OPTIMIZATION OF AIR CONDITIONING CYCLING

A Thesis

by

SWAROOPH NIRMAL SESHADRI

Submitted to the Office of Graduate Studies of
Texas A&M University
in partial fulfillment of the requirements for the degree of

MASTER OF SCIENCE

August 2011

Major Subject: Mechanical Engineering

Optimization of Air Conditioning Cycling

OPTIMIZATION OF AIR CONDITIONING CYCLING

A Thesis

by

SWAROOPH NIRMAL SESHADRI

Submitted to the Office of Graduate Studies of
Texas A&M University
in partial fulfillment of the requirements for the degree of

MASTER OF SCIENCE

Approved by:

Chair of Committee,	Bryan Rasmussen
Committee Members,	Won-Jong Kim
	Jeff Haberl
Head of Department,	Dennis O'Neal

August 2011

Major Subject: Mechanical Engineering

ABSTRACT

Optimization of Air Conditioning Cycling. (August 2011)

Swarooph Nirmal Seshadri, B.E, Madras Institute of Technology, Chennai

Chair of Advisory Committee: Dr. Bryan Rasmussen

Systems based on the vapor compression cycle are the most widely used in a variety of air conditioning applications. Despite the vast growth of modern control systems in the field of air conditioning systems, industry standard control is still thermostat based on-off control, in other words cycle control. This thesis proposes an approach to find the optimal profiles for the expansion valve and the evaporator fan for an air conditioning system for a given period of on-off cycle of the compressor. The research will consist of two phases, the development of a simulation model and an experimental analysis.

In this thesis, the profiles for the expansion valve and the evaporator fan are parameterized by an S-curve equation so that the optimization problem will have less numbers of parameters. The first step is a simulation model that predicts startup/shutdown characteristics. This model is used as a tool to understand the effect that the S-curve parameters has on the system cycle efficiency. Several key vapor compression system dynamics are identified as causes for increasing/decreasing system's cyclic efficiency. Refrigerant migration and fan delay at shutdown are determined as crucial issues that have an effect on the system's cyclic efficiency. A

direct search optimization algorithm, namely the simplex search algorithm, is then used to search for the optimal S-curve parameters. Valve/fan strategies that ultimately resulted in a better superheat control are assessed as the most energy efficient. Extensive experimental tests conducted on a 3-ton residential air conditioner are then presented to intuitively understand the effect of expansion valve and evaporator fan cycling in a real system. A real time optimization method is explored and the feasibility, recommendations for a successful online method are proposed. The heuristics for the expansion valve and evaporator fan profiles from the optimization results could be easily hard coded into any commercial air conditioning system to perform the much preferred cycle control. Thus a significant improvement in the energy performance was observed without the use of any advanced control techniques.

DEDICATION

To Saroja Paati

ACKNOWLEDGEMENTS

I would like to thank my thesis advisor, Dr. Bryan Rasmussen, for his constant support and patience throughout the length of my research. I would also like to thank Dr. Won-Jong Kim and Dr. Haberl for serving on my advisory committee. I would like to thank my colleagues at Thermo-Fluids Control Laboratory namely Matt, Bhaskar, Nataraj, Bala and Alex for their insightful discussions and relieving laughter. I am grateful to all my friends who fill up my life with beautiful moments. Finally I would like to thank my parents and my sister for believing in my abilities and letting me follow my dream.

NOMENCLATURE

$HVAC\&R$	Heating, Ventilation, Air Conditioning and Refrigeration
A_i	Internal surface area of heat exchanger
A_o	External surface area of heat exchanger
C_d	Coefficient of Discharge of the expansion valve
COP	Instantaneous Coefficient of Performance
COP_{ss}	Coefficient of Performance at steady state condition
EEV	Electronic Expansion Valve
E_w	Heat exchanger tube wall energy
FCV	Finite Control Volume
h	Enthalpy of the refrigerant
H	Energy due to refrigerant flow
$ICOP_{cycle}$	Inverse Coefficient of Performance per on/off cycle of the compressor
MB	Moving Boundary
$\dot{m}_{air}$	Mass flow rate of the air over the evaporator
$\dot{m}_{in}$	Mass flow rate of the refrigerant flowing into the evaporator
$\dot{m}_k$	Mass flow rate of the refrigerant flowing through the compressor
$\dot{m}_{out}$	Mass flow rate of the refrigerant flowing out of the evaporator
$\dot{m}_v$	Mass flow rate of the refrigerant flowing through the valve
P	Pressure

P_c	Condenser pressure
P_e	Evaporator pressure
P_{in}	Pressure at expansion valve inlet
P_{out}	Pressure at expansion valve outlet
Q	Instantaneous cooling
Q_a	Energy due to heat transfer between heat exchanger tube wall and air
Q_{ss}	Cooling at steady state condition
Q_w	Energy due to heat transfer between refrigerant and heat exchanger tube wall
T_a	Temperature of air
T_r	Temperature of the refrigerant
T_w	Temperature of heat exchanger tube wall
T_{cao}	Air temperature at condenser outlet
T_{cro}	Refrigerant temperature at condenser outlet
T_{eao}	Air temperature at evaporator outlet
T_{ero}	Refrigerant temperature at evaporator outlet
T_{eai}	Air temperature at evaporator inlet
U	Refrigerant energy
u	Internal energy of the refrigerant
u_v	Percentage opening of the EEV
V_k	Volume of the compressor

W	Instantaneous work input to the system

Greek symbols

α_i	Heat transfer coefficient between refrigerant and heat exchanger tube wall
α_o	Heat transfer coefficient between heat exchanger tube wall and air
ΔP	Pressure differential across the valve
∇f	Gradient of a function f
$\nabla^2 f$	Hessian of a function f
ρ	Density of the refrigerant
ρ_w	Density of heat exchanger tube wall material
η_a	Adiabatic efficiency of the compressor
η_k	Volumetric efficiency of the compressor
ρ_k	Density of refrigerant at compressor inlet
ω_k	Compressor speed in rotations per second

TABLE OF CONTENTS

Page

LIST OF FIGURES

FIGURE Page

FIGURE Page

FIGURE Page

FIGURE Page

FIGURE Page

FIGURE Page

FIGURE Page

FIGURE Page

FIGURE Page

LIST OF TABLES

1. INTRODUCTION

The energy consumption of Heating, Ventilation, Air-Conditioning and Refrigeration (HVAC&R) systems amounts to as much as 56% of energy use in an average U.S household [1]. The projections for residential energy consumption per capita by 2035 show a sharp decline [2]. This is under the assumption that customers adhere to the best energy standards despite the cost. However in reality this is not really true since the majority of consumers are cost conscious. So, an effort has to be made towards higher energy efficiency that need not involve substantial investment from the consumer's end.

Vapor compression systems are the most widely used type of AC&R systems because, they are relatively inexpensive and a rugged technology. Despite the advent of modern controls systems, the final implementation of control of vapor compression based AC&R systems is fairly simple. Conventional cycle control is cycling the electronic expansion valve and the heat exchanger fans on and off simultaneously with the compressor. From the energy efficiency perspective, there is no reason to believe that it is the optimal strategy. This thesis addresses this question by investigating the optimal expansion valve and the evaporator fan cycles, given an on-off cycle of the compressor.

The rest of the section is organized as follows. Subsection 1.1 gives a brief overview of vapor compression systems and the need for compression cycling. This is followed by a literature review on startup/shut down modeling and cycling control.

This thesis follows the style of *IEEE Transactions on Automatic Control.*

1.1 Background

1.1.1 Vapor Compression Cycle

The single stage vapor compression system essentially has four components, namely: compressor, condenser, expansion valve and evaporator. Figure 1.1 gives a schematic of such a system.

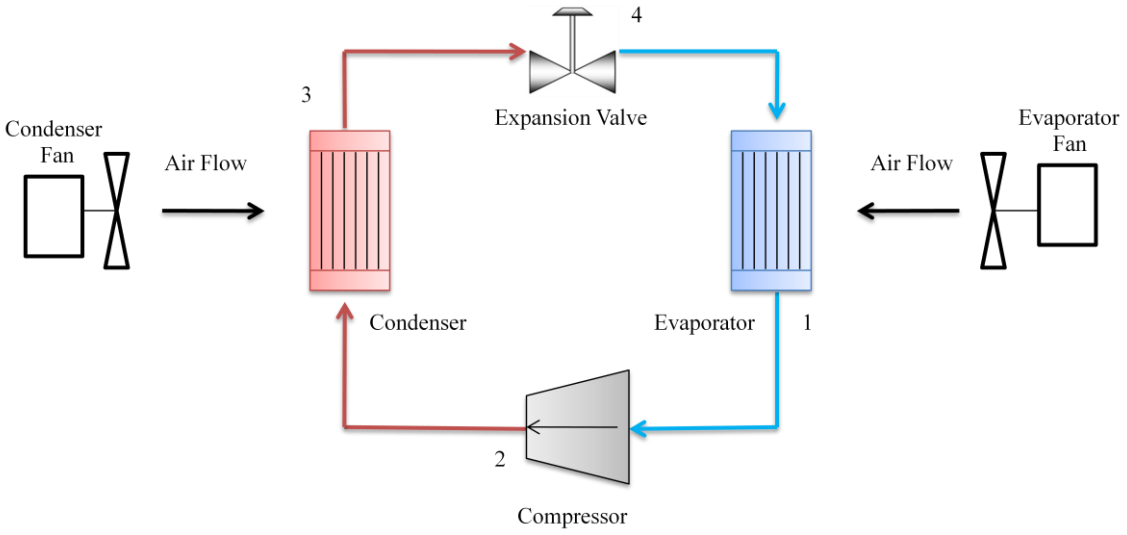

Figure 1.1 Components of a Vapor Compression System

The ideal vapor compression cycle consists of four processes: isentropic compression at the compressor, isobaric heat rejection in the condenser, isenthalpic expansion in the expansion valve and isobaric heat absorption in the evaporator. Figure 1.2 shows the pressure versus enthalpy diagram of an ideal single stage vapor compression cycle.

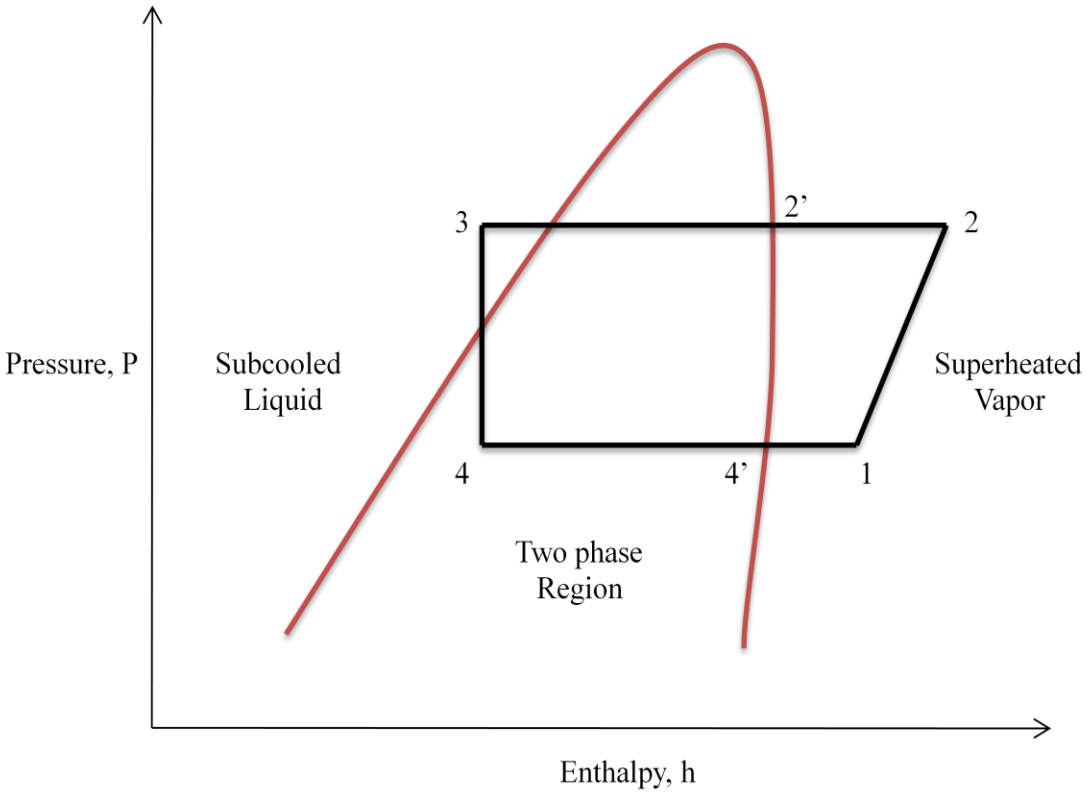

Figure 1.2 P-h Diagram of Actual Single Stage Vapor Compression Cycle

The first stage of the cycle starts at 1 which is at the compressor inlet. Here the refrigerant is at a low pressure and is gaseous. The compressor then compresses the refrigerant into a high pressure vapor that is fed to the inlet of the condenser at 2. The condenser is a heat exchange element in the cycle, where heat is rejected by the refrigerant to an external fluid. At the outlet of the condenser the refrigerant is a high pressure liquid at 3. The refrigerant expands and cools down through the expansion valve to the low pressure region of the cycle. At the outlet of the valve the refrigerant is in the two phase region at 4. The final stage of the cycle is in the evaporator, which is the second heat exchange element. Here, heat is absorbed by the refrigerant from an external

fluid thus evaporating. This results in the refrigerant being superheated at the evaporator outlet at 1.

From the control engineering point of view, the inputs to the system are: the compressor on/off signal, the expansion valve opening, the evaporator and the condenser fan speeds. The expansion valve referenced here is assumed to be an electronic expansion valve. The valve opening can be controlled by simple electric circuitry thus making advanced controls possible. Other types of expansion valves that could be used in the vapor compression system are orifice expansion valve, automatic expansion valve and the thermal expansion valve. The fans are assumed to be variable speed fans and hence the mass flow rate of air can be controlled at both the heat exchangers using electrical signals. Another type of fan that could be employed is a single speed fan where the fan is either on or off.

1.1.2 Compressor Cycling

Cycling a compressor on and off is the usual way to control the cooling capacity of HVAC&R systems. This kind of simple control is popular because of the low cost and easy availability of timing and logic circuits, solid state relays and temperature measurement. In this context, control refers to capacity control where the objective is to match the heat capacity output of the HVAC&R system to the load. Such kind of capacity modulation schemes are required in order to maintain a certain thermal comfort in the conditioned space. One of the easiest ways to do capacity modulation in residential and small scale commercial HVAC&R systems is to control the speed of the compressor.

By this method, there are three distinct ways to achieve capacity control. The conventional cycling of HVAC&R systems to modulate capacity is to turn on and off a fixed speed compressor. The cycle periods here could be as long as 20 minutes. The cycle length here is determined by a temperature sensing device such as a thermostat. But there are a number of problems associated with such a scheme. The foremost is the fact that the indoor air temperature and humidity fluctuation is very wide. This would be a cause for thermal discomfort during the long off cycles. Most of the times the fans are off during the off cycles and this means the air circulation in the room also varies a lot. The second problem is the system efficiency. Long cycles such as this would result in higher cyclic losses and lower thermodynamic efficiencies for the heat exchangers. One way to get around this problem would be to use the variable speed approach. Unlike conventional cycling where the compressor is either on or off, here the compressor is made to run at different speeds suited to the cooling load at that time, to provide the needed heat capacity output. Thus even at part load conditions the system would be operating at high efficiencies. The system is continuously running aiming to match the load at all times, hence the indoor temperature and humidity is maintained in a tighter manner. This results in a much better thermal comfort. However, the downside to this approach is the requirement of an inverter and its drive circuits to do speed control for the compressor. There are electrical losses associated with the inverter and also the cost associated to design and install such a system is high.

More recently a new method has been explored to do capacity control through rapid cycling of the compressor. By rapid cycling, the compressor cycle period could

vary from 5s to 100s. Here the on time percentage of the compressor is controlled to match the heat capacity output of the system to the load. This is comparable to the speed control in the variable speed systems. As the cycling frequency is increased, the system performance seems to get close to that of the variable speed systems and when the cycle is lengthened the system tends to act more like the conventional cycling systems. Thus efficiencies that are close to that of the variable speed systems could be achieved without the use of an inverter. Because the system is cycling so fast, the indoor air temperature and humidity fluctuation is not wide and remains within an acceptable bound. Thermal comfort hence is not sacrificed.

With such cycling techniques helping to achieve better system efficiencies (Table 1.1), there is a need to look at optimizing such cycles. Research has gone into finding the optimized duty cycle and scheduling of the compressors corresponding to a cooling load profile [3], [4], [5], [6] and [7]. However for those cycles, the expansion valve and the heat exchanger fan cycling also needs to be looked at to see if the cycle efficiency can be further improved.

Table 1.1 Cycling Techniques - Summary

METHOD	CYCLE LENGTH	THERMAL DISCOMFORT	EFFICIENCY		MAIN FEATURE
			Full load	Part Load	
Conventional ON-OFF	$\geq$ 20 mins	High	High	Low	Cheap
Variable Speed	-	Very Low	High	Comparable	Costly
Rapid Cycling	5s – 100s	Very Low	High	Depends on OFF period	Compressor Wear

1.2 Literature Survey

The most important work in the field of dynamic modeling of vapor compression systems and cycle control, pertaining to this research is presented here. Review of dynamic modeling of vapor compression systems is important for the development of the simulation model. Secondly, cycle control techniques need to be studied to understand the advantages and disadvantages of existing cycling controls.

1.2.1 Modeling

The heat exchangers' model of the vapor compression system, developed in this thesis uses Finite Control Volume (FCV) technique. This belongs to a modeling approach that is spatially dependant where the heat exchanger is divided into a number of constant volumes. A lumped parameter approach is then applied to each of the control volumes, thus producing a discretized distributed parameter approach. Another popular technique is the Moving Boundary (MB) technique that estimates the point in a heat exchanger at which phase change occurs. Here the heat exchanger length is divided dynamically depending on the refrigerant phase. Bendapudi [8] extensively compared the two modeling techniques and concluded that the main advantage of the MB models is their speed of execution while giving accuracies really close to the FCV models. Although FCV models are slower, they are better suited to capture the startup transients. Since this thesis requires a model that has accurate transient characteristics during cycling, the FCV approach is used. The work done by Wedekind and Stoecker [9] looked at the transient behavior of evaporators as early as 1968 and was the first to describe the concept of a transition point that later laid the foundation for the MB

technique. Wedekind, Bhatt et al. [10] also developed a void fraction method. Due to this work, the assumption that the positions of effective dry out point for an evaporator during pure evaporation and the effective point of complete condensation for the condenser, is almost the same throughout the process became popular. Dhar's doctoral thesis [11] gives a detailed description about modeling transient behavior of refrigeration systems. The MB approach was used here to predict the refrigerant side dynamics of the system. Experimental validation was done on a window air conditioner to study the transients. Gruhle and Isermann [12] suggested the first noteworthy distributed parameter approach for modeling in 1985. They obtained the model in a state space form but no experimental validation was presented. MacArthur and Grald were successful in validating a distributed model with experimental data in 1987 [13]. In 1992 the MB equivalent was developed by the same authors [14]. Mithraratne [15] showed a distributed parameter based numerical model of an evaporator controlled by a thermostatic expansion valve. Unlike [12], the model here was implemented by solving nonlinear differential equations at discrete time steps. The lumped parameter approach usually fails to capture some important dynamics. However, Chi and Didion presented a useful transient model that followed a lumped parameter approach [16]. Data taken from a 4-ton air to air heat pump was used to validate the model. Bendapudi [17] gives a very good literature review on the modeling of vapor compression systems.

Losses due to the relative inefficiency of the HVAC&R systems when subjected to cycling have been assessed in detail by several researchers. This is important to understand a HVAC&R system's cyclic performance and to calculate an appropriate

performance metric for the system. Murphy and Goldschmidt [18] noted that the transient losses due to cycling vary for heating and cooling modes. This meant that the efficiency not only depended on the thermal mass of the heat exchangers but also the thermostat setting. Wang and Wu [19] inferred that the startup transients are heavily influenced by the shutdown transients. They showed refrigerant migration to be a major factor contributing to cyclic efficiency by using thermostatic valve without bleed ports to stop flow at shutdown and that by preventing refrigerant migration motor power input during startup can be decreased by 4%. Mulroy and Didion [20] developed an exponential equation (equation 2.1) to predict the instantaneous cooling capacity of a refrigeration system under startup condition.

$$Q = Q_{ss}\left(1 - e^{-t/\tau_1}\right)\left(1 + K.e^{-t/\tau_2}\right) \quad 1.1$$

Gado [21] in his doctoral thesis defines transient losses as a simple integral equation as follows,

$$Loss = \frac{\int (Q_{ss} - Q)dt}{\int Q\, dt} \quad 1.2$$

Equation 1.2 defines the area between the air side capacity and the steady state cooling as the overall transient loss. Kapadia et al. [22] compared the transient losses occurring during startup for two different refrigerants namely R-22 and R-410A. They concluded for their set up that R-410A showed lesser transient losses because of refrigeration migration.

1.2.2 Cycle Control

Subsection 1.1.2 briefed upon the need for compressor cycling and the different types. Marquand, Tassou et al. [23] compared three different types of compressor cycling for capacity modulation namely fixed speed compressor on/off, two speed compressor on/off and the variable speed approach. The economic aspect of the different approaches was also discussed. They concluded that installing a two-speed switch for the compressor is much preferred because of the relatively low cost of installation and small payback time compared to the variable speed inverter. Janssen et al. [24] studied the cycling losses occurring in domestic appliances. They attributed the cycling losses to three factors namely, thermodynamic efficiency of heat exchangers, start/stop losses and compressor efficiency. They also observed that closing the line between the condenser and the expansion device during the off period of the compressor results in less start/stop losses. Thus, higher efficiencies could be obtained by increasing the cycle rate but the efficiency would never match a continuously running system. Wicks [25] compared the on/off method to the frequency modulation method and found that capacity control is better achieved by continuously varying compressor speed rather than on/off of the compressor because the former used less electricity. Leva, Piroddi et al. [26] note that the on/off solution is less frequently explored compared to its counterpart the variable speed despite its vast application in commercial HVAC&R systems. They continue to note that when cost is a factor, on/off is preferred over variable speed even though performance reduces and controller complexity increases.

Ilic, Bullard and Hjrnak [27] and Poort and Bullard [28] explore the advantages of rapid cycling. They concluded that rapid cycling could give performance comparable to the much costlier variable speed compressor speed control. However they do inform that the cycle lengths have to be lengthened so as to reduce the number of startup spikes and increase the compressor reliability by reducing the wear.

The work done by Mulroy [29] in 1986 is of much interest for this thesis since; he looked at the effect of keeping the fan on during the off cycle of the compressor on the efficiency of the system. The measure of cyclic efficiency in this work is of particular interest. The ratio of total capacity produced over the cycle to the total power input to the system was taken in the efficiency as follows,

$$Cyclic\ Efficiency = \frac{\int Q\ dt / \int W\ dt}{COP_{ss}} \tag{1.3}$$

where COP_{ss} is the steady state Coefficient of Performance of the system when the system is continuously running. The objective function for use in the optimization in this thesis is very similar to the above equation and is explained in the proposed approach.

A look into the literature of optimal on/off strategies in HVAC&R systems is of interest. Jian and Zaheruddin [5] developed a dynamic model of a chilled water cooling system and presented the optimal lead time for the compressor switching on time and staying on time given a cooling load profile. The cost function used here consists of 2 terms namely, temperature performance and energy performance. Honglian, Larsen et al. [4] present a very simple model of an AC system, considering it as a unit that just removes energy from another room. They used a fast, computationally easy method to achieve results close to optimal solution for the compressor cycle input by considering

an objective function that involved thermal comfort, energy efficiency and compressor weariness (number of switches). The method was compared to a finite prediction horizon model predictive control where the computations are very demanding. Chang, Lin et al. [3] and Rampazzo [7] presented different methods for optimal chiller sequencing. They considered parameters like loading limit and minimal down time for a chiller. The objective was to find the sequence for operating the chillers while reducing the number of switches thus improving equipment life. While Chang, Lin et al. [3] used a branch and bound method to solve the problem, Rampazzo [7] used a genetic algorithm based method. Li and Alleyne [6] present a method to obtain the optimal algorithm for compressor on/off using relay feedback. An objective function consisting of temperature performance, energy consumption and component wear was taken into account. Finally a compressor profile of on/off sequences was obtained to suit according to the weights of the terms in the stated objective function.

To summarize, no previous work was done regarding the optimal cycles for the expansion valve and the fans for the HVAC&R systems. Significant research has only gone into scheduling of compressors and finding the optimal profile for the compressor. Hence, there is a need to explore the strategies for the actuators given the compressor on/off cycle as they could have significant effect on system's cyclic efficiency. This would also reveal key vapor compression system dynamics on the refrigerant and the air side as causes for increase or decrease in a system's cyclic efficiency.

2. STARTUP/SHUTDOWN MODELING

This section describes the modeling of the various components in the vapor compression based HVAC&R systems which were listed in Subsection 1.1.1. The models were drawn from the work done by Rasmussen [30] and Gupta [31]. The heat exchangers were modeled using the Finite Control Volume (FCV) approach and the compressor, valve were modeled using algebraic relationships. The section is organized as follows: firstly the modeling assumptions are stated followed by each of the components' description.

2.1 Modeling Assumptions

The first assumption was that the actuating components namely the compressor and the electronic expansion valve could be modeled with algebraic relationships. This was because the dynamics of the system were expected to be dominated by the heat exchangers. Since the compressor and the electronic expansion valve are generally much faster compared to the heat exchanger dynamics, this assumption did not hinder the transient accuracy of the model. The compression was assumed to be isentropic and the expansion in the electronic expansion valve to be isenthalpic. The heat exchangers themselves were modeled as long thin horizontal tubes hence the refrigerant flow could be modeled as one dimensional flow. In reality, due to turbulence, the flow would be three dimensional; however, using appropriate correlations for calculating heat transfers, the effects can be captured. The heat transfer occurring at the heat exchangers were

assumed to be isobaric, in which case the pressure drop due to change in momentum of the refrigerant could be neglected. Hence equations involving conservation of momentum could be ignored. A Finite Control Volume based approach was used to model the heat exchangers. Here the length of the heat exchanger was discretized into several control volumes. The cross sectional flow area of the refrigerant was assumed constant within a given control volume. Finally axial conduction of the refrigerant is assumed negligible.

The important point to note here is that the model presented here was not validated against the experimental system described in Section 3. This was because validating a model for such a complex system is a difficult task in itself. Since the model was going to serve as a tool to understand the patterns of system efficiency corresponding to different types of expansion valve and evaporator fan cycles, an approximate model was deemed enough for the purpose. The model was configured such that the dynamics resembled the experimental system in most important cases and was not tested for all operating conditions. The model thus aided to guess better in terms of a starting point for optimizations.

2.2 Compressor

The compressor was modeled using two relationships. The first determined the mass flow rate of the refrigerant at the compressor outlet. Equation 2.1 involving an empirically derived volumetric efficiency η_k was used.

$$\dot{m}_k = \rho V_k \omega_k \eta_k \qquad 2.1$$

$$\eta_k = \eta(\omega_k, \frac{P_{out}}{P_{in}}) \quad 2.2$$

The second expression estimated the outlet enthalpy. This was done based on the assumption that compression was adiabatic with an isentropic efficiency η_a. The equations 2.3 and 2.4 describe the relationship.

$$\eta_a = \frac{h_{out,isentropic} - h_{in}}{h_{out} - h_{in}} \quad 2.3$$

$$h_{out} = \frac{1}{\eta_a}[h_{out,isentropic} + h_{in}(\eta_a - 1)] \quad 2.4$$

An empirical map was created for η_a as a function of the speed of the compressor and the pressure ratio similar to η_k as in equation 2.2.

2.3 Electronic Expansion Valve

The mass flow rate through the electronic expansion valve was modeled based on the following orifice equation,

$$\dot{m}_v = C_d\sqrt{\rho(P_{in} - P_{out})} \quad 2.5$$

$$C_d = f_1(u_v, \Delta P) \quad 2.6$$

C_d, the discharge coefficient of the valve was a semi empirical map that depended on the valve command u_v and the pressure differential across the valve $\Delta P = P_{in} - P_{out}$. The valve was assumed to be isenthalpic so; enthalpy at the exit of the valve was the same as the enthalpy at its inlet.

$$h_{v,out} = h_{v,in} \quad 2.7$$

2.4 Evaporator

As noted before, FCV based modeling approach used in Gupta [31] was adopted for the simulation model. In this, the evaporator was divided into *n* control volumes and a lumped parameter approach was applied to each of the control volumes. By increasing the number of control volumes, the model approaches the distributed parametric model which resembles a heat exchanger in reality. The governing differential equations were obtained by listing the equations involving conservation of refrigerant energy, mass and tube wall energy and then applying the simplicity assumptions explained in Subsection 2.1.

In the FCV evaporator model, the state of the refrigerant in a particular control volume is determined by the enthalpy of the refrigerant at the exit of that control volume. If the enthalpy is greater than the saturated vapor enthalpy then the refrigerant is superheated vapor and if the enthalpy is less than or equal to the saturated vapor enthalpy, the refrigerant is in two phase. The evaporator usually has a two phase fluid entering it and a superheated evaporator leaving it. Thus the evaporator has 2 regions namely: two phase region and superheated region. Here the transition is assumed to be gradual as shown in Figure 2.1.

There might be modeling errors associated with the inaccurate placement of the transition region. This could be avoided by increasing the number of control volumes. In the figure $\dot{m}_{in}$, h_{in} and $\dot{m}_{out}$, h_{out} are the mass flow rates and the enthalpies at the inlet and the exit of the evaporator. $\dot{m}_{e,k}$, $h_{e,k}$ are mass flow rates and the average enthalpy in the k^{th} control region. h_k is the enthalpy at the exit of k^{th} region that determines the

state of the refrigerant in the k^{th} region. The following subsections describe the equations that are used in modeling the FCV heat exchanger.

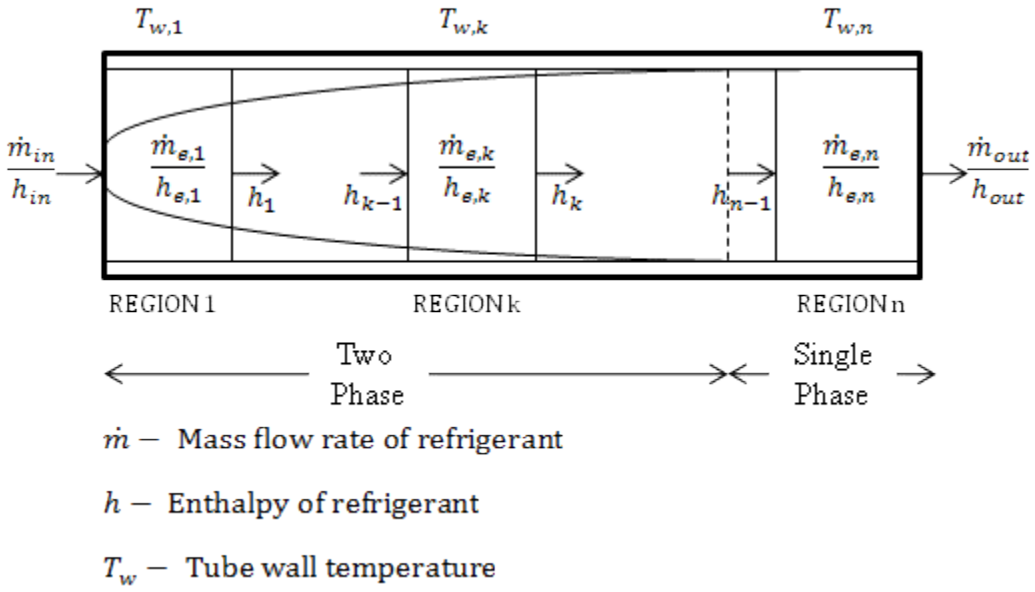

Figure 2.1 FCV Evaporator Model

2.4.1 Conservation of Refrigerant Energy

The rate of change of refrigerant energy in the system is given by equation 2.8. Here, $\dot{H}_{in}$ is the rate of energy into the region due to refrigerant flow, $\dot{H}_{out}$ is the rate of energy leaving the region due to refrigerant flow and $\dot{Q}_w$ is the rate of energy due to heat transfer between the refrigerant and the tube wall. At a point the rate of energy due to refrigerant flow is given by equation 2.9 where $\dot{m}$ is the refrigerant mass flow rate and h is the refrigerant enthalpy at that point. The rate of energy due to heat transfer to the tube wall $\dot{Q}_w$ is given by equation 2.10 where α_i is the lumped parameter heat transfer

coefficient between the fluid and the tube wall, T_w and T_r are the lumped parameter tube wall and refrigerant temperatures. α_i was calculated using a correlation as suggested by Wattelet et al. [32]. The main feature of this correlation is the implicit capability to handle pool boiling condition which is necessary to model shutdown dynamics of the evaporator. For a detailed analysis the reader is encouraged to refer [32]. Gnielinski [33] correlation was used for calculating the heat transfer coefficient during single phase heat transfer. Expanding all the necessary terms, the conservation of refrigerant energy for all the control regions are derived in equation 2.11.

$$\dot{U} = \dot{H}_{in} - \dot{H}_{out} + \dot{Q}_w \tag{2.8}$$

$$\dot{H} = \dot{m}\, h \tag{2.9}$$

$$\dot{Q}_w = \alpha_i A_i (T_w - T_r) \tag{2.10}$$

$$\begin{bmatrix} \dot{U}_1 \\ \vdots \\ \dot{U}_k \\ \vdots \\ \dot{U}_n \end{bmatrix} = \begin{bmatrix} \dot{m}_{in} h_{in} - \dot{m}_1 h_1 + \alpha_{i,1} A_{i,1} (T_{w,1} - T_{r,1}) \\ \vdots \\ \dot{m}_{k-1} h_{k-1} - \dot{m}_k h_k + \alpha_{i,k} A_{i,k} (T_{w,k} - T_{r,k}) \\ \vdots \\ \dot{m}_{n-1} h_{n-1} - \dot{m}_{out} h_{out} + \alpha_{i,n} A_{i,n} (T_{w,n} - T_{r,n}) \end{bmatrix} \tag{2.11}$$

2.4.2 Conservation of Mass

The conservation of refrigerant mass is given by difference of the amount of refrigerant entering the region and the amount leaving it. Equation 2.12 gives the conservation of refrigerant mass for all regions. These can be composed into a single equation by adding them to give equation 2.13 where, $\dot{m}_{in}$ and $\dot{m}_{out}$ are the mass flow rates of the refrigerant entering and exiting the heat exchanger.

$$\begin{bmatrix} \dot{m}_{e,1} \\ \vdots \\ \dot{m}_{e,k} \\ \vdots \\ \dot{m}_{e,n} \end{bmatrix} = \begin{bmatrix} \dot{m}_{in} - \dot{m}_1 \\ \vdots \\ \dot{m}_{k-1} - \dot{m}_k \\ \vdots \\ \dot{m}_{n-1} - \dot{m}_{out} \end{bmatrix} \tag{2.12}$$

$$\dot{m}_e = \dot{m}_{in} - \dot{m}_{out} \tag{2.13}$$

2.4.3 Conservation of Tube Wall Energy

The rate of change of tube wall energy is given by the equation 2.14 where, $\dot{Q}_a$ is the rate of heat transfer between the tube wall and the external fluid. $\dot{Q}_a$ is given by equation 2.15 where, α_o is the lumped parameter heat transfer coefficient between the tube wall and the external fluid. A_o is the outside surface area and T_a is the lumped parameter external fluid temperature for each region. Finally, substituting for the necessary terms equation 2.16 presents the law of conservation of tube wall energy for all regions.

$$\dot{E}_w = \dot{Q}_a - \dot{Q}_w \tag{2.14}$$

$$\dot{Q}_a = \alpha_o A_o (T_a - T_w) \tag{2.15}$$

$$\begin{bmatrix} \dot{E}_{w,1} \\ \vdots \\ \dot{E}_{w,k} \\ \vdots \\ \dot{E}_{w,n} \end{bmatrix} = \begin{bmatrix} \alpha_{o,1} A_{o,1} (T_{a,1} - T_{w,1}) - \alpha_{i,1} A_{i,1} (T_{w,1} - T_{r,1}) \\ \vdots \\ \alpha_{o,k} A_{o,k} (T_{a,k} - T_{w,k}) - \alpha_{i,k} A_{i,k} (T_{w,k} - T_{r,k}) \\ \vdots \\ \alpha_{o,n} A_{o,n} (T_{a,n} - T_{w,n}) - \alpha_{i,n} A_{i,n} (T_{w,n} - T_{r,n}) \end{bmatrix} \tag{2.16}$$

2.4.4 Governing Equations

A nonlinear state space of form in equation 2.17 was used to describe the entire model. The detailed derivation found in Gupta [31] is presented in the Appendix. This contains *2n+1* states (Enthalpy of *n* regions + Wall Temperature of *n* regions + Pressure

across the heat exchanger). These are contained in the state vector *x*, as expressed in equation 2.18. *u* and *y* are the input and output vectors described in equations 2.19 and 2.20 respectively. *Z(x,u)* and *f(x,u)* are shown in equation 2.21 and 2.22 respectively.

$$Z(x,u)\,.\,\dot{x} = f(x,u) \tag{2.17}$$

$$x = [\;\; P_e \quad h_{e,1} \quad \cdots \quad h_{e,k} \quad \cdots \quad h_{e,n} \quad T_{w,1} \quad \cdots \quad T_{w,k} \quad \cdots \quad T_{w,n} \;\;]^T \tag{2.18}$$

$$u = [\;\; \dot{m}_{in} \quad \dot{m}_{out} \quad h_{in} \quad T_{a,in} \quad \dot{m}_{air} \;\;]^T \tag{2.19}$$

$$y = \left[P_e \;\; h_{out} \;\; T_{w,1} \;\; \cdots \;\; T_{w,k} \;\; \cdots \;\; T_{w,n} \;\; T_{a,out} \;\; T_{r,out} \;\; \dot{m}_{e,1} \;\; \cdots \;\; \dot{m}_{e,k} \;\; \cdots \;\; \dot{m}_{e,n}\right]^T \tag{2.20}$$

$$Z(x,u) = \begin{bmatrix} Z_{11} & Z_{12} & 0 \\ Z_{21} & Z_{22} & 0 \\ 0 & 0 & Z_{33} \end{bmatrix}_{(2n+1)X\,(2n+1)} \tag{2.21}$$

$$f(x,u) = \begin{bmatrix} \dot{m}_{in}(h_{in} - h_1) + \alpha_{i,1}A_{i,1}(T_{w,1} - T_{r,1}) \\ \vdots \\ \dot{m}_{in}(h_{k-1} - h_k) + \alpha_{i,k}A_{i,k}(T_{w,k} - T_{r,k}) \\ \vdots \\ \dot{m}_{in}(h_{n-1} - h_{out}) + \alpha_{i,n}A_{i,n}(T_{w,n} - T_{r,n}) \\ \dot{m}_{in} - \dot{m}_{out} \\ \alpha_{o,1}A_{o,1}(T_{a,1} - T_{w,1}) - \alpha_{i,1}A_{i,1}(T_{w,1} - T_{r,1}) \\ \vdots \\ \alpha_{o,k}A_{o,k}(T_{a,k} - T_{w,k}) - \alpha_{i,k}A_{i,k}(T_{w,k} - T_{r,k}) \\ \vdots \\ \alpha_{o,n}A_{o,n}(T_{a,n} - T_{w,n}) - \alpha_{i,n}A_{i,n}(T_{w,n} - T_{r,n}) \end{bmatrix}_{(2n+1)X1} \tag{2.22}$$

2.5 Condenser

FCV based modeling approach was used for modeling the condenser also. In this the condenser was divided into *n* control volumes and a lumped parameter approach was

applied to each of the control volumes. By increasing the number of control volumes, the model approaches the dynamics of a heat exchanger in reality.

In the FCV condenser model, the state of the refrigerant in a particular control volume is determined by the enthalpy of the refrigerant at the exit of that control volume. If the enthalpy is greater than the saturated vapor enthalpy then the refrigerant is superheated vapor, if the enthalpy of the refrigerant is less than or equal to the saturated vapor enthalpy, the refrigerant is in two phase and if the enthalpy of the refrigerant is less than the saturated liquid enthalpy, then the refrigerant is a sub-cooled liquid. The condenser usually has the refrigerant entering it as a superheated vapor and leaving it as a sub-cooled liquid. Thus the condenser has 3 regions namely: superheated region, two phase region and sub-cooled region. Here the transition is assumed to be gradual as shown in Figure 2.2.

The governing differential equations are obtained by listing the equations involving conservation of refrigerant energy, mass and tube wall energy and then applying the simplicity assumptions just like what was done for the evaporator. In fact the governing equations for the condenser are the same as evaporator as presented in Subsection 2.4, equations 2.33 through 2.53. One thing of importance to note here is the correlation that was used to calculate α_i, the lumped parameter heat transfer coefficient between the condenser wall and the refrigerant. Dobson et al. [34] was used to calculate α_i for two phase conditions. Since the condenser model has to be valid during shutdown, the correlation was included with a film condensation expression to handle this condition. The formula for estimating heat transfer correlation during film

condensation was adopted from [35]. For a detailed analysis the reader is encouraged to refer [35] and [35]. Gnielinski [33] correlation was used for estimating heat transfer coefficient during single phase.

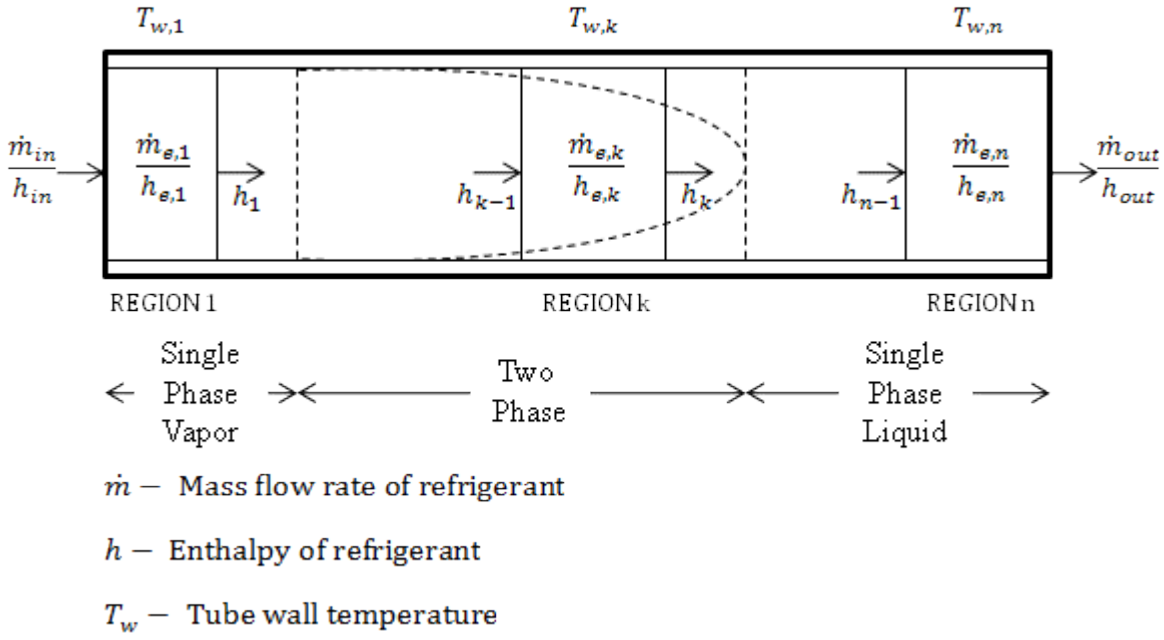

Figure 2.2 FCV Condenser Model

3. EXPERIMENTAL SYSTEM

The experimental system used was a 3-ton residential air conditioner from TRANE available at the Thermo-Fluid Controls Laboratory in Texas A&M University, College Station. The system is shown in Figure 3.1. The system was instrumented with sensors like pressure sensors, thermocouples, a mass flow rate sensor, humidity sensors etc. The actuators used in the systems are an electronic expansion valve from Parker and two variable speed fans. The variable speed fans were made to run at different speeds to adjust the mass flow rate of air (external fluid) over the evaporator and the condenser. The system was charged with R-410A refrigerant by a two stage fixed speed scroll compressor. Figure 3.1 is a picture of the main parts of the system. The schematic of the system showing the placement of the various sensors and the actuators are shown in Figure 3.2.

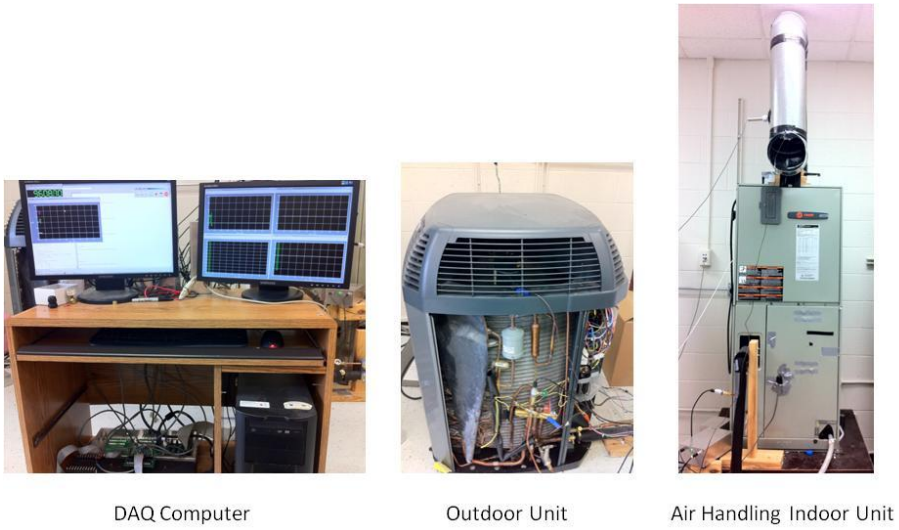

Figure 3.1 3-ton Residential Air conditioner Experimental System from TRANE

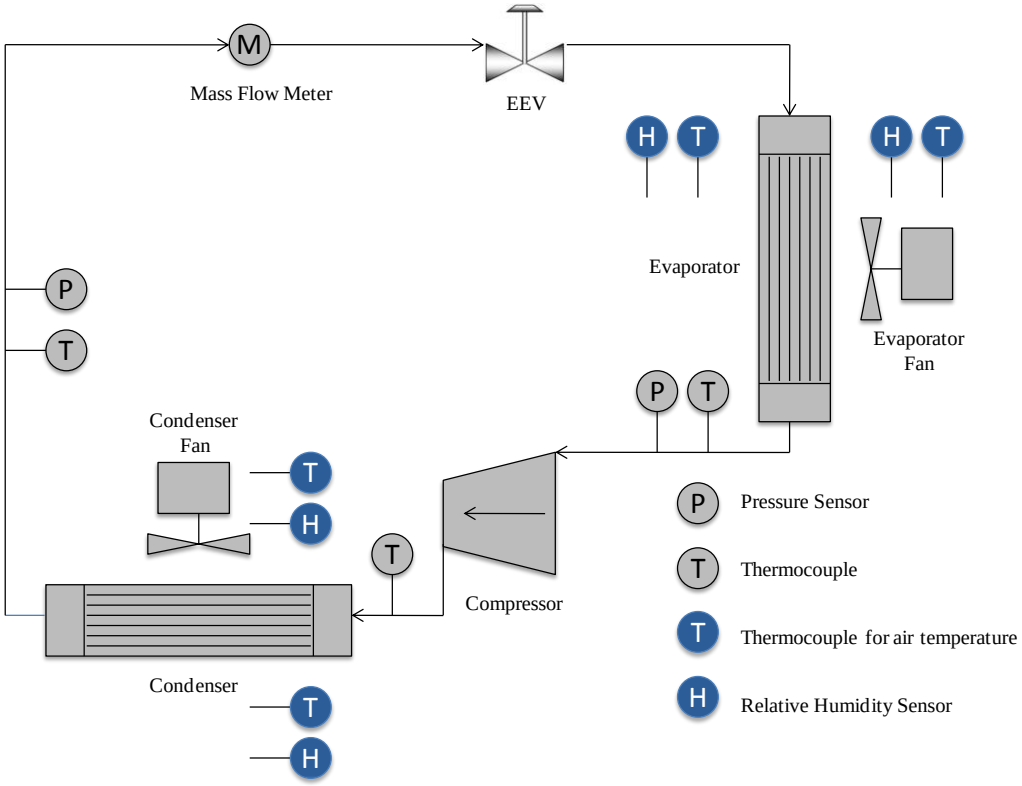

Figure 3.2 TRANE Experimental System Schematic

The information about the essential components used in the system is listed in Table 3.1.

Table 3.1 Components of TRANE Experimental System

Component	**Manufacturer**	**Model Number**
Air Conditioning System	Trane	XL 16i
EEV	Parker	020432-00
Thermocouple	Omega	GTMQSS-062U-6
Pressure sensor	Omega	PX309-500G5V
Relative Humidity Sensor	Omega	HX94AVW
Mass flow meter	McMillan	102 Range 8
Data Acquisition Board	Measurement Computing	PCI-DAS6071
DAQ software	Wincon for MATLAB	Wincon 5.0

Sample cycling results are shown in Figure 3.3 – 3.6.

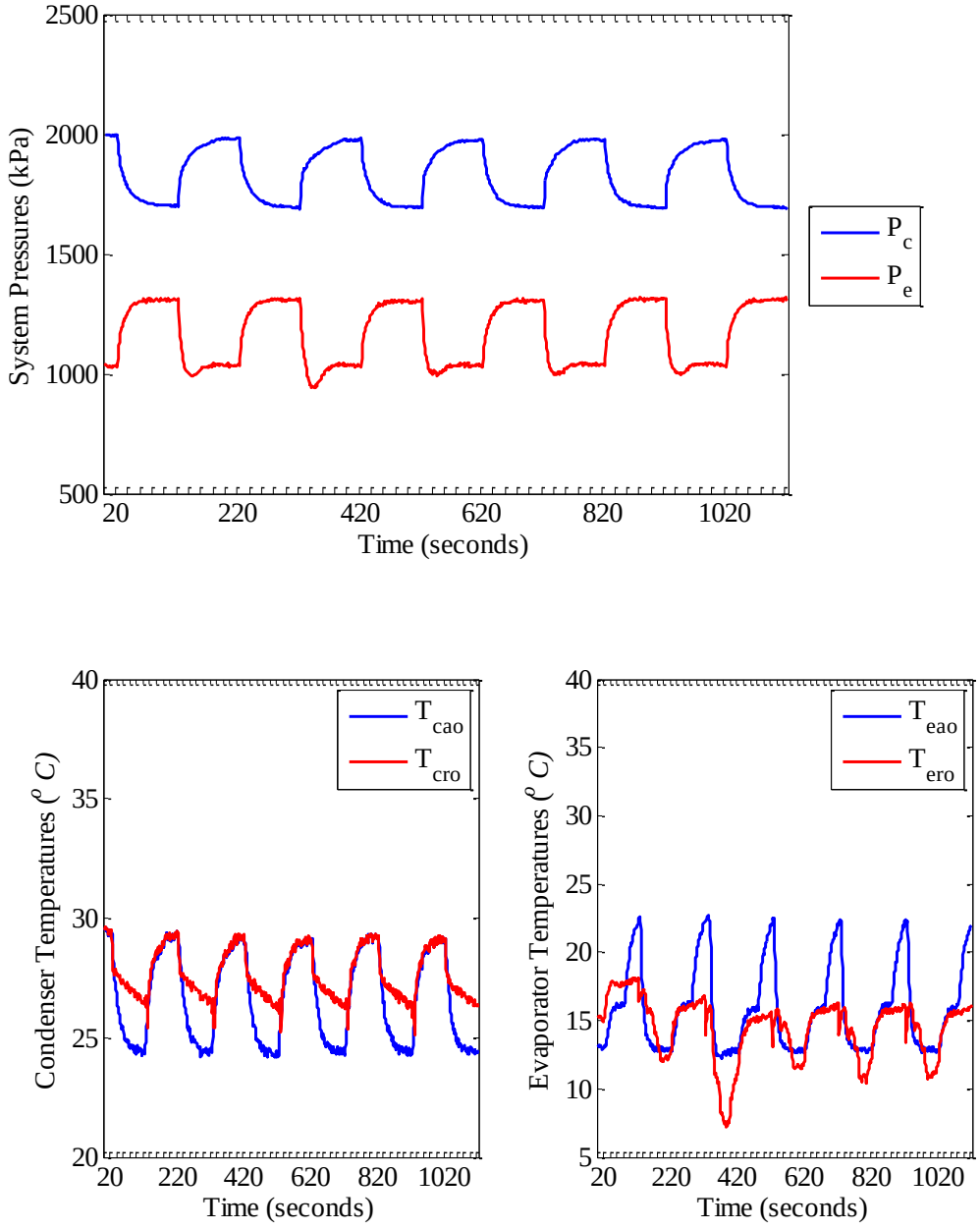

Figure 3.3 System Pressures and Temperatures – Sample Cycling - Experiment

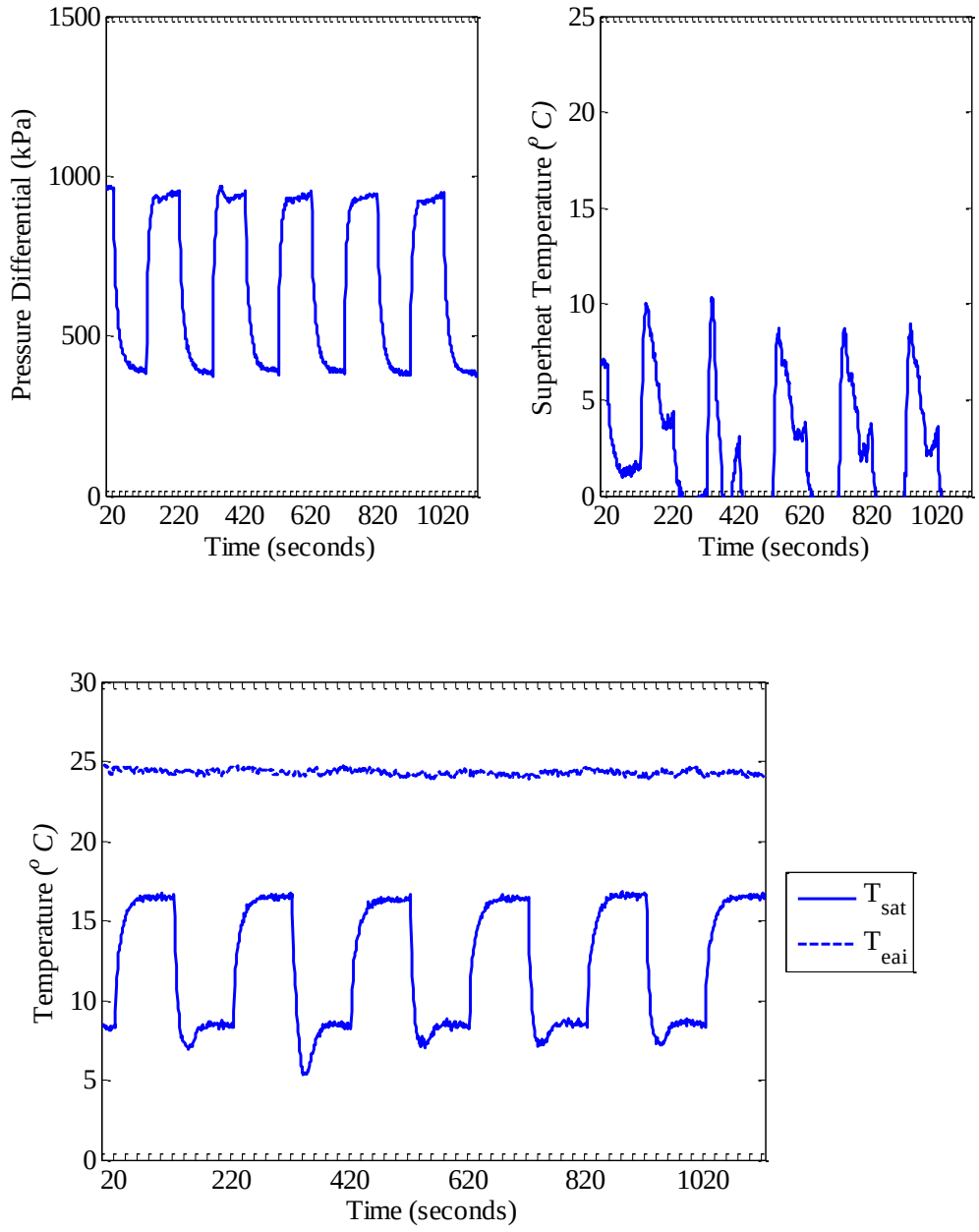

Figure 3.4 Pressure Differential and Superheat – Sample Cycling – Experiment

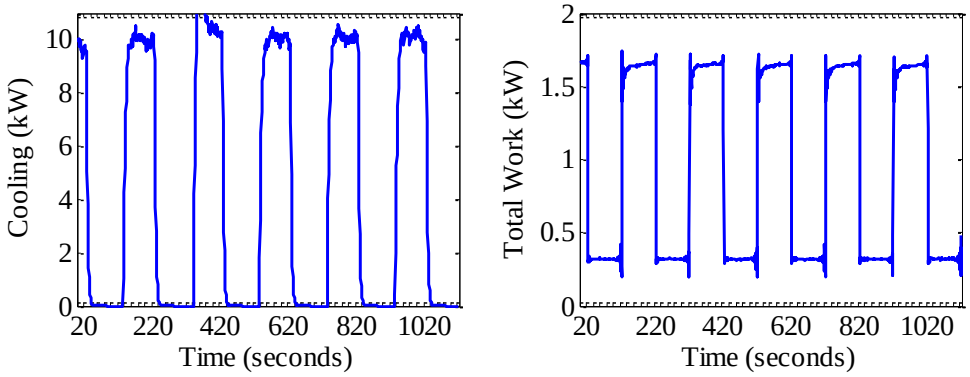

Figure 3.5 Cooling, Work and COP_{Cycle} – Sample Cycling – Experiment

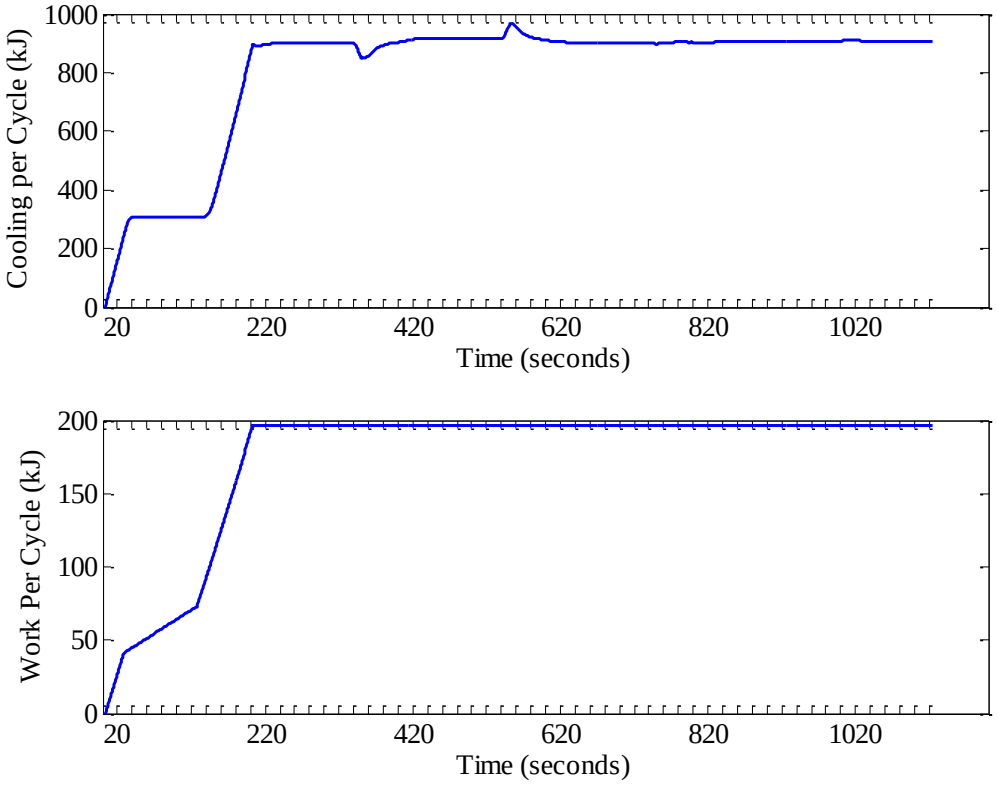

Figure 3.6 Work, Cooling Per Cycle – – Sample Cycling – Experiment

4. OPTIMIZATION ALGORITHM

There are a number of optimization techniques available, based on the type of the problem required to solve and the amount of information needed to solve the problem. This section summarizes the common optimization methods considered for use in this thesis and justifying the specific choice of a minimization algorithm. Much of this section is drawn from [36] which is a popular textbook on optimization methods.

4.1 Classical Optimization Methods

This subsection lists the most popularly applied optimization techniques by classifying them according to the type of optimization problem it solves. The optimization methods thus can be broadly put into two categories:

- Unconstrained optimization
    - Newton's method
    - Simplex search
- Constrained optimization
    - Active-set method
    - Interior point method
    - Sequential quadratic programming

4.1.1 Unconstrained Optimization

These methods are used to solve problems of type specified in equation 4.1. Basically, there are no constraints on the parameter x to minimize the function $f(x)$ except that it lies in the n-dimensional Euclidean space R^n.

$$min_x \quad f(x),$$
$$s.t. \quad x \in R^n \tag{4.1}$$

4.1.1.1 Newton's Method

Newton's Method for minimization is an ideal method to solve minimization problems. Here the first order necessary condition for optimality is that the gradient of the function $f(x)$ be zero as shown in equation 4.2.

$$\nabla f(x) = 0 \tag{4.2}$$

The next set of iterates is given by equation 4.2,

$$x(k+1) = x(k) + p(k) \tag{4.3}$$

Where $p(k)$, the step size is the solution to the Newton' s equations,

$$\left[\nabla^2 f\left(x(k)\right)\right] p(k) = [\nabla f(x(k))] \tag{4.4}$$

The step size is solved for by solving a linear system of equations rather than computing the inverse of a Hessian, $\nabla^2 f\left(x(k)\right)$. Hessian is the matrix of second order derivatives of $f(x)$.

Newton's method is never used in its classical form and is altered in two ways: to improve reliability and to reduce iteration cost. There are three very important aspects to an algorithm that defines its performance namely: derivatives, calculations and storage. Usually the method involves computation of second derivatives, solving of system of

equations and matrix storage. The most popular way to reduce the costs associated to these aspects is to calculate just the first derivative and then approximate the Hessian. There are other methods that strive to avoid solving of equations or even use less storage [36]. However these compromises do have their downsides. They tend to have slower rates of convergence and use cheaper iterations to solve problems.

The **Steepest Descent algorithm** is the simplest Newton-type method. Though of not much practical use, the algorithm is useful for theoretical understanding. The algorithm reduces the costs associated with the Newton's method by employing cheaper iterations i.e., lower costs per iteration. However the disadvantage is that it is very slow.

Next is the **Quasi-Newton method**. Unlike the previous method this is very practical and much preferred. The characteristic of this method is that it approximates the Hessian by a matrix B_k from the information of first derivative itself. Since the storage of the approximate Hessian becomes really costly as the number of parameters increases, the algorithm is mostly used for small scale and medium scale problems. There are a number of formulae used to approximate the Hessian. Following are some of the more popular ones:

- DFP [37]
- BFGS [38, 39]
- Broyden [40]
- Symmetric Rank 1

Techniques that are used to guarantee convergence help control the optimization routine when in the danger of going out of hand. There are two widely used types of these global strategies:

- Line Search Methods
- Trust Region Methods

MATLAB command *fminunc* could be used for unconstrained minimization. The command allows the user to choose from a variety of algorithms.

4.1.1.2 Simplex Search

The Nelder Mead simplex method is a direct search non gradient optimization technique [41]. In the sense, the algorithm is a numerical optimization technique so it does not require the calculation of derivatives. For a problem involving *n* variables, a simplex of *n+1* vertices is constructed and a comparison of the objective function values at the various vertices is performed. The simplex then changes its shape to converge on the minimum local to that region. The method consists of the following steps:

1. **Name** the vertices as

   $$x_1, x_2, x_3, x_4 \dots x_{n+1}$$

   Such that the **order** of the function values at the vertices:

   $$f(x_1) \leq f(x_2) \leq \cdots \leq f(x_{n+1}) \quad 4.5$$

2. **Calculate** the center of gravity x_0 of all points except x_{n+1}.
3. **Reflect:** The reflected point is computed as the following equation shows,

   $$x_r = x_{n+1} + \alpha(x_0 - x_{n+1}) \quad 4.6$$

   If the reflected point is computed such that

$$f(x_1) \leq f(x_r) \leq f(x_n) \quad 4.7$$

then x_{n+1} is replaced by x_r to obtain a new simplex and the iteration is terminated.

4. **Expand:** If the x_r is the best point so far i.e.,

$$f(x_r) < f(x_1) \quad 4.8$$

Then the expanded point x_e is computed as,

$$x_e = x_{n+1} + \gamma(x_0 - x_{n+1}) \quad 4.9$$

If the expanded point is computed such that

$$f(x_e) \leq f(x_r) \quad 4.10$$

then x_{n+1} is replaced by x_e to obtain a new simplex and the iteration is terminated. However if that is not the case generate the new simplex with x_r instead of x_{n+1} and terminate the iteration.

5. **Contract:** This instruction is processed when it is certainly known by the end of previous step that

$$f(x_r) \geq f(x_n) \quad 4.11$$

The contracted point is hence computed as follows,

$$x_c = x_{n+1} + \rho(x_0 - x_{n+1}) \quad 4.12$$

If the contracted point is such that

$$f(x_c) \leq f(x_{n+1}) \quad 4.13$$

Then the new simplex is generated by replacing x_{n+1} with x_c. Otherwise the algorithm goes to the next step.

6. **Shrink:** This step replaces all but the best point i.e., x_1 using the following expression,

$$x_i = x_1 + \sigma(x_i - x_1) \quad for\ all\ i \in \{2,3,\dots,n+1\} \tag{4.14}$$

This effectively shrinks the simplex around the vertex with the lowest function value. The iteration is then terminated.

α, γ, ρ and σ are respectively the reflection, the expansion, the contraction and the shrink coefficient. Standard values are $\alpha = 1$, $\gamma = 2$, $\rho = 1 / 2$ and $\sigma = 1 / 2$.

As already noted the method uses very less information at each stage (no need of first or second order derivative calculations) and no account is kept of past positions. The method works well for unknown and discontinuous surfaces. However there is a certain disadvantage of getting trapped at local minima. This is because the simplex method has no idea about the global surface and keeps adapting to only the surface local to the initial guess value. Also as the solution converges onto a minimum the algorithm becomes really slow as it tries to find a better minimum by wasting more iteration. MATLAB command *fminsearch* could be used for unconstrained minimization using simplex search

4.1.2 Constrained Optimization

These are optimization problems subjected to equality constraints, inequality constraints or both. They could be further classified into methods that deal with linear and non linear problems. The non-linearity could be with respect to the objective

function, the constraints themselves or both. A general mixed problem with linear equality and inequality constraints could be formulated as follows,

$$min_x \quad f(x),$$

$$s.t. \quad Ax \geq b, \qquad Cx = d \tag{4.15}$$

Such problems are difficult to solve because of the huge number of possible infeasible points. However, there are feasible-point methods that allow the algorithm to move from one feasible iterate to another. The advantage of such an approach is that because of assured feasibility one can transform the equality constrained problems into unconstrained minimization problems and then use the techniques described in Subsection 4.1.1 so that solution could be obtained far more easily. Following are some of these methods:

4.1.2.1 Active-Set Method

This method is used to solve a non-linear problem with linear inequality constraints. The basic principle of this method relies on the fact that the active set of constraints at the optimal solution does not necessarily have all the inequality constraints. Thus if this active set of constraints is known a priori, then the rest of the constraints can be relaxed thus solving the problem as an equality constrained problem. Unfortunately in real world problems there is no way of knowing which set of constraints constitute the active set. The active set method iterates what is called a working set of constraints that includes or excludes a constraint to/from the set based on whether the current iteration is near the optimum or not. One of the main responsibilities of the method is the strategy it adopts to change this working set. The other component

of the method is how it chooses the search direction. This is done based on the condition that the direction leads to a feasible descent. For a given feasible initial starting point x let the working set be W, and then the corresponding equality constrained problem is in equation 4.16.

$$\begin{aligned} min_x \quad & f(x), \\ s.t. \quad & \bar{A}x = \bar{b} \end{aligned} \tag{4.16}$$

where $\bar{A}$ is the coefficient matrix of the constraints and $\bar{b}$ its corresponding right hand side vector. A search direction p is chosen such that equation 4.17 is satisfied.

$$\bar{A}p = 0 \tag{4.17}$$

4.1.2.2 Interior Point Method

Interior Point method is another really popular feasible point method. Here the feasibility of the solution to all the iterations is maintained by constructing a barrier around the feasible region. This is achieved by transforming the objective function by including a barrier/penalty term. Thus when the algorithm is operating in the vicinity of the boundary of the feasible region the penalty term penalizes the function by assuming an infinite value. This drives the algorithm to operate in the interior of the feasible region.

Also called penalty methods because of the use of penalty terms, they aim to use unconstrained minimization techniques to solve non-linear problems with non-linear constraints as in equation 4.18.

$$min_x \quad f(x),$$

$$s.t. \quad b(x) \geq 0, \qquad c(x) = 0 \tag{4.18}$$

As noted before, the objective function $f(x)$ is transformed by including a penalty term that increases for any constraint violation. A general expression to describe the transformed objective function $T(x)$ is in equation 4.19.

$$\min T(x) = f(x) + r_k P(x). \tag{4.19}$$

Here $P(x)$ is the penalty function that keeps the iteration results feasible and r_k is a scalar value that acts like a tuning parameter which determines how much the function should be penalized. $P(x)$ could assume any generally used barrier functions such as the inverse function or the barrier function [42].

4.1.2.3 Sequential Quadratic Programming

As the name suggests, the method solves a quadratic problem at each iteration k [43]. Consider the problem in the equation 4.18 only with the equality constraints. The Lagrangian for this problem could be formulated as in equation 4.20,

$$l(x, \lambda) = f(x) - \lambda^T b(x). \tag{4.20}$$

The Lagrangian is a technique used in constrained optimization problems wherein the solution is a stationary point of the Lagrangian [36]. Thus the first order optimality condition is

$$\nabla l(x^*, \lambda^*) = 0. \tag{4.21}$$

If k is the current iteration then for the pair $\big(x(k), \lambda(k)\big)$, Newton's method defines

$$\big(x(k+1), \lambda(k+1)\big) = \big(x(k), \lambda(k)\big) + (p(k), w(k)) \tag{4.22}$$

where the step $\big(p(k), w(k)\big)$ is defined by the linear system

$$\begin{bmatrix} \nabla^2 l(x(k),\lambda(k)) & -\nabla g(x(k)) \\ -\nabla g(x(k))^T & 0 \end{bmatrix} \begin{bmatrix} p(k) \\ w(k) \end{bmatrix} = - \begin{bmatrix} \nabla l(x(k),\lambda(k)) \\ -g(x(k) \end{bmatrix}. \quad 4.23$$

From this system the quadratic program is obtained in equation 4.24 by making the assumption that the pair $(x(k),\lambda(k))$ is close to the optimum value.

$$\min \ \frac{1}{2} p \,.\, \nabla^2 l(x(k),\lambda(k)) p + \nabla l(x(k),\lambda(k)) + l(x(k),\lambda(k))$$
$$s.t \ \ \nabla g(x(k))^T p + g(x(k)) = 0 \quad 4.24$$

This is a convex program with a unique $(p(k), w(k))$. This is determined by the optimality conditions as described in equation 4.25.

$$\nabla^2 l(x(k),\lambda(k)) p + \nabla l(x(k),\lambda(k)) - \nabla g(x(k)) w = 0$$
$$\nabla g(x(k))^T p + g(x(k)) = 0 \quad 4.25$$

Sequential quadratic programming converges locally so, the technique could be adopted with a globalization strategy such as line search or trust region as noted in Subsection 4.1.1.1. Based on such a strategy there are a number of different SQP algorithms. In order to prevent the method from going out of the feasible region a barrier function could be included as mentioned in Subsection 4.1.2.2.

4.2 Choice of Algorithm

The optimization algorithm was picked based on three important factors. First of all, methods that required the objective function be put in a specific form for it to solve, were all eliminated. Finding an analytical expression for the objective function $f(x)$ explicitly in terms of the input x was nearly impossible. Methods like quadratic programming which require formulating problem matrices for describing the objective

function explicitly as a function of input x were thus out of the race. An extension of this logic would be to eliminate all the methods that require the user to supply the gradient and/or the hessian information. No analytical expression for the objective function meant, there was no way to derive expressions for the gradient and/or the hessian. Thus it was evident that a numerical, non-gradient optimization technique was needed.

Secondly, because there were no constraints on the problem except for the bounds on the parameters, it was decided that the optimization routine would be tested with both the unconstrained minimization methods. These methods were implemented using the MATLAB commands *fminunc* and *fminsearch* respectively. The *fminsearch* simplex search showed better descent per iteration compared to the *fminunc* algorithms. Thus the convergence rate for the simplex search was also marginally better compared to the other unconstrained minimization algorithms. One downside to using MATLAB's simplex search was that the optimization parameters' bound could not be specified in the problem. This was dealt with by manually penalizing the objective function near the boundary regions. Steep barriers were constructed near the vicinity of the boundary such that optimization parameters would not go out of bounds.

Finally, since the surface of the objective function was largely unknown, the simplex search promised better robustness with respect to the search ability. In the unfortunate circumstance that the algorithm was trapped in a local minima, an early termination of the routine was done and a new starting point was initialized.

5. SIMULATION

In this section the simulation approach for optimizing the expansion valve and the evaporator fan cycles and the associated results are discussed in detail. The first subsection will deal with the cost function that was used for the optimization. A cyclic efficiency quantity called $ICOP_{Cycle}$ is defined for this purpose. In the next subsection, the parameterization of the expansion valve and the evaporator fan profiles are discussed. A generalized S-curve model is described to parameterize the actuator profiles. This is followed by the presentation of the trends in objective function with respect to the expansion valve and evaporator fan profile parameters. This would later serve as a reference to justify the solution provided by the optimization algorithm. The simulations also help in choosing the parameters and their starting guesses to be used in the final optimization problem. Refrigeration migration is identified as a cause for decrease in system efficiency whereas a fan delay strategy at shutdown causes an increase in system's cyclic efficiency. The last subsection deals with the optimization results. These results are compared with practical control scheme strategies to see how they perform in practice. Superheat control is identified as a key issue that influences a system's cyclic efficiency.

5.1 Objective Function

A dynamic simulation model implemented using the model library developed by Rasmussen [30] and Gupta [31] was used. The model incorporates the FCV techniques discussed earlier.

The Coefficient of Performance (COP) is the measure of energy efficiency of an air conditioning system and is calculated as follows,

$$\mathrm{COP} = \frac{\mathrm{Q_{TOTAL}}}{\mathrm{W_{TOTAL}}} \tag{5.1}$$

Where Q_{TOTAL} is the total cooling performed and W_{TOTAL} is the required work input to perform the cooling during a cycle. The work input is comprised of both the fan and the compressor work. The units for both cooling and work are in kilowatts (kW). Cooling calculations are done on the air side since the experimental refrigerant mass flow meter is not accurate under low flow condition, which is mostly the case during valve shutoff. Since most of the optimization routines in MATLAB are designed to solve minimization problems, an inverse COP was considered instead of COP. Also, what is of interest in this thesis is the energy efficiency over the entire cycle and not the instantaneous efficiency at discrete points of time throughout the duration of the cycle. So the cost function that was used for optimization is the cycle inverse COP. The expression to calculate the cycle inverse COP is as follows,

$$ICOP_{Cycle} = \frac{\int_{\mathrm{T}}^{\mathrm{T}+\mathrm{T_{Cycle}}} \mathrm{W} - \int_{0}^{\mathrm{T}} \mathrm{W}}{\int_{\mathrm{T}}^{\mathrm{T}+\mathrm{T_{Cycle}}} \mathrm{Q} - \int_{0}^{\mathrm{T}} \mathrm{Q}}\, dt \tag{5.2}$$

where T is the ending time of the previous cycle as well as the starting time of the current cycle and T_{Cycle} is the cycle period. Based on equation 5.2 as the objective function, the optimal expansion valve and evaporator fan cycling was found.

5.2 Parameterization

The goal of the optimization routine was to find an optimal expansion valve and evaporator fan profile given a cycle of the compressor. The simplest solution was to make the optimization algorithm search for the valve position/evaporator fan speed at each discrete time instant of the cycle that would result in an overall energy optimum for the cycle. However, this brute force optimization would result in a problem that involves n- parameters, where n is the number of samples required to draw the expansion valve and the evaporator fan profiles. This was a nearly impossible task computationally speaking, since the time that any optimization algorithm would take to converge on a solution might stretch to a number of days. Thus, in order to make the problem manageable, the valve position/evaporator fan speed profiles were parameterized using an S-curve model. The model Y (t) was defined by the following equation,

$$Y(t) = A + \frac{K - A}{(1 + Qe^{-B(t-M)})^{1/v}} \tag{5.3}$$

where A is the lower asymptote, K is the upper asymptote, B is the growth rate and M is the time of maximum growth. The values Q and v are governed by the initial condition of the curve; hence they were kept constant throughout the simulations. In case of the parameter K, the value was chosen such that it was equal to the operating condition in which the air conditioning model needed to run during its steady state ON condition. In

case of the valve opening K was mainly decided by the amount of superheat that was desired when the system is ON and in case of the fan speed it was governed by the energy balance of the system. Since there were two transients: startup and shutdown, two S-curves were employed so that the individual slope (e.g. $B_{Shutdown}$ and $B_{Startup}$) and time (e.g. $M_{Shutdown}$ and $M_{Startup}$) could be varied independently. A two level curve like the S-curve was justified for the optimal shape because it was expected that the expansion valve would be closed and the evaporator fan would be switched off at some point during the off cycle. The effects of varying the S-curve parameters are presented in the Figure 5.1. As can be seen, the parameter B determines the slope of the transient for the input profiles. The parameter M decides the delay/lead operation of the input actuators. Finally the parameter A equals the state of the input during the OFF cycle.

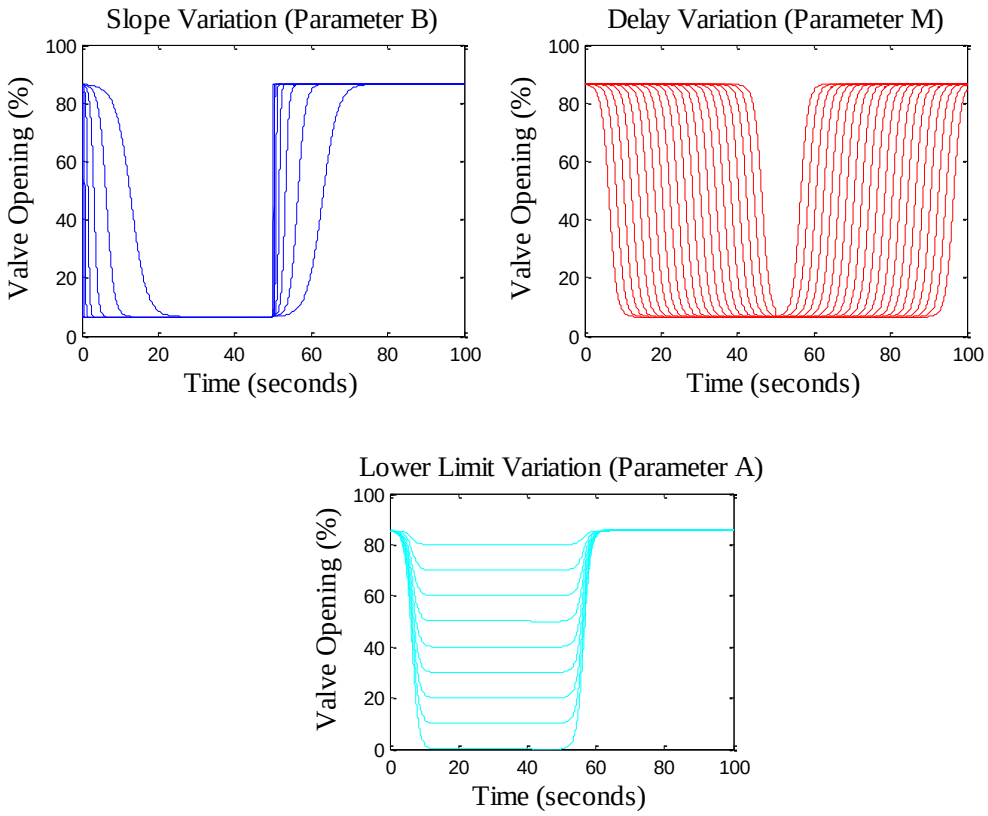

Figure 5.1 S-curve Variations with Parameters

5.3 COP_{Cycle} Trends

In this subsection a series of simulation tests is presented that would showcase the effect of the various S-curve parameters on the $ICOP_{Cycle}$. These simulations were conducted separately for the expansion valve and the evaporator fan so that individual responses of $ICOP_{Cycle}$ to the different S-curve parameters could be established. The simulations were run for two different cycle lengths to see the effect cycle length has on $ICOP_{Cycle}$. In order to visualize the efficiency changes better, normalized COP_{Cycle}

was used as in equation for plotting the trends. Thus it is evident that for the benchmark cycle normalized COP_{Cycle} is 1.

$$Normalized\ \ COP_{Cycle} = \frac{{}^{1}/_{ICOP_{Cycle}}}{COP_{Benchmark\ Cycle}} \tag{5.4}$$

5.3.1 Short Cycle

Simulation results obtained for a short cycle length of 200 seconds are presented here. This was to understand how normalized COP_{Cycle} varies with respect to the S-curve parameters during rapid cycling times. Under such circumstances, the pressures and temperatures will not go to equilibrium during the off cycle. Thus, what trend normalized COP_{Cycle} followed with various S-curve parameters investigated.

5.3.1.1 Gross Trends

To prove that the normalized COP_{Cycle} changes are significant enough to merit a further detailed investigation, a quick comparison of some possible cycling schemes was done. Figure 5.2 shows the gross trends for the various cycling schemes. With the benchmark for comparison at 1 the other cycling schemes are presented. Benchmark cycling is defined as the scheme where the expansion valve and the evaporator fan cycle simultaneously with the compressor. The 'All on' condition is where neither the valve nor the fan cycles. Both are always on at their steady state ON condition while the compressor is the only cycling component. 'Valve Cycle Fan on' is the condition where the valve cycles in sync with the compressor and the fan is on throughout the duration of the cycle. 'Fan Cycle Valve on' is the opposite condition where the evaporator fan cycles in sync with the compressor and the valve is at its steady state ON condition

always. ‘Part Valve Cycle Fan Cycle’ is when the valve stays at its ON condition for 20s AFTER compressor shutdown before going to its OFF position. The fan however cycles simultaneously with the compressor. ‘Part Fan Cycle Valve Cycle’ is when the evaporator fan stays at its ON condition for 20s AFTER compressor shutdown before going to its OFF position and the valve cycles synchronous with the compressor. In this thesis, whenever the valve or the fan stays on or off for extended amount of time compared to the compressor cycle, it is referred to as part cycling. These are tabulated in Table 5.1.

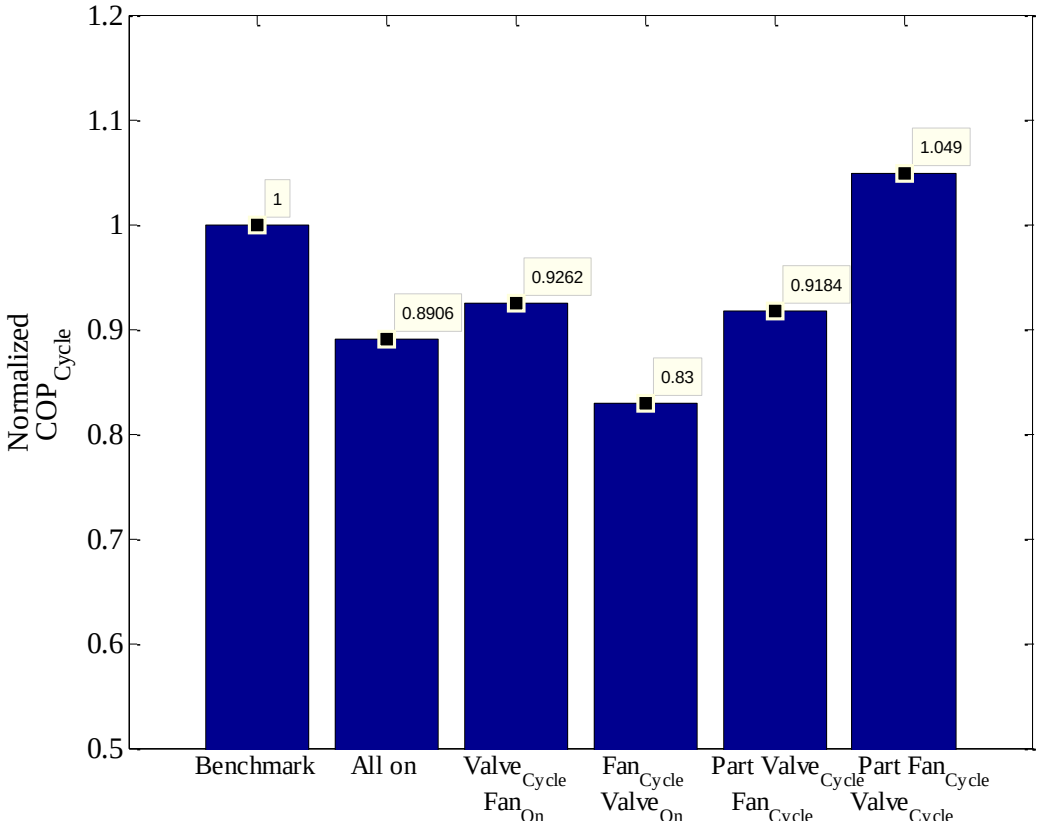

Figure 5.2 COP_{Cycle} Gross Trends of Various Cycling Schemes – Short Cycle

Table 5.1 Gross Trends Cycling Schemes

CYCLING SCHEME	EXPANSION VALVE		EVAPORATOR FAN	
	OFF CYCLE	ON CYCLE	OFF CYCLE	ON CYCLE
Benchmark	OFF	ON	OFF	ON
All on	ON	ON	ON	ON
Valve Cycle Fan On	OFF	ON	ON	ON
Fan Cycle Valve On	ON	ON	OFF	ON
Part Valve Cycle Fan Cycle	ON for first 20 seconds then OFF	ON	OFF	ON
Part Fan Cycle Valve Cycle	OFF	ON	ON for first 20 seconds then OFF	ON

From Figure 5.2 it was evident that 'All on' and 'Fan Cycle Valve On' conditions were having the worst performance. In order to explain the physical reason of why this happens the following figures are presented.

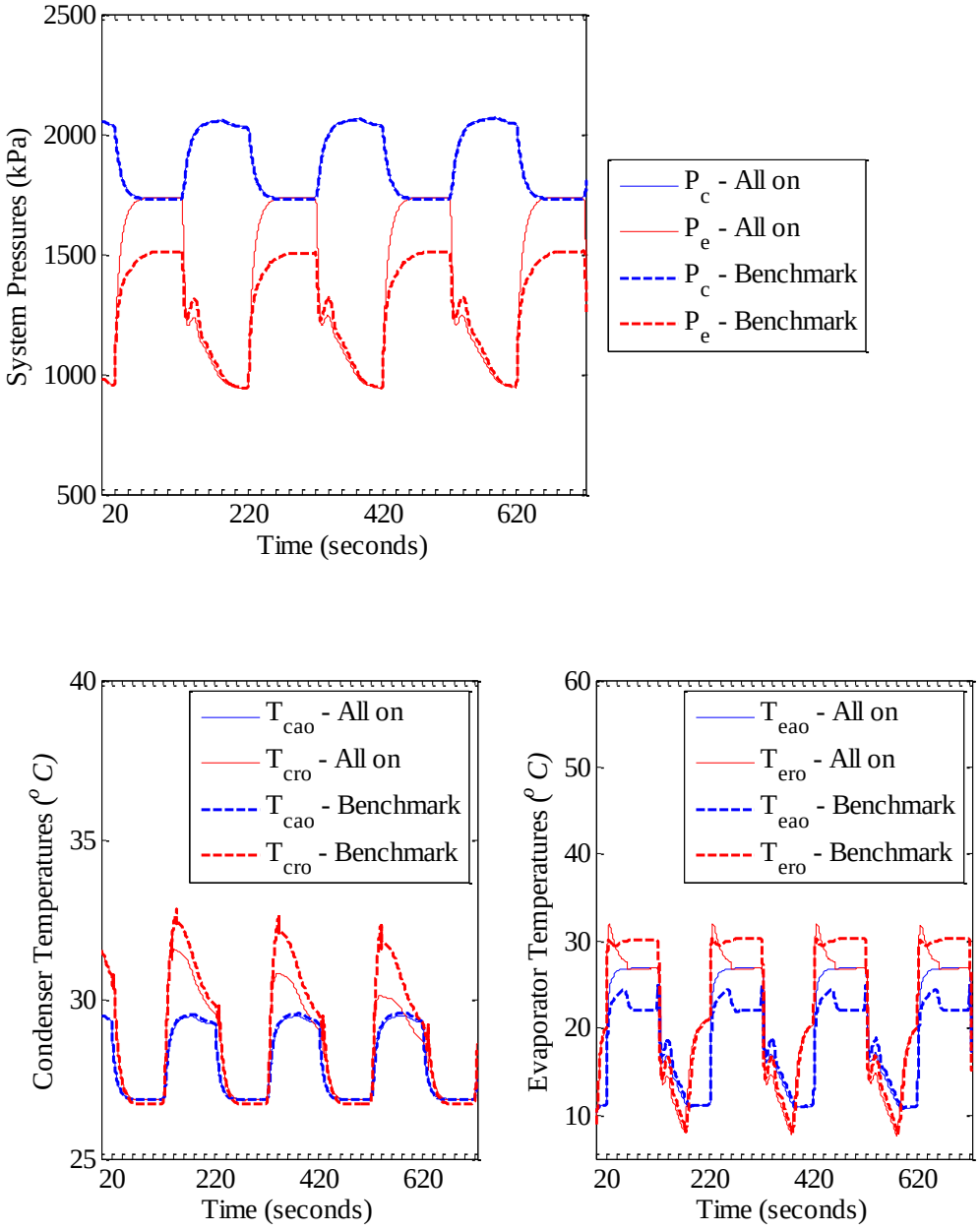

Figure 5.3 System Pressures and Temperatures – All On Vs Benchmark – Short Cycle

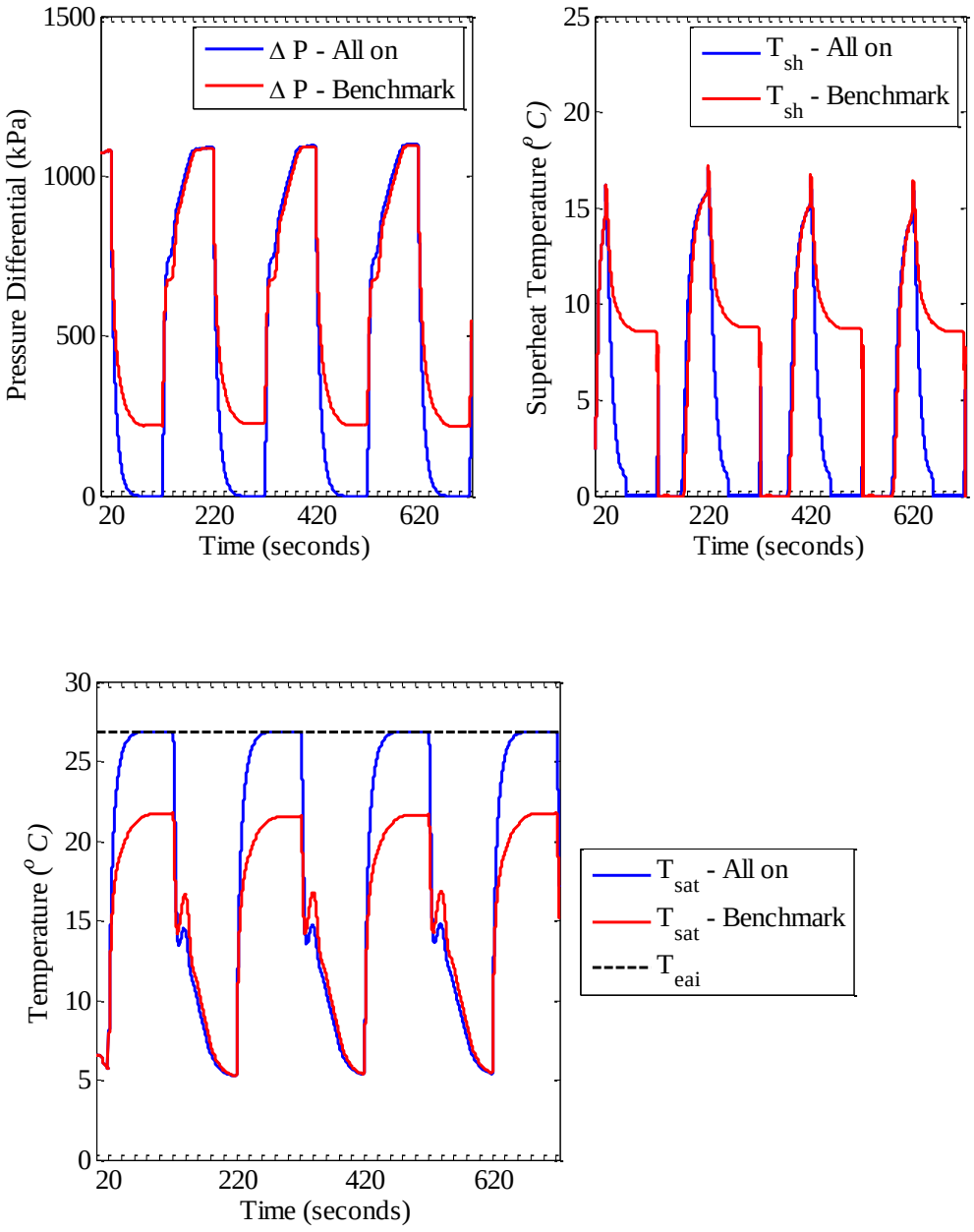

Figure 5.4 Pressure Differential and Superheat – All On Vs Benchmark – Short Cycle

Figure 5.3 shows the variation in the pressures and temperatures between the benchmark and the all on condition. The striking change between the two is the pressure

curve. In the all on condition since the valve is on during the on cycle, the pressures equalized whereas in the benchmark the valve is closed so the pressures do not equalize. Since the refrigerant flow to the evaporator is effectively cut off in the benchmark condition, the refrigerant is completely vaporized and superheated. The effect of valve cycling on superheat is evident from Figure 5.4.

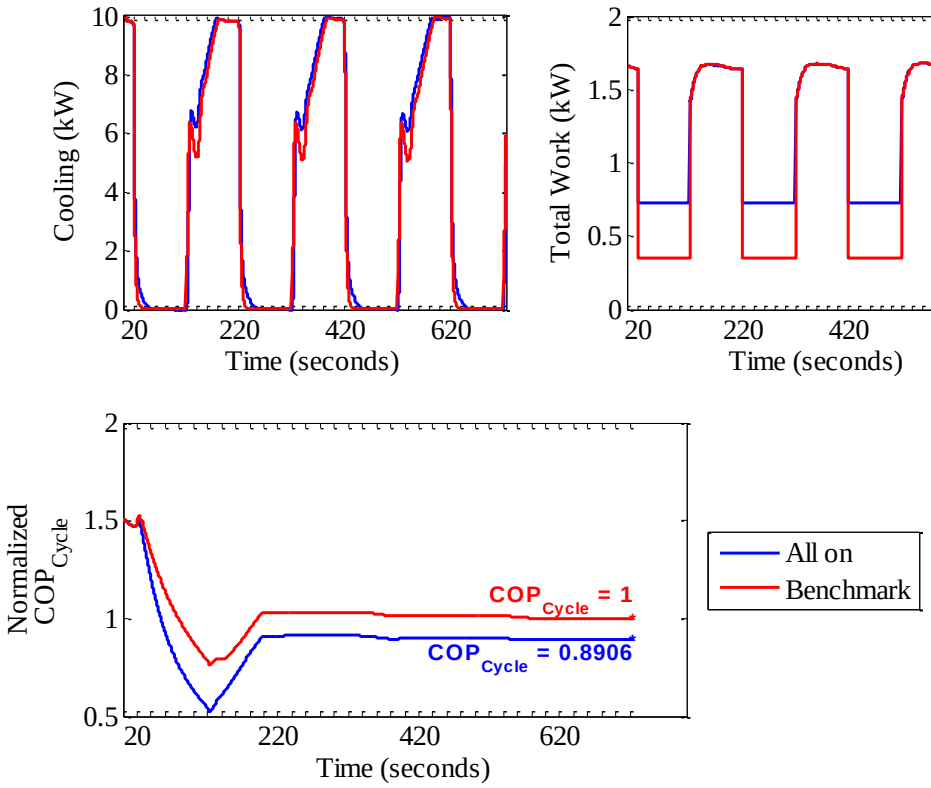

Figure 5.5 Cooling, Work and COP_{Cycle} – All On Vs Benchmark – Short Cycle

Here the superheat temperature for the all on condition drops almost as soon as the compressor is OFF however the benchmark condition holds superheat for a longer time.

The valve cycling also plays an important role in maintaining a good pressure differential across the off cycle. This influences the startup efficiency as it avoids refrigerant migration.

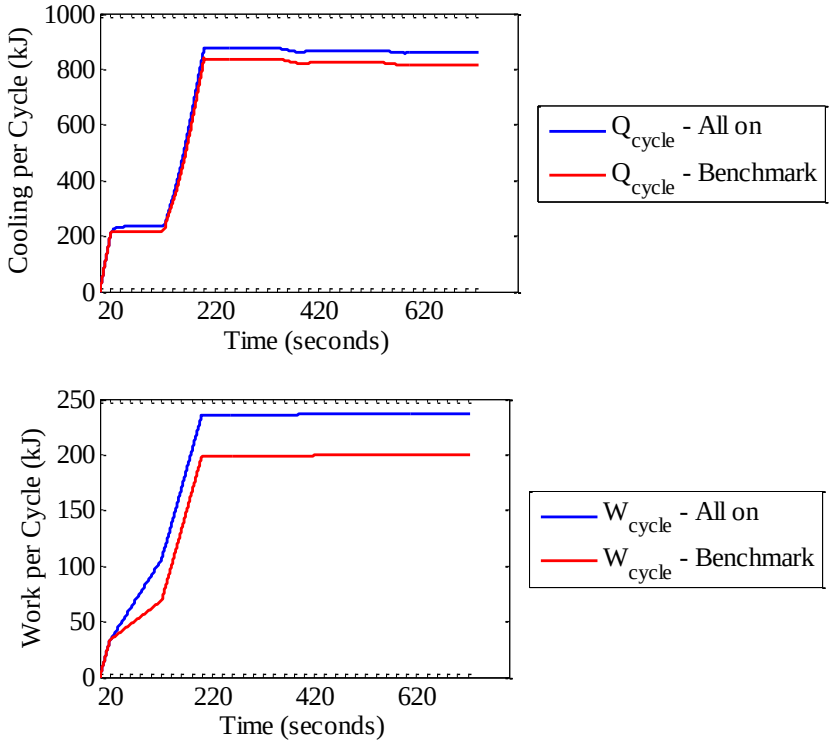

Figure 5.6 Work, Cooling Per Cycle – All On Vs Benchmark – Short Cycle

The instantaneous cooling and work for the two conditions are as shown in Figure 5.5. As expected the COP_{Cycle} for the all on condition is much less when compared to the benchmark condition which can be attributed to the evaporator fan power during the OFF cycle. Switching on the fan during the OFF cycle did result in a trickle of cooling but, most of the time during the OFF cycle the evaporator fan was ON

doing nothing. So the trade off of the small amount of the cooling obtained to the work during off cycle did not work in favor of the cyclic efficiency. This is observed in Figure 5.6 which shows the cooling and work per cycle.

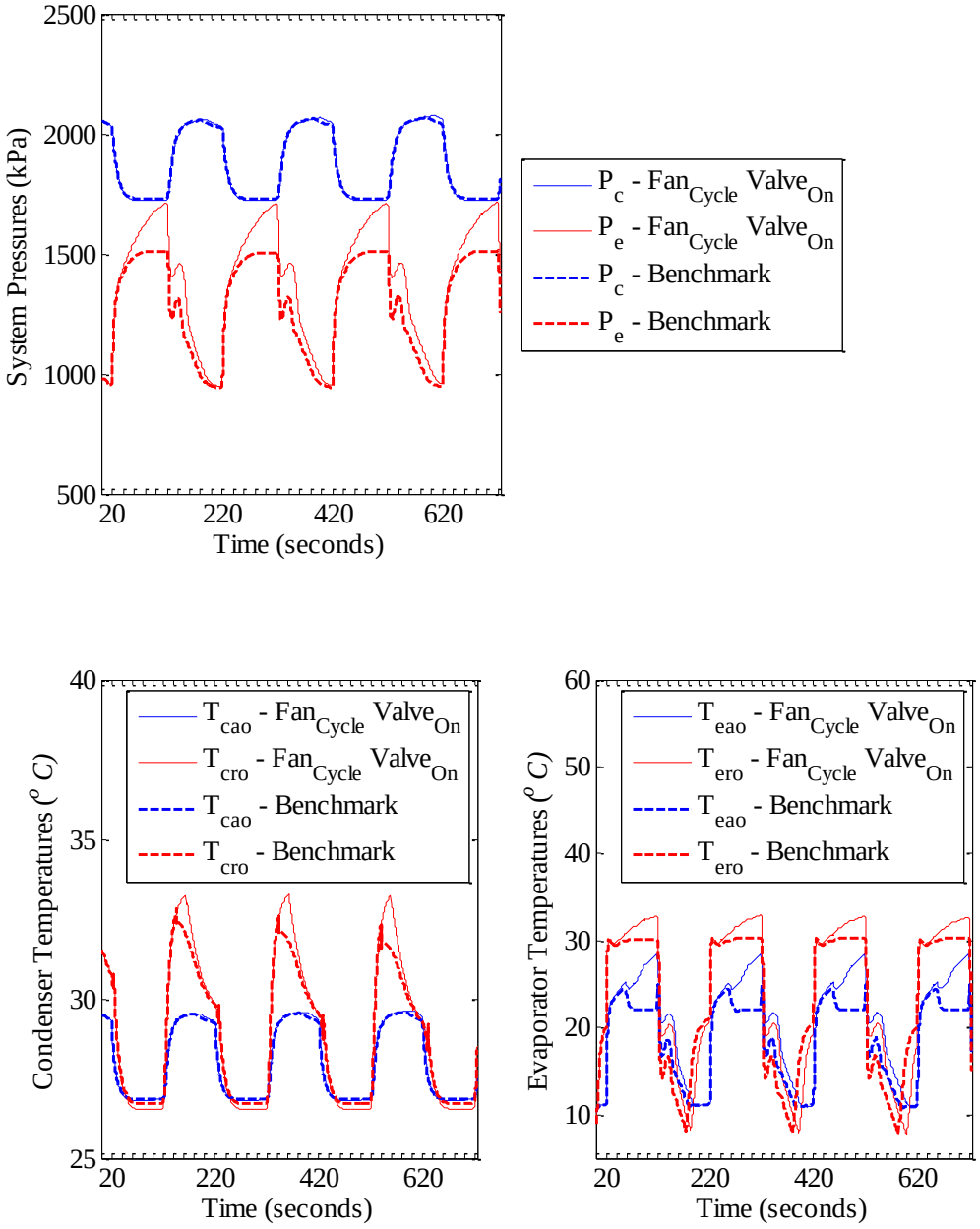

Figure 5.7 System Pressures and Temperatures – Fan Cycle Valve On Vs Benchmark – Short Cycle

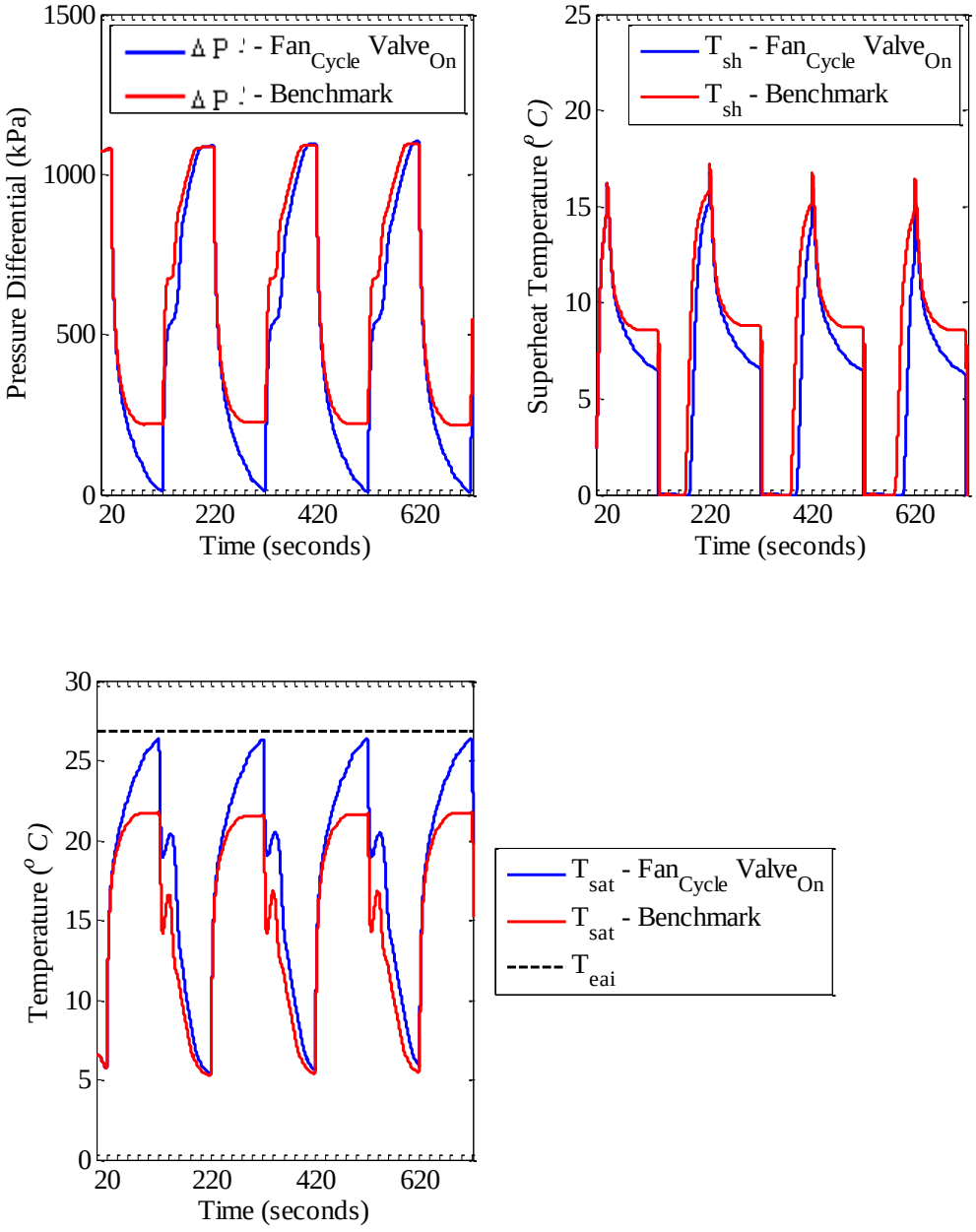

Figure 5.8 Pressure Differential and Superheat – Fan Cycle Valve On Vs Benchmark – Short Cycle

The next condition to be compared with benchmark is the 'Fan Cycle Valve On' condition. Figure 5.3 showed that this condition had the worst efficiency. Following is a discussion that analyzes the case. Figure 5.7 shows the variation in the pressures and temperatures between the benchmark and the 'Fan Cycle Valve On' condition. Similar to the all on condition since the valve is on during the on cycle of 'Fan Cycle Valve On', the pressures equalized whereas in the benchmark the valve is closed so the pressures do not equalize. Here also the superheat temperature drops similar to the all on condition almost as soon as the compressor is OFF as shown in Figure 5.8. The instantaneous cooling and work for the two conditions are as shown in Figure 5.9.

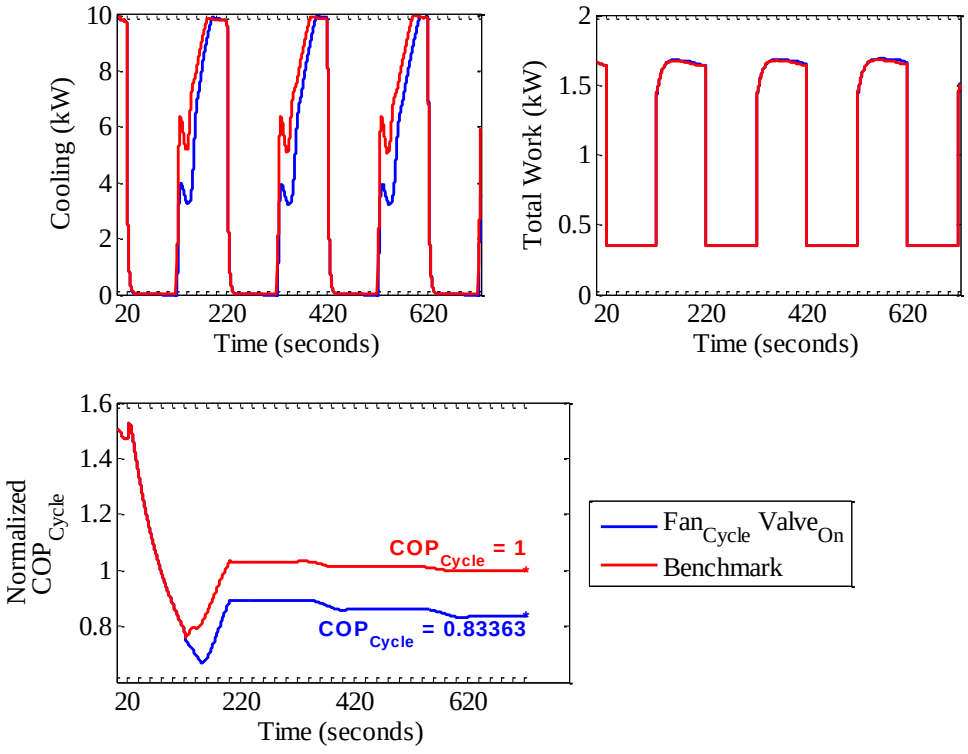

Figure 5.9 Cooling, Work and COP_{Cycle} – Fan Cycle Valve On Vs Benchmark – Short Cycle

Since the fan is OFF at the instant of startup and the pressures are already equalized, the 'Fan Cycle Valve On' condition takes some time to build up to the full cooling capacity. The problem of refrigerant redistribution during startup is showcased here. The fact that the valve did not shut off the flow to the evaporator meant that the compressor had to do more work during startup to pump the entire refrigerant from the evaporator through the condenser.

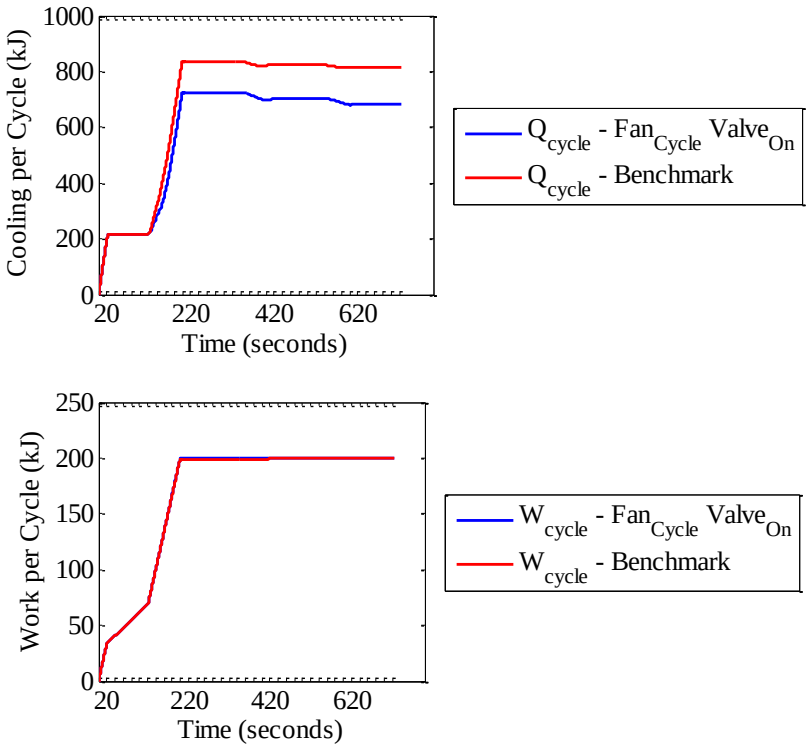

Figure 5.10 Work, Cooling Per Cycle – Fan Cycle Valve On Vs Benchmark – Short Cycle

Since the power consuming components namely the compressor and the evaporator fan are cycled likewise in both the benchmark and the 'Fan Cycle Valve On'

condition, the work per cycle is the same for both the conditions as shown in Figure 5.10. Ultimately since the 'Fan Cycle Valve On' condition gives less cooling per cycle, it is the least efficient. The next case to analyze is the 'Valve Cycle Fan On' condition.

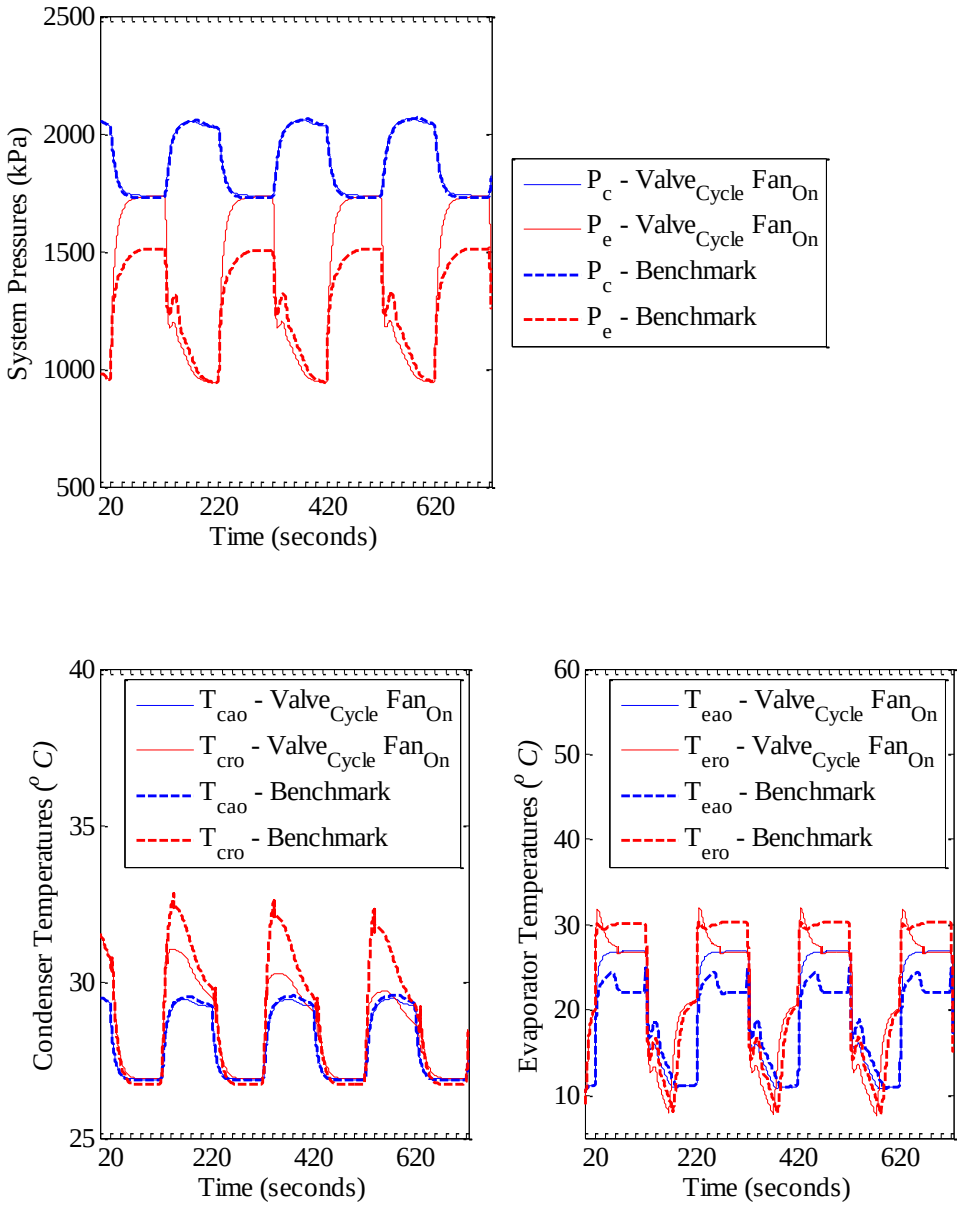

Figure 5.11 System Pressures and Temperatures – Valve Cycle Fan On Vs Benchmark – Short Cycle

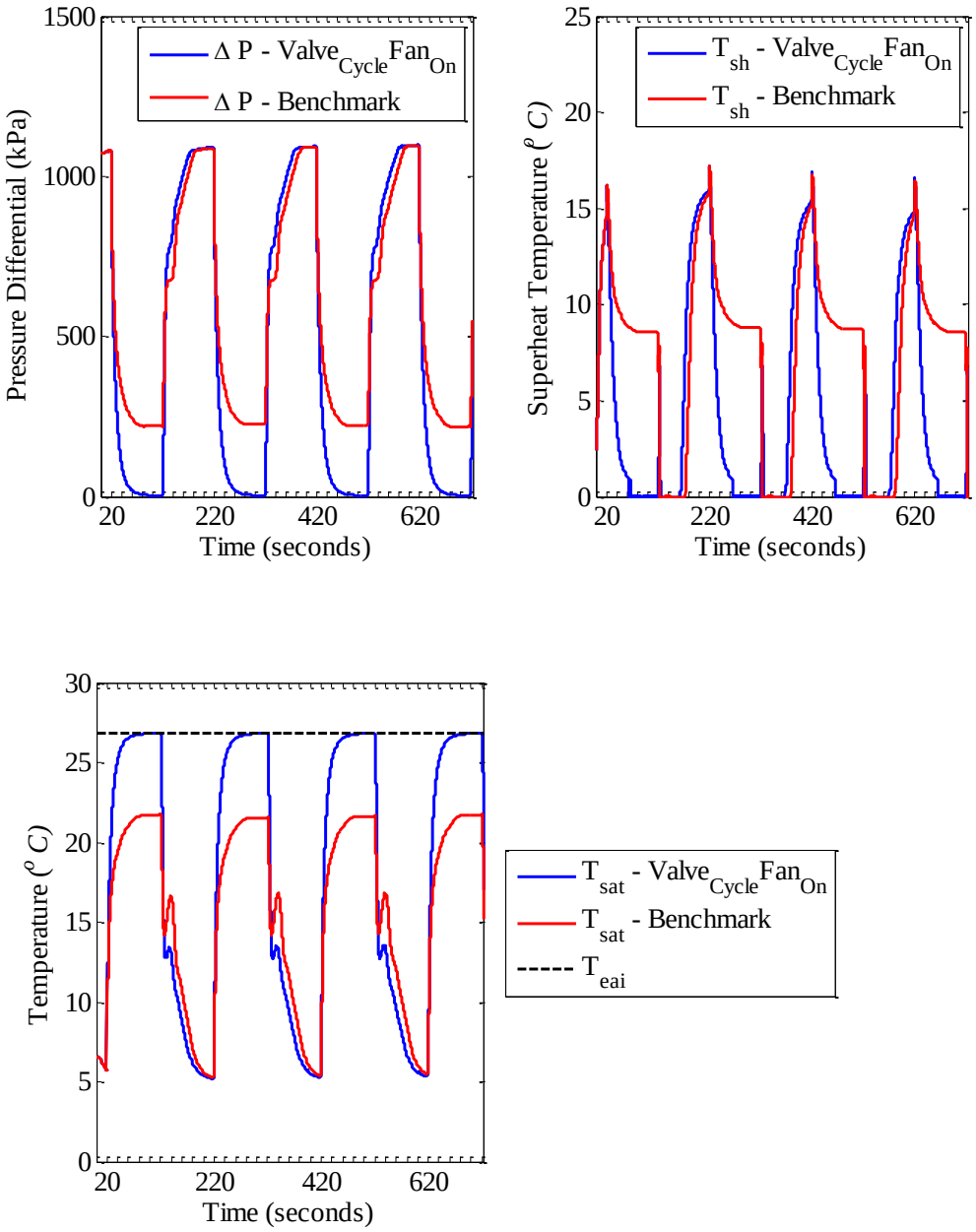

Figure 5.12 Pressure Differential and Superheat – Valve Cycle Fan On Vs Benchmark – Short Cycle

Figure 5.11 shows the pressures and temperatures of the two conditions namely: benchmark and 'Valve Cycle Fan On'. The first noticeable fact is that despite valve

cycling the pressures have equalized. This is because since the fan is still on, the heat transfer is faster in this condition when compared to benchmark during the off cycle. This can be seen from the superheat temperatures for the two conditions as shown in Figure 5.12. For the 'Valve Cycle Fan On' condition superheat is lost much faster once the compressor is shutdown. Unlike the 'Fan Cycle Valve On' condition the pressure builds up faster during startup facilitating full capacity cooling faster as shown in Figure 5.13. Thus there is a net increase in the amount of cooling per cycle. This is because since the valve shuts off at compressor shutdown, it traps some refrigerant in the condenser thus not having to pump entire refrigerant at startup (redistribution).

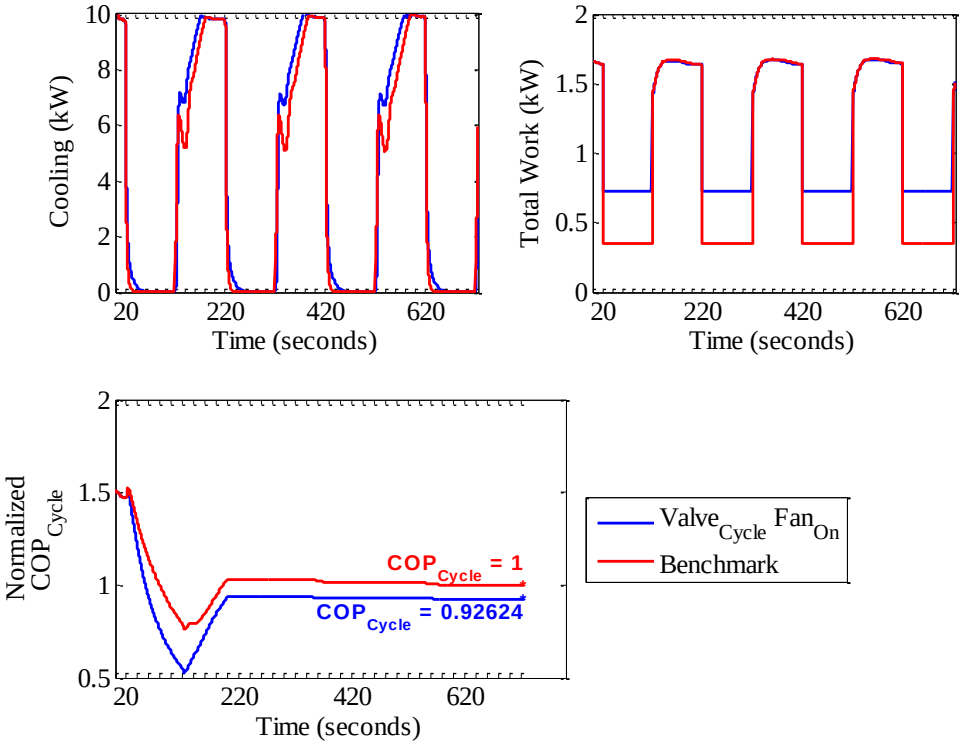

Figure 5.13 Cooling, Work and COP_{Cycle} – Valve Cycle Fan On Vs Benchmark – Short Cycle

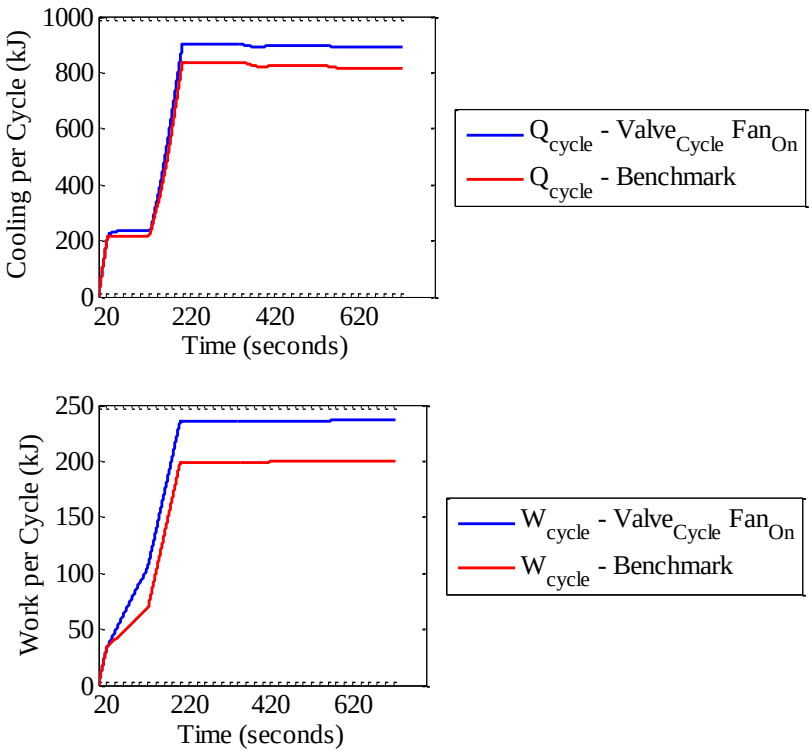

Figure 5.14 Work, Cooling Per Cycle – Valve Cycle Fan On Vs Benchmark – Short Cycle

The relative inefficiency of the 'Valve Cycle Fan On' scheme compared to the benchmark can be attributed to the evaporator fan being on throughout the duration of the cycle. Thus it consumes some power even when not providing any cooling in the off cycle thus having higher work per cycle as shown in Figure 5.14. The 'Valve Cycle Fan On' condition gives better cooling both during startup and shutdown. The startup cooling behavior is because of the prevention of refrigerant migration during shutdown and the shutdown cooling behavior is just because the fan is on during the OFF cycle to extract some potential cooling before the refrigerant reaches saturated conditions. 'Valve Part Cycle' is the next condition that is compared with the benchmark. This condition differs

from the benchmark in the aspect that the valve remains on for a part time (20 seconds) after shutdown.

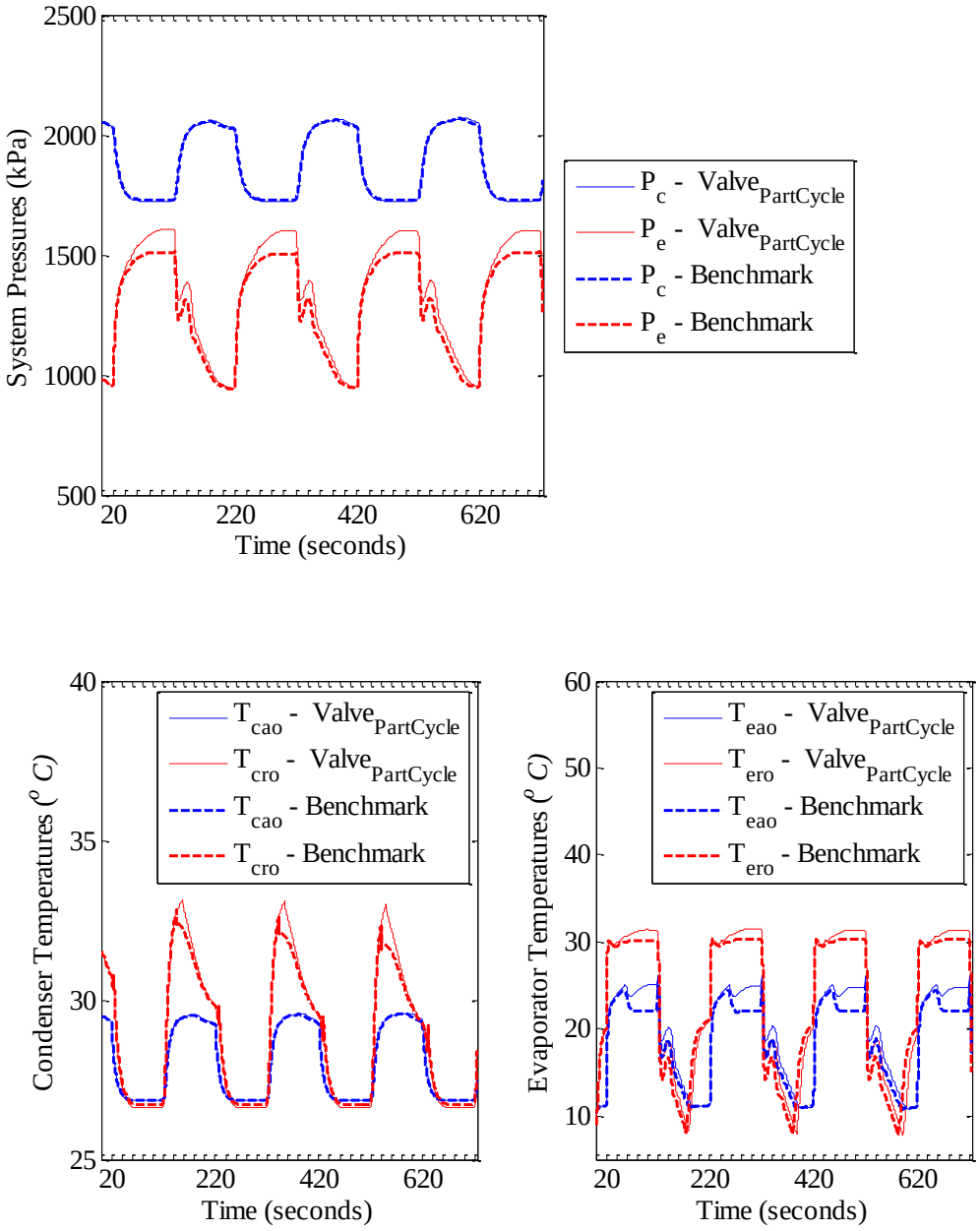

Figure 5.15 System Pressures and Temperatures – Valve Part Cycle Vs Benchmark – Short Cycle

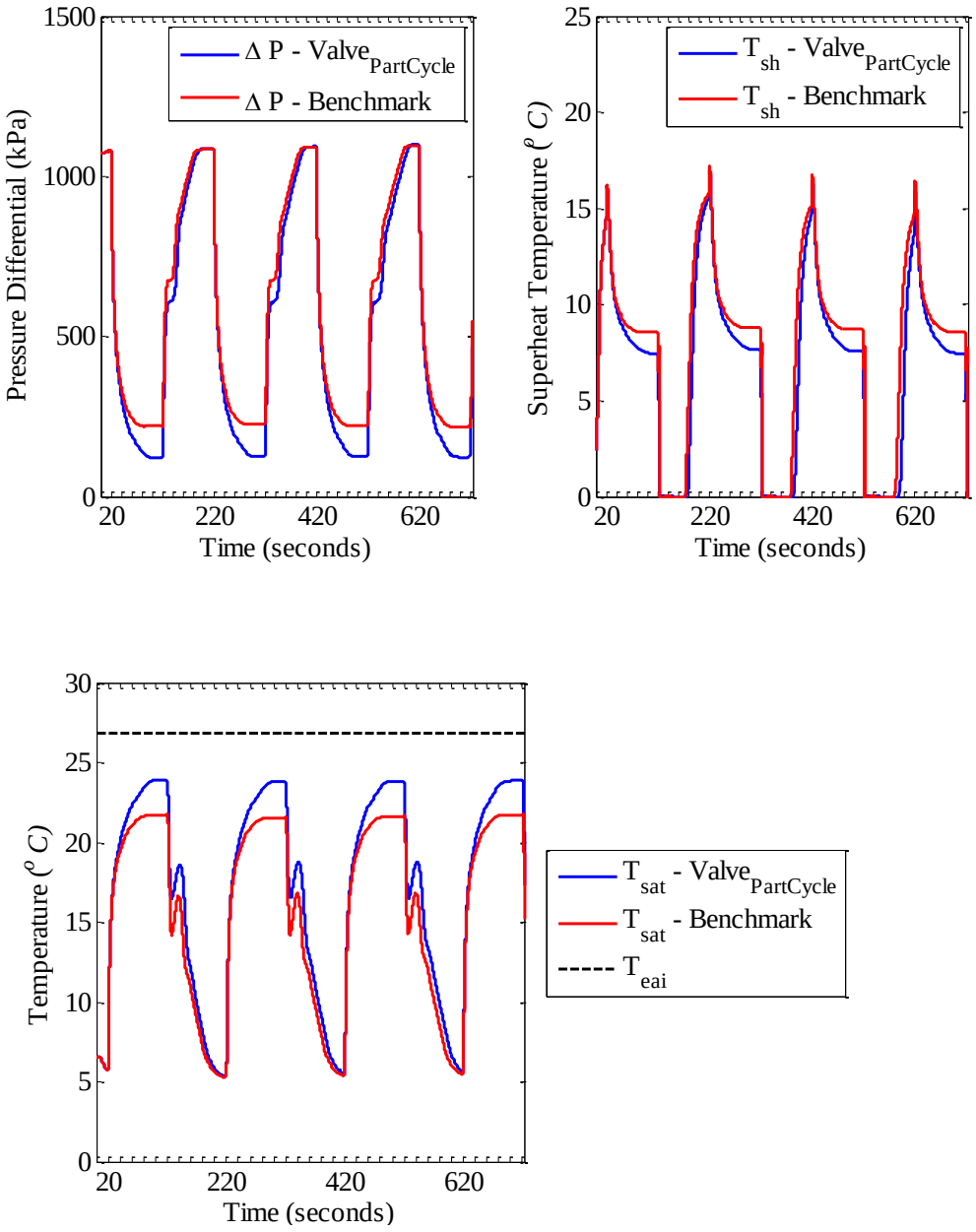

Figure 5.16 Pressure Differential and Superheat – Valve Part Cycle Vs Benchmark – Short Cycle

Figure 5.15 shows that the system pressures and temperatures for the benchmark and 'Valve Part Cycle' differ during off cycle. Because the valve is open for 20s after shutdown in 'Valve Part Cycle', the evaporator pressure has more time to move towards the saturated pressure at the ambient temperature. However the valve is closed after 20s so the evaporator pressure settles at a higher pressure than benchmark during off cycle. Also evaporator is now holding more refrigerant than in benchmark cycle which means during startup it will take relatively more time for the compressor to build up the pressure difference as shown in Figure 5.16 in the pressure differential and hence the full cooling capacity as shown in Figure 5.17. Figure 5.17 also shows the normalized COP_{Cycle}.

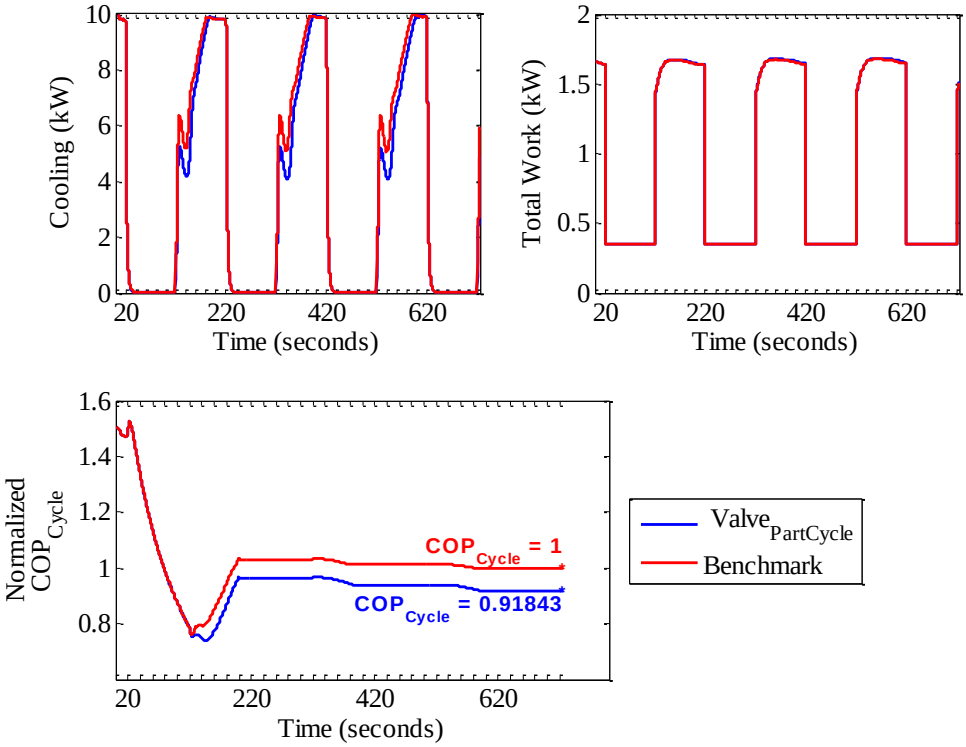

Figure 5.17 Cooling, Work and COP_{Cycle} – Valve Part Cycle Vs Benchmark – Short Cycle

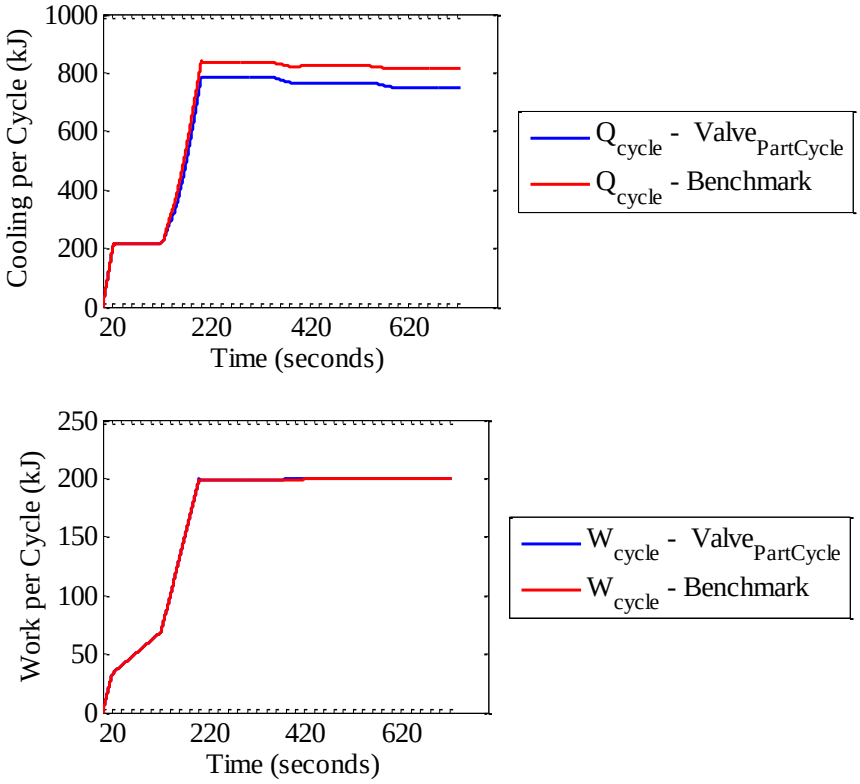

Figure 5.18 Work, Cooling Per Cycle – Valve Part Cycle Vs Benchmark – Short Cycle

There is no extra cooling obtained at shutdown since the fan is shutoff during shutdown along with the compressor. Since the power consuming components namely the compressor and the evaporator fan are cycled likewise in both the benchmark and the 'Valve Part Cycle' condition, the work per cycle is the same for both the conditions as shown in Figure 5.18. Ultimately since the 'Valve Part Cycle' condition gives less cooling per cycle, it is less efficient. The final comparison is 'Fan Part Cycle' with benchmark. In 'Fan Part Cycle' the evaporator fan stays on for 20 seconds more after

shutdown and then switches off while the expansion valve cycles along with the compressor.

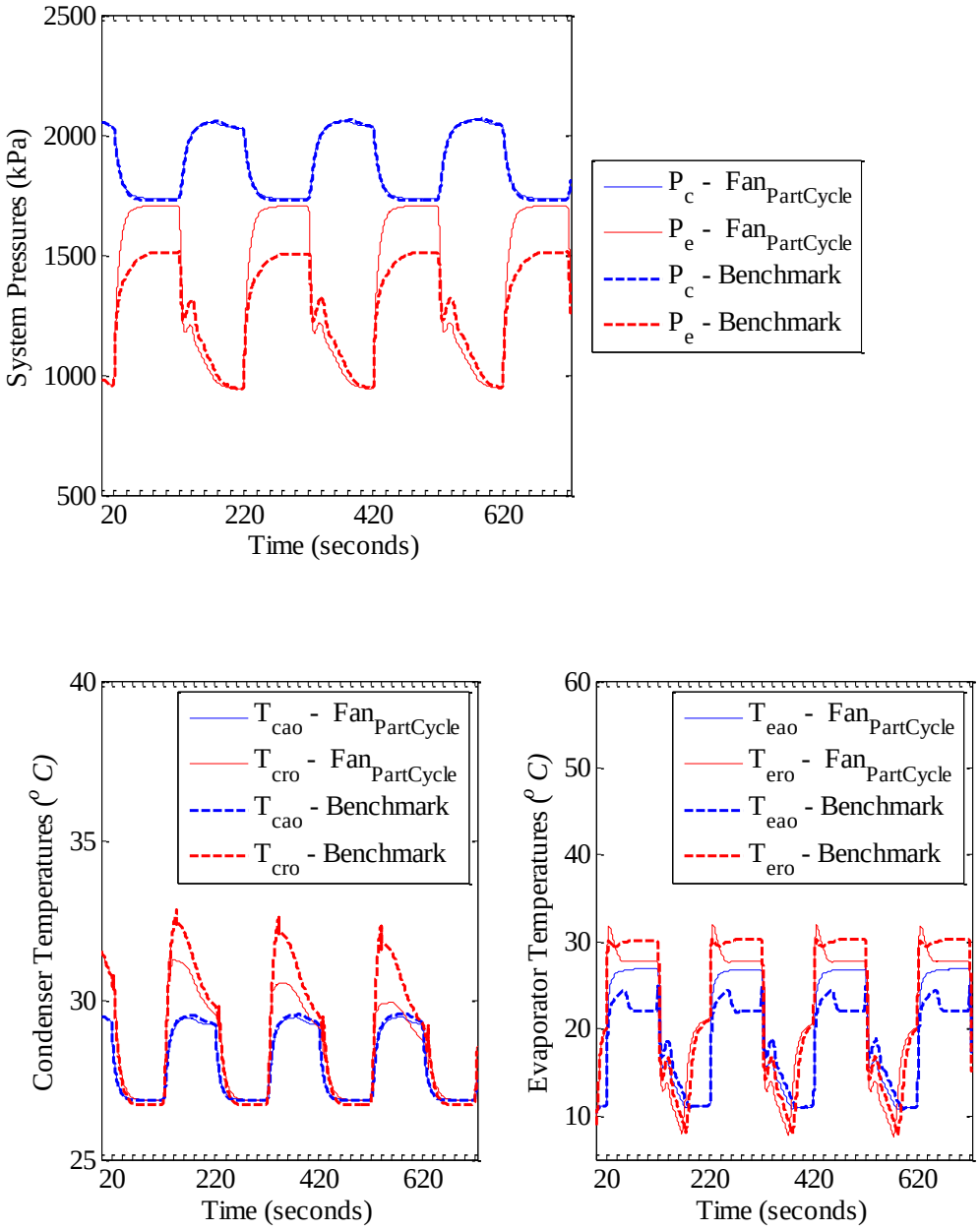

Figure 5.19 System Pressures and Temperatures – Fan Part Cycle Vs Benchmark – Short Cycle

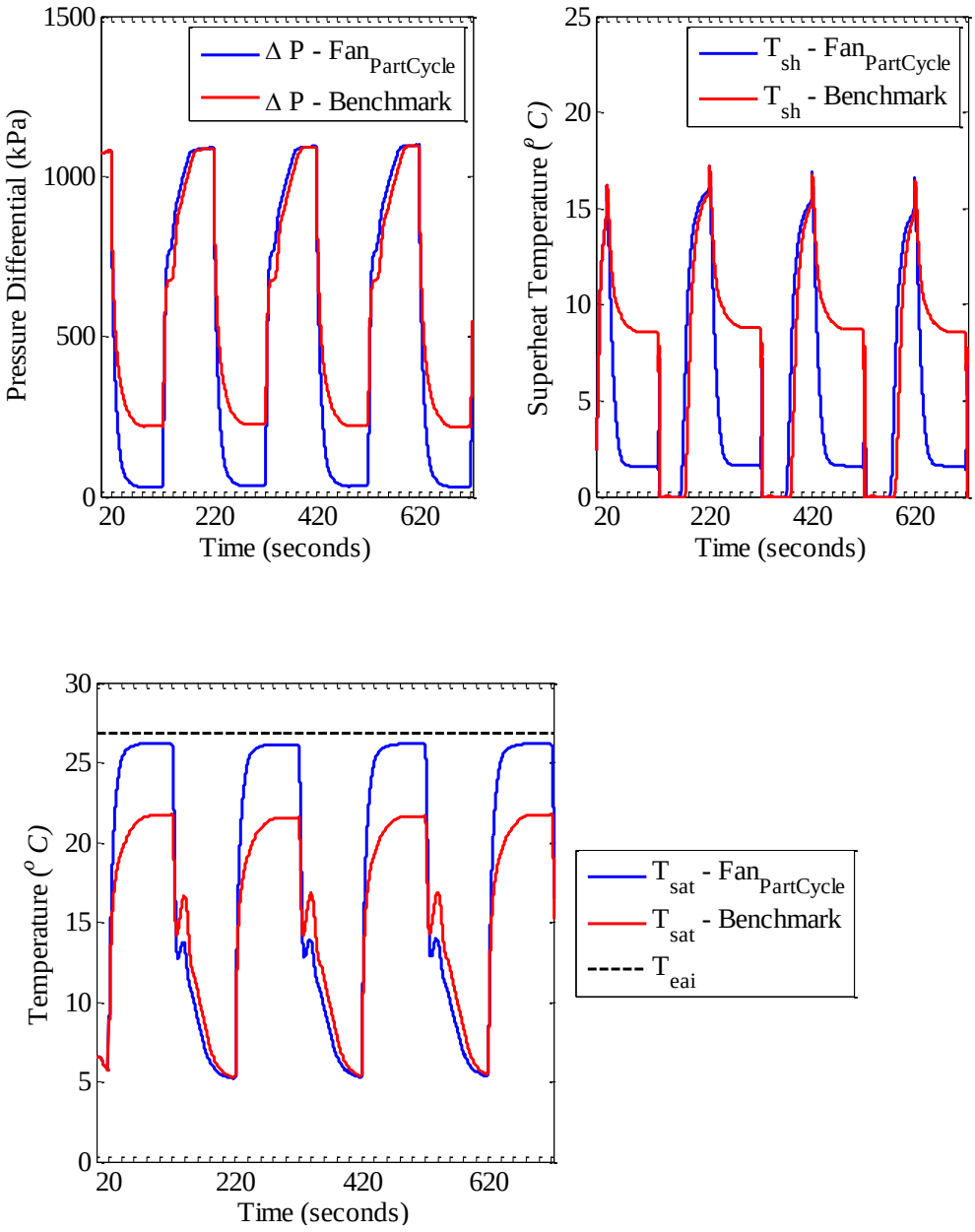

Figure 5.20 Pressure Differential and Superheat – Fan Part Cycle Vs Benchmark – Short Cycle

In 'Fan Part Cycle' condition the pressures almost equalize as shown in Figure 5.19. This is because of the faster heat transfer during shutdown since the fan is on for

20 seconds after shutdown. This is also evident with the way superheat drops at shutdown for 'Fan Part Cycle' as shown in Figure 5.20. This extended heat transfer does extract some potential cooling off the refrigerant during shutdown when compared to benchmark. Since the valve is also cycling refrigeration migration to evaporator is avoided thus pressure build up during startup is faster. This also facilitates more cooling during startup as shown in Figure 5.21. Figure 5.21 also shows the instantaneous power consumed from which the fan staying on for 20 seconds after shutdown can be inferred.

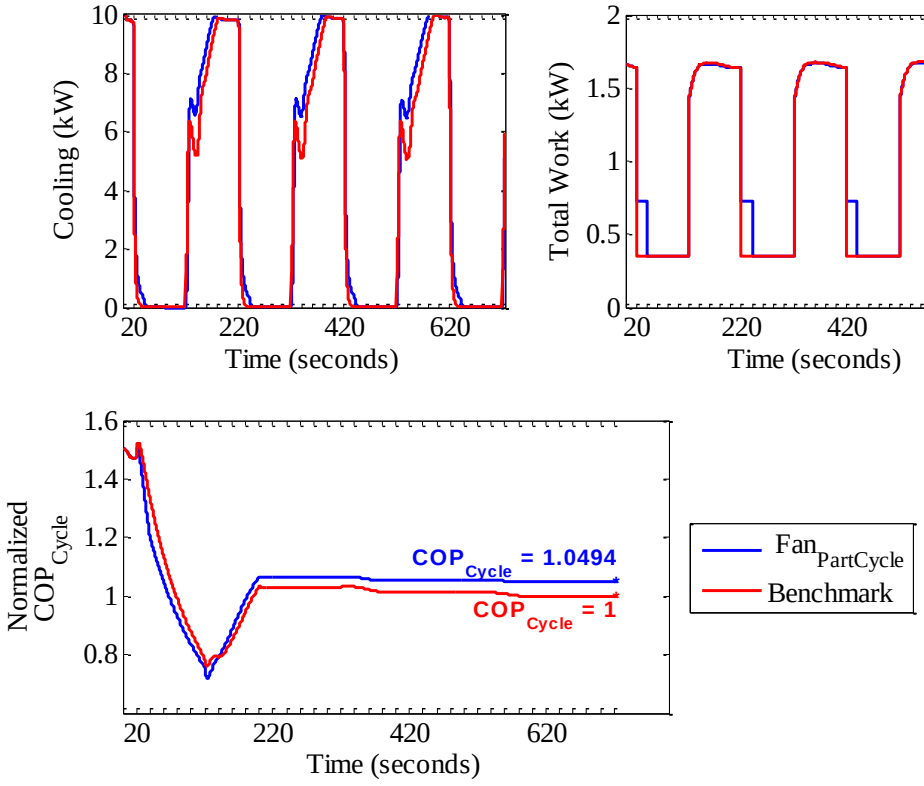

Figure 5.21 Cooling, Work and COP_{Cycle} – Fan Part Cycle Vs Benchmark – Short Cycle

Figure 5.21 also shows that there is an increase in cyclic efficiency of the system under 'Fan Part Cycle' condition. This is because as Figure 5.22 shows, the net increase in cooling obtained per cycle is more than enough to trade off the increased power consumption caused by the fan being on for 20 seconds after shutdown.

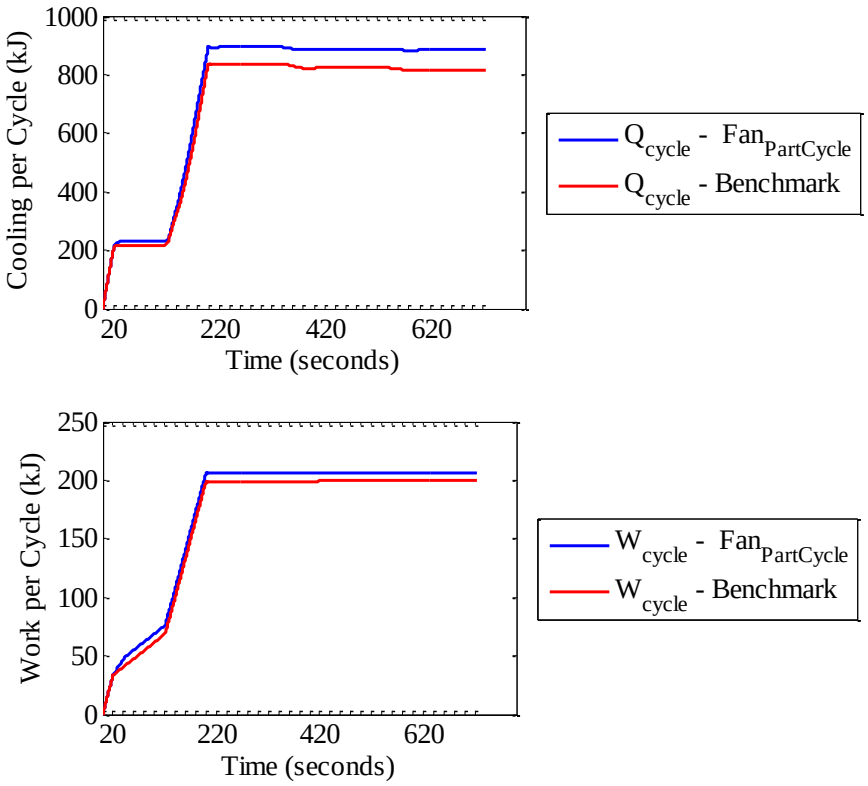

Figure 5.22 Work, Cooling Per Cycle – Fan Part Cycle Vs Benchmark – Short Cycle

Overall, the various cycling schemes show the important dynamics that affects the cyclic efficiency of the system. There is still a need to investigate the expansion valve and the evaporator fan cycling S-curve parameters individually.

5.3.1.2 Expansion Valve

The expansion valve was first considered as the cycling component, while the evaporator fan was assumed to be running for the entire length of the cycle.

The values of the S-curve parameters used for this simulation are specified in Table 5.2. Higher values of slope correspond to steeper transients in the S-curve. Negative time values mean a lead operation (act before the compressor) whereas positive value means a delayed operation (act after the compressor).

Table 5.2 Simulation S-curve Parameters Range for Detailed Trends

Shutdown Slope	**Startup Slope**	**Shutdown Time (in seconds)**	**Startup Time (in seconds)**
0.5 to 32	0.5 to 32	-20 to 20	-20 to 20

The detailed trend analysis was one dimensional in the sense, when one parameter was varied according to the range in Table 5.2, the other parameters were held constant at their benchmark values. Figure 5.23 present the results of the detailed trend analysis for the individual S-curve parameters for the expansion valve profile.

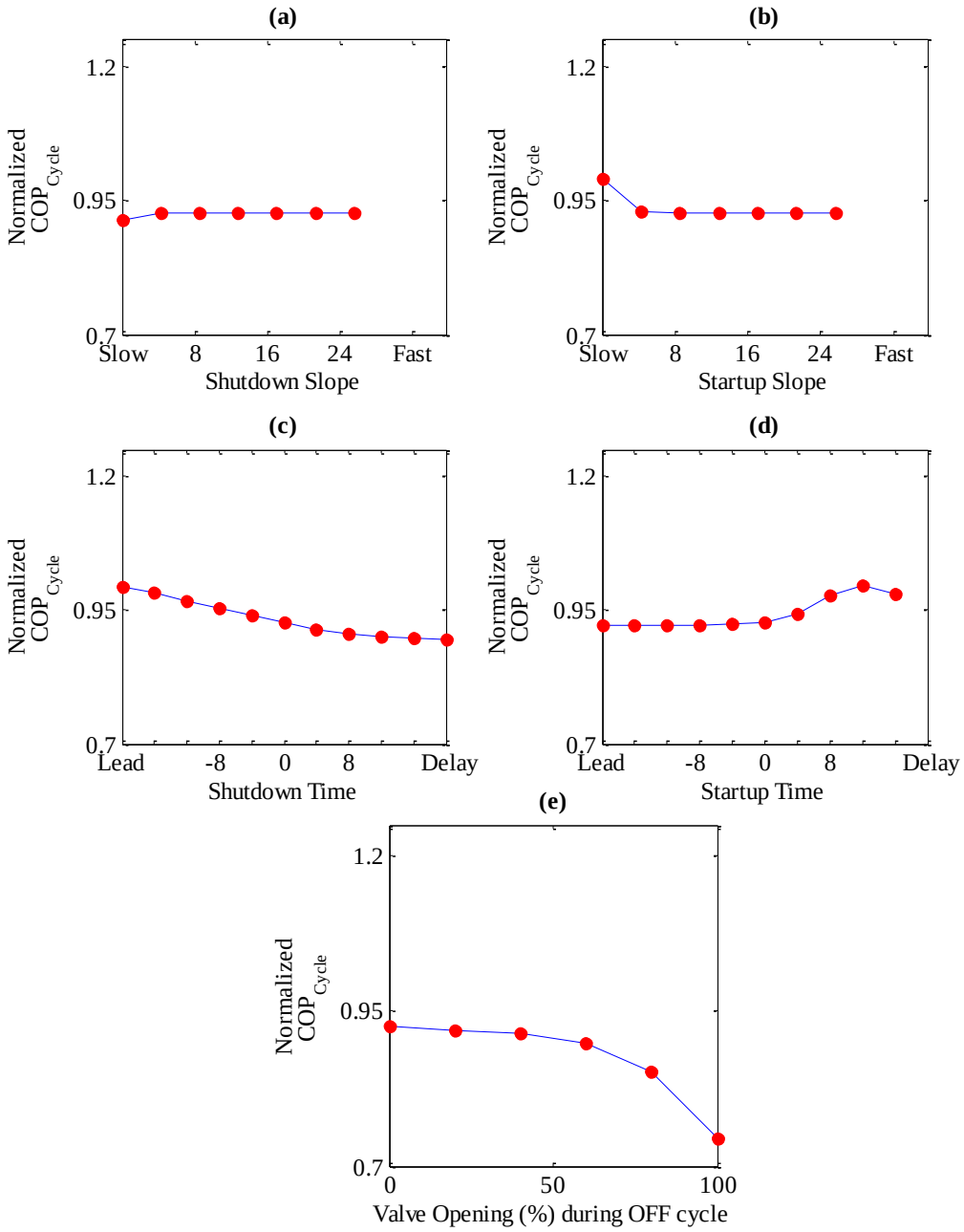

Figure 5.23 Detailed Trends in COP_{Cycle} – Expansion Valve – Short Cycle

Figure 5.23(a) and 5.23(b) show the effect of shutdown slope and startup slope respectively on COP_{Cycle}. They show the relatively negligible effect that the slope has in the system efficiency. Figure 5.23(e) shows the trend of COP_{Cycle} when the valve opening during the off cycle was changed as the parameter. This characteristic notes that the valve has to be strictly closed during the off cycle for the best cyclic efficiency of the system. Thus any small leakage in the valve means loss of system efficiency. Figure 5.23(c) presents the effect of shutdown time on COP_{Cycle}. Leading the valve closing with respect to compressor shutdown is observed to have efficiency comparable to benchmark even when the fan is not being cycled. Figure 5.23(d) shows the effect of startup time on COP_{Cycle} where trends show that a slight delay of the valve opening at startup is preferred for better cyclic efficiency. In order to justify why these conditions present have such efficiency characteristics, the following analyses are done.

The 'Valve Shutdown Lead' condition is interesting in the sense; it gives efficiency nearly equal to that of the benchmark despite the fan not being cycled. Figure 5.24 presents the system pressures and temperatures. The pressures for the 'Valve Shutdown Lead' condition equalize during the off cycle and that is because of the extended heat transfer of the fan being on throughout the cycle. The effect of valve is felt at the startup.

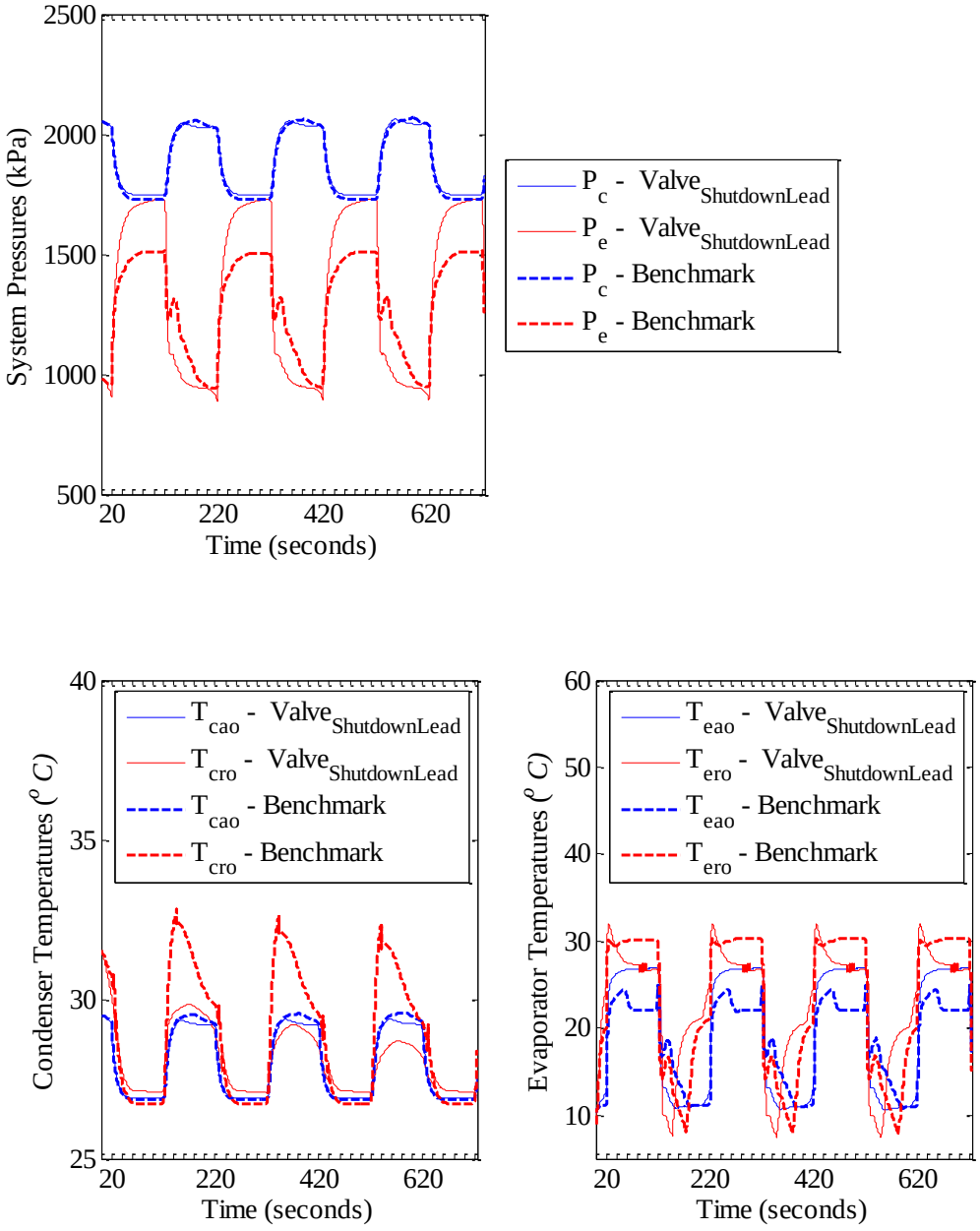

Figure 5.24 System Pressures and Temperatures – Valve Shutdown Lead Vs Benchmark – Short Cycle

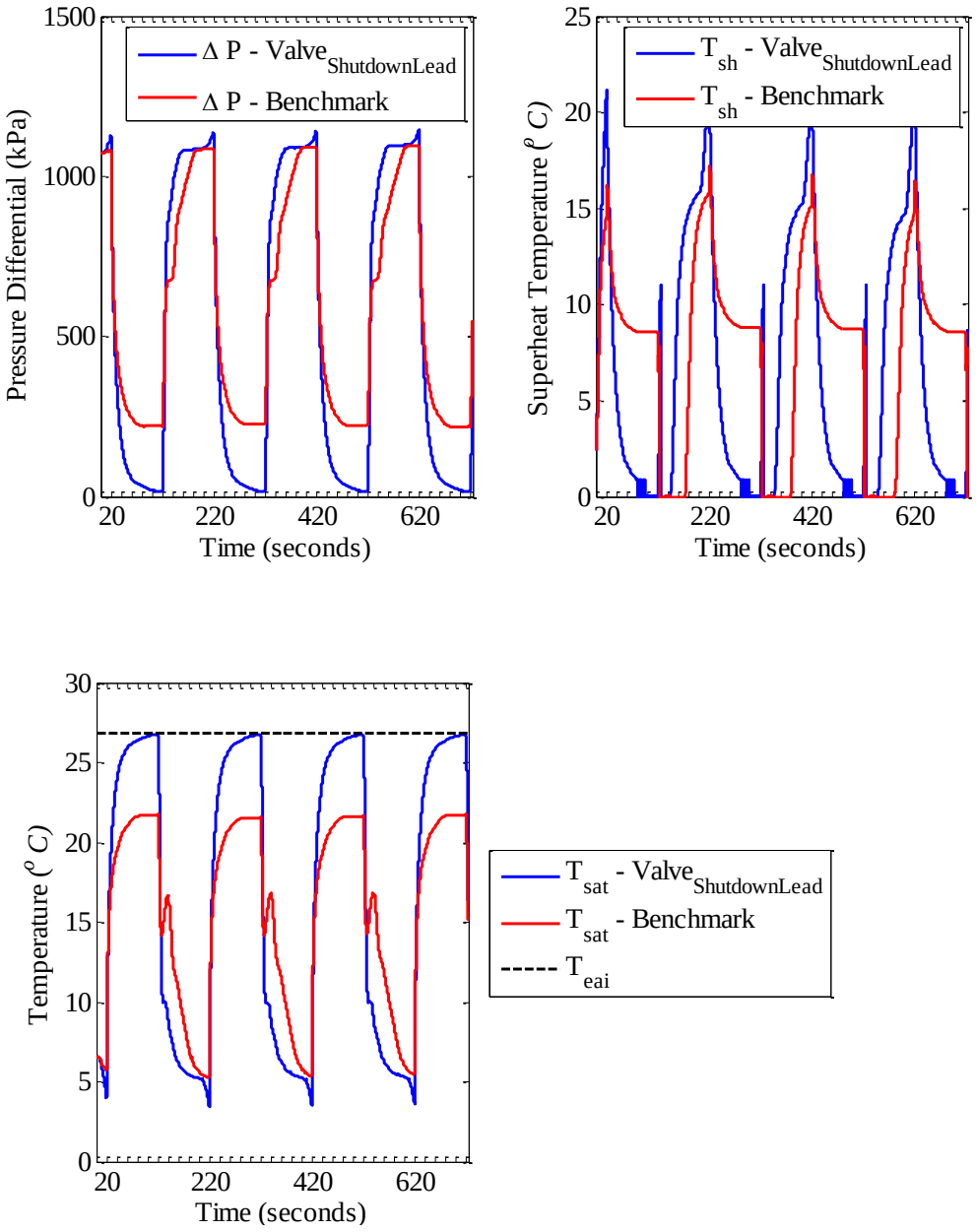

Figure 5.25 Pressure Differential and Superheat – Valve Shutdown Lead Vs Benchmark – Short Cycle

Since the valve is leading the compressor shutdown, this condition has less amount of refrigerant in the evaporator compared to the benchmark. This means that

most of the refrigerant mass is stored in the condenser during the off cycle thus preventing refrigerant migration. This facilitates faster pressure build up and superheat as shown in Figure 5.25 and reaches full cooling capacity faster at startup as shown in Figure 5.26.

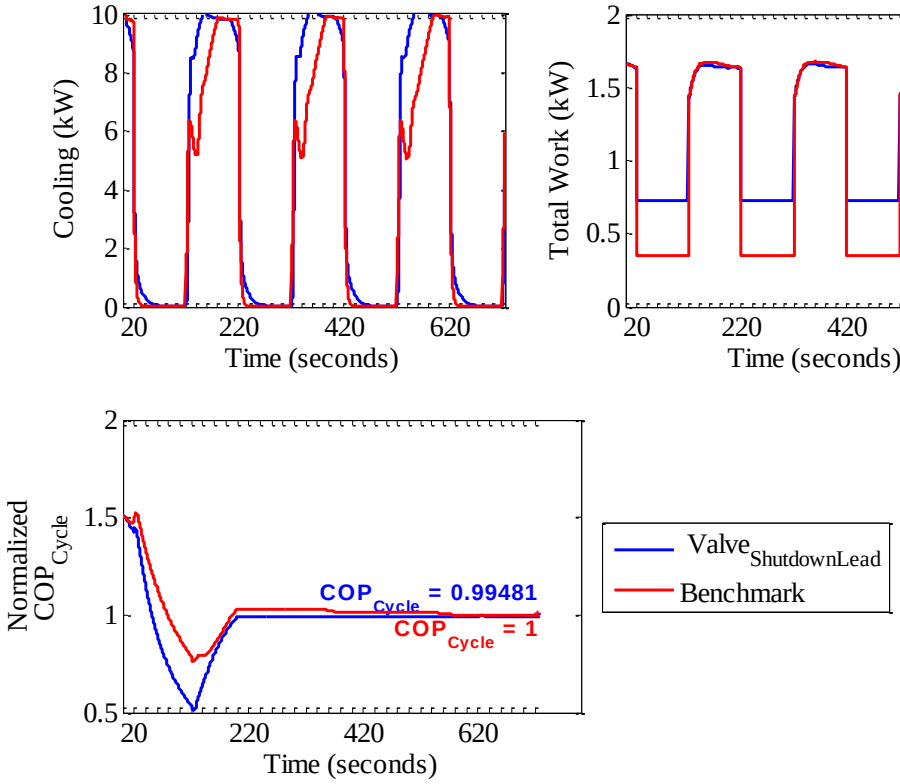

Figure 5.26 Cooling, Work and COP_{Cycle} – Valve Shutdown Lead Vs Benchmark – Short Cycle

As has been the case with the discussions before, the relative inefficiency of 'Valve Shutdown Lead' is attributed to the fan being on throughout the cycle. Perhaps if the fan had been part cycling at shutdown there would have been an improvement in efficiency. This condition is dealt next. Figure 5.27 shows that the high cooling obtained

during the cycle compared to benchmark is not enough to tradeoff the higher work due to the fan on condition.

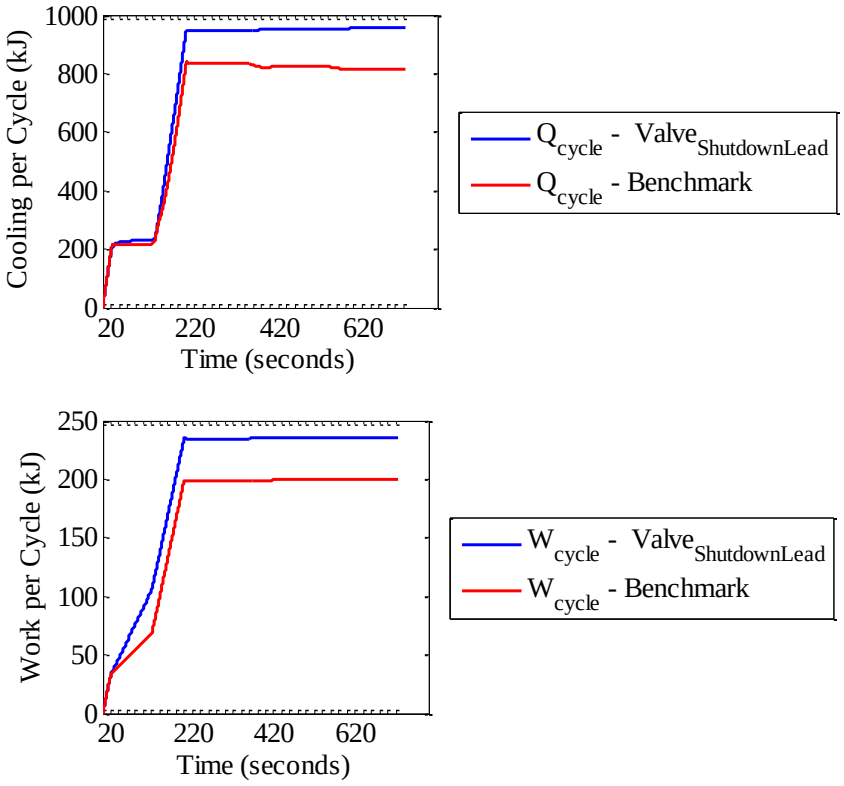

Figure 5.27 Work, Cooling Per Cycle – Valve Shutdown Lead Vs Benchmark – Short Cycle

The final valve cycling scheme to analyze is 'Valve Startup Delay'. Here the valve waits for some time before opening with respect to compressor startup. Despite having a different valve command when compared to 'Valve Shutdown Lead', this condition more or less achieves the same efficiency albeit for different reasons. Figure

5.28 show the system pressures and temperatures for the 'Valve Startup Delay' and benchmark conditions.

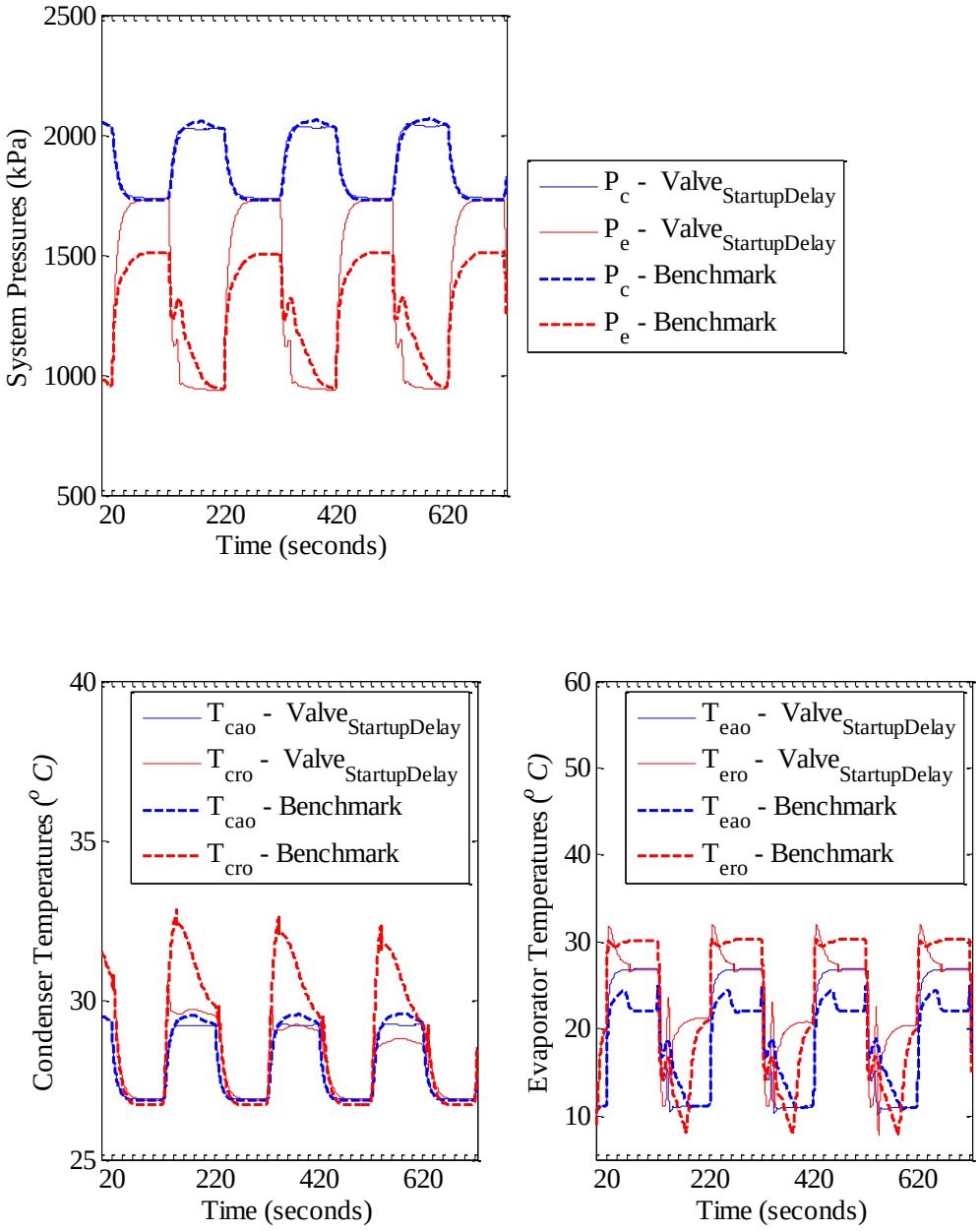

Figure 5.28 System Pressures and Temperatures – Valve Startup Delay Vs Benchmark – Short Cycle

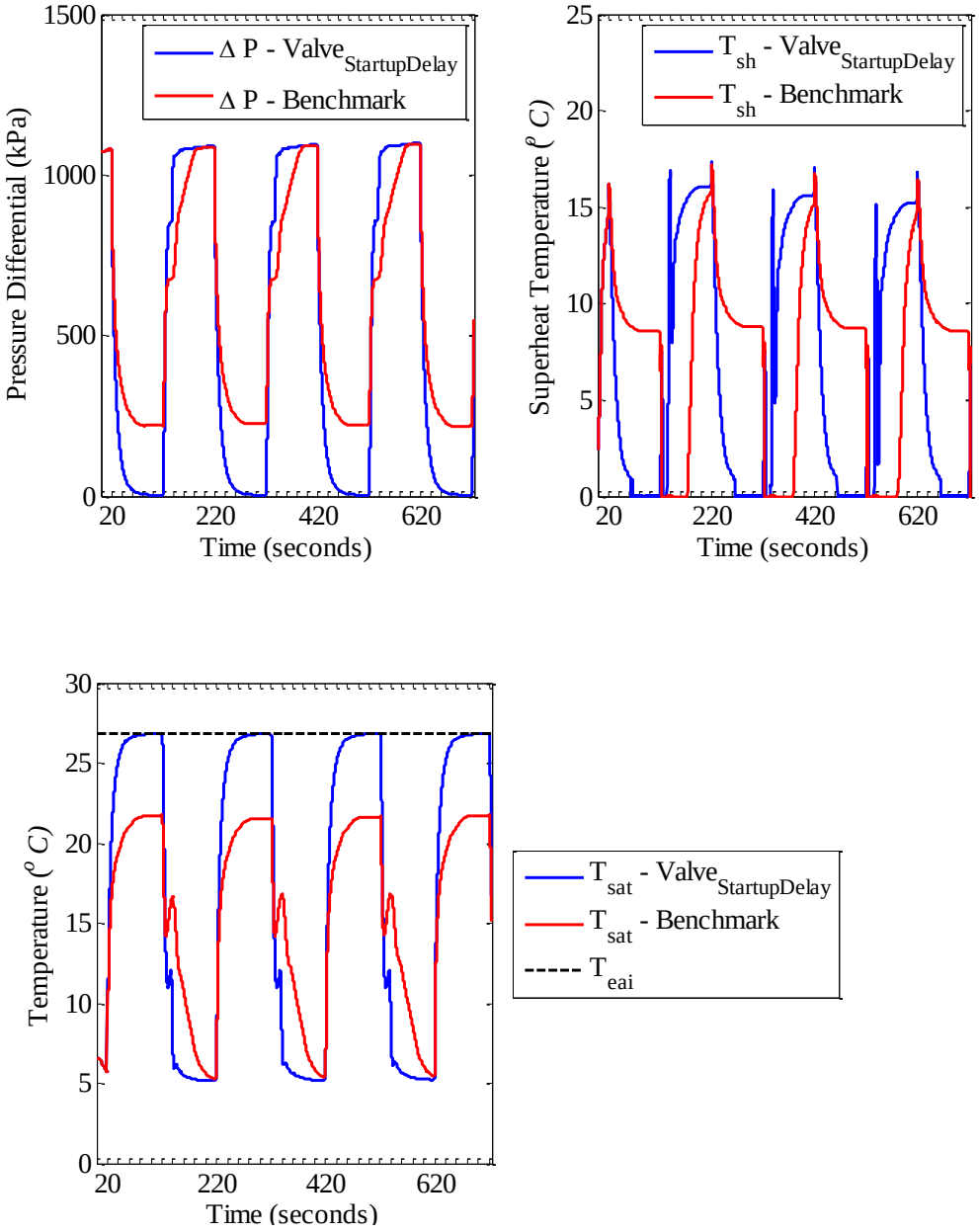

Figure 5.29 Pressure Differential and Superheat – Valve Startup Delay Vs Benchmark – Short Cycle

One of the striking features by closing the valve at startup is that the superheat and the pressure differential builds up almost instantaneously compared to compressor

startup as shown in Figure 5.29. This results in almost instantaneous full cooling capacity as shown in Figure 5.30.

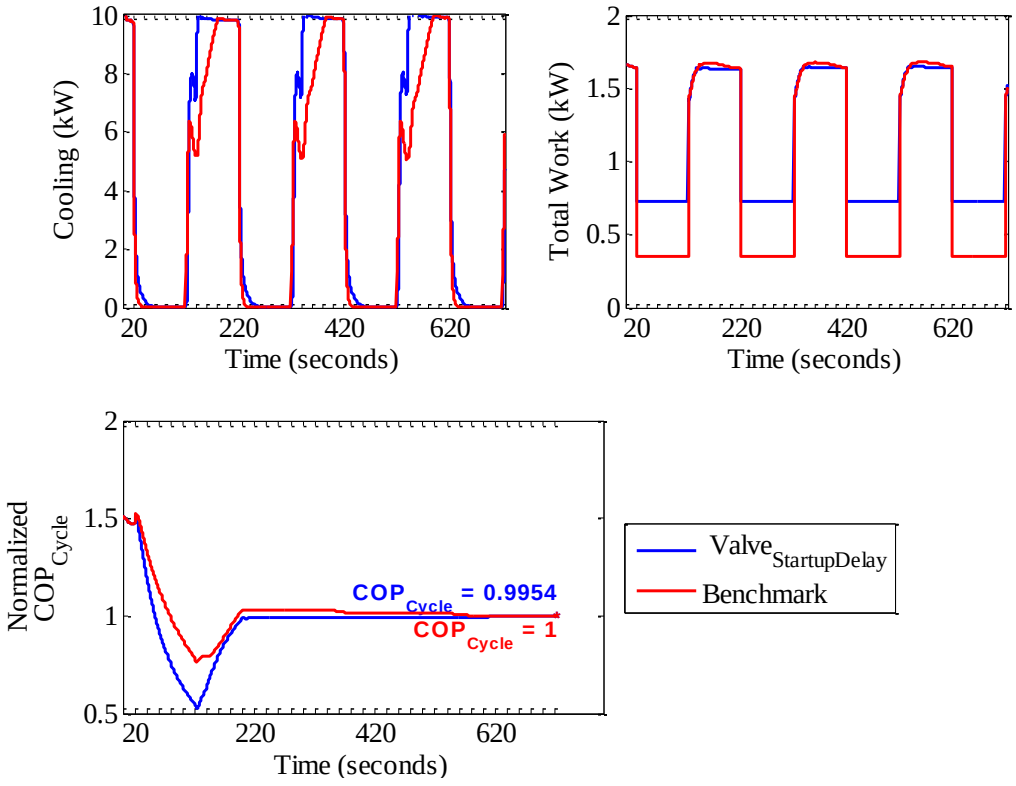

Figure 5.30 Cooling, Work and COP_{Cycle} – Valve Startup Delay Vs Benchmark – Short Cycle

The fan being on during the off cycle is advantageous initially since it extracts some potential cooling off the refrigerant pumped into the evaporator. But, for the rest of the off cycle, the fan is on just consuming power and providing any cooling. This results in the relative inefficiency of the system as shown in Figure 5.30. Figure 5.31 shows the

cooling and work per cycle comparison of 'Valve Startup Delay' and benchmark conditions.

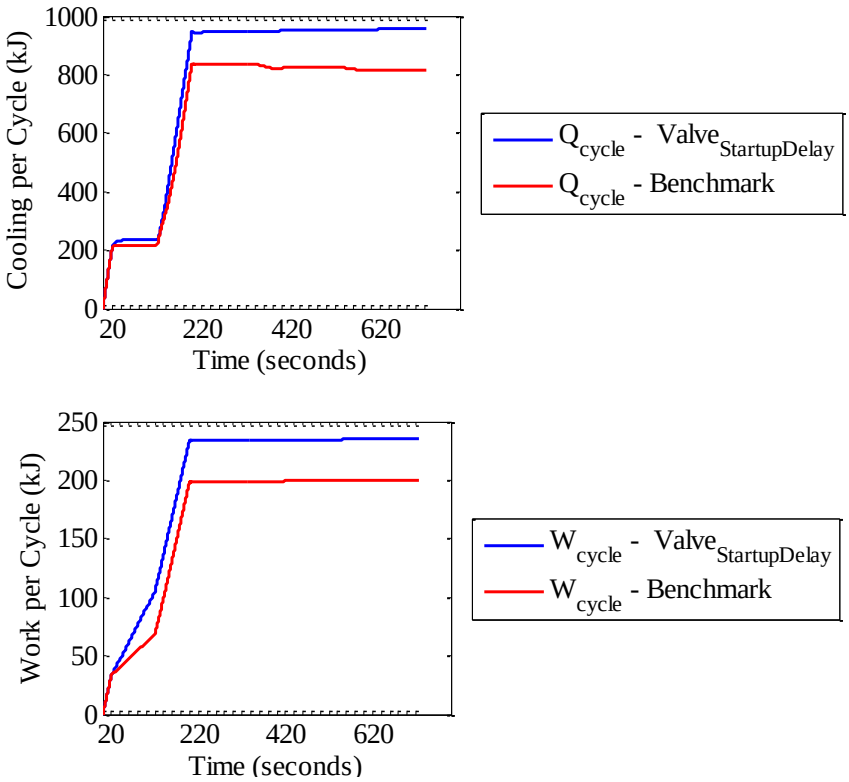

Figure 5.31 Work, Cooling Per Cycle – Valve Startup Delay Vs Benchmark – Short Cycle

The conclusions that were drawn from the trend analysis for the valve are summarized in Table 5.3.

Table 5.3 Trend Analysis Summary for Expansion Valve – Short Cycle

Expansion valve cycle S-curve parameter	Recommendations for better cycle efficiency	Representative figures
Shutdown Slope	No significant change	Figure 5.23(a)
Startup Slope	No significant change	Figure 5.23(b)
Shutdown Time	Lead (Valve closed before compressor shutdown)	Figure 5.23(c)
Startup Time	Delay (Valve opened before compressor startup)	Figure 5.23(d)
Valve opening (%) during OFF cycle	Zero	Figure 5.23(e)

On an overall note, with the OFF position fixed at zero and the slope effects ignored (since they have relatively less impact on cyclic efficiency), the valve startup and shutdown times played a big role in the overall optimization of the system as seen in Figure 5.23(c) and (d). This meant that the optimization procedure could be reduced to just a two parameter problem from the original five parameters of the S-curve. Valve cycling mainly affects the startup efficiency of the system by pulling down the pressure faster and thus achieving full cooling capacity faster.

5.3.1.2 Evaporator Fan

The effects of evaporator fan S-curve parameters on COP_{Cycle} is analyzed here. For these analyses the valve was cycling in sync with the compressor. The valve was not

left on throughout the cycle since the effect of fan cycling could not be captured by cycling the fan alone. This approach was also justified since the previous subsection has already established that valve cycling is mandatory for good startup efficiency.

Similar to the expansion valve analysis, the detailed trend analysis was one dimensional where, one parameter was varied according to the range in Table 5.2, the other parameters were held constant at their benchmark values. Figure 5.32 present the results of the detailed trend analysis for the individual S-curve parameters for the evaporator fan profile.

Figure 5.32(a) and 5.32(b) show the effect of shutdown slope and startup slope respectively on COP_{Cycle}. They show the relatively negligible effect that the slope has in the system efficiency. Figure 5.32(e) shows the trend of COP_{Cycle} when the air mass flow rate (kg/s) during the off cycle was changed as the parameter. Physically this means leaving the fan on at the specified speed throughout the off cycle. This characteristic notes that the fan has to be strictly OFF during the off cycle for the best cyclic efficiency of the system. Figure 5.32(c) presents the effect of shutdown time on COP_{Cycle}. Delaying the fan switching off with respect to compressor shutdown is observed to have higher efficiency compared to benchmark when the valve is also cycling. Figure 5.32(d) shows the effect of startup time on COP_{Cycle} where trends show that the fan is better off with starting along with the compressor rather than lead/delay it during startup. The effect of delaying the fan during shutdown has already been discussed in Subsection 5.3.1.1 when analyzing the 'Fan Part Cycle' condition. The reasons were also analyzed in the same discussion.

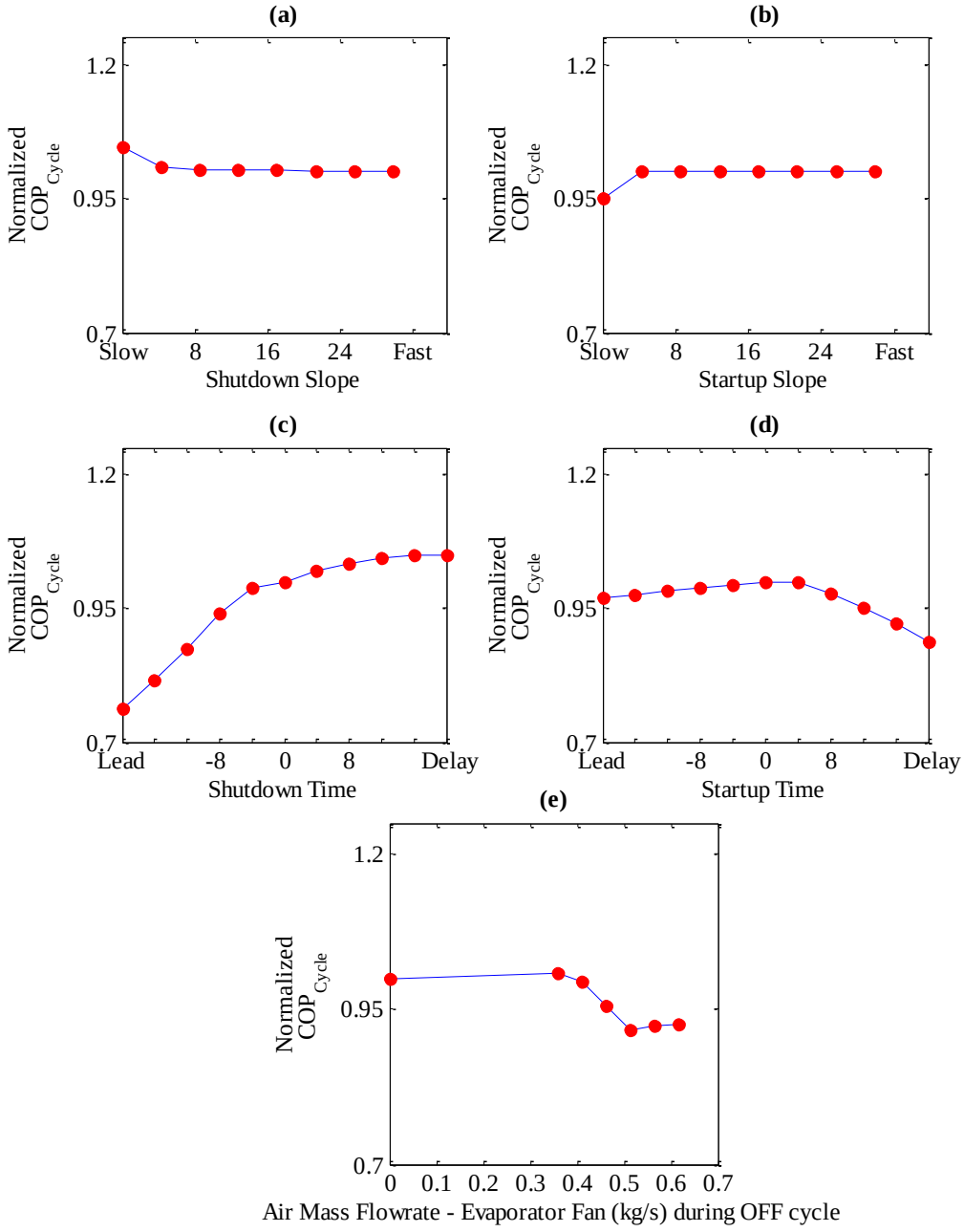

Figure 5.32 Detailed Trends in COP_{Cycle} – Evaporator Fan – Short Cycle

The conclusions that were drawn from the trend analysis are summarized in Table 5.4. On an overall note, with the OFF position fixed at zero and the slope effects ignored (since they have relatively less impact on cyclic efficiency), the fan startup time synchronous with the compressor startup, the shutdown time played a big role in the overall optimization of the system as seen in Figure 5.32(c). This meant that the optimization procedure could be reduced to a single parameter problem from the original five parameters of the S-curve. Fan cycling results in power regulation on the cycle while providing better cooling during shutdown thus, improving the cyclic efficiency of the system.

Table 5.4 Trend Analysis Summary for Evaporator Fan – Short Cycle

Evaporator fan cycle S-curve parameter	**Recommendations for better cycle efficiency**	**Representative figures**
Shutdown Slope	No significant change	Figure 5.32(a)
Startup Slope	No significant change	Figure 5.32(b)
Shutdown Time	Delay (Fan OFF after compressor shutdown)	Figure 5.32(c)
Startup Time	With (Fan ON at compressor startup)	Figure 5.32(d)
Air mass flow rate during OFF cycle	Zero	Figure 5.32(e)

5.3.2 Long Cycle

Simulation results obtained for a long cycle length of 1000 seconds are presented here. This was to understand how COP_{Cycle} varies with respect to the S-curve parameters during conventional cycling times. Also, since the longer cycle gives enough time for the pressures and temperatures to assume equilibrium, the effect of not having a pressure/temperature differential on the optimum expansion valve, evaporator fan profile was an interesting study.

5.3.2.1 Gross Trends

To prove that the normalized COP_{Cycle} changes are significant enough to merit a further detailed investigation, a quick comparison of some possible cycling schemes is done. Figure 5.33 shows the gross trends for the various cycling schemes. With the benchmark for comparison at 1 the other cycling schemes are presented as described in Table 5.2. From the figure 'All on' and 'Valve Cycle Fan On' conditions were having the worst performance. This is different from what was observed in short cycle, where 'Fan Cycle Valve On' had the worst efficiency.

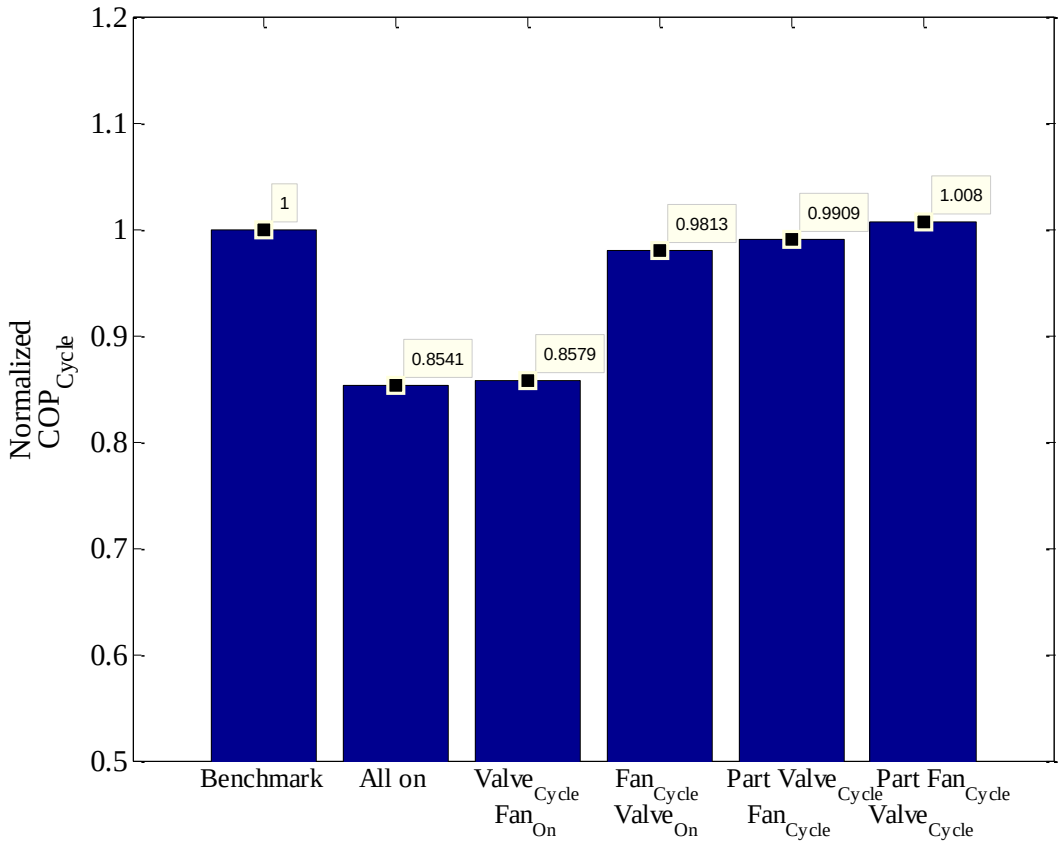

Figure 5.33 COP_{Cycle} Gross Trends of Various Cycling Schemes – Long Cycle

A quick glance at Figure 5.33 tells that the cycling schemes do not discern that much among them when it comes to magnitude of the COP_{Cycle} change like it did in the case of short cycle. The COP_{Cycle} remains more or less constant which mean the valve and the fan cycling parameters might have less effect on it. To explain why these conditions do not change the cyclic efficiency much the following analysis needs to be done. The first case is the 'All on' condition.

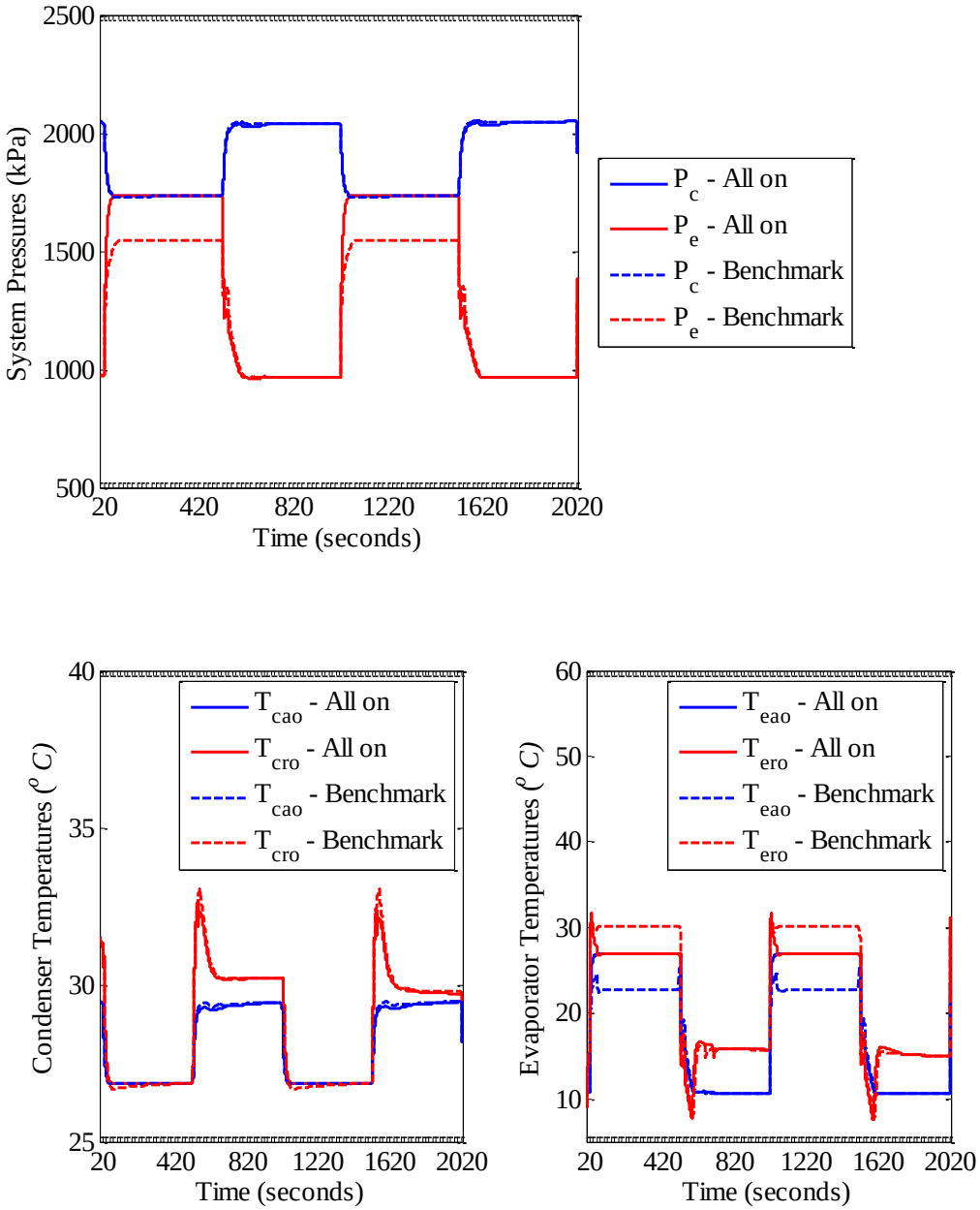

Figure 5.34 System Pressures and Temperatures – All On Vs Benchmark – Long Cycle

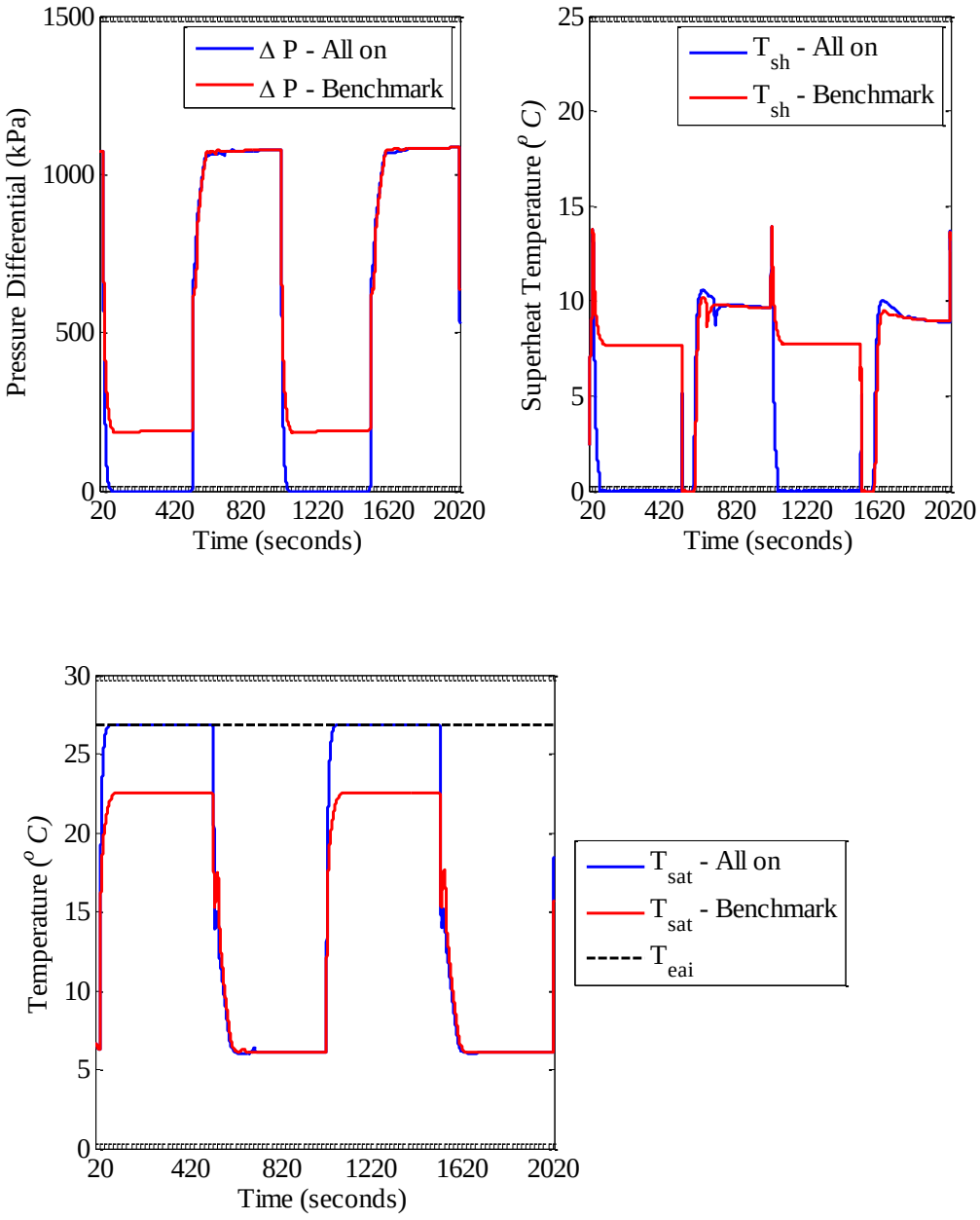

Figure 5.35 Pressure Differential and Superheat – All On Vs Benchmark – Long Cycle

Figure 5.34 presents the system pressures and temperatures. It shows that for the all on condition, the evaporator and the condenser pressures equalize during the off cycle. Figure 5.35 agrees with this where it shows the pressure differential also going to zero for the off cycle. Figure 5.36 shows the instantaneous cooling and power consumed. Despite the fan being on throughout the cycle in the all on condition, there is not that much cooling gained by having the fan on.

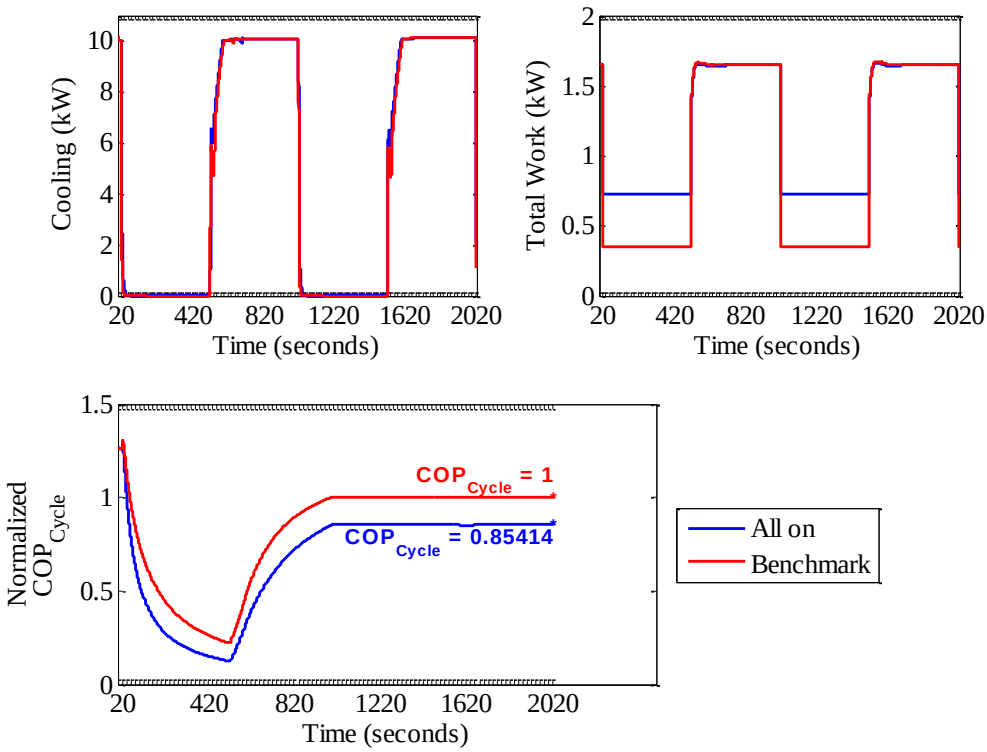

Figure 5.36 Cooling, Work and COP_{Cycle} – All On Vs Benchmark – Long Cycle

In the long cycle the penalty for having the fan on throughout the length of the cycle is much more when compared to the short cycle. Since the potential cooling that

could be obtained during the initial part of the off cycle is always going to be relatively less compared to the fan power consumption throughout the length of the off cycle, leaving the fan on all the way on is perhaps the worst cycling scheme. The fan consumes power while not providing any cooling for the bulk part of the cycle. This is why fan cycling was shown to be more important in the long cycle compared to valve cycling in the gross trends Figure 5.33. Figure 5.37 shows this for the all on condition. For about the same cooling as benchmark, the all on condition consumes needless power during the off cycle thus resulting in inefficiency of the cycling scheme.

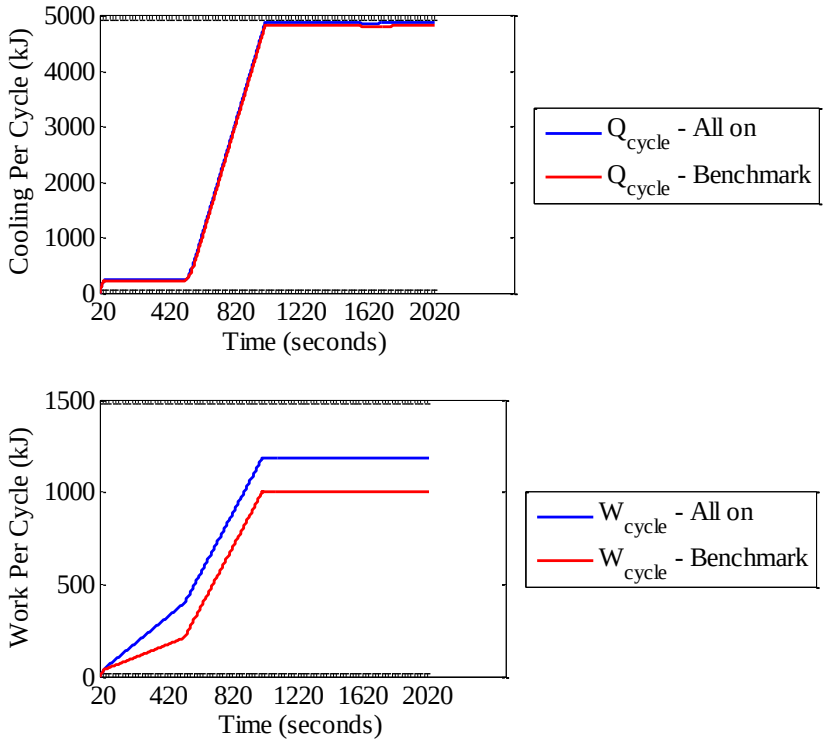

Figure 5.37 Work, Cooling Per Cycle – All On Vs Benchmark – Long Cycle

The gross trends showed 'Valve Cycle Fan On' condition to have almost same efficiency as the all on condition. The reasons for this scheme to perform so poorly is explained below. Figure 5.38 shows the system pressures and temperatures for the comparison of 'Valve Cycle Fan On' with the benchmark.

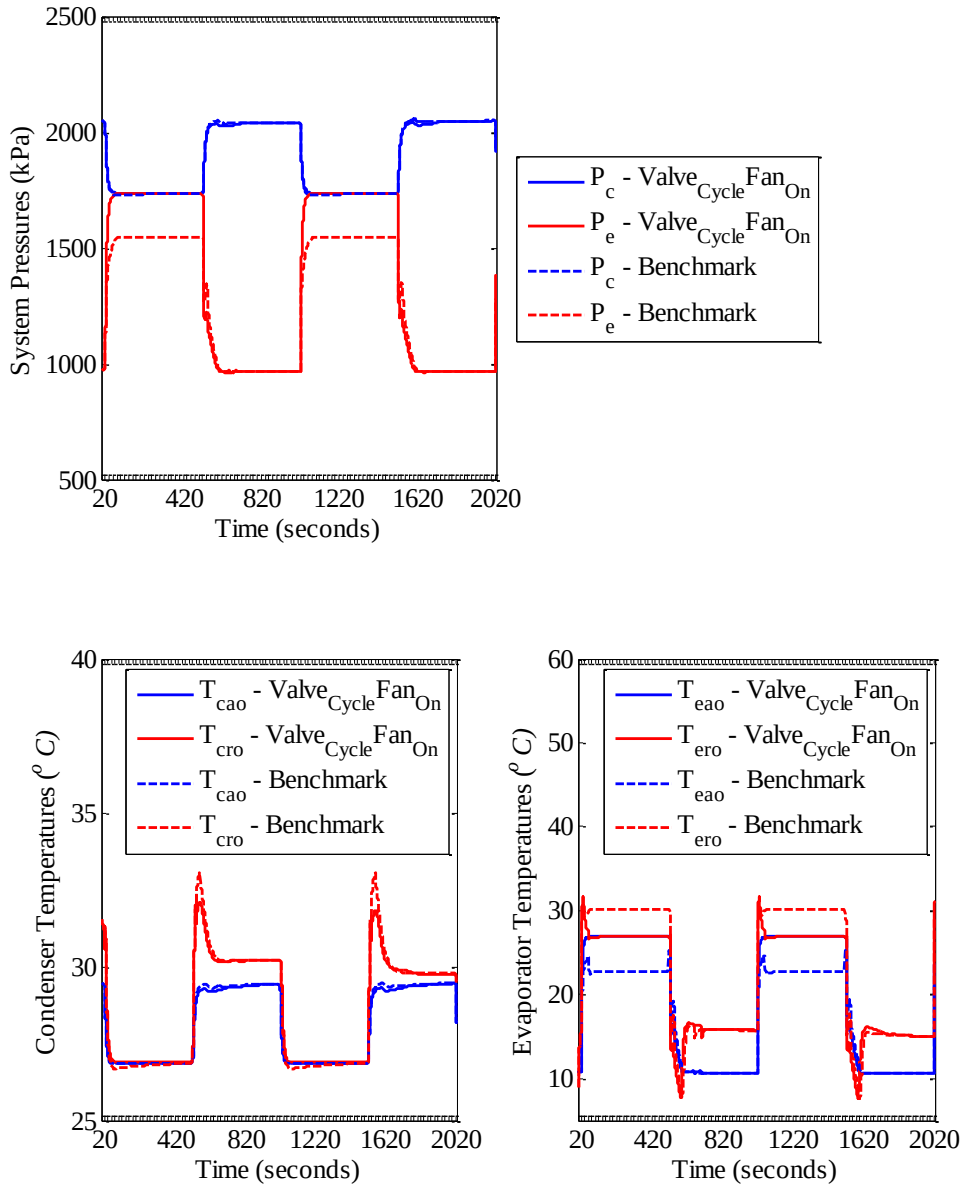

Figure 5.38 System Pressures and Temperatures – Valve Cycle Fan On Vs Benchmark – Long Cycle

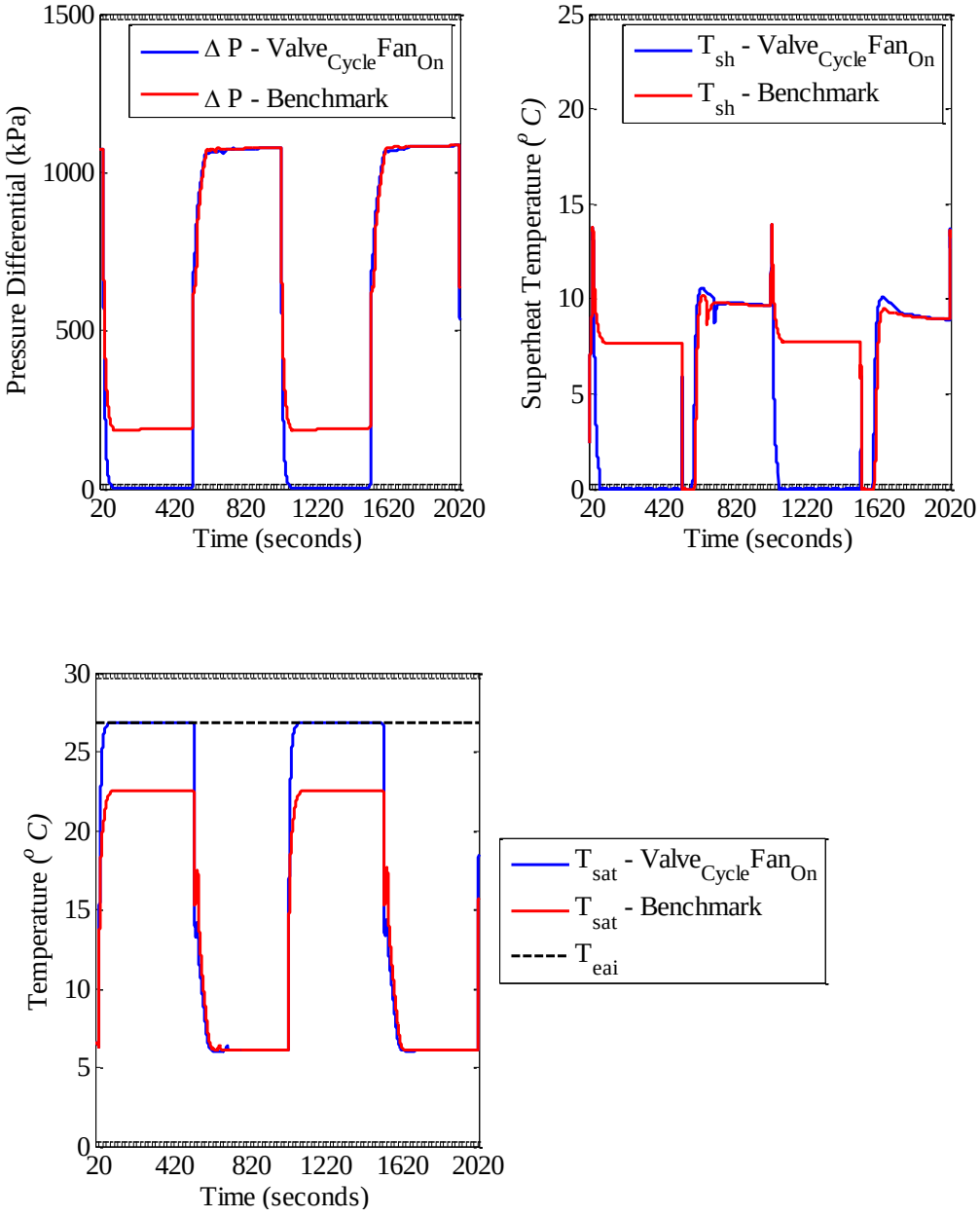

Figure 5.39 Pressure Differential and Superheat – Valve Cycle Fan On Vs Benchmark – Long Cycle

The ‘Valve Cycle Fan On’ condition is bad for the same reasons as the all on condition. Figure 5.39 shows the pressure differential going to zero during the off cycle. Figure 5.40 shows the instantaneous cooling and the power consumed. The inefficiency of the ‘Valve Cycle Fan On’ condition is because of the fan being on throughout the off cycle resulting in no significant cooling at all. Since the off cycle length is long here the effect of having the fan on unnecessarily is magnified.

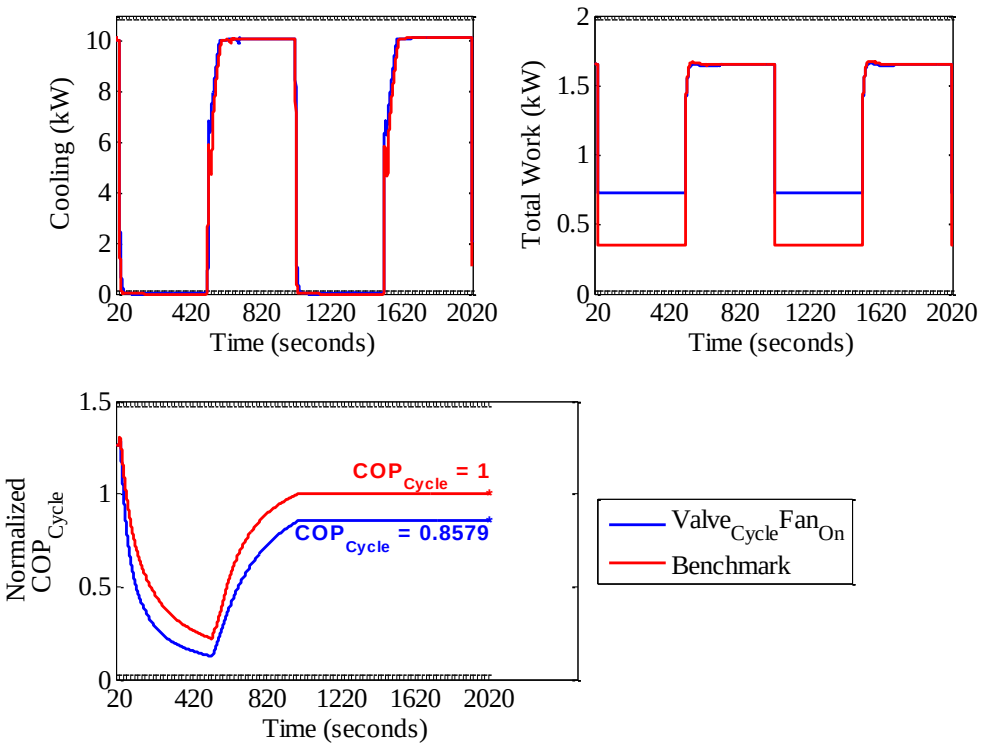

Figure 5.40 Cooling, Work and COP_{Cycle} – Valve Cycle Fan On Vs Benchmark – Long Cycle

Figure 5.41 shows the cooling and the work per cycle. Similar to the all on condition, for about the same amount of cooling as benchmark, the 'Valve Cycle Fan On' scheme takes significantly more power resulting in the reduction of COP_{Cycle}.

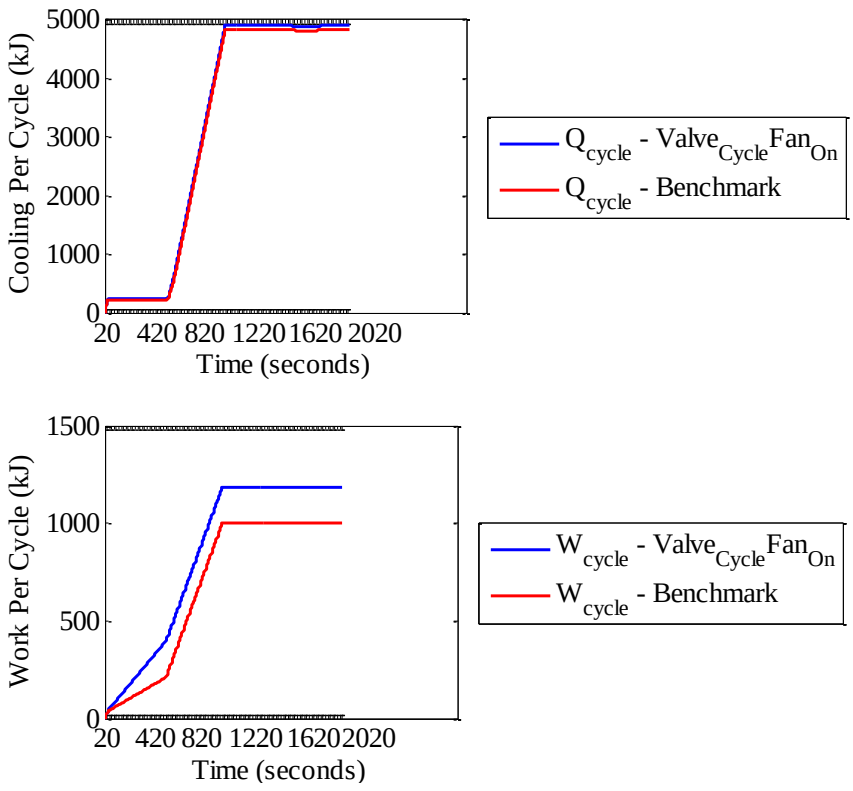

Figure 5.41 Work, Cooling Per Cycle – Valve Cycle Fan On Vs Benchmark – Long Cycle

The next case is 'Fan Cycle Valve On' which had one of the worst efficiencies in the short cycle. For the long cycle, the efficiency is nearly as good as benchmark. The following plots help in understanding the physical reason behind this reversal of trends.

Figure 5.42 shows the system pressures and temperatures. The pressures equalize for this condition since the valve is on throughout the length of the cycle.

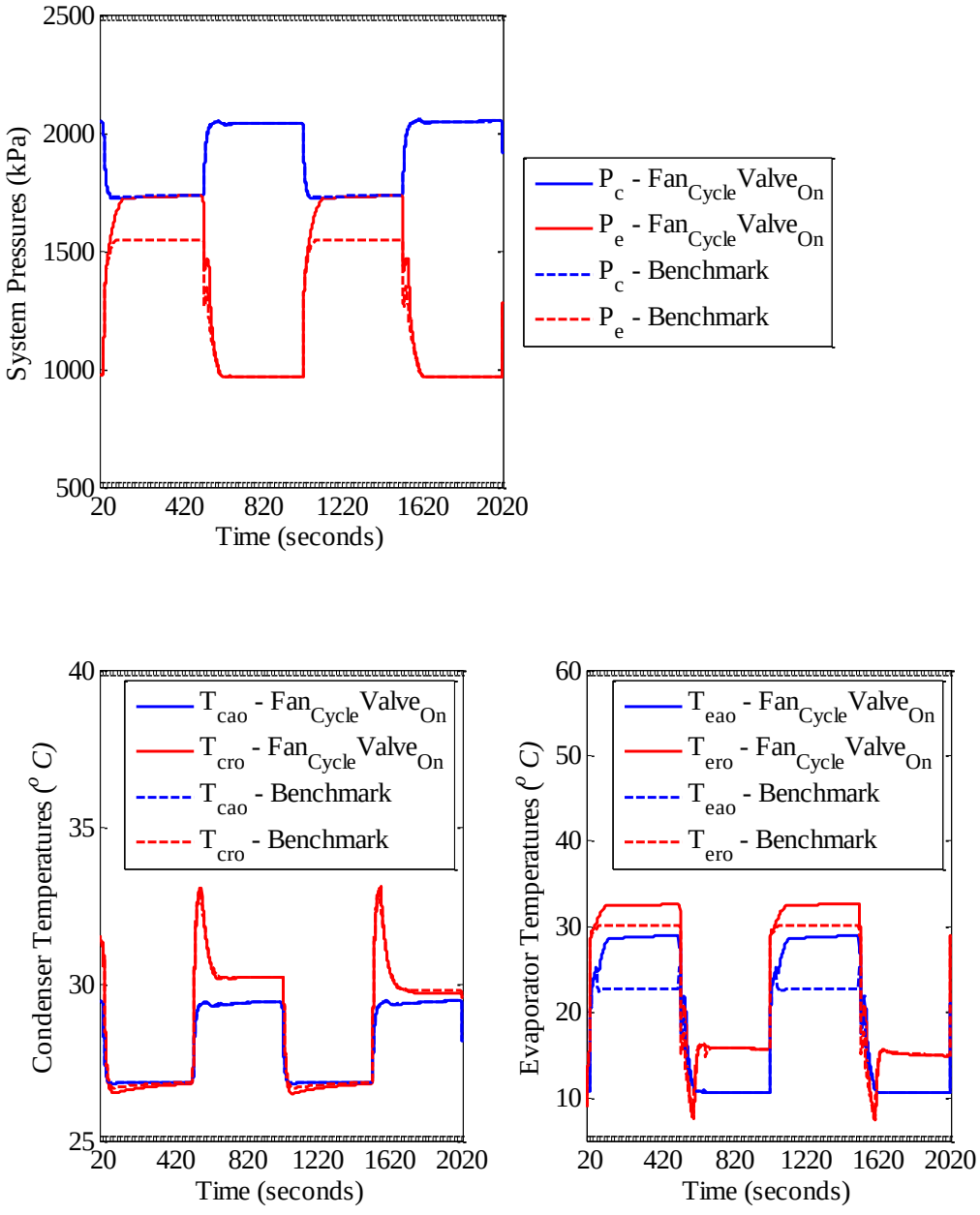

Figure 5.42 System Pressures and Temperatures – Fan Cycle Valve On Vs Benchmark – Long Cycle

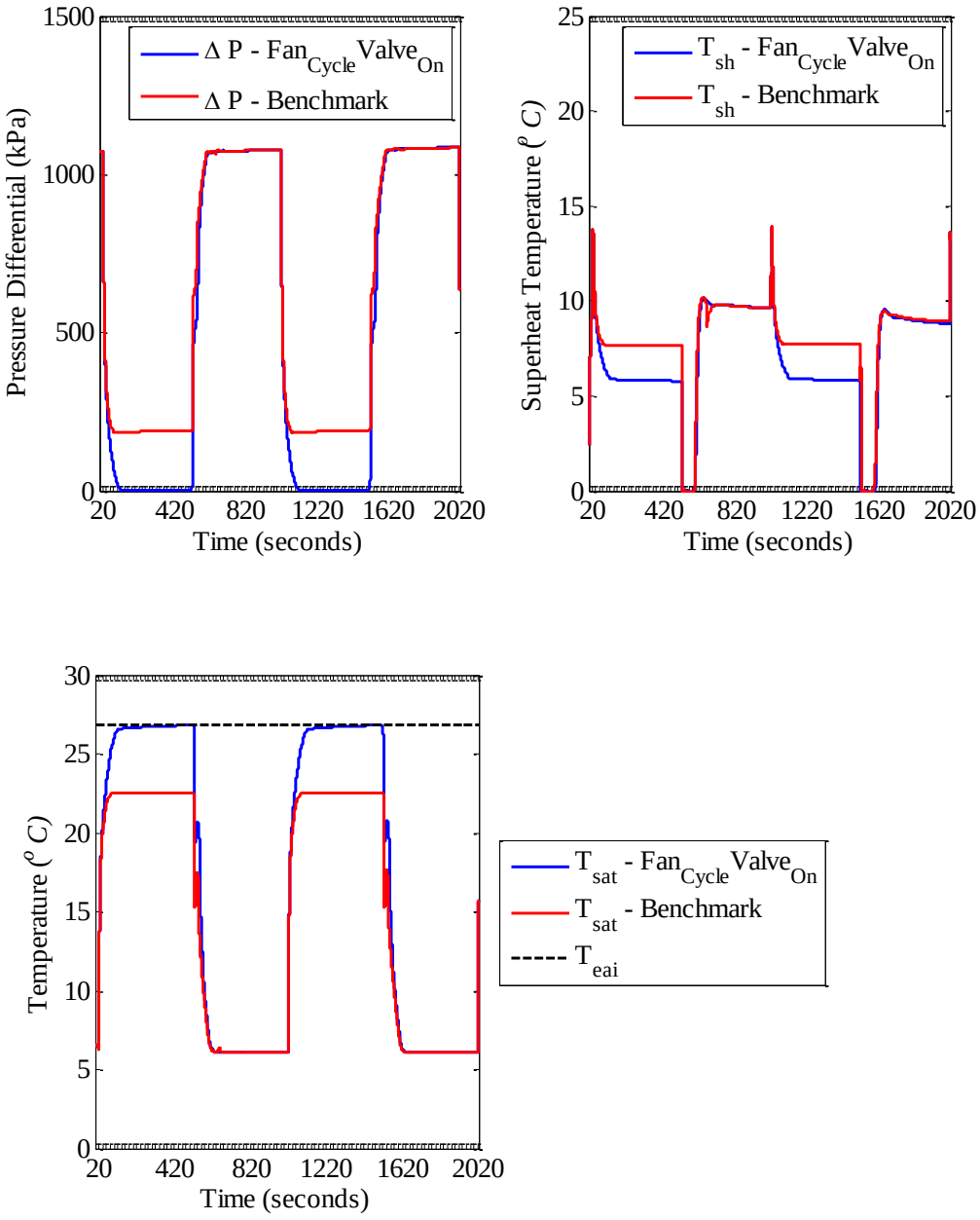

Figure 5.43 Pressure Differential and Superheat – Fan Cycle Valve On Vs Benchmark – Long Cycle

Figure 5.43 shows the pressure differential and superheat for 'Fan Cycle Valve on' and benchmark conditions. Figure 5.44 shows the instantaneous cooling and work curves.

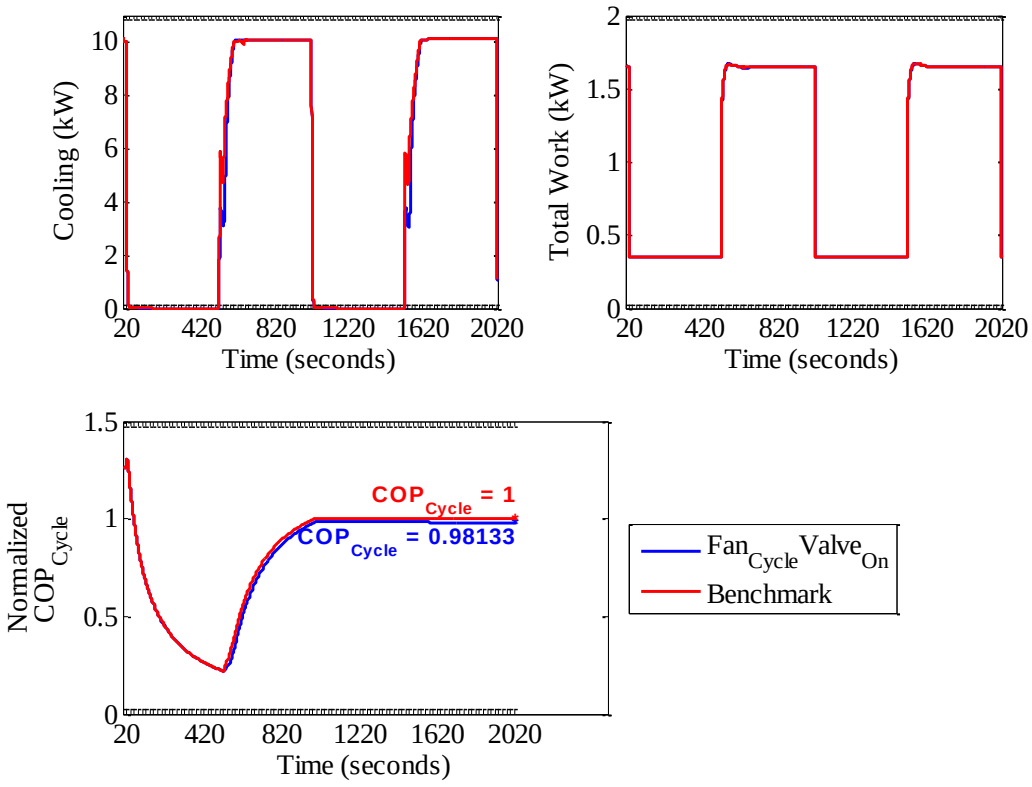

Figure 5.44 Cooling, Work and COP_{Cycle} – Fan Cycle Valve On Vs Benchmark – Long Cycle

Since the valve is open during the off cycle an appreciable amount refrigerant gets stored in the evaporator in other words, there is refrigerant migration. At startup this refrigerant has to be redistributed through the circuit which takes a little more time than benchmark where the valve shuts off to limit the amount of refrigerant in the evaporator

avoiding migration. Thus 'Fan Cycle Valve On' condition takes a little more time to build up pressure. Because of this some cooling is lost during startup as shown in Figure 5.44. This is the reason for the 'Fan Cycle Valve On' condition to have less efficiency than benchmark. Figure 5.45 reaffirms this by showing the less cooling per cycle for the same amount of work per cycle.

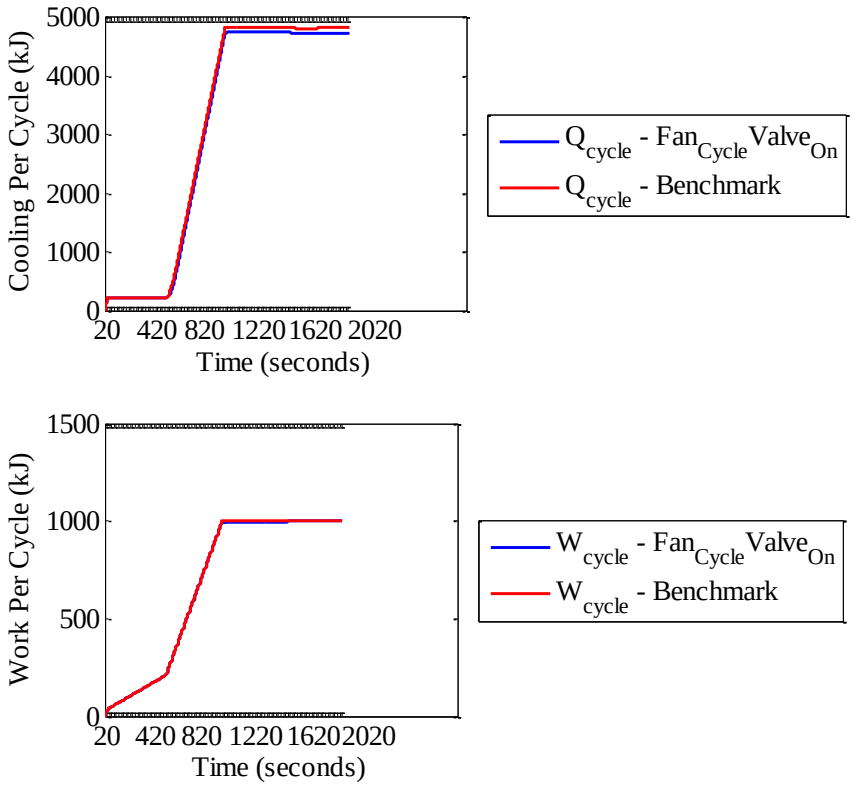

Figure 5.45 Work, Cooling Per Cycle – Fan Cycle Valve On Vs Benchmark – Long Cycle

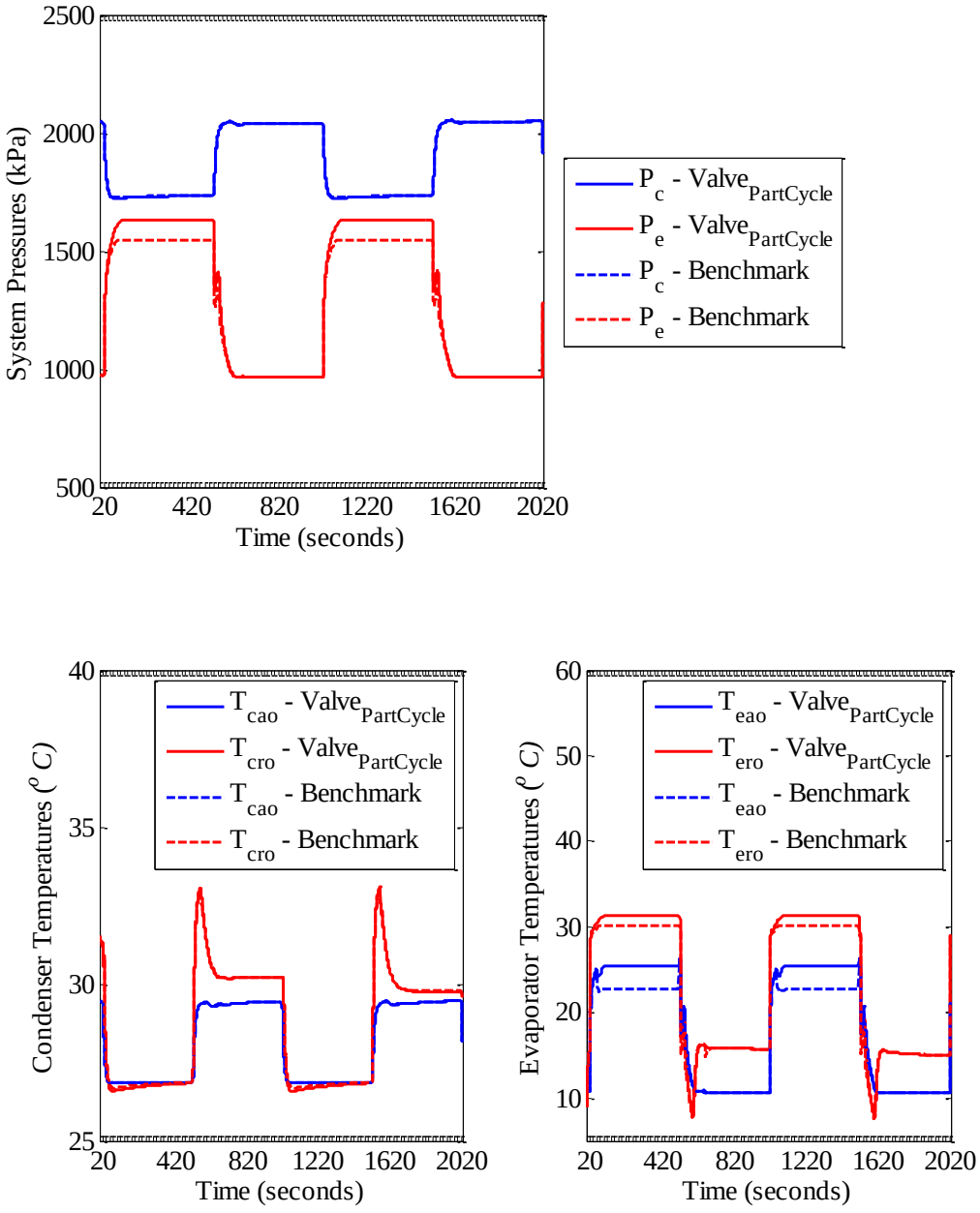

Figure 5.46 System Pressures and Temperatures – Valve Part Cycle Vs Benchmark – Long Cycle

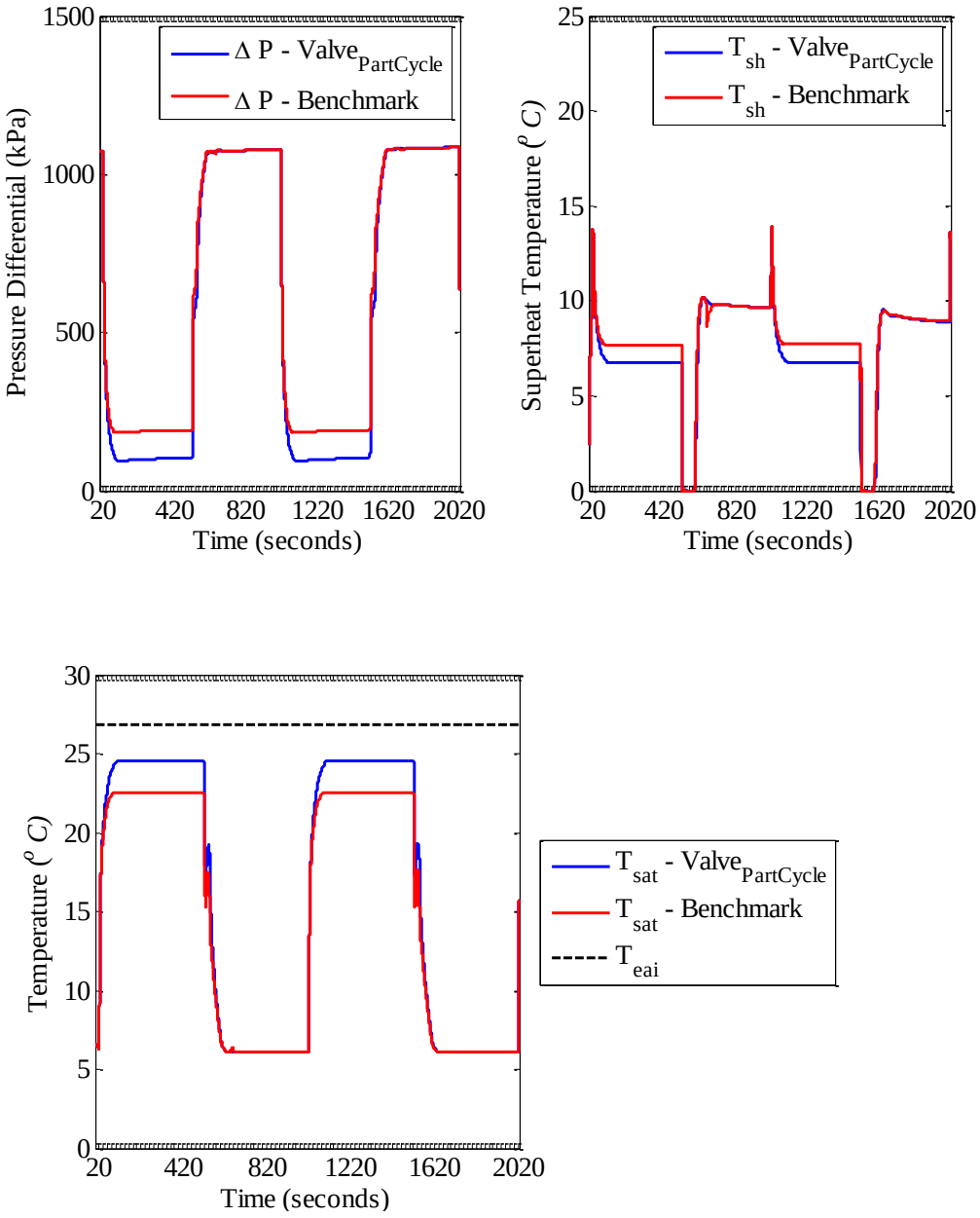

Figure 5.47 Pressure Differential and Superheat – Valve Part Cycle Vs Benchmark – Long Cycle

The system pressures and temperatures of 'Valve Part Cycle' are shown in Figure 5.46. 'Valve Part Cycle' differs from the benchmark in the aspect that, the valve stays on for 20 seconds more during shutdown. Since the valve is on for more time during shutdown the pressure differential during off cycle is less than that of the benchmark as shown in Figure 5.47. This also results in some extra refrigerant mass to be stored in the evaporator compared to benchmark. Again the redistribution problem arises, which results in some loss in startup cooling as shown in Figure 5.48.

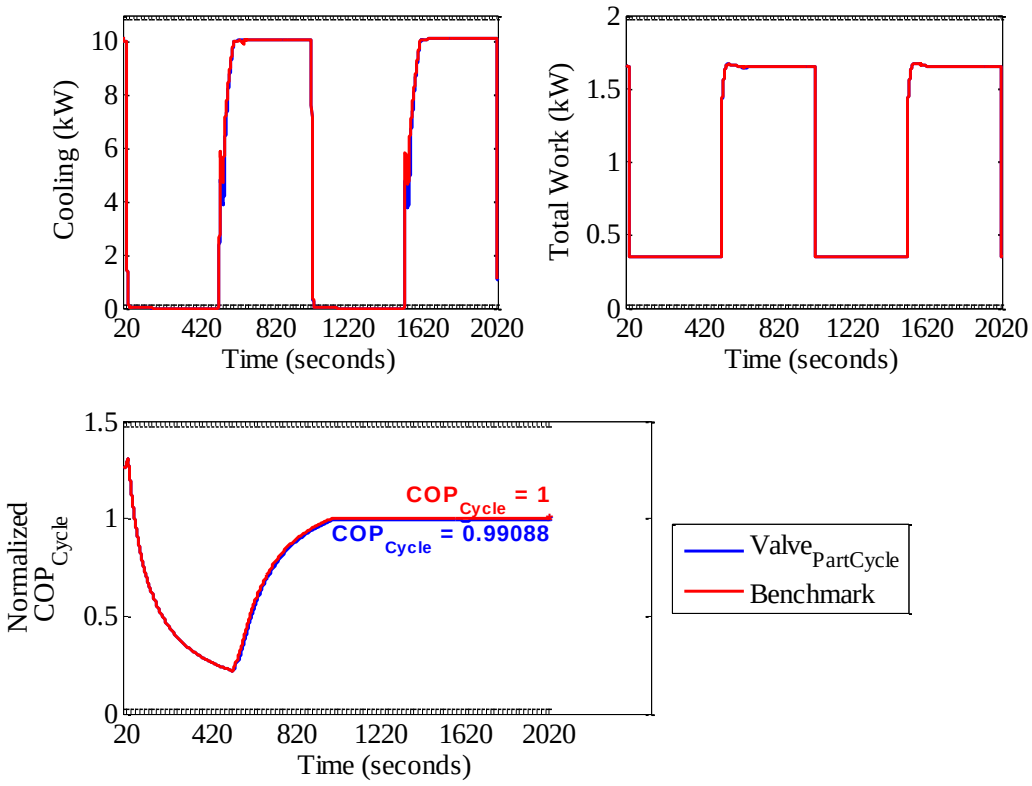

Figure 5.48 Cooling, Work and COP_{Cycle} – Valve Part Cycle Vs Benchmark – Long Cycle

But the cycle is very long which means the effect of this problem on the cyclic efficiency as a whole is not that great. Thus despite having some intentional 'valve leakage' during shutdown, given the length of the cycle, the efficiency comes close to benchmark. The slightly less cooling per cycle of the 'Valve Part Cycle' condition is shown in Figure 5.49.

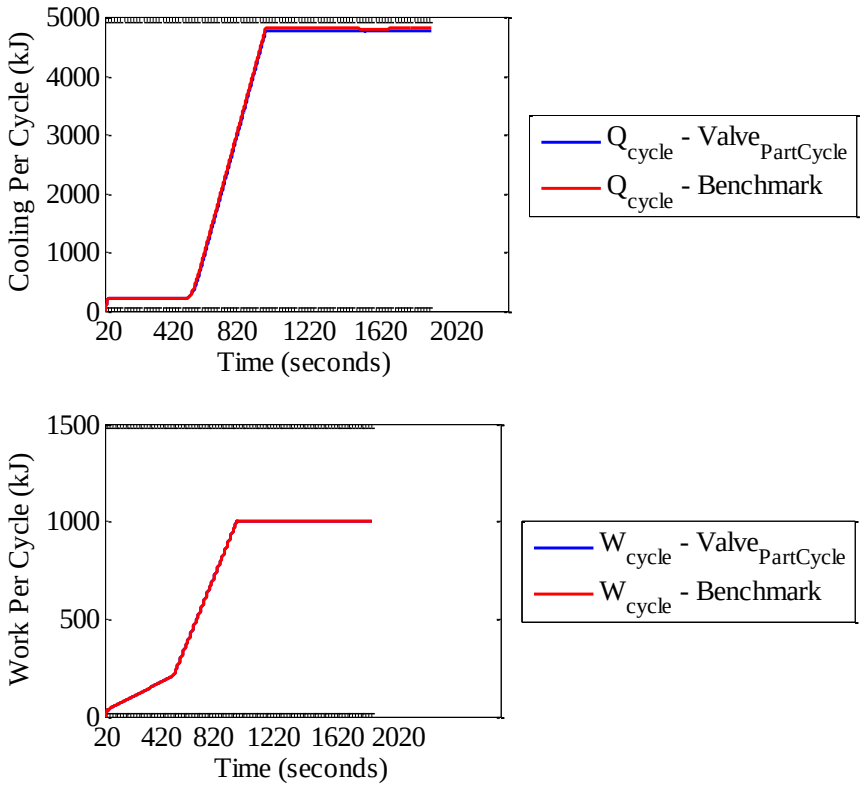

Figure 5.49 Work, Cooling Per Cycle – Valve Part Cycle Vs Benchmark – Long Cycle

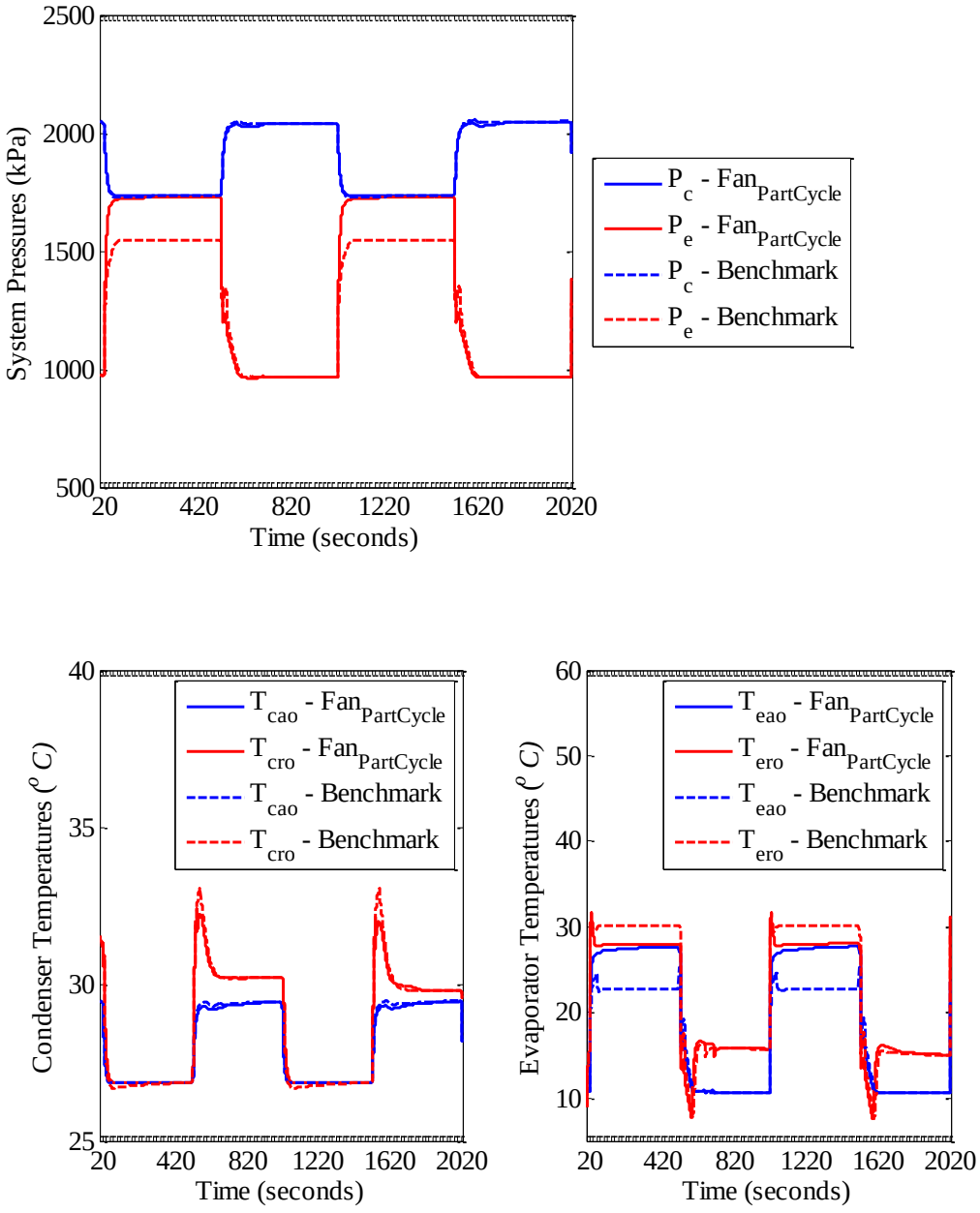

Figure 5.50 System Pressures and Temperatures – Fan Part Cycle Vs Benchmark – Long Cycle

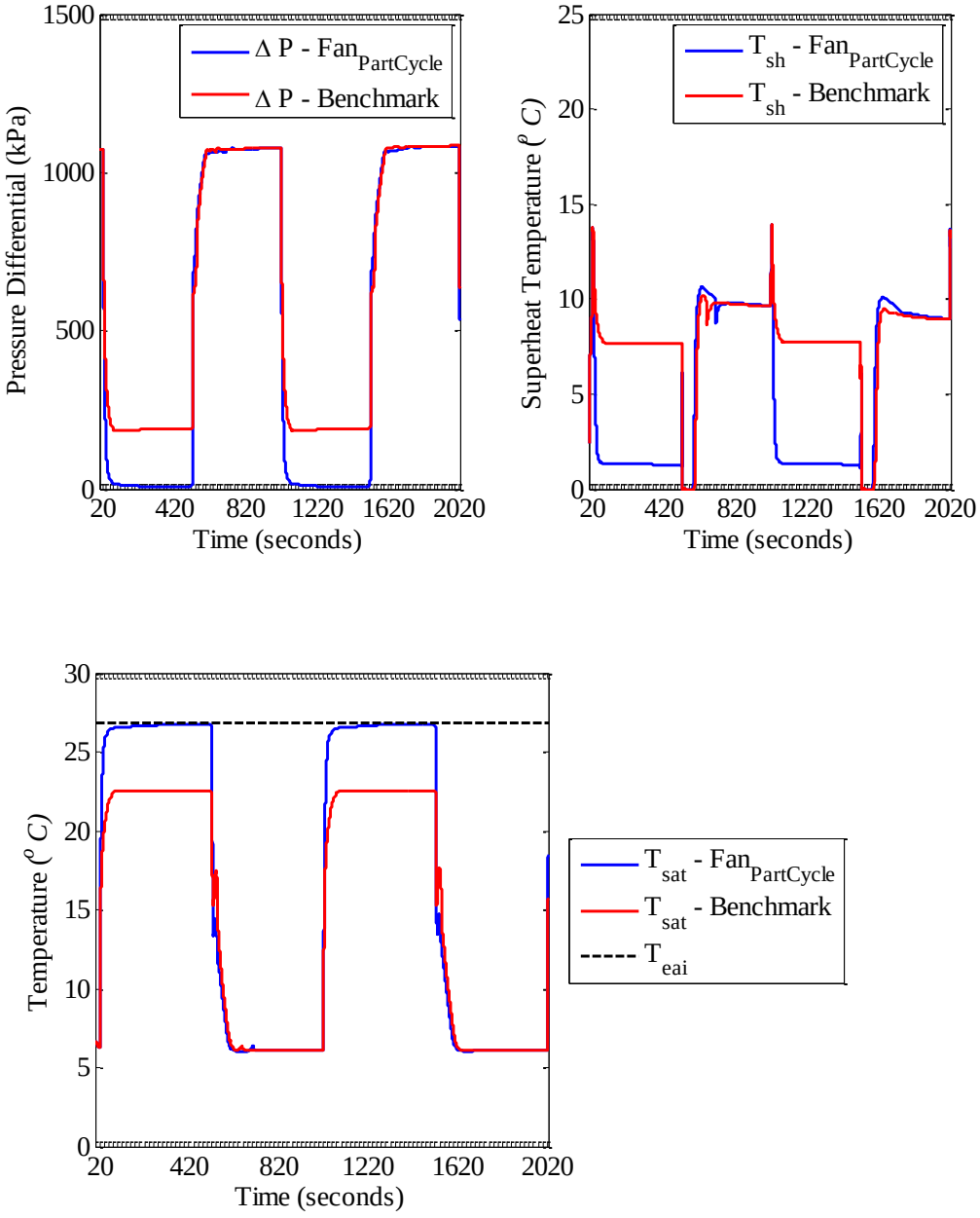

Figure 5.51 Pressure Differential and Superheat – Fan Part Cycle Vs Benchmark – Long Cycle

The final case to compare against benchmark is 'Fan Part Cycle' where the fan remains on for 20 seconds after shutdown. Figure 5.50 shows the system pressures and temperatures in this case. Figure 5.51 shows the pressure differential and superheat for the same. The instantaneous cooling curve in Figure 5.52 shows a tiny increase in both startup and shutdown cooling.

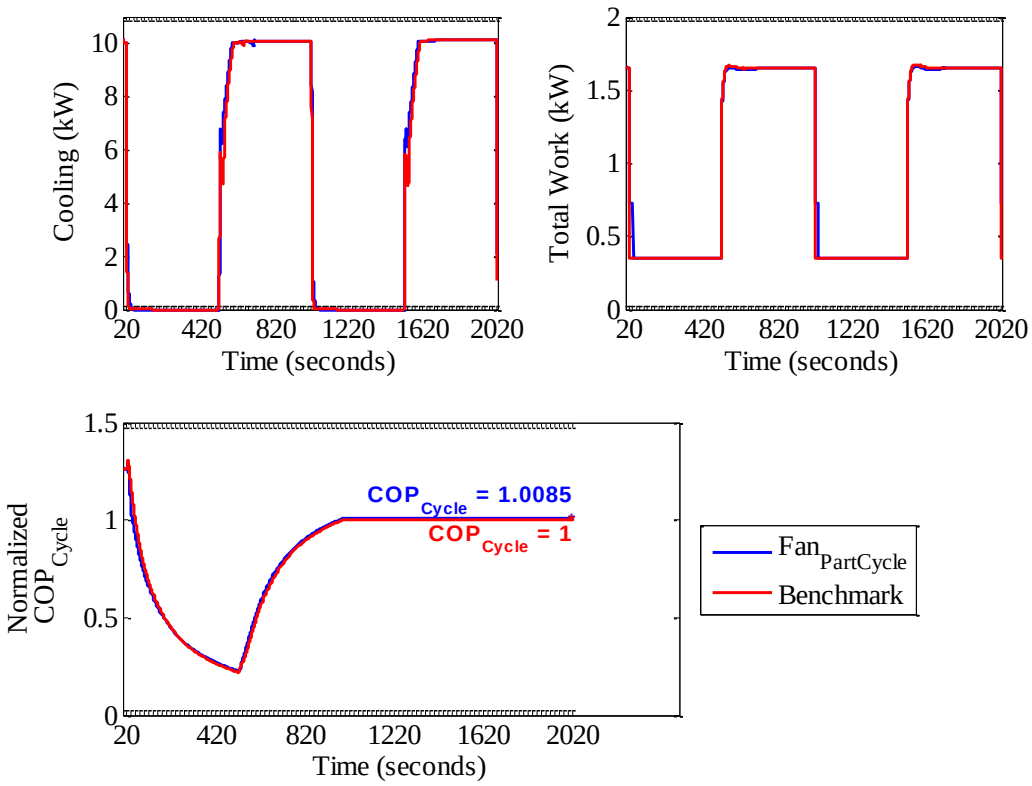

Figure 5.52 Cooling, Work and COP_{Cycle} – Fan Part Cycle Vs Benchmark – Long Cycle

Since the fan is on for more time during shutdown, the extended heat transfer extracts some potential cooling off the refrigerant during shutdown when compared to benchmark. Since the valve is also cycling refrigeration migration to evaporator is avoided thus pressure build up during startup is faster.

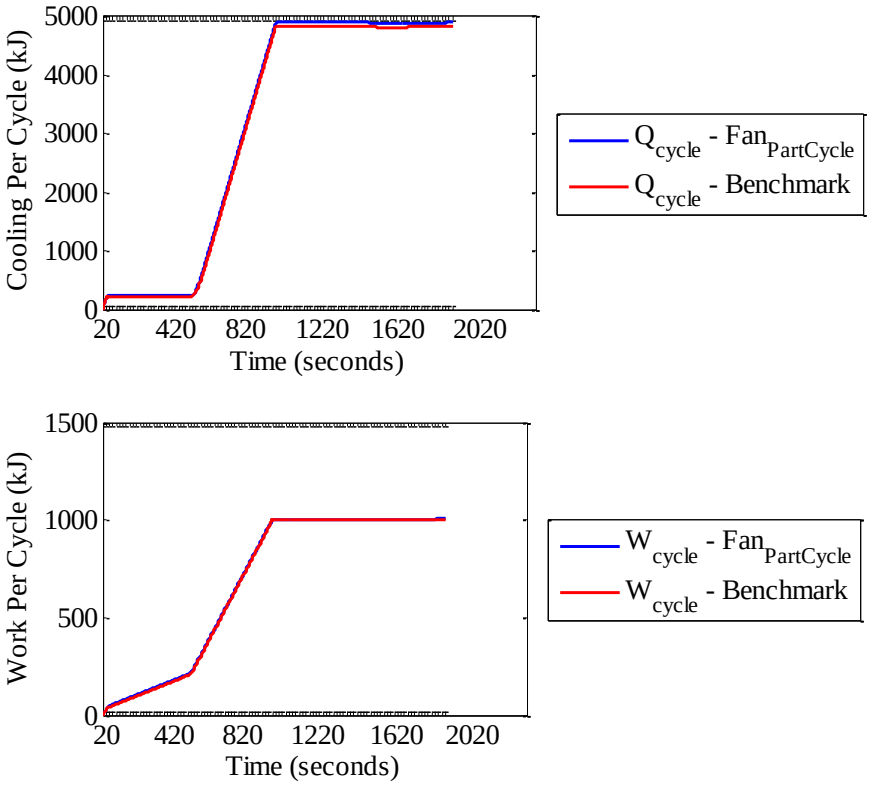

Figure 5.53 Work, Cooling Per Cycle – Fan Part Cycle Vs Benchmark – Long Cycle

Overall, the various cycling schemes show the important dynamics that affects the cyclic efficiency of the system. Comparing the long cycle to the short cycle, there is not much room to improve in terms of efficiency change. One of the discerning characteristic in the long cycle is the major effect of fan cycling on cyclic efficiency. Whereas valve cycling was of primary importance in short cycle, it is intuitive to think that fan cycling plays a major part in the long cycle. This is because, switching of the fan during the long off cycle allows for less power consumption thus giving efficiencies close to benchmark. The relatively less effect of valve cycling here compared to short cycle is attributed to the fact that the longer period of the cycle allows for the pressures and temperatures to settle to equilibrium and any losses in startup efficiencies as such will be insignificant given the length of the cycle. At this point it is expected that changing the S-curve parameters would not yield much change in the COP_{Cycle}. To prove this fact, the following subsections investigate the individual effect of expansion valve and the evaporator fan cycling S-curve parameters on COP_{Cycle}.

5.3.2.2 Expansion Valve

The expansion valve was first considered as the cycling component, while the evaporator fan was assumed to be running for the entire length of the cycle. The values of the S-curve parameters used for this simulation are specified in Table 5.2. The detailed trend analysis was one dimensional where, one parameter was varied, the other parameters were held constant at their benchmark values.

Figure 5.54(a) and 5.54(b) show the effect of shutdown slope and startup slope respectively on COP_{Cycle}. Figure 5.54(c) presents the effect of shutdown time on COP_{Cycle}. Figure 5.54(d) shows the effect of startup time on COP_{Cycle} . Figure 5.54(e) shows the trend of COP_{Cycle} when the valve opening during the off cycle was changed as the parameter. They show the relatively negligible effect on the system's cyclic efficiency when compared to short cycle. Thus the assumed benchmark valve cycling has the best cyclic efficiency when considering valve cycling separately. The conclusions that were drawn from the trend analysis for the valve are summarized in Table 5.5 and they are nothing but benchmark parameters.

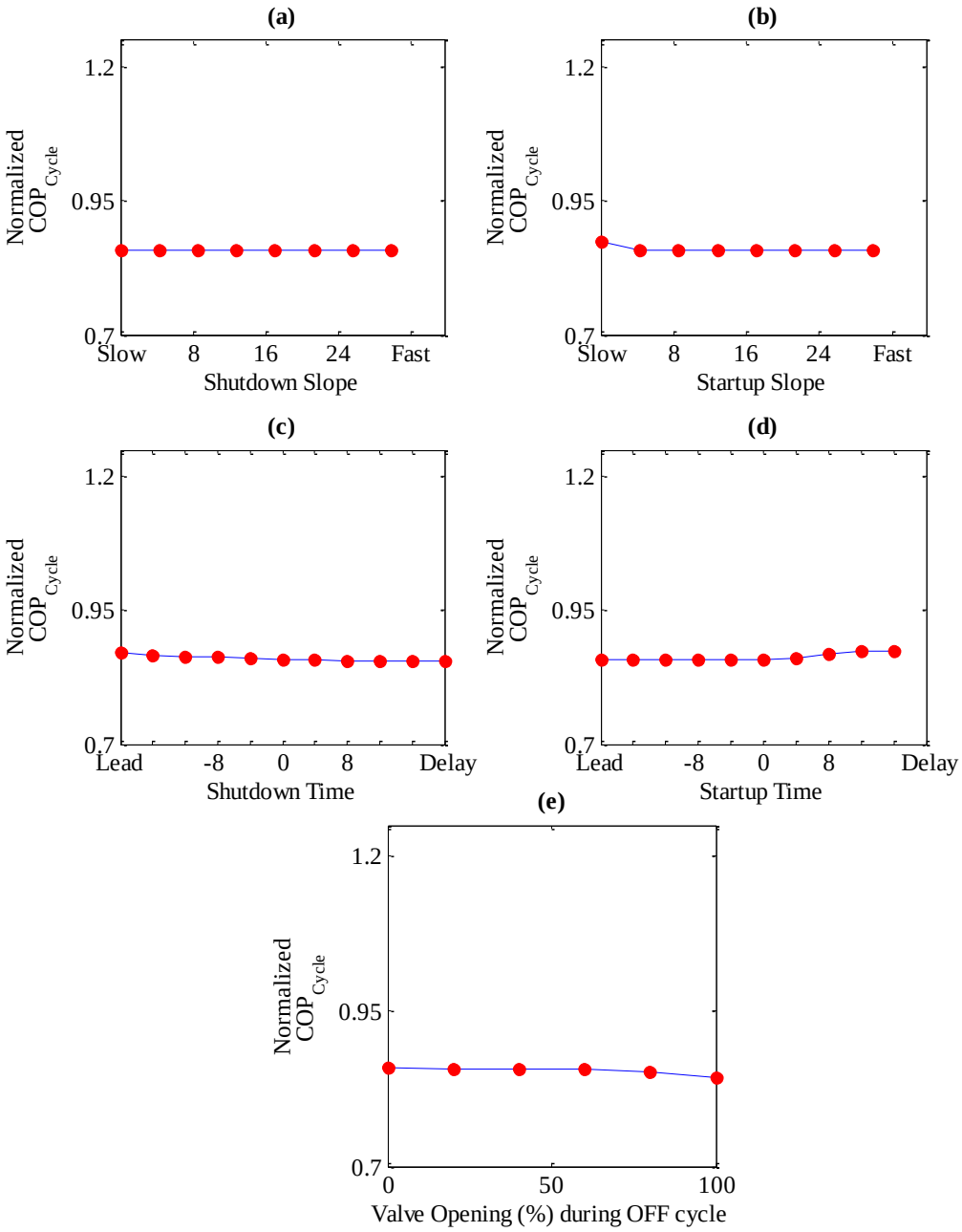

Figure 5.54 Detailed Trends in COP_{Cycle} – Expansion Valve – Long Cycle

Table 5.5 Trend Analysis Summary for Expansion Valve – Long Cycle

Expansion valve cycle S-curve parameter	Recommendations for better cycle efficiency	Representative figures
Shutdown Slope	No significant change	Figure 5.23(a)
Startup Slope	No significant change	Figure 5.23(b)
Shutdown Time	With compressor	Figure 5.23(c)
Startup Time	With compressor	Figure 5.23(d)
Valve opening (%) during OFF cycle	Zero	Figure 5.23(e)

5.3.2.3 Evaporator Fan

The effect of evaporator fan S-curve parameters on $ICOP_{Cycle}$ was then analyzed for the long cycle of 1000 seconds. For these analyses the valve was undergoing benchmark cycling. Similar to the expansion valve analysis, the detailed trend analysis was one dimensional where, one parameter was varied according to the range in Table 5.2, the other parameters were held constant at their benchmark values. Figure 5.55 present the results of the detailed trend analysis for the individual S-curve parameters for the evaporator fan profile.

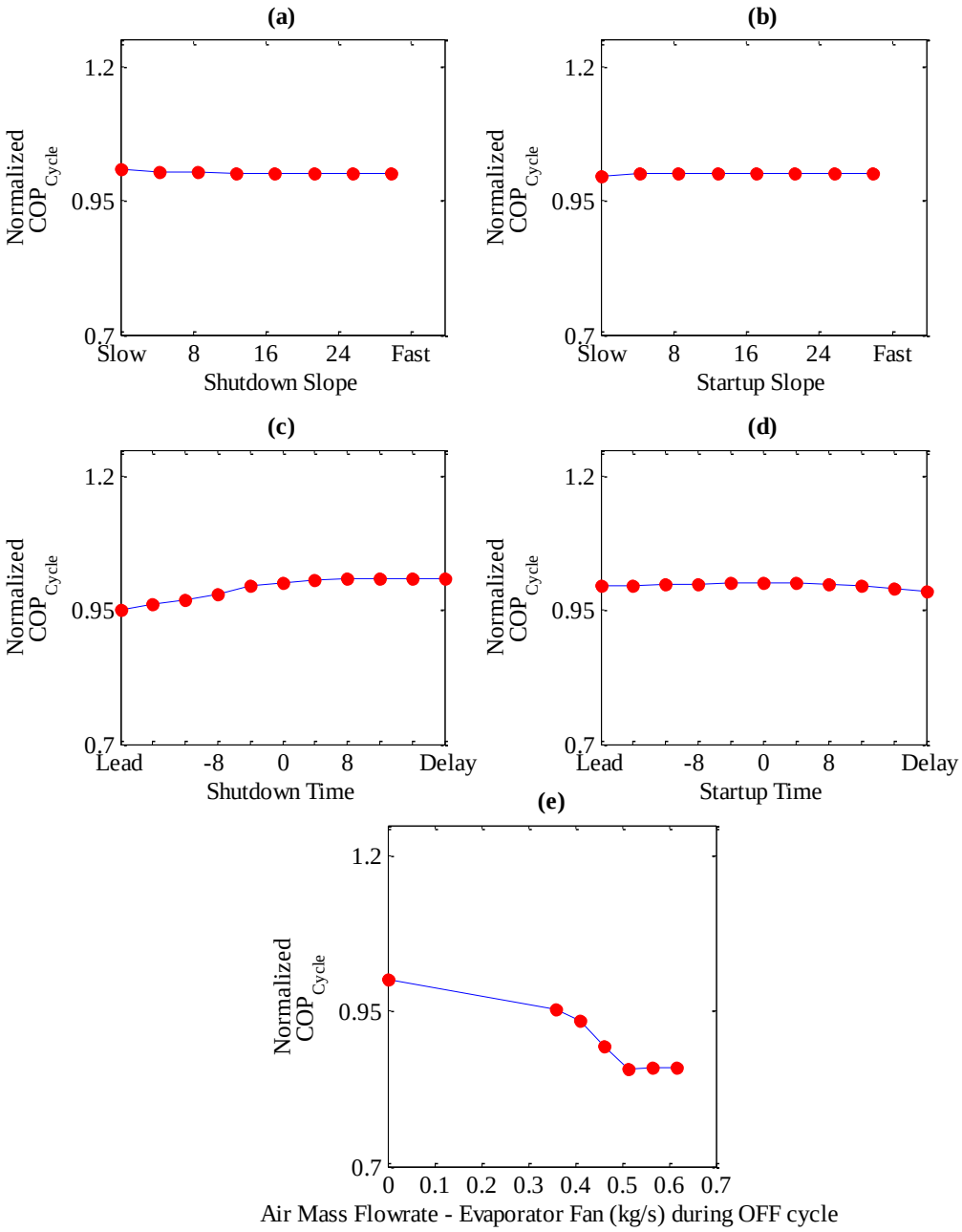

Figure 5.55 Detailed Trends in COP_{Cycle} – Evaporator Fan – Long Cycle

Figure 5.55 shows that fan cycling has more effect on the cyclic efficiency than valve cycling when it comes to long cycle. Figures 5.55(a) and (b) show the negligible effects that the startup and shutdown slopes have on COP_{Cycle}. Figure 5.55(c) shows the effect of fan shutdown time on COP_{Cycle}. There is a very slight increase in efficiency for delaying the fan switching off, about 1%. This case was discussed previously in Subsection 5.1.1.1 as 'Fan Part Cycle'. By defining satisfactory performance as one where the efficiency gain is within 2% of best gain, the benchmark condition of turning the fan off along with the compressor can be termed satisfactory. Figure 5.55(d) shows the negligible effect of startup time on the system efficiency. The only parameter which had any impact on system efficiency was the fan speed during the off cycle presented in Figure 5.55(e). Since the fan would be consuming power for any speed greater than zero, setting the fan to run at speed greater than zero throughout the off cycle is not advised. In such cases, the fan consumes power while not providing any cooling in return, thus leading to loss of efficiency. The conclusions that were drawn from the trend analysis are summarized in Table 5.6.

As already discussed at the end of Subsection 5.3.2.1, there is not much room for improvement in the efficiency of the long cycle when altering the profile of the benchmark valve and fan. Thus the recommendations for the expansion valve and evaporator fan profiles remain same as benchmark.

Table 5.6 Trend Analysis Summary for Evaporator Fan – Long Cycle

Evaporator fan cycle S-curve parameter	Recommendations for better cycle efficiency	Representative figures
Shutdown Slope	No significant change	Figure 5.55(a)
Startup Slope	No significant change	Figure 5.55(b)
Shutdown Time	Best: Delay Satisfactory: With Compressor	Figure 5.55(c)
Startup Time	Best : With Compressor	Figure 5.55(d)
Air mass flow rate during OFF cycle	Zero	Figure 5.55(e)

5.4 Optimization

Benchmark cycling involves cycling the expansion valve and the evaporator fan along with the compressor. The optimization parameters for the expansion valve and the evaporator fan profiles were as follows:

1. Shutdown time
2. Startup time

The optimization was carried out in 2 parts. The first part was just the expansion valve optimization where the evaporator fan was cycling with benchmark parameters. Secondly the evaporator fan profile was optimized while expansion valve was

performing cycling according to benchmark conditions. As discussed in Subsection 4.2 the Nelder Mead simplex algorithm was used to determine the minimum because of the already stated advantages. Since the short cycle displayed significant changes in efficiency with respect to the valve and the fan S-curve parameters, the optimization was carried out only for this cycle length.

5.4.1 Expansion Valve Optimization

This subsection presents and explains the results of the optimization carried out for the expansion valve. The aim was to find out the optimum parameters for the expansion valve namely: startup time and shutdown time. Table 5.7 presents the initial guess and the results. Figure 5.56 shows the resulting expansion valve cycle.

Table 5.7 Expansion Valve Optimization Results

Expansion valve cycle S-curve parameter	**Guess**	**Solution**
Shutdown time (seconds)	0	-19.9940
Startup time (seconds)	0	8.0623

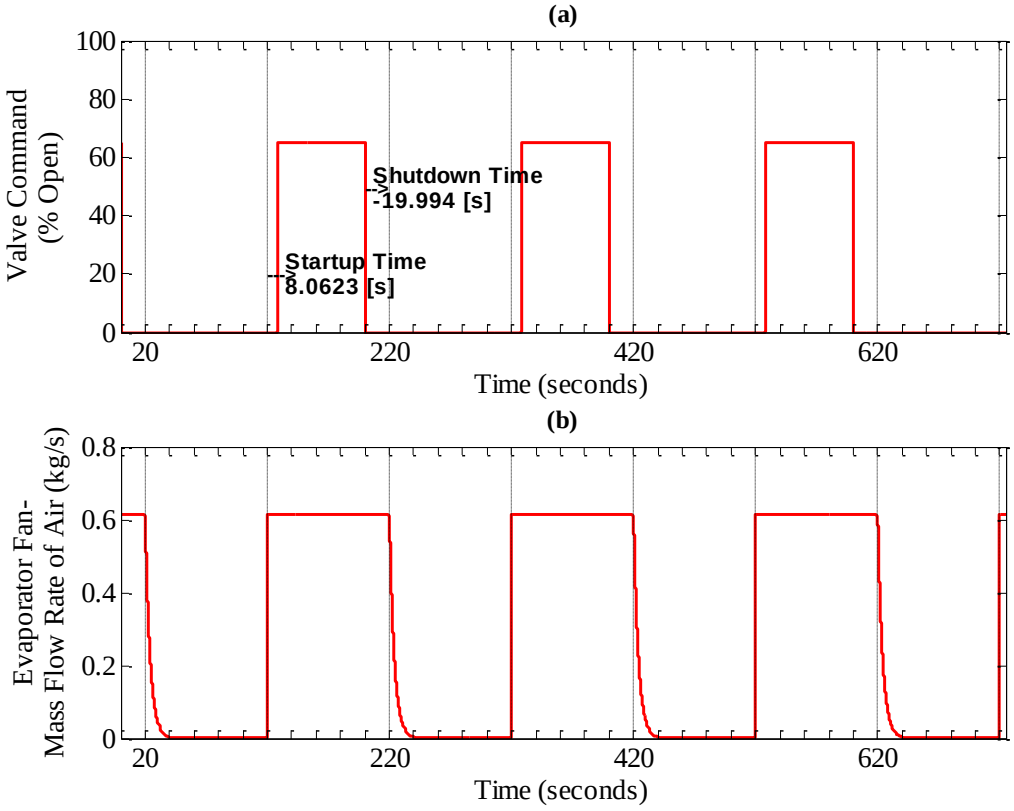

Figure 5.56 Expansion Valve Optimization Results

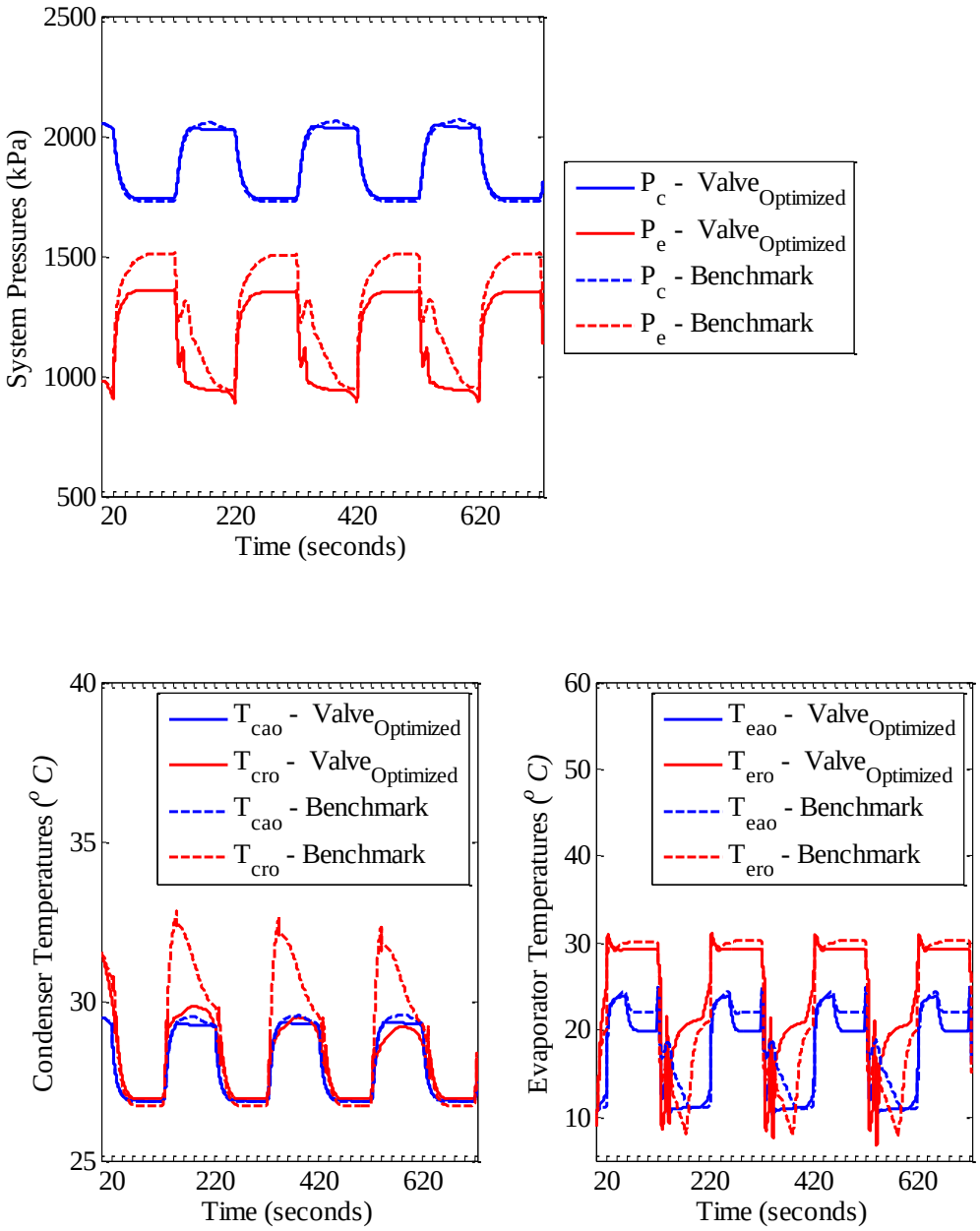

Figure 5.57 System Pressures and Temperatures – Valve Optimized Vs Benchmark – Optimization

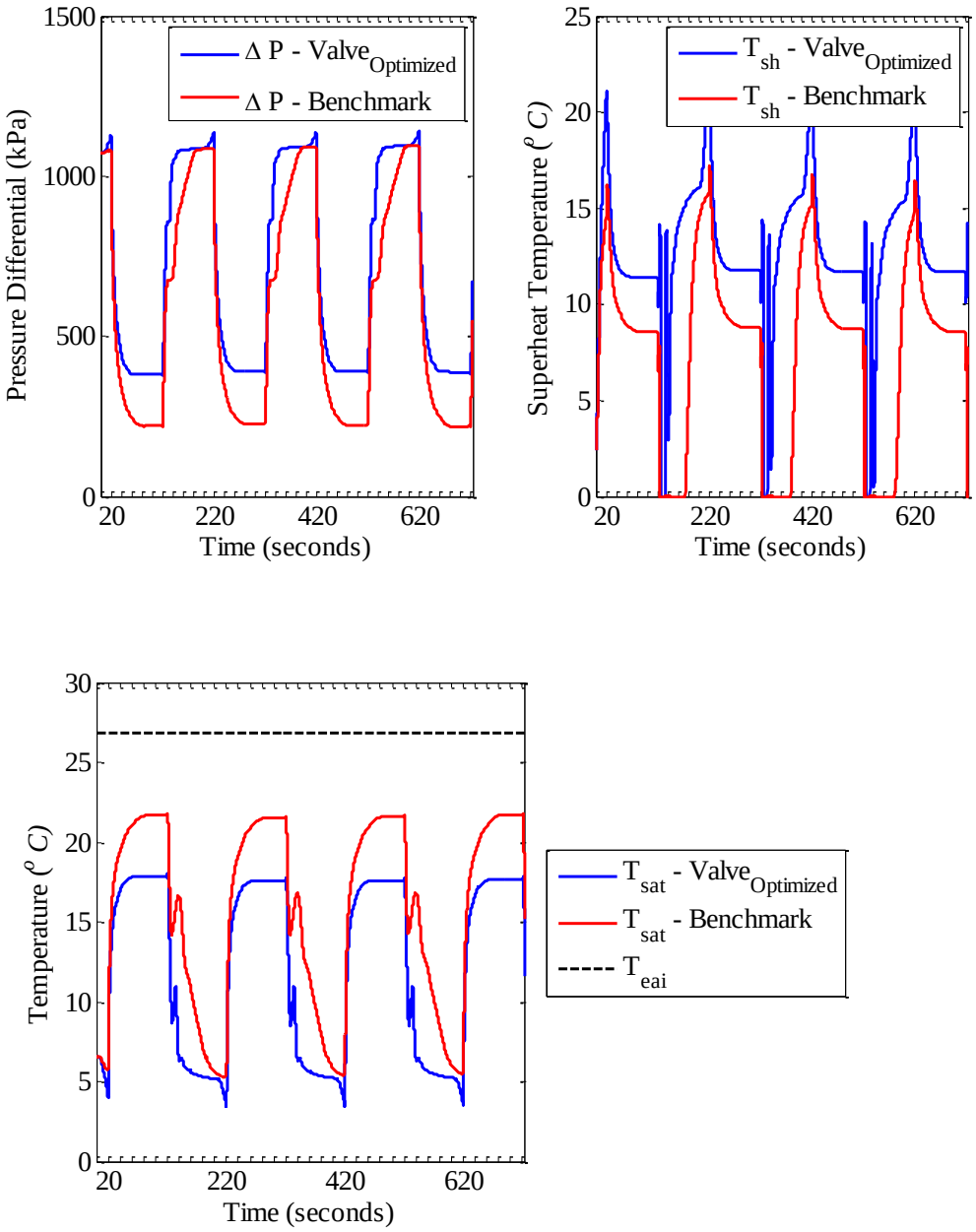

Figure 5.58 Pressure Differential and Superheat – Valve Optimized Vs Benchmark – Optimization

Figures 5.57 – 5.60 help in understanding the physical reason behind why this sort of valve cycling is preferred in this context. Figure 5.57 show the system pressures and temperatures of the 'Valve Optimized' and the benchmark condition. 'Valve Optimized' condition inflicts a better pressure pull down at startup because of the delay. This also affects the superheat as shown in Figure 5.58. The refrigerant is superheated very quickly in this case whereas the benchmark condition takes a while to get superheated. By delaying the valve at shutdown the system's pressure differential is also maintained higher.

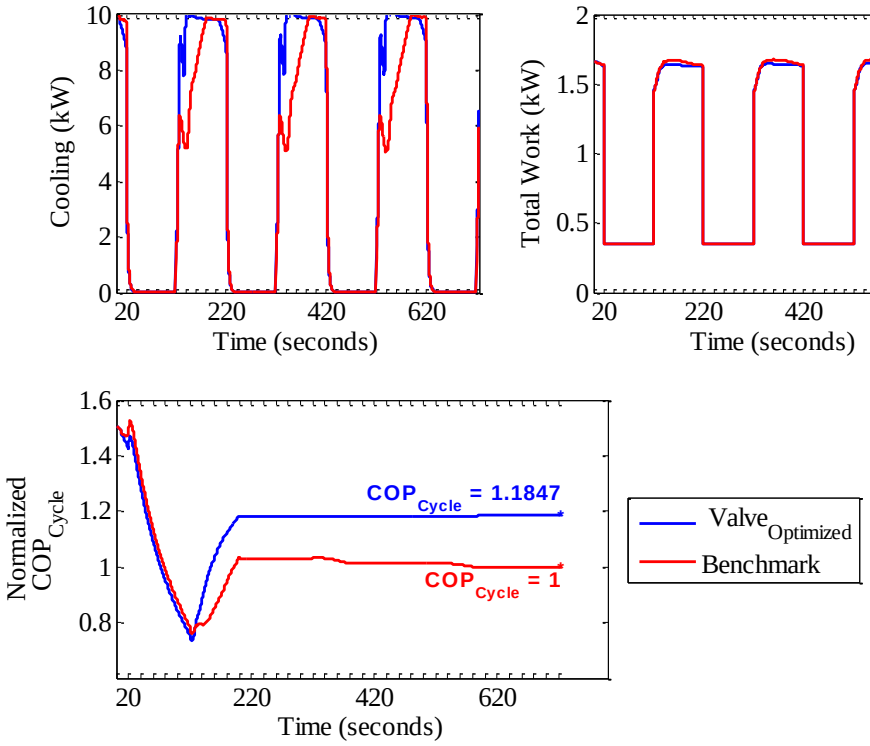

Figure 5.59 Cooling, Work and COP_{Cycle} – Valve Optimized Vs Benchmark – Optimization

Figure 5.59 shows the superior startup cooling for 'Valve Optimized'. The cooling during startup reaches full capacity almost instantaneously. This is because of how quickly the refrigerant at the evaporator outlet gets superheated. Since 'Valve Optimized' has much faster superheat response, the cooling performance is vastly better. Figure 5.60 shows the consequential high cooling per cycle for this condition. Most of this is because of the valve delaying at startup to get to superheat faster. Since the fan and compressor are cycling with benchmark conditions, the work per cycle for 'Valve Optimized' is same as benchmark.

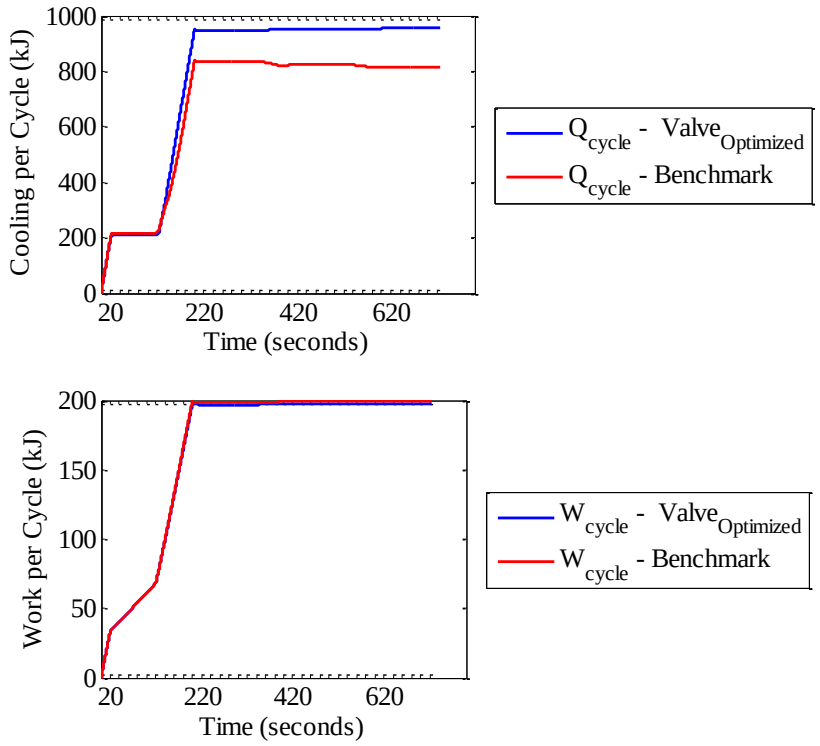

Figure 5.60 Work, Cooling Per Cycle – Valve Optimized Vs Benchmark – Optimization

The ‘Valve Optimized’ Cycle shows a really high improvement in efficiency about 18% compared to benchmark. The practical implications of such a scheme are discussed later.

5.4.2 Evaporator Fan Optimization

This subsection presents and explains the results of the optimization carried out for the evaporator fan. The aim was to find out the optimum parameters for evaporator fan startup and shutdown time. Table 5.8 presents the initial guess and the results. Figure 5.61 shows the resulting evaporator fan cycle.

Table 5.8 Evaporator Fan Optimization Results

Expansion valve cycle **S-curve parameter**	**Guess**	**Solution**
Shutdown time (seconds)	0	17.7971
Startup time (seconds)	0	2.4043

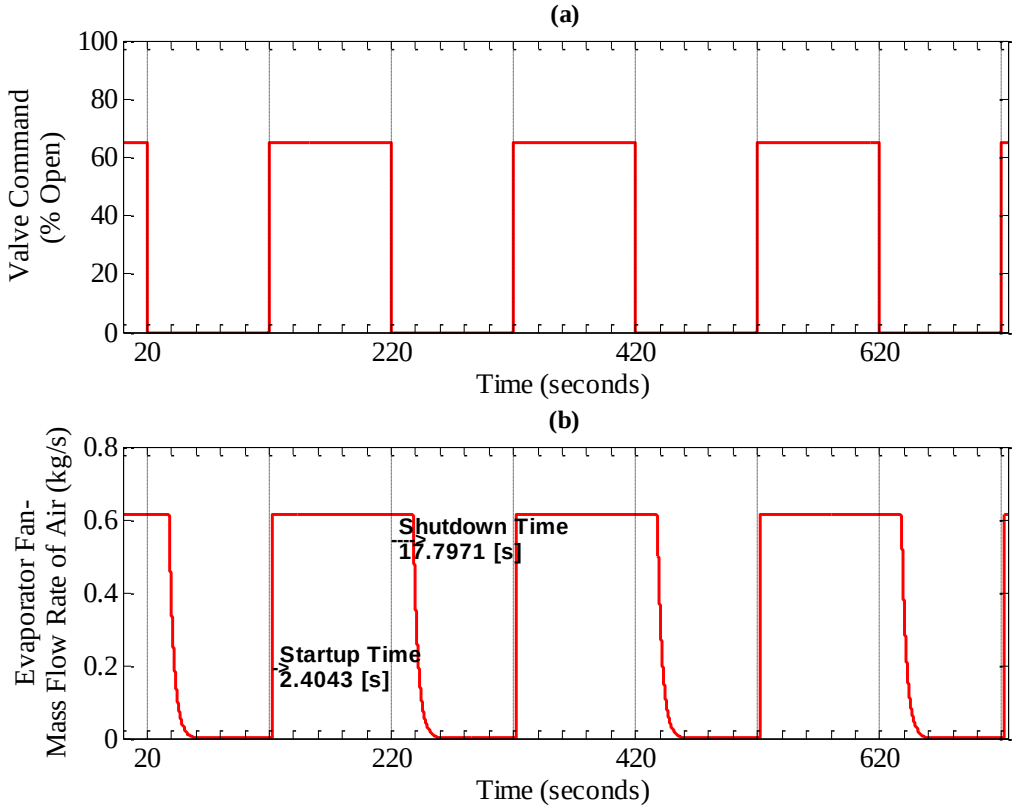

Figure 5.61 Evaporator Fan Optimization Results

Figures 5.62 – 5.66 show the dynamics of the 'Fan Optimized' cycle when compared to benchmark. Figure 5.62 shows the system pressures and temperatures. The pressures in the 'Fan Optimized' cycle almost equalize despite the valve being closed at shutdown and the entire of off cycle. This is because the fan is on for some time beyond shutdown because of the delay. This facilitates an extended heat transfer which can be seen from the superheat plot in Figure 5.63.

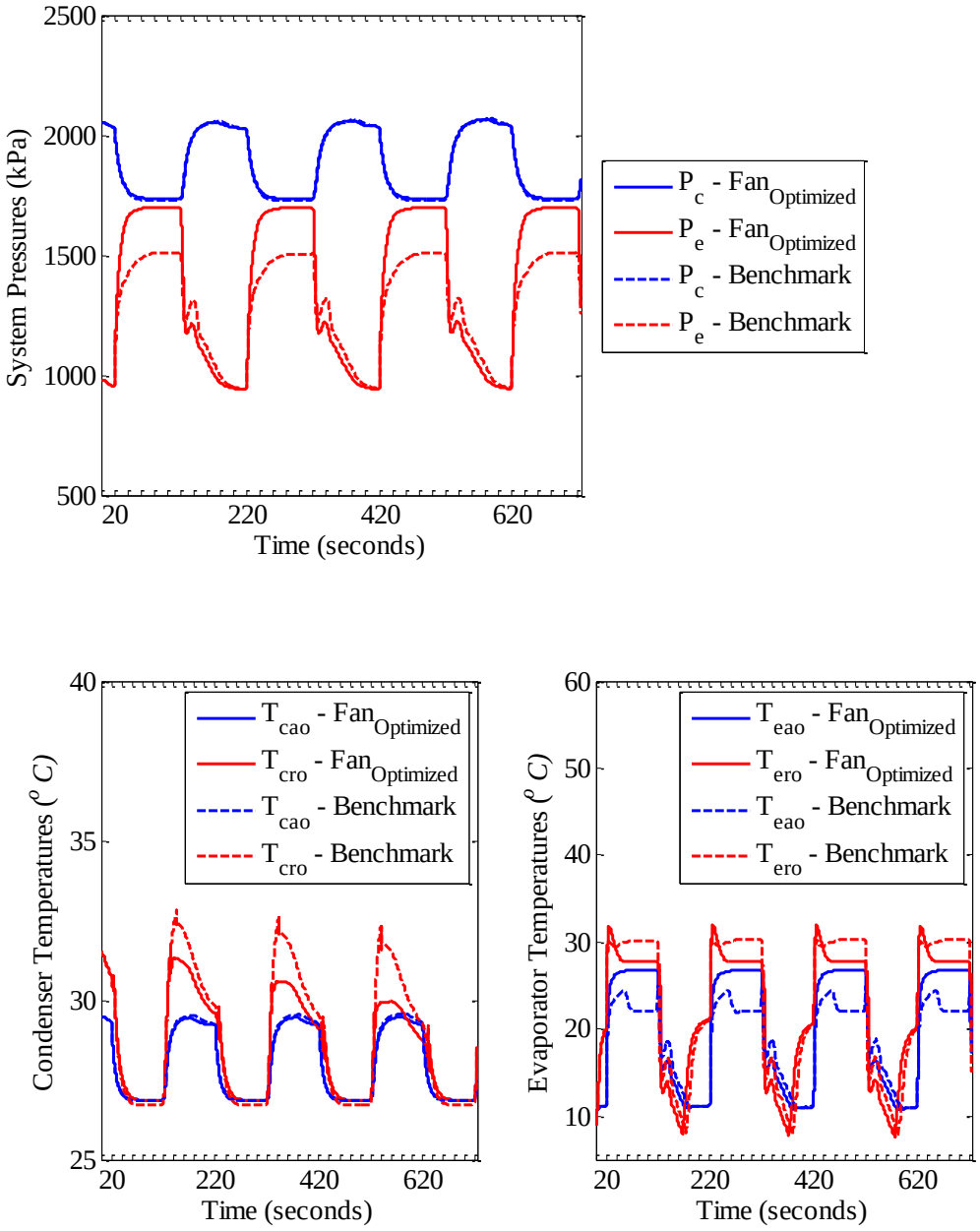

Figure 5.62 System Pressures and Temperatures – Fan Optimized Vs Benchmark – Optimization

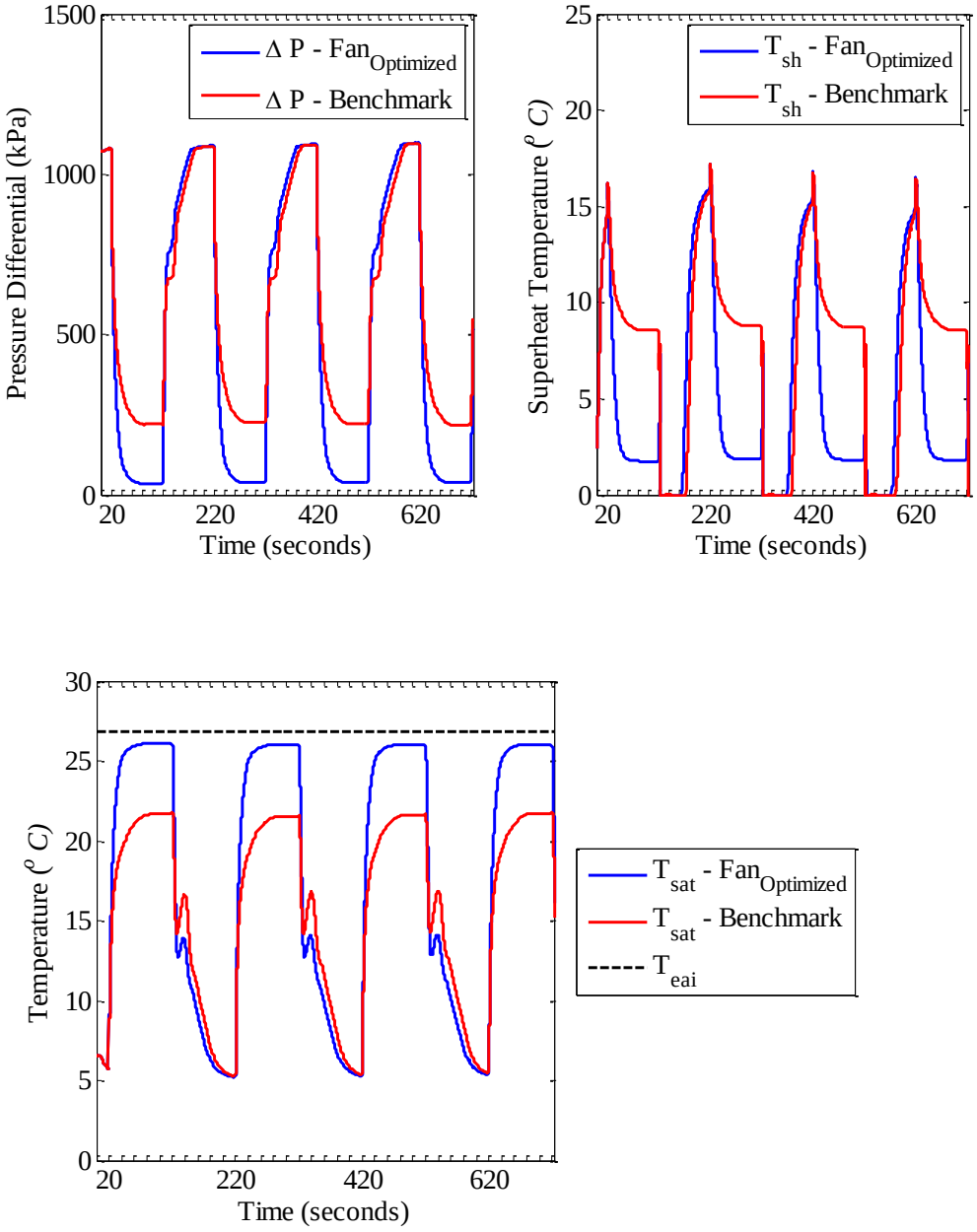

Figure 5.63 Pressure Differential and Superheat – Fan Optimized Vs Benchmark – Optimization

Figure 5.64 shows the instantaneous cooling and power consumption. 'Fan Optimized' cycling results in a 5% increase in efficiency because the delay of the fan during shutdown extracts some potential cooling. This cycling scheme is very much similar to the 'Fan Part Cycle' discussed in Subsection 5.3.1.1. The small delay at startup facilitates a faster pressure build up and superheat. Despite the fan being off for the first few seconds of startup, the instantaneous cooling reaches its capacity faster because of the faster build up of pressure and superheat as shown in Figure 5.63. Figure 5.64 also shows the fan being part on after shutdown consuming some extra power compared to benchmark.

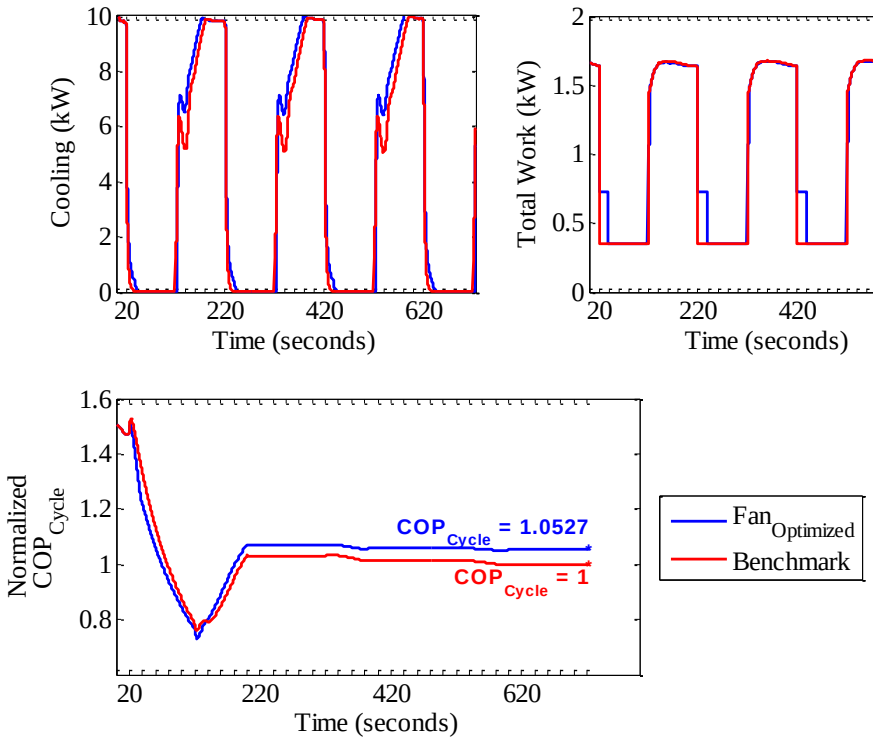

Figure 5.64 Cooling, Work and COP_{Cycle} – Fan Optimized Vs Benchmark – Optimization

However this extra power does result in some extra cooling in the initial part of the off cycle. Figure 5.65 shows the cooling per cycle and work per cycle for 'Fan Optimized' condition. Work per cycle is higher than benchmark because the fan is on for more time than benchmark.

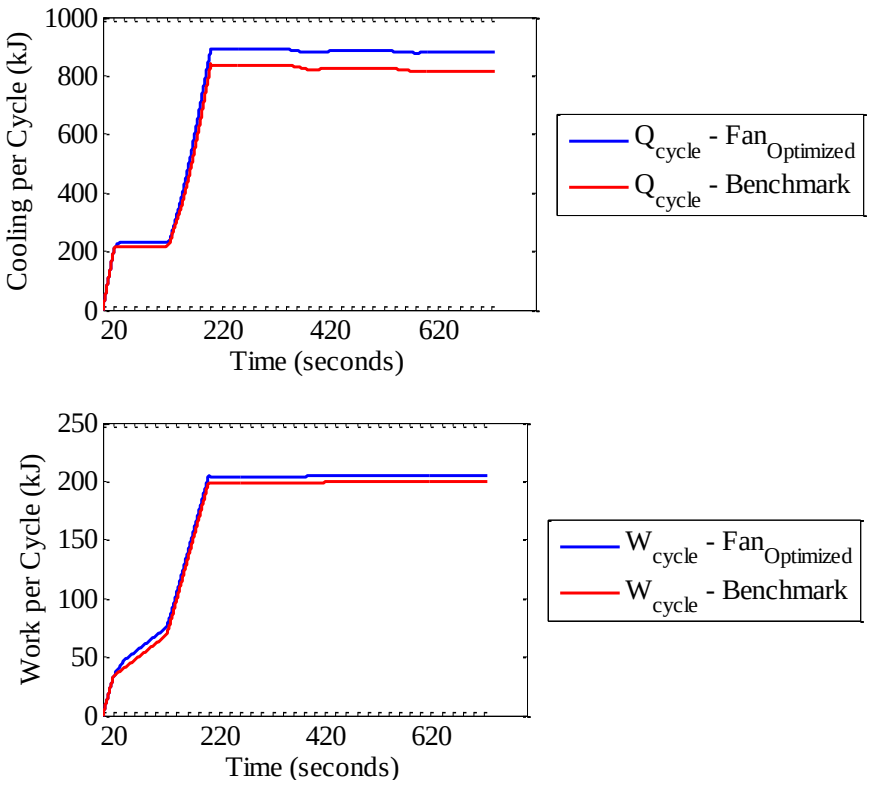

Figure 5.65 Work, Cooling Per Cycle – Fan Optimized Vs Benchmark – Optimization

5.4.3 Combined Optimization

In this subsection the results of the simultaneous optimization of expansion valve and evaporator fan are presented. A comparison of individual optimization results put together and the simultaneous optimization will shed light on the coupling of the two problems. The parameters to be optimized in the simultaneous optimization are as follows:

- Expansion valve shutdown time
- Expansion valve startup time
- Evaporator fan shutdown time
- Evaporator fan startup time

The initial guess and the results of the simultaneous optimization are shown in Table 5.9. The resulting valve and fan cycles are shown in Figure 5.66. Figures 5.67 – 5.70 compare the simultaneous optimization to the combined effect of the individual optimizations put together.

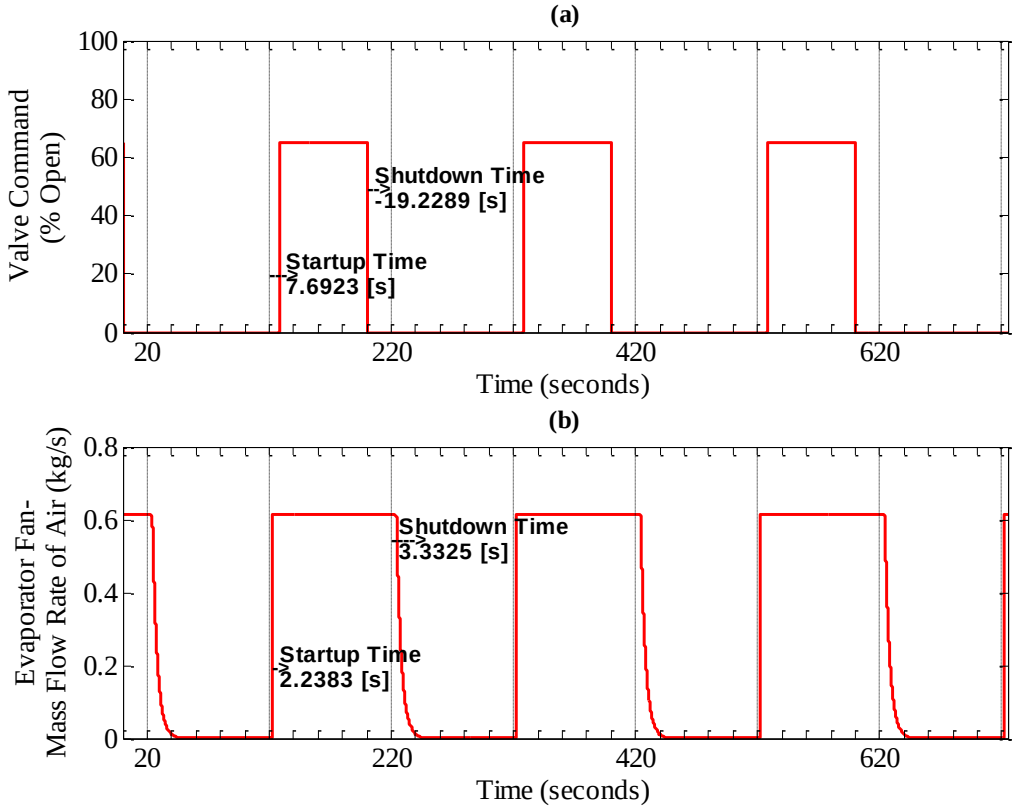

Figure 5.66 Combined Optimization Results

Table 5.9 Combined Optimization Results

Cycle	S-curve parameter	Guess	Solution
Expansion Valve	Shutdown time (seconds)	0	-19.2289
	Startup time (seconds)	0	7.6923
Evaporator Fan	Shutdown time (seconds)	0	3.3325
	Startup time (seconds)	0	2.2383

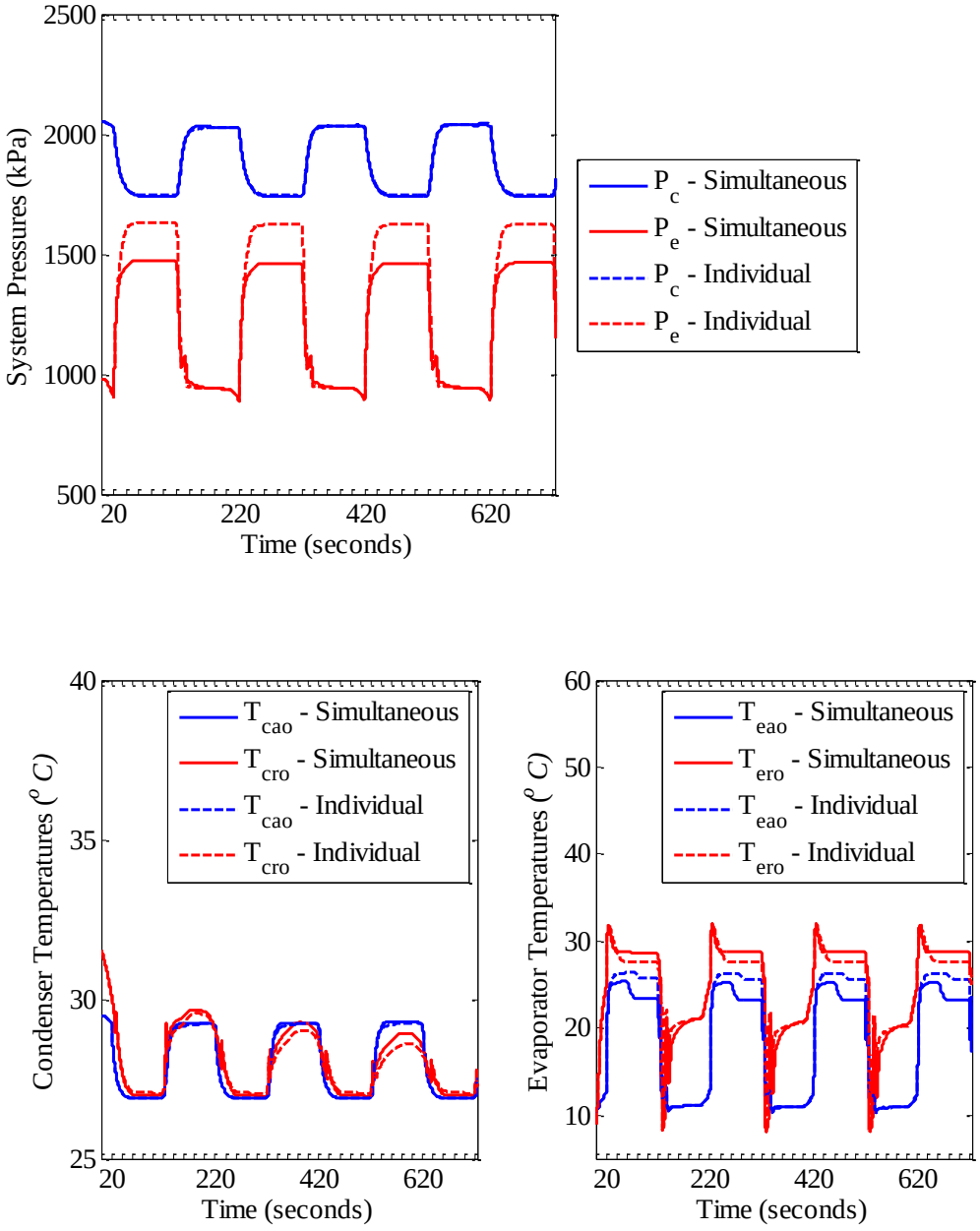

Figure 5.67 System Pressures and Temperatures – Simultaneous Vs Individual – Optimization

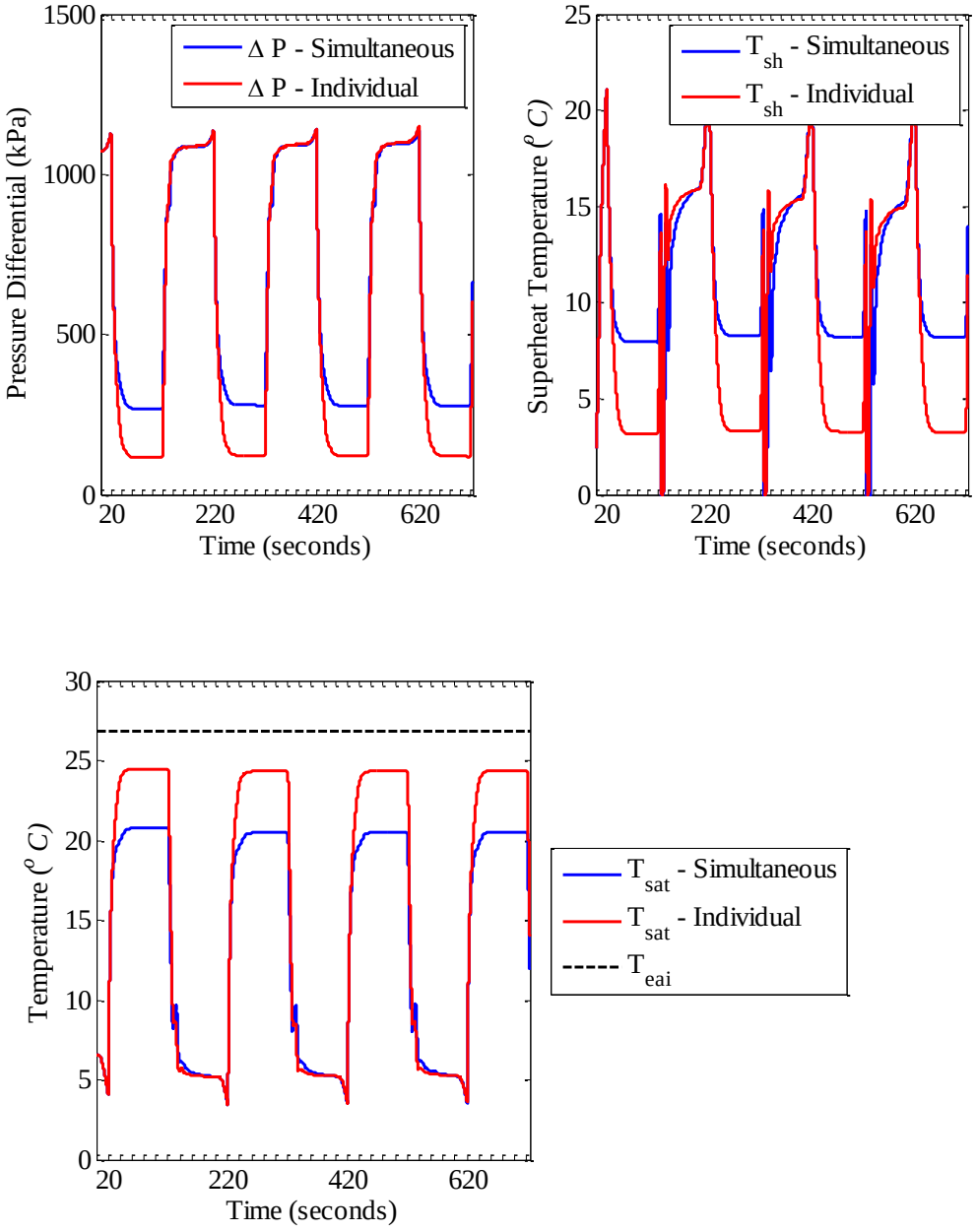

Figure 5.68 Pressure Differential and Superheat – Simultaneous Vs Individual – Optimization

Figure 5.67 shows the system pressures and temperatures of the simultaneous (case 1) and the combined effect of the individual optimization (case 2). The evaporator pressure settles at a higher value in case 2 because the fan is on for more time in case 2 than case 1. This is also evident in the pressure differential plot in Figure 5.68 where the pressure differential for case 1 is much higher in the off cycle than for case 2. Figure 5.69 shows that the change in efficiency between the two approaches is just off by 2%. The slightly higher efficiency for case 1 is because the fan is on for less time during the off cycle thus consuming less power overall as in Figure 5.70.

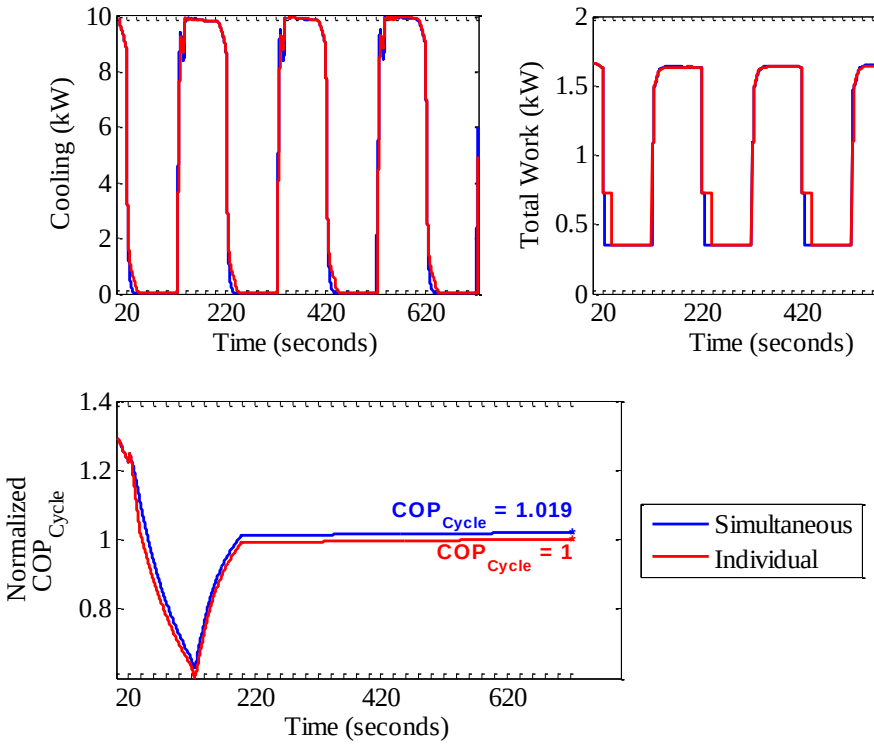

Figure 5.69 Cooling, Work and COP_{Cycle} – Simultaneous Vs Individual – Optimization

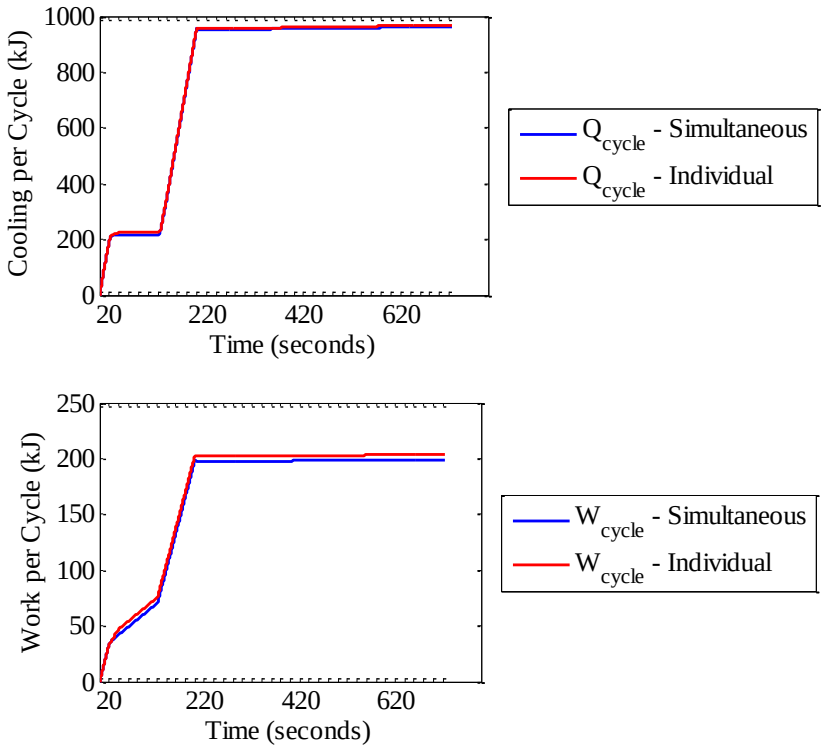

Figure 5.70 Work, Cooling Per Cycle – Simultaneous Vs Individual – Optimization

Thus the way in which the optimization procedure was carried out did not make much difference since they are only off by 2%. Anything within 2% of best gain has already been termed as a satisfactory performance. Hence the final recommendations based on the optimization simulations are given in Table 5.10. These are very much in keeping with the recommendations obtained after the trend analysis in Tables 5.2 and 5.3.

Table 5.10 Final Recommendations for Expansion Valve and Evaporator Fan Cycles

Actuator	S-curve parameter	Recommendations for better cycle efficiency
Expansion Valve	Shutdown Time	Lead
	Startup Time	Delay
Evaporator Fan	Shutdown Time	Delay
	Startup Time	Delay

5.4.4 Discussion

The benchmark set in this thesis is valve and fan cycling synchronously with the compressor. However in practice the valve is controlled for superheat by a controller. There is a need to look at how the optimized cycle does in practice. So a comparison of the optimized cycle to a superheat controlled cycle is done here. There are two types of control that is compared with the optimized cycle.

- Control Scheme 1: Valve position is determined by the superheat controller through the on and off cycle.

- Control Scheme 2: Valve position is determined by the superheat controller through the on cycle. During the off cycle the controller is over ridden and is completely shut off to avoid migration.

The controller used in the two schemes was a simple PI controller. With the controlled cycles as the new benchmark set at 1, a comparison with the optimized cycle is done. There is a vast change in efficiency of the optimized cycle with respect to control scheme 1. The main reason for this inefficiency is that the controller is still in action during the off cycle. This lets some refrigerant into the evaporator which presents the migration problem. However in the optimized cycle, the valve shuts off before the compressor shuts down thus preventing the refrigerant from occupying the evaporator. The valve command for control scheme 1 is shown in Figure 5.71. During the off cycle the valve is still open at some percentage.

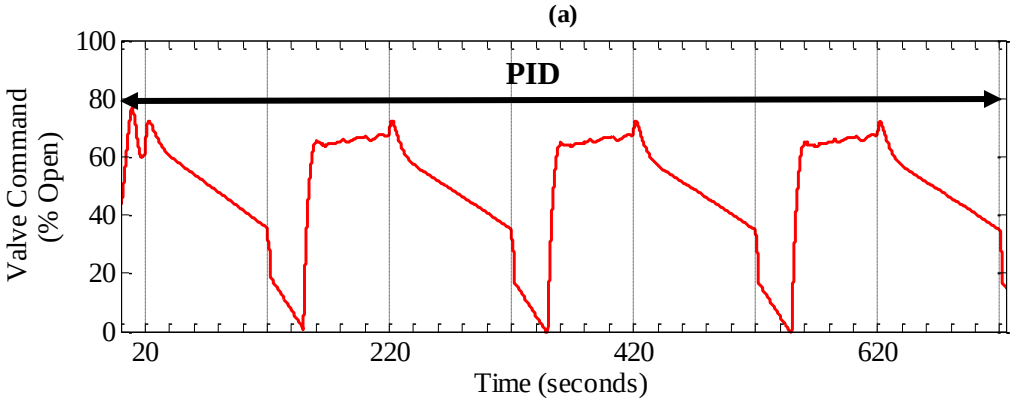

Figure 5.71 Valve Command for Control Scheme 1

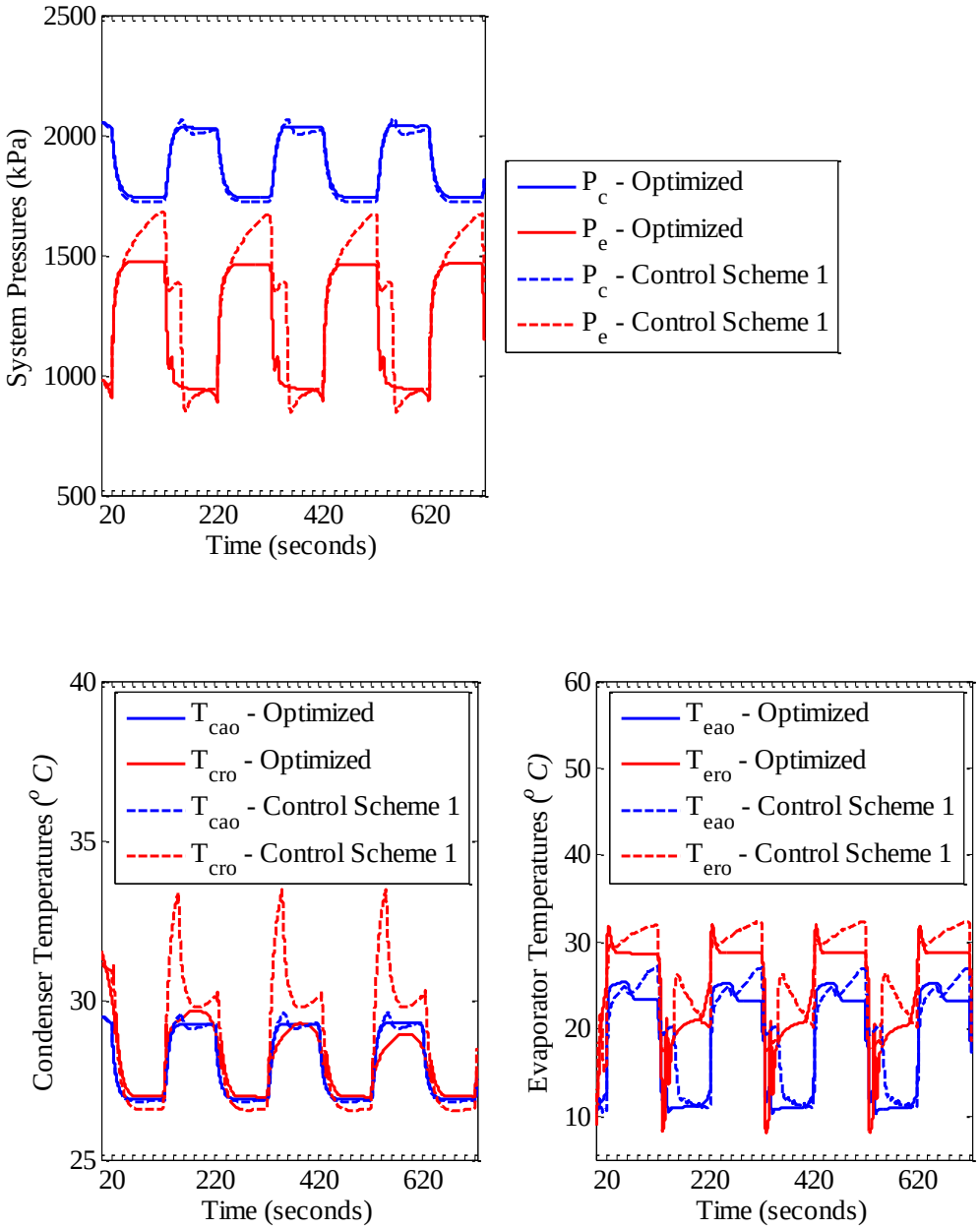

Figure 5.72 System Pressures and Temperatures – Optimized Vs Control Scheme 1

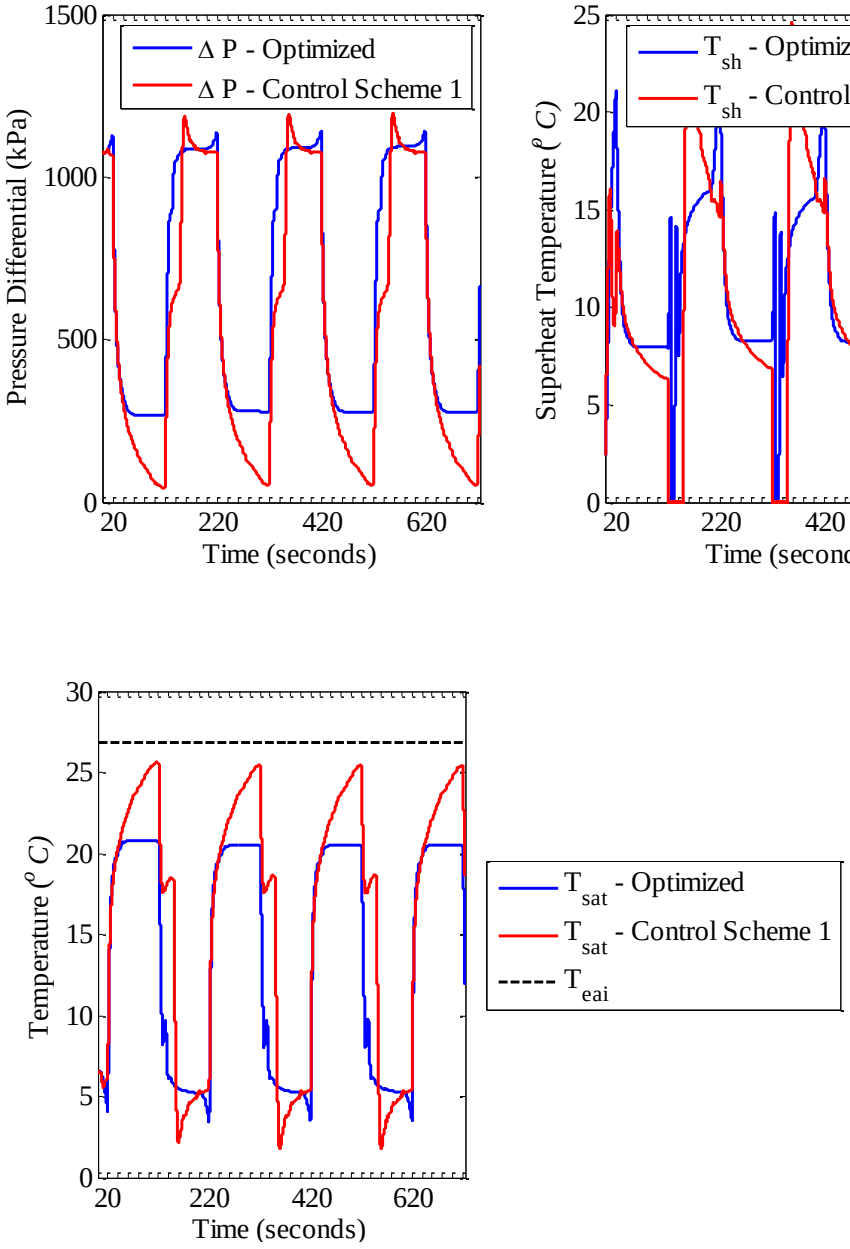

Figure 5.73 Pressure Differential and Superheat – Optimized Vs Control Scheme 1

Figure 5.72 presents the system pressures and temperatures. Since the valve is not completely shut off during the off cycle for control scheme 1, the pressures get closer to each other when compared to the optimized condition. The optimized cycle has a faster superheat build up as shown in Figure 5.73. This is the reason for the cooling to reach its rated capacity so fast for the optimized cycle. Figure 5.74 shows the instantaneous cooling got at the startup. The power consumed by the compressor and the fan are almost similar for both the conditions.

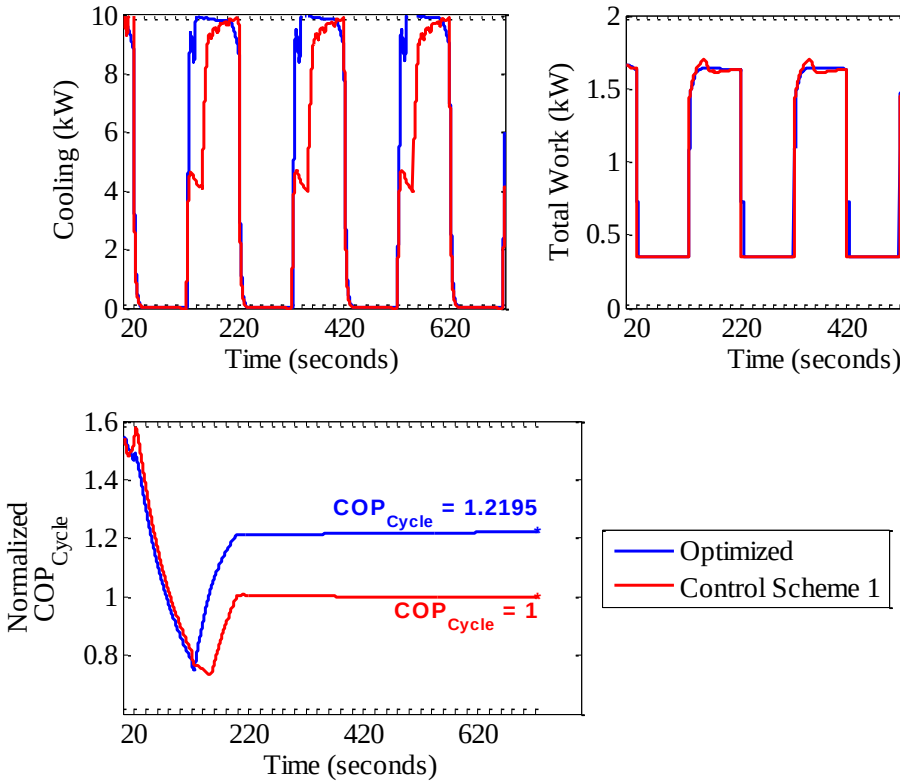

Figure 5.74 Cooling, Work and COP_{Cycle} – Optimized Vs Control Scheme 1

Figure 5.75 shows the cooling and work per cycle. Because of the better startup performance the optimized cycle has significantly more cooling compared to control scheme 1.

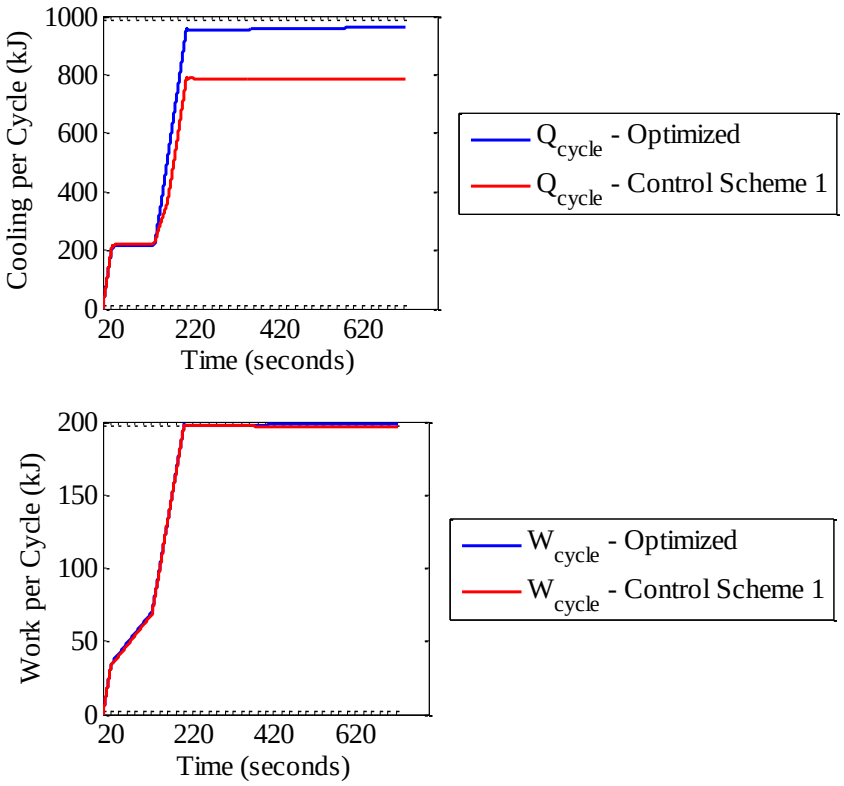

Figure 5.75 Work, Cooling Per Cycle – Optimized Vs Control Scheme 1

The final comparison is between the optimized cycle and control scheme 2. The valve command for control scheme 2 is shown in Figure 5.76. Basically the control signal gets multiplied by the compressor signal so that the controller works only during

the on cycle whereas in the off cycle it is switched off and the valve goes to zero position. This method aims to couple the controller's ability to attain superheat faster while also turning off the valve during shutdown for better startup performance. Figures 5.77 – 5.80 compare control scheme 2 with the optimized cycle.

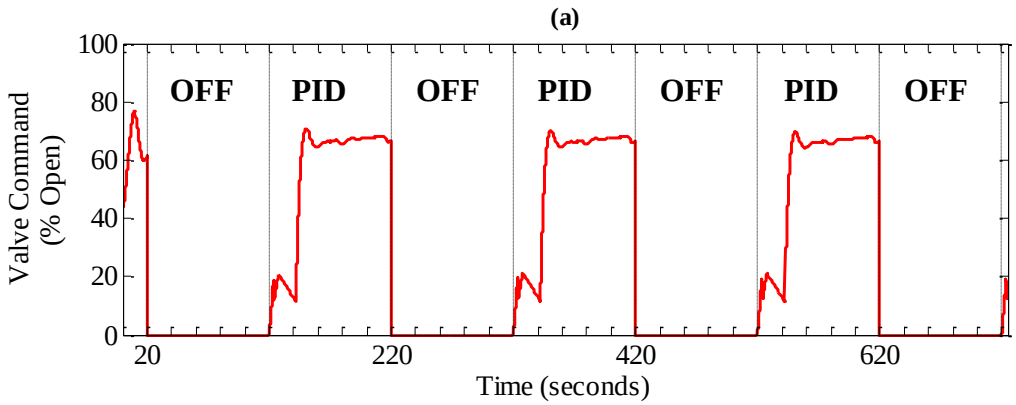

Figure 5.76 Valve Command for Control Scheme 2

Figure 5.77 shows the system pressures and temperatures. The pressures look almost the same but for the off cycle when, control scheme 2 does lose a bit of the pressure differential as shown in Figure 5.78. The superheat during the on cycle is also almost similar. However the controller is still relatively sluggish to push the superheat up. Control scheme 2 thus is slower compared to the optimized cycle. This is evident from the instantaneous cooling curve as shown in Figure 5.79.

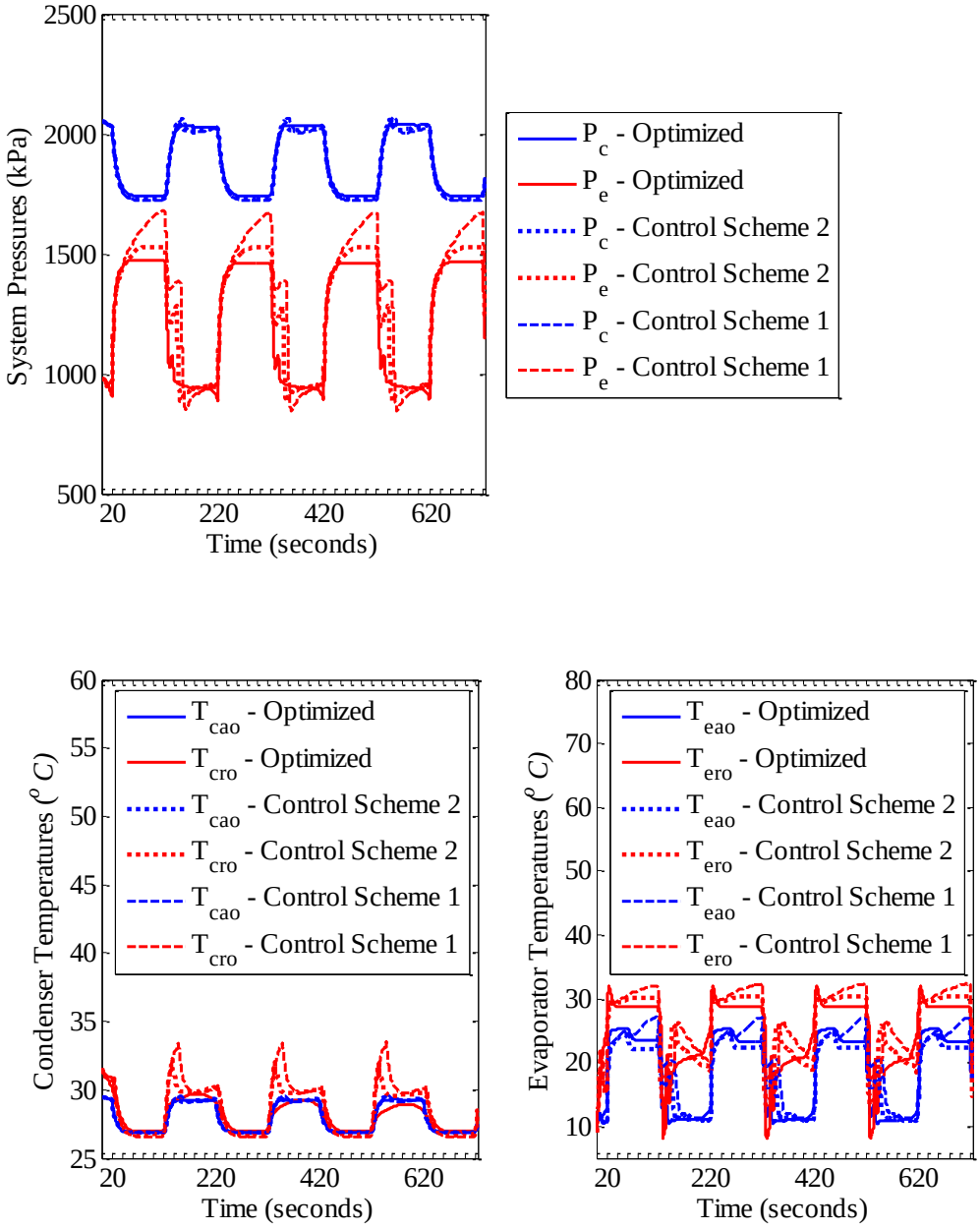

Figure 5.77 System Pressures and Temperatures – Optimized Vs Control Scheme 2 Vs Control Scheme 1

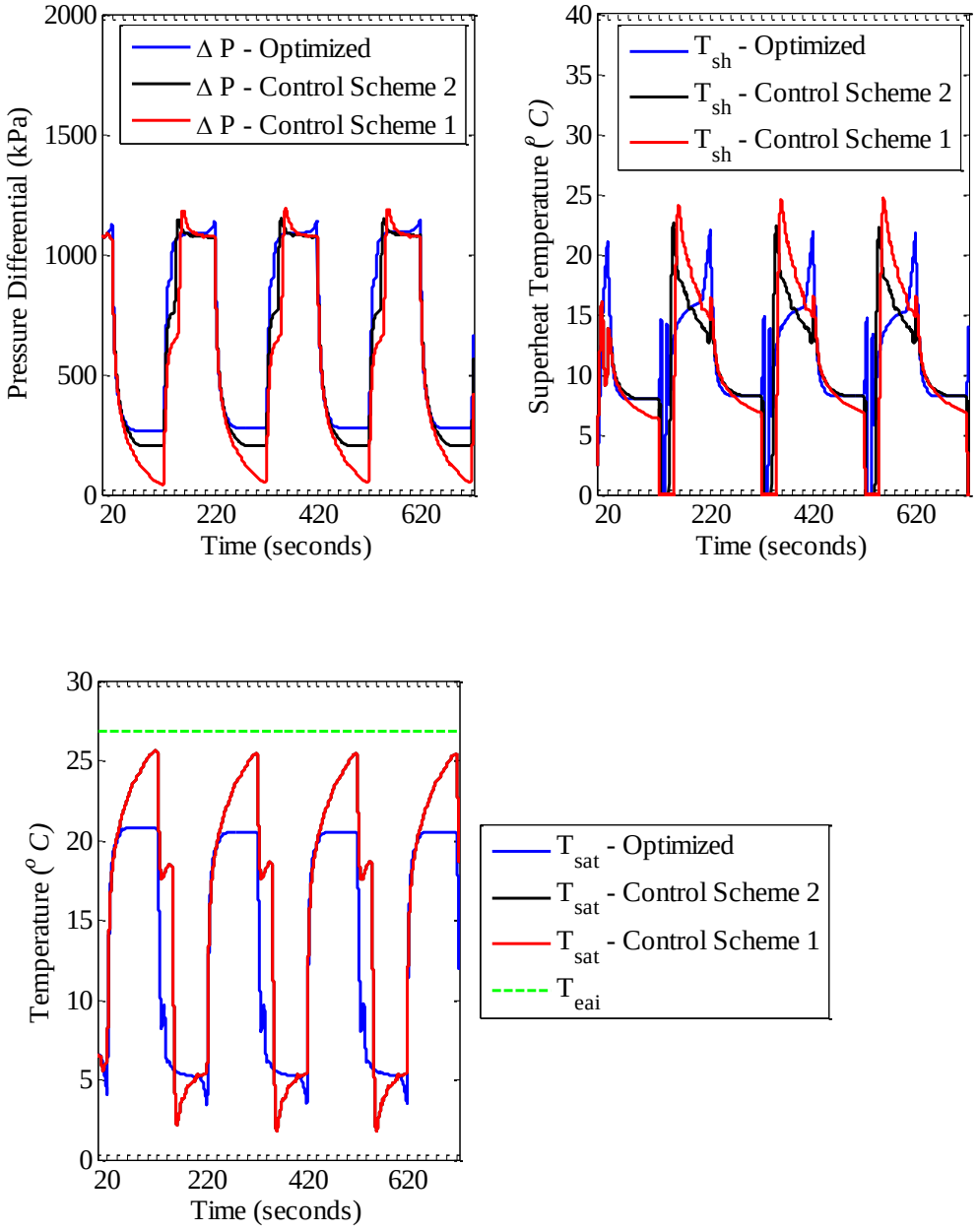

Figure 5.78 Pressure Differential and Superheat – Optimized Vs Control Scheme 2 Vs Control Scheme 1

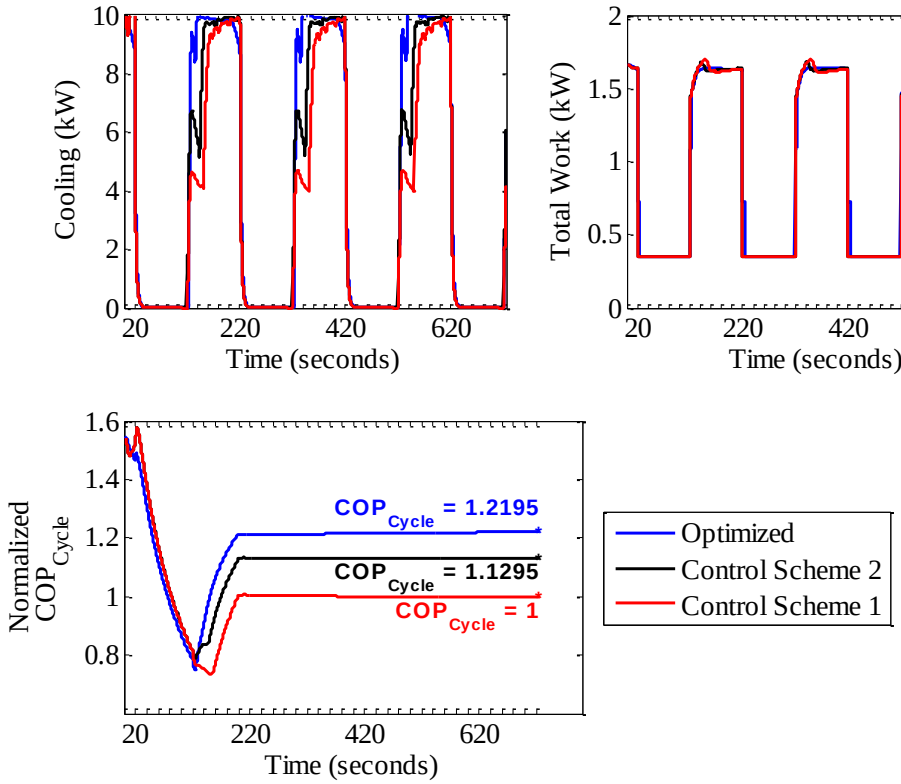

Figure 5.79 Cooling, Work and COP_{Cycle} – Optimized Vs Control Scheme 2 Vs Control Scheme 1

The cooling during startup for the optimized cycle is still superior compared to control scheme 2. The interesting thing here is that by forcing the valve to shutoff at shutdown, control scheme 2 has proven that the startup performance gets better when compared to scheme 1. Figure 5.80 shows the cooling and work per cycle. As observed because of the significantly extra startup cooling, the cooling per cycle of the optimized cycle is higher than control scheme 2.

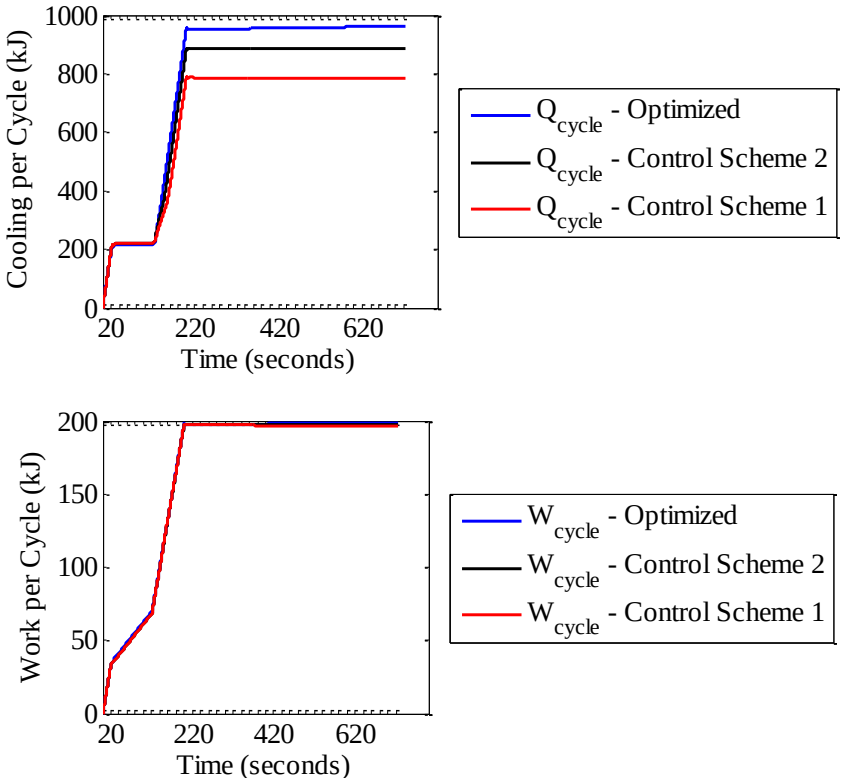

Figure 5.80 Work, Cooling Per Cycle – Optimized Vs Control Scheme 2 Vs Control Scheme 1

The comparisons of control scheme 1 and control scheme 2 with the optimized cycle shows that the optimized cycle does better. The main reason is how the cycle regulates superheat. By forcing control scheme 1 to cut off the valve during off cycle, there is an increase in the startup performance. Also it proves that just using the superheat controller is not that efficient a strategy so in practice the controller should at least be turned off during the off cycle. A more sophisticated superheat controller might match the optimized cycle in terms of efficiency.

6. EXPERIMENTS

The experiments that were conducted on the TRANE system discussed in Section 3 are elaborated in this section. The experimental approach to obtaining the trends is very similar to that used in simulation. More details on the nature of the experiments and the approach used to collect data are given in the Appendix. First the cyclic efficiency trends for various cycling schemes are discussed. Refrigerant migration during off cycle is noted as the biggest effect on decreasing system efficiency whereas fan delay is identified as a strategy that increases system's cyclic efficiency. Secondly, recommendations and feasibility of a successful real time optimization approach are presented. Factors like experimental conditions and time taken for a solution are considered here to propose the recommendations.

6.1 Experimental COP_{Cycle} Trends

In this subsection a series of experimental tests is presented that would showcase the effect of the various S-curve parameters on the $ICOP_{Cycle}$. These simulations were conducted separately for the expansion valve and the evaporator fan so that individual responses of $ICOP_{Cycle}$ to the different S-curve parameters could be established. The experiments were run for two different cycle lengths to see the effect cycle length has on $ICOP_{Cycle}$. In order to visualize the efficiency changes better, normalized COP_{Cycle} was used as in equation for plotting the trends. Thus it is evident that for the benchmark cycle normalized COP_{Cycle} is 1.

6.1.1 Short Cycle

Experimental results obtained for a short cycle length of 200 seconds are presented here. This was to understand how normalized COP_{Cycle} varies with respect to the S-curve parameters during rapid cycling times. Under such circumstances, the pressures and temperatures will not go to equilibrium during the off cycle. Thus, what trend normalized COP_{Cycle} followed with various S-curve parameters was an interesting thing to study.

6.1.1.1 Gross Trends

Similar to the simulation approach, there is a necessity to look at whether the normalized COP_{Cycle} changes are significant enough to merit a further detailed investigation. A quick comparison of some possible cycling schemes was done to identify this. Figure 6.1 shows the gross trends for the various cycling schemes. With the benchmark for comparison at 1 the other cycling schemes are presented. To refresh what the various cycling schemes mean refer Table 5.2. From the figure it was evident that 'All on' and 'Fan Cycle Valve On' conditions were having the worst performance. In order to explain the physical reason behind the efficiency changes, the following analyses are presented.

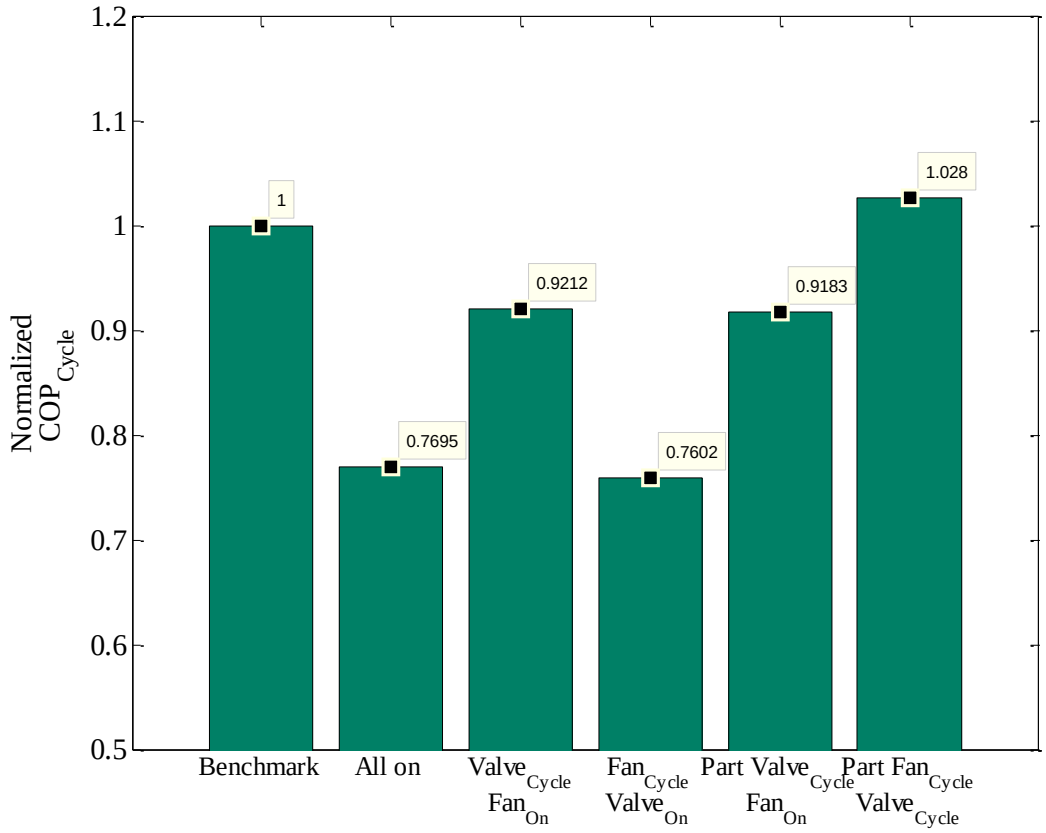

Figure 6.1 COP_{Cycle} Gross Trends of Various Cycling Schemes – Short Cycle – Experiment

Figure 6.2 presents the system pressures and temperatures for the ‘’All on’ and the benchmark conditions. The striking change between the two is the pressure curve. In the all on condition since the valve is on during the on cycle, the pressures equalized whereas in the benchmark the valve is closed so the pressures do not equalize.

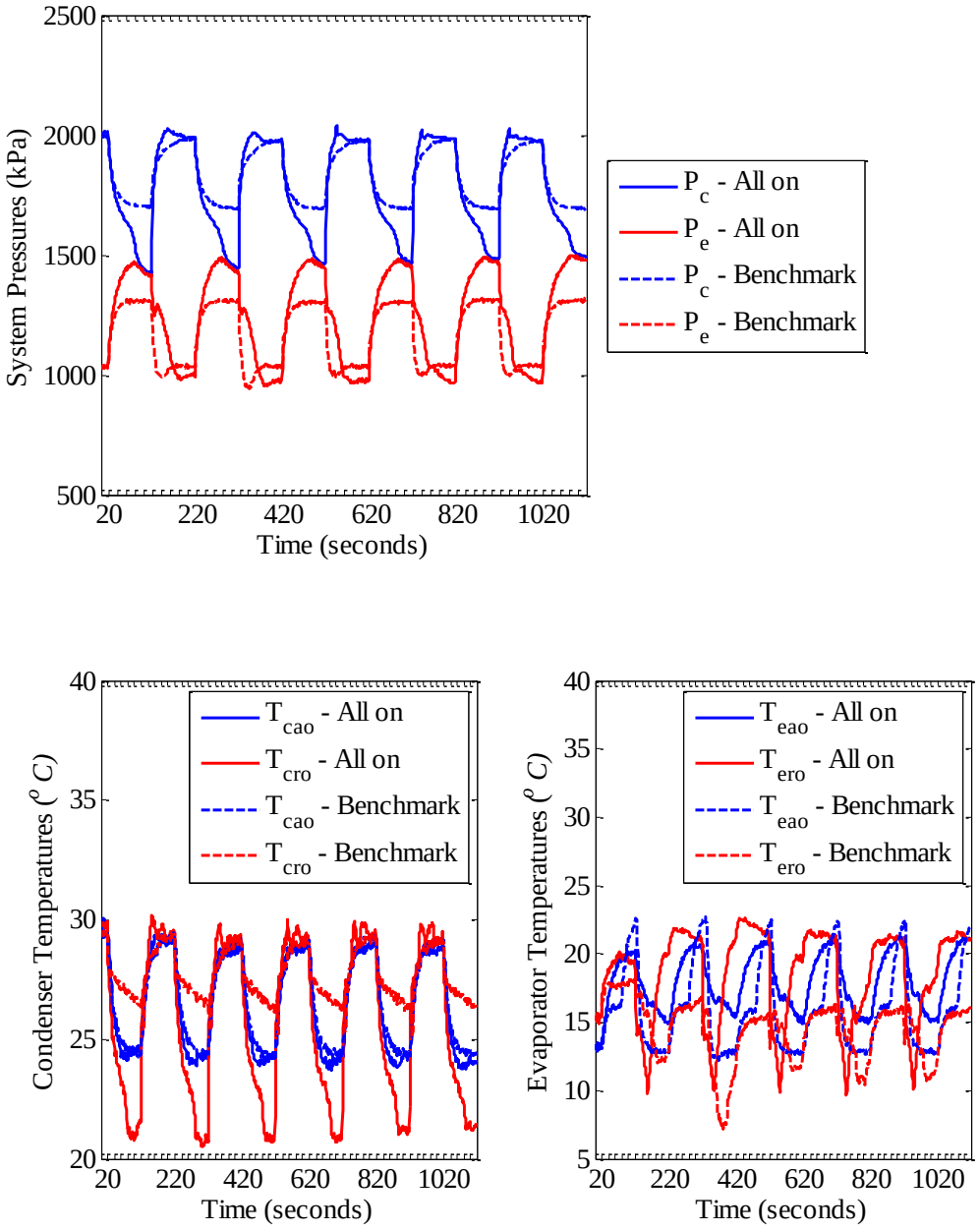

Figure 6.2 System Pressures and Temperatures – All On Vs Benchmark – Short Cycle - Experiment

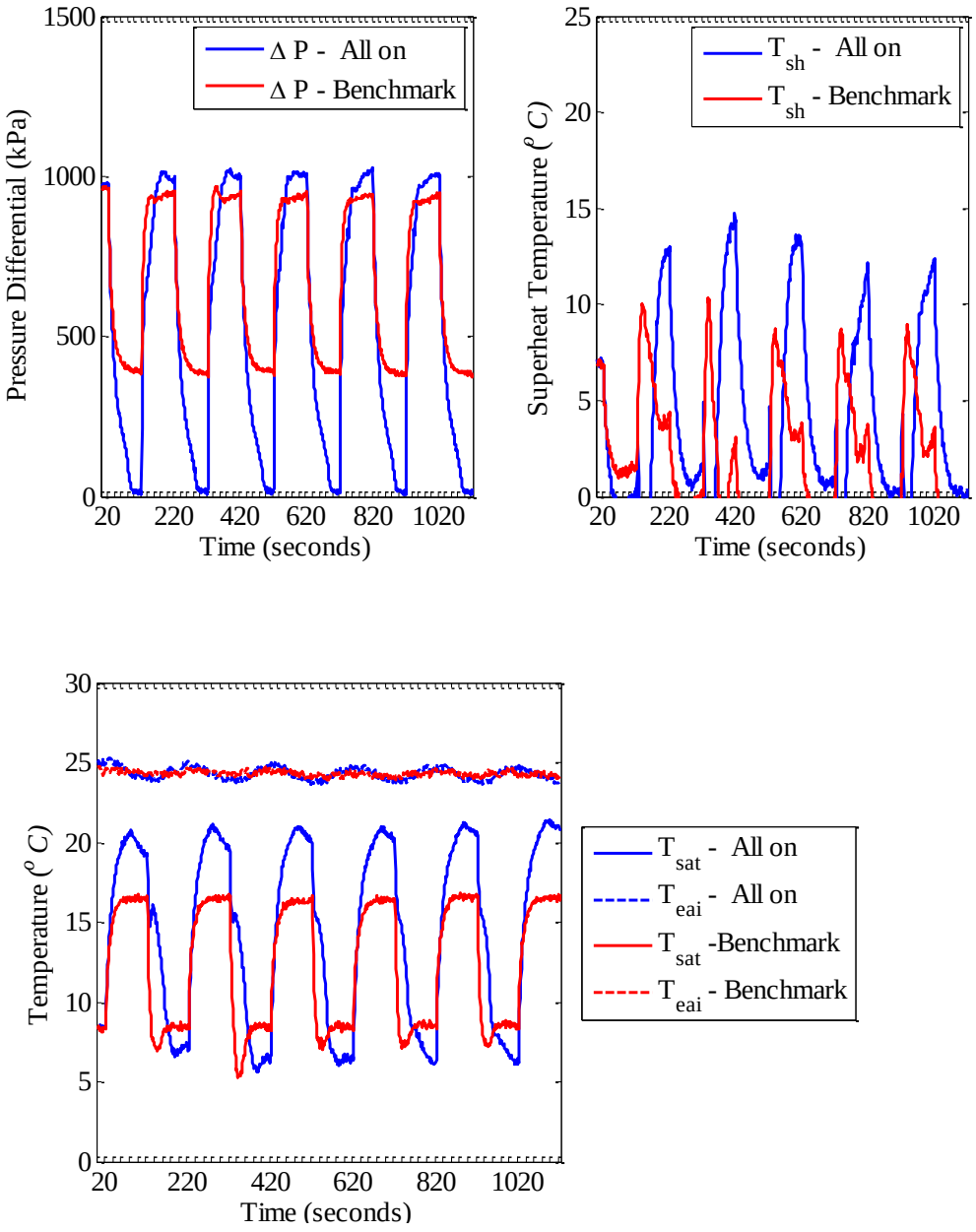

Figure 6.3 Pressure Differential and Superheat – All On Vs Benchmark – Short Cycle – Experiment

The effect of valve cycling on superheat is evident from Figure 6.3. Here the superheat temperature for the all on condition takes more time for it to build-up whereas in the benchmark since the valve is being cycled superheat is obtained faster. The valve cycling also plays an important role in maintaining a good pressure differential across the off cycle. This influences the startup efficiency as it avoids refrigerant migration. The instantaneous cooling and work for the two conditions are as shown in Figure 6.4.

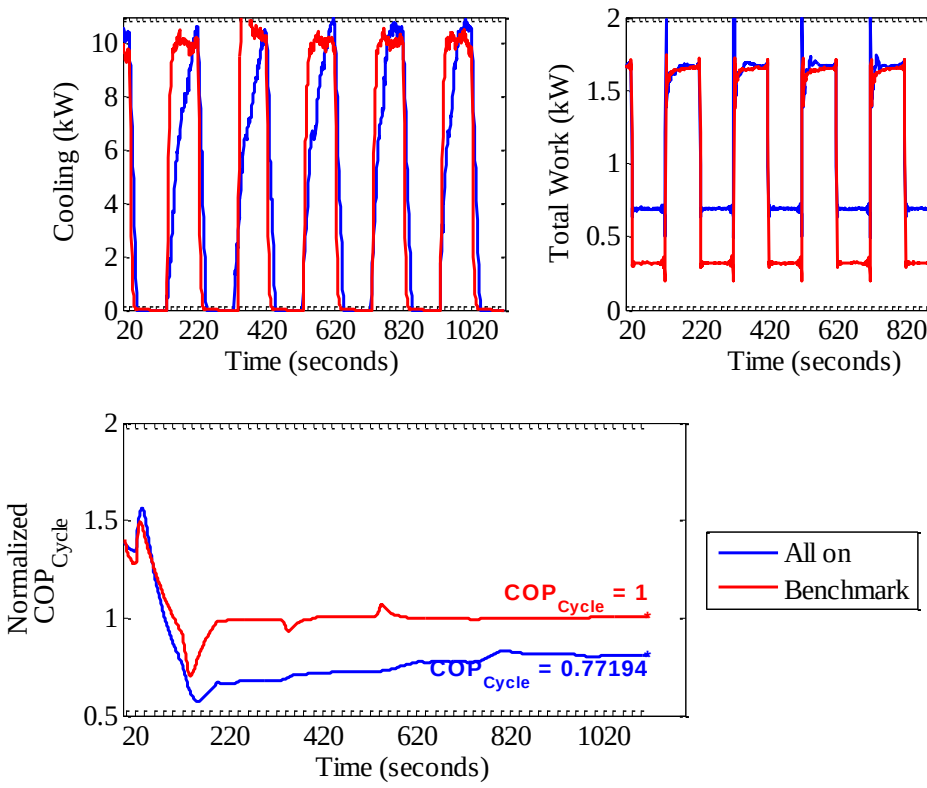

Figure 6.4 Cooling, Work and COP_{Cycle} – All On Vs Benchmark – Short Cycle - Experiment

The COP_{Cycle} for the all on condition is much less when compared to the benchmark condition as expected. A bulk of this loss in cyclic efficiency can be attributed to the evaporator fan power during the OFF cycle. Switching on the fan during the OFF cycle did result in a trickle of cooling but, most of the time during the OFF cycle the evaporator fan was ON doing nothing. So the trade off of the small amount of the cooling obtained to the work during off cycle did not work in favor of the cyclic efficiency. This is observed in Figure 6.5 which shows the cooling and work per cycle. Work done during the all on condition was much more compared to benchmark while giving nearly the same amount of cooling in return.

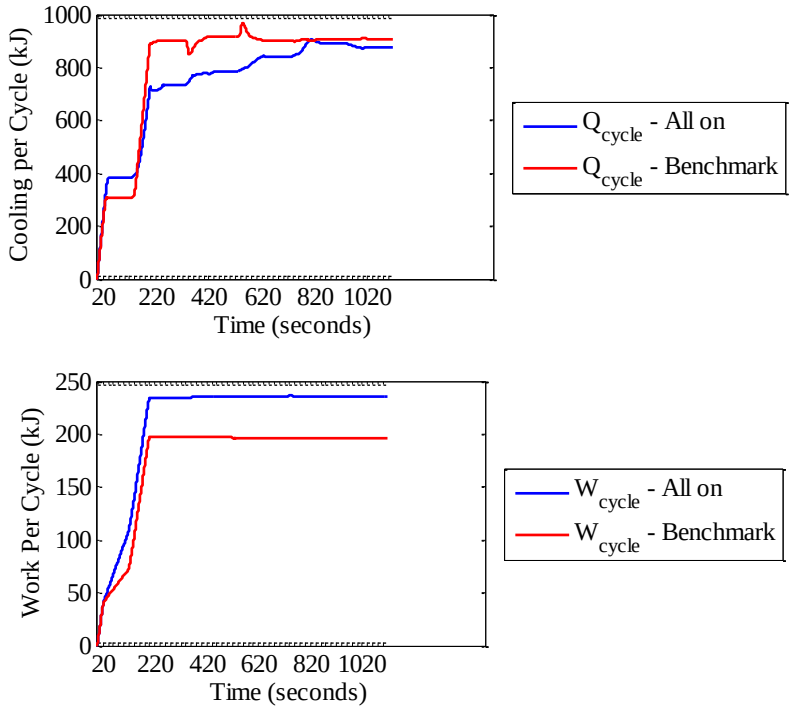

Figure 6.5 Work, Cooling Per Cycle – All On Vs Benchmark – Short Cycle - Experiment

The next condition to be compared with benchmark is the 'Fan Cycle Valve On' condition. Figure 6.1 showed that this condition had the worst efficiency. Following is a discussion that analyzes the case.

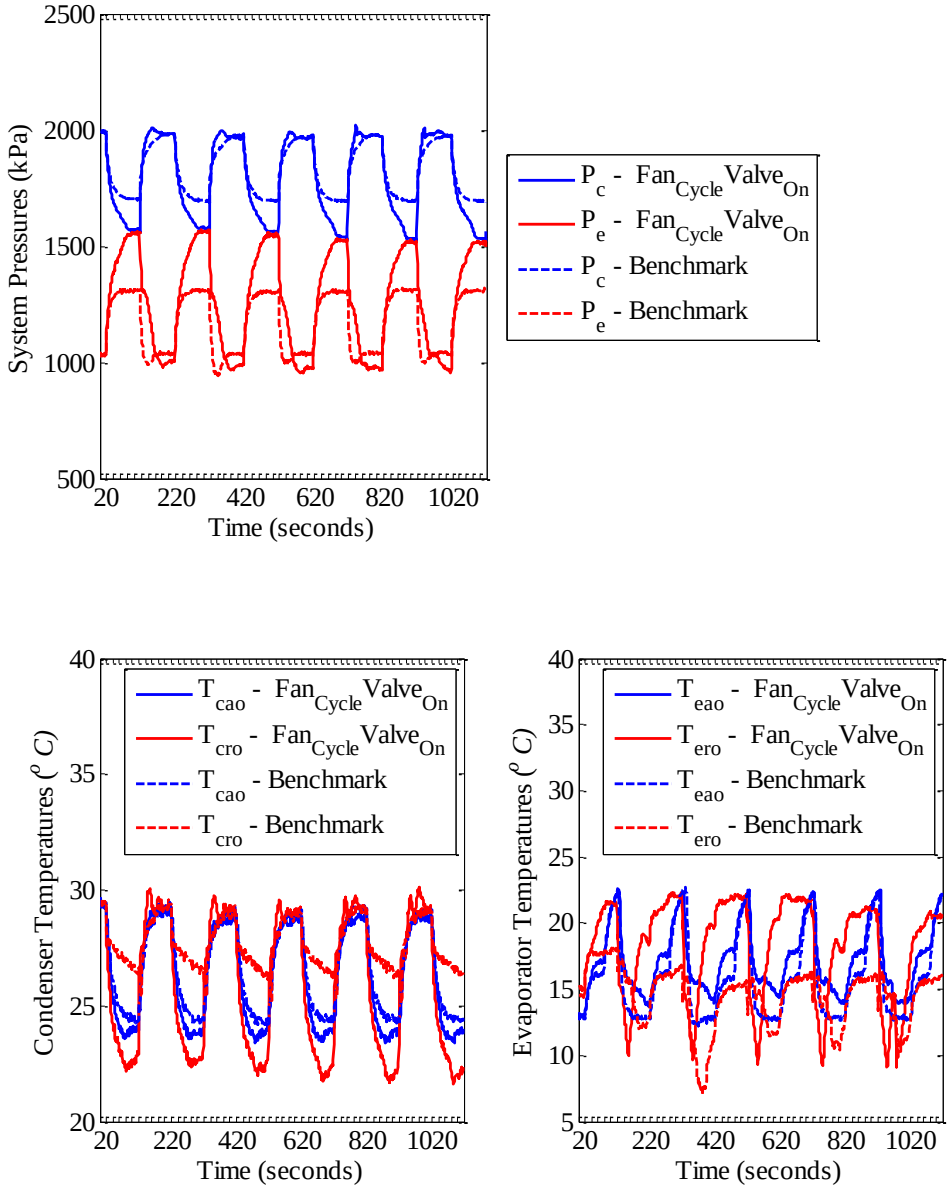

Figure 6.6 System Pressures and Temperatures – Fan Cycle Valve On Vs Benchmark – Short Cycle - Experiment

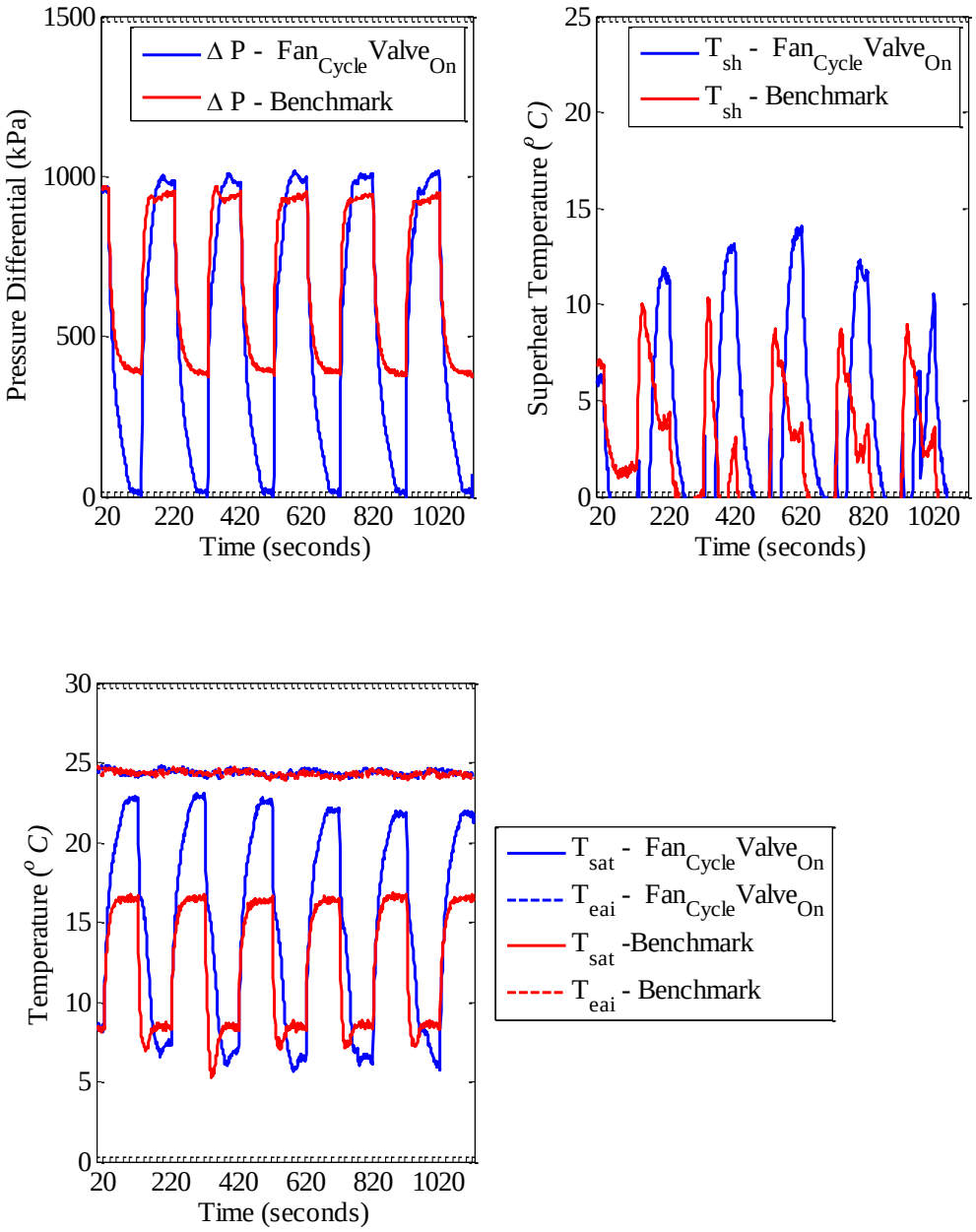

Figure 6.7 Pressure Differential and Superheat – Fan Cycle Valve On Vs Benchmark – Short Cycle – Experiment

Figure 6.6 shows the variation in the pressures and temperatures between the benchmark and the 'Fan Cycle Valve On' condition. Similar to the all on condition since

the valve is on during the on cycle of 'Fan Cycle Valve On', the pressures equalized whereas in the benchmark the valve is closed so the pressures do not equalize. Here also the superheat temperature take more time to rise similar to the all on condition as shown in Figure 6.7. The instantaneous cooling and work for the two conditions are as shown in Figure 6.8.

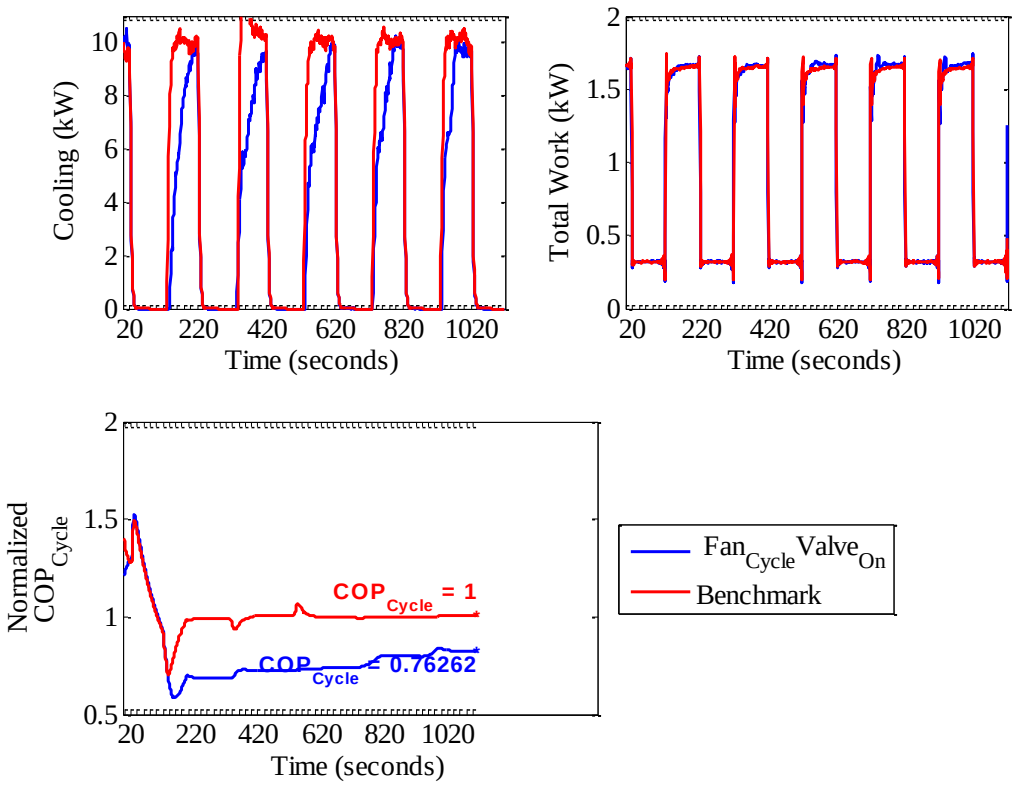

Figure 6.8 Cooling, Work and COP_{Cycle} – Fan Cycle Valve On Vs Benchmark – Short Cycle - Experiment

Since the fan is OFF at the instant of startup and the pressures are already equalized, the 'Fan Cycle Valve On' condition takes some time to build up to the full

cooling capacity. The problem of refrigerant redistribution during startup is showcased here. The fact that the valve did not shut off the flow to the evaporator meant that the compressor had to do more work during startup to pump the entire refrigerant from the evaporator through the condenser.

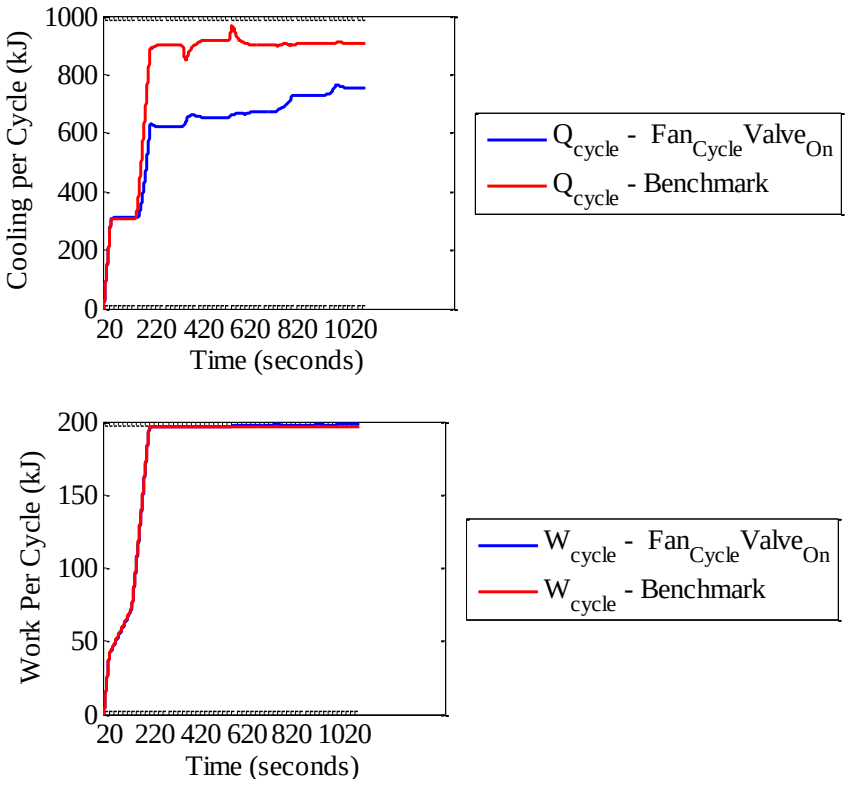

Figure 6.9 Work, Cooling Per Cycle – Fan Cycle Valve On Vs Benchmark – Short Cycle - Experiment

Since the power consuming components namely the compressor and the evaporator fan are cycled likewise in both the benchmark and the 'Fan Cycle Valve On'

condition, the work per cycle is the same for both the conditions as shown in Figure 6.9. Ultimately since the 'Fan Cycle Valve On' condition gives less cooling per cycle, it is the least efficient. The next case to analyze is the 'Valve Cycle Fan On' condition.

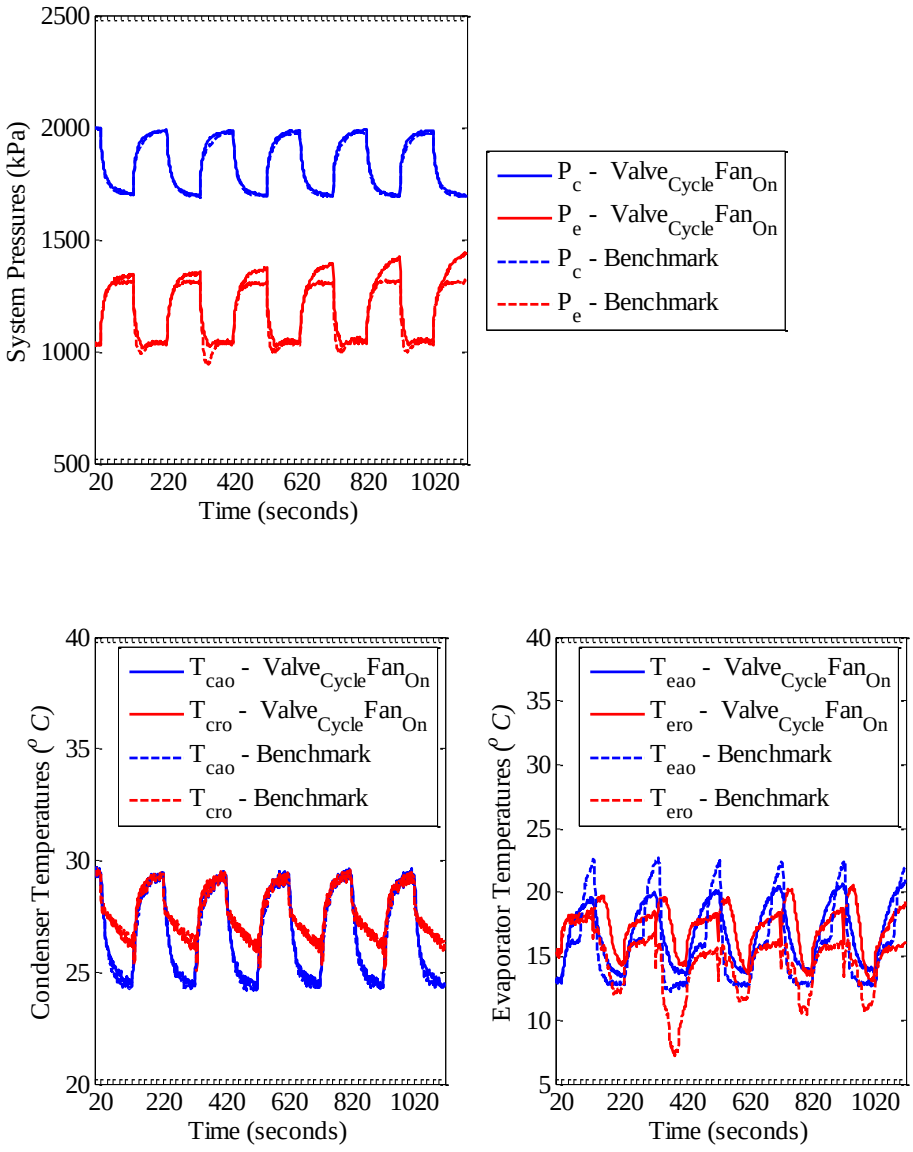

Figure 6.10 System Pressures and Temperatures – Valve Cycle Fan On Vs Benchmark – ShortCycle - Experiment

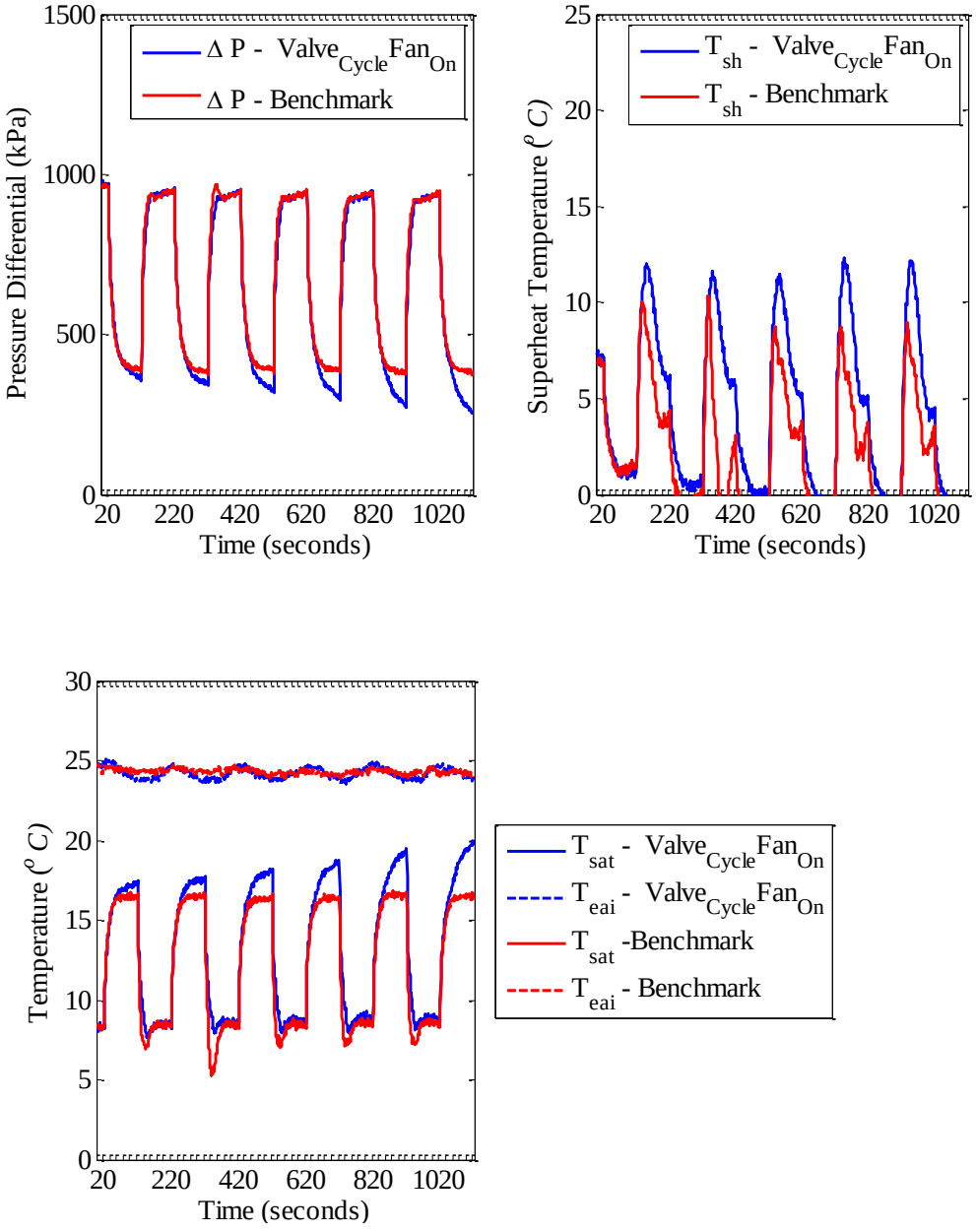

Figure 6.11 Pressure Differential and Superheat – Valve Cycle Fan On Vs Benchmark – Short Cycle – Experiment

Figure 6.10 shows the pressures and temperatures of the two conditions namely: benchmark and 'Valve Cycle Fan On'. The first noticeable fact is that the pressures are almost the same for the two. This is because valve is cycling in both cases which maintains the pressure differential across the off cycle as shown in Figure 6.11. Since the fan is on throughout the cycle in the 'Valve Cycle Fan On' condition, there is a net increase in the amount of cooling because of the extra cooling obtained during shutdown and the initial part of the off cycle as shown in Figure 6.12. Figure 6.12 also shows the power consumed by the evaporator fan during the off cycle for the 'Valve Cycle Fan On' condition.

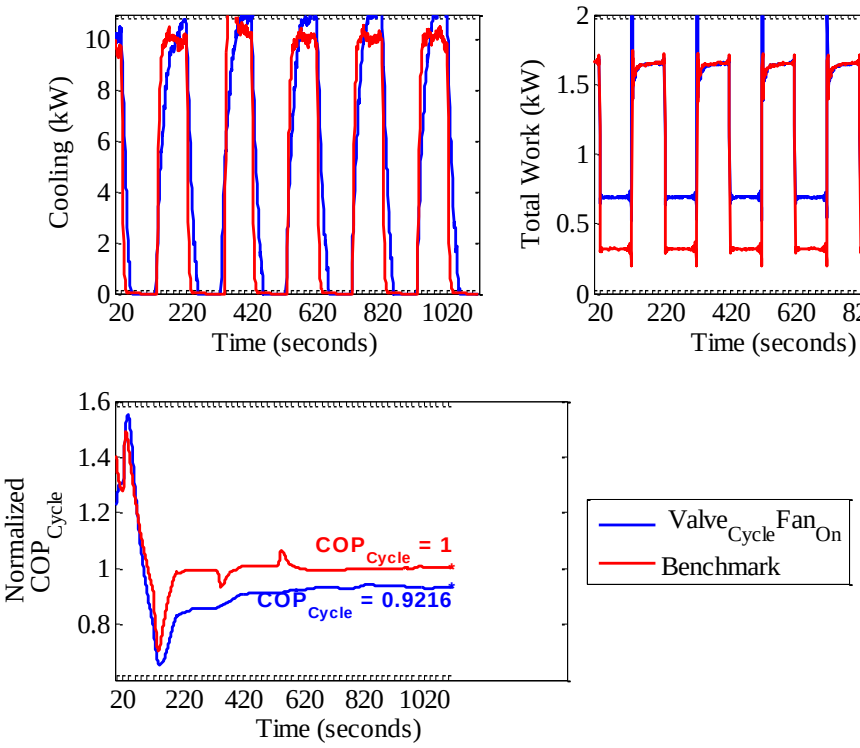

Figure 6.12 Cooling, Work and COP_{Cycle} – Valve Cycle Fan On Vs Benchmark – Short Cycle - Experiment

The relative inefficiency of the 'Valve Cycle Fan On' scheme compared to the benchmark can be attributed to the evaporator fan being on throughout the duration of the cycle. Thus it consumes some power even when not providing any cooling in the off cycle. The 'Valve Cycle Fan On' condition gives better cooling during shutdown because the fan is on during the OFF cycle to extract some potential cooling before the refrigerant reaches saturated conditions. The cooling and the work per cycle is shown in Figure 6.13.

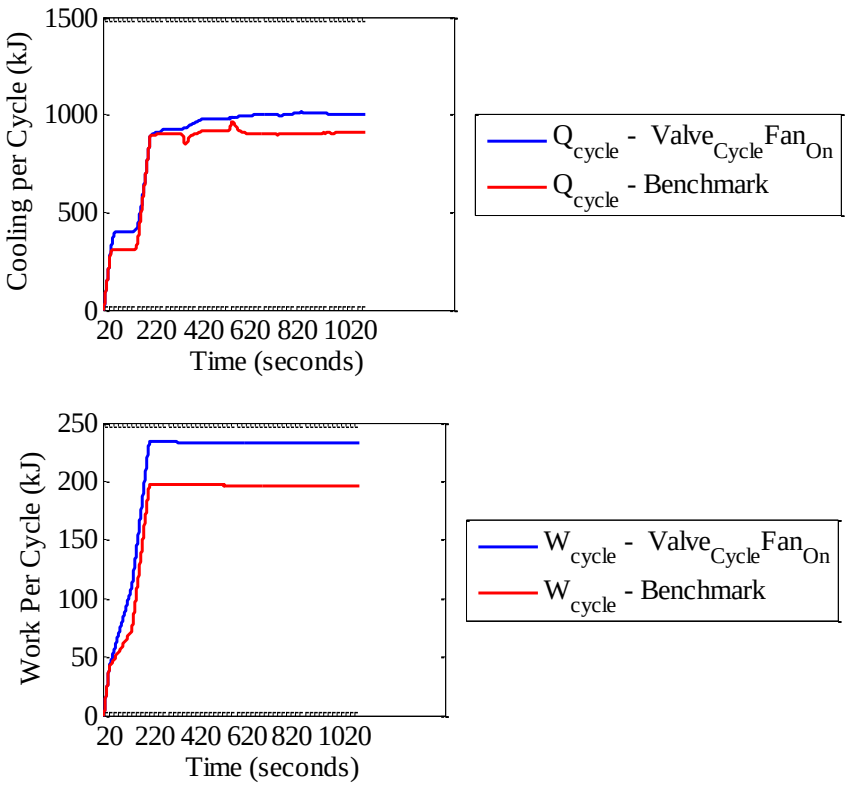

Figure 6.13 Work, Cooling Per Cycle – Valve Cycle Fan On Vs Benchmark – Short Cycle - Experiment

'Valve Part Cycle' is the next condition that is compared with the benchmark. This condition differs from the 'Valve Cycle Fan On' in the aspect that the valve remains on for a part time (20 seconds) after shutdown.

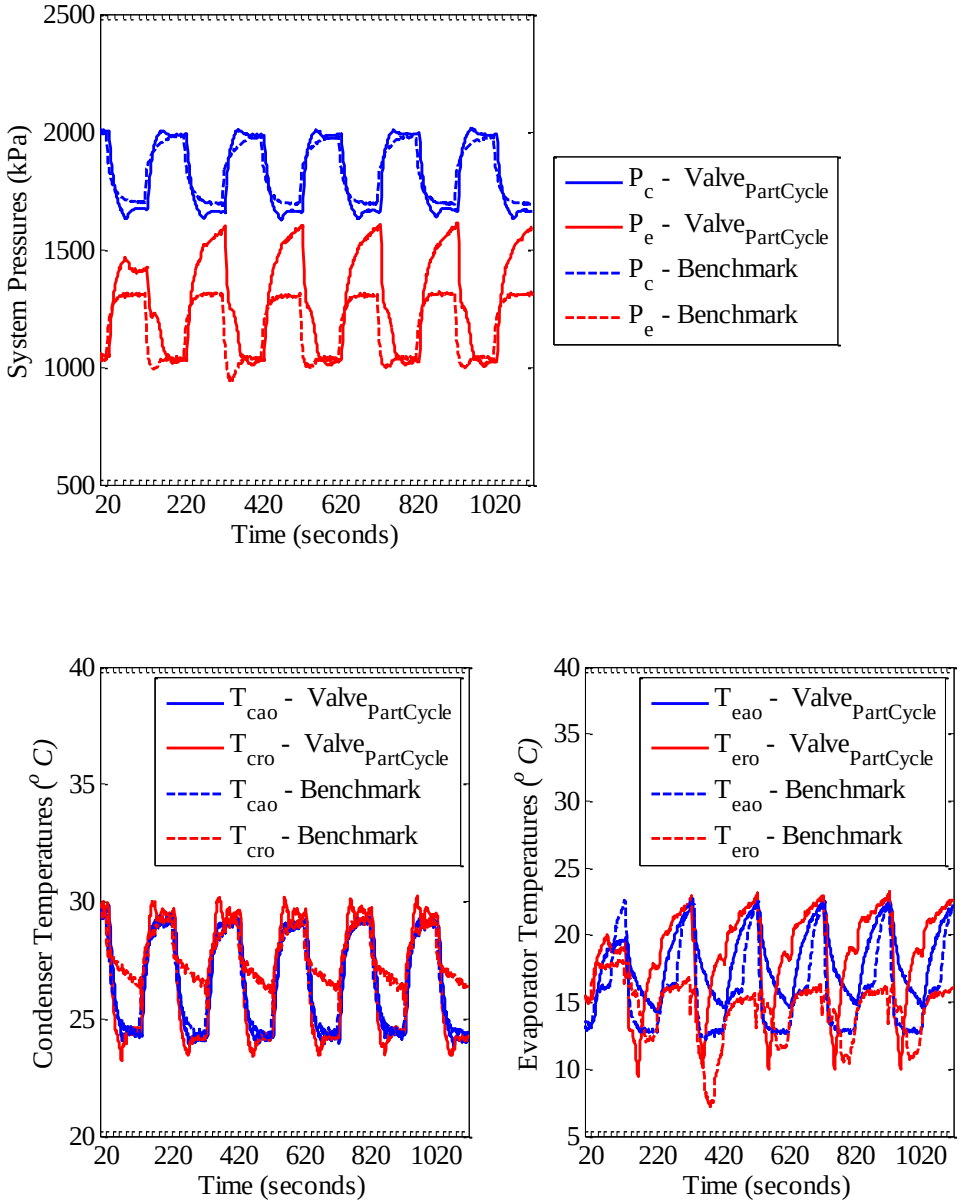

Figure 6.14 System Pressures and Temperatures – Valve Part Cycle Vs Benchmark – Short Cycle - Experiment

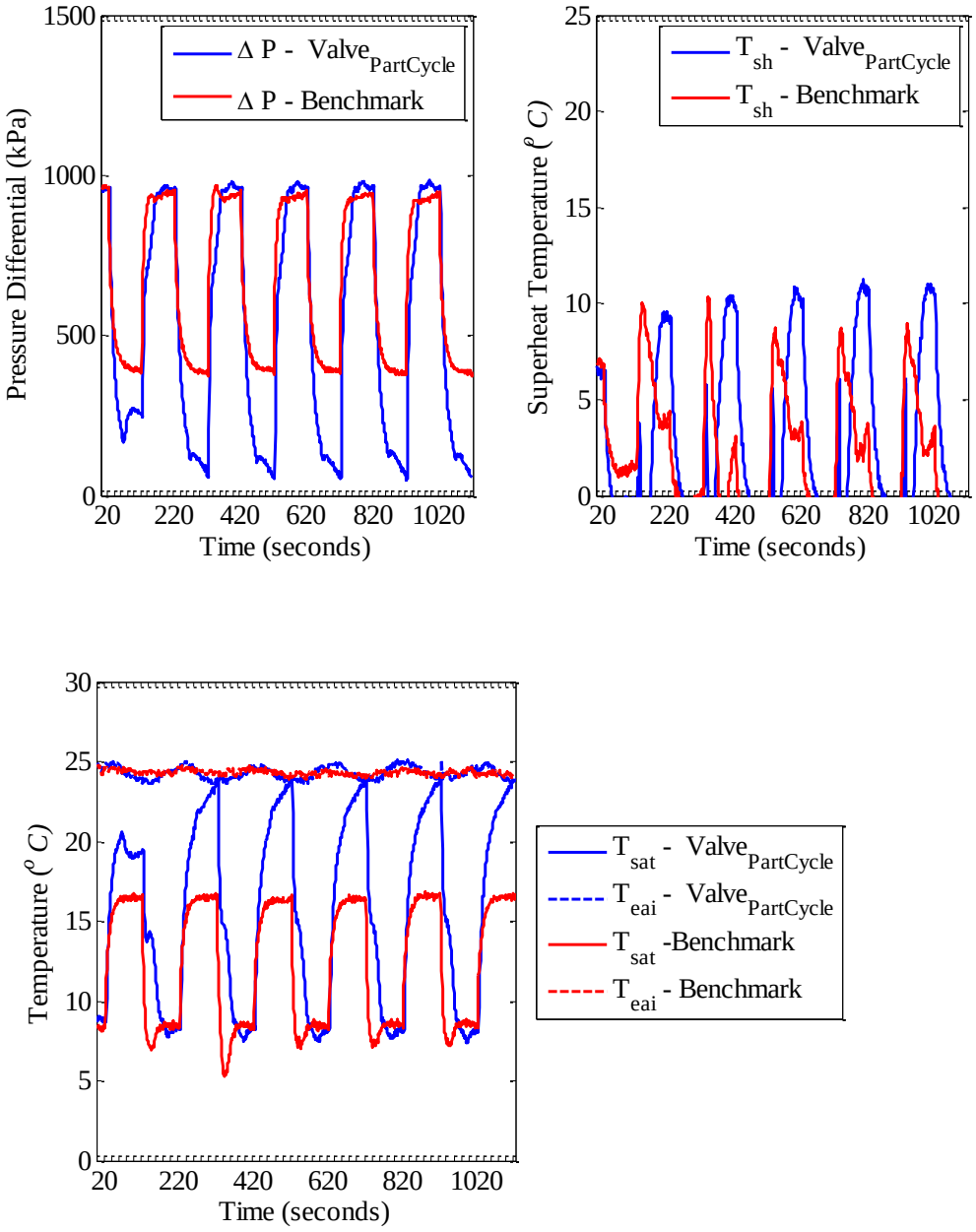

Figure 6.15 Pressure Differential and Superheat – Valve Part Cycle Vs Benchmark – Short Cycle – Experiment

In this case, the system pressures almost equalize as shown in Figure 6.14. This is because of the valve being opened at shutdown that moves more refrigerant into the

evaporator. This has its effect at startup also, where because of this extra refrigerant migration to the evaporator, the pressure differential and the superheat build up is slower as shown in Figure 6.15. Figure 6.16 shows the instantaneous cooling, work and the normalized COP_{Cycle}. The refrigerant migration problem is shown in the cooling curve also as it takes more time now to reach its full cooling capacity. Since the fan is on during the off cycle, there is some potential cooling obtained during the initial part of the off cycle. However, thereafter the fan just consumes power with no more cooling to be obtained.

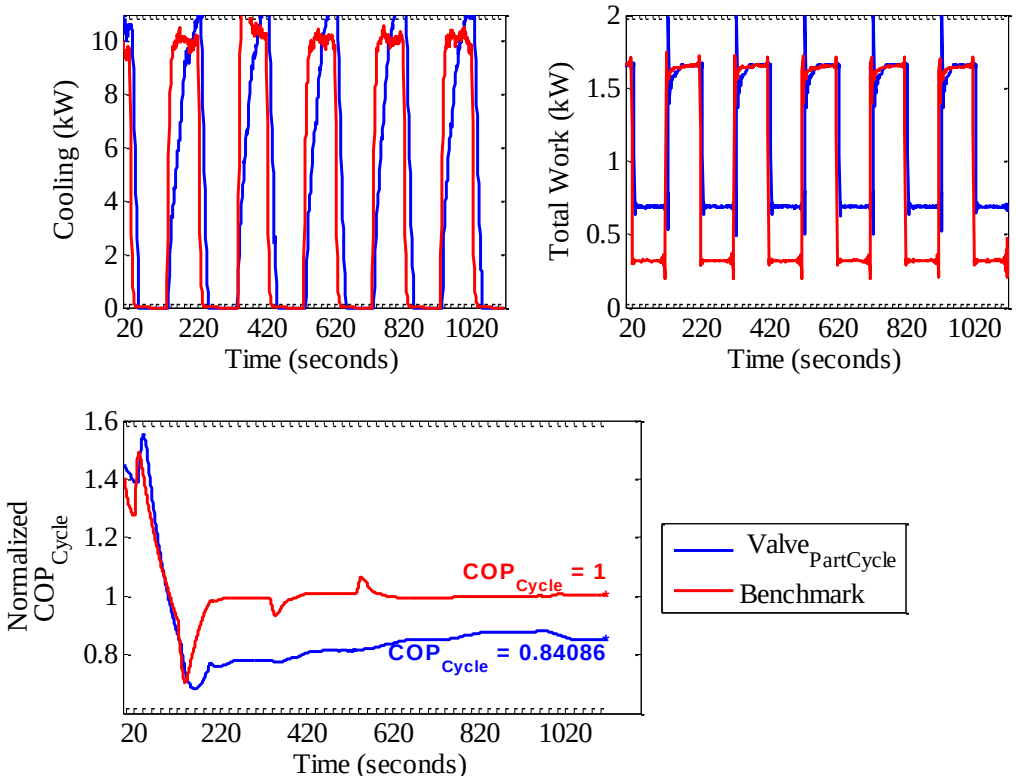

Figure 6.16 Cooling, Work and COP_{Cycle} – Valve Part Cycle Vs Benchmark – Short Cycle - Experiment

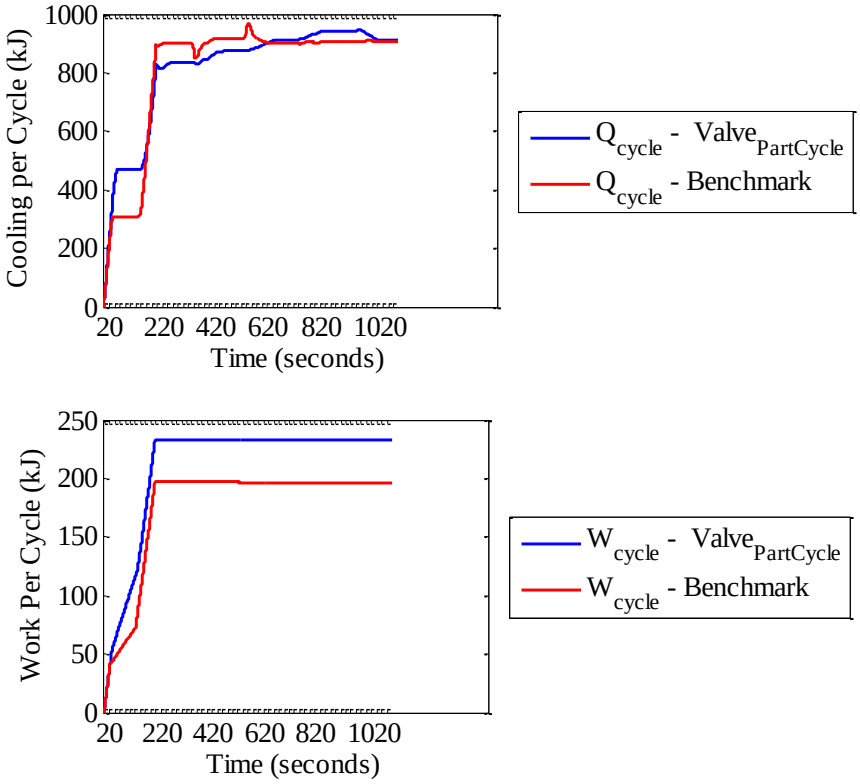

Figure 6.17 Work, Cooling Per Cycle – Valve Part Cycle Vs Benchmark – Short Cycle – Experiment

Figure 6.17 shows the work and cooling per cycle for the two conditions. These plots confirm that the slightly extra cooling obtained during shutdown for the 'Valve Part Cycle' condition is traded off by the power consumed by the fan during the off cycle. The next comparison is between 'Fan Part Cycle' and benchmark. 'Fan Part Cycle' differs from the benchmark due to the fact that the fan stays on for 20 seconds more after shutdown in 'Fan Part Cycle'.

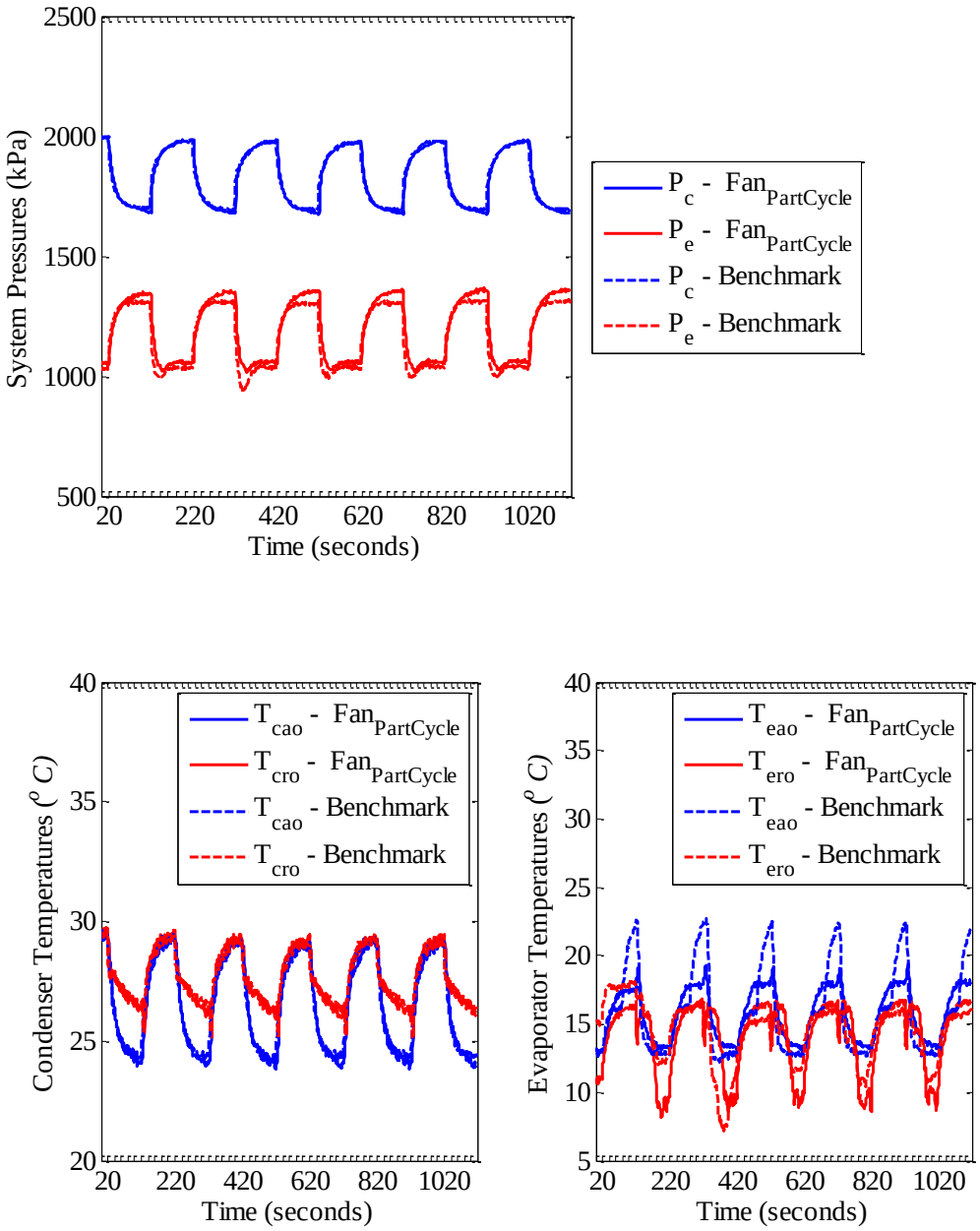

Figure 6.18 System Pressures and Temperatures – Fan Part Cycle Vs Benchmark – Short Cycle - Experiment

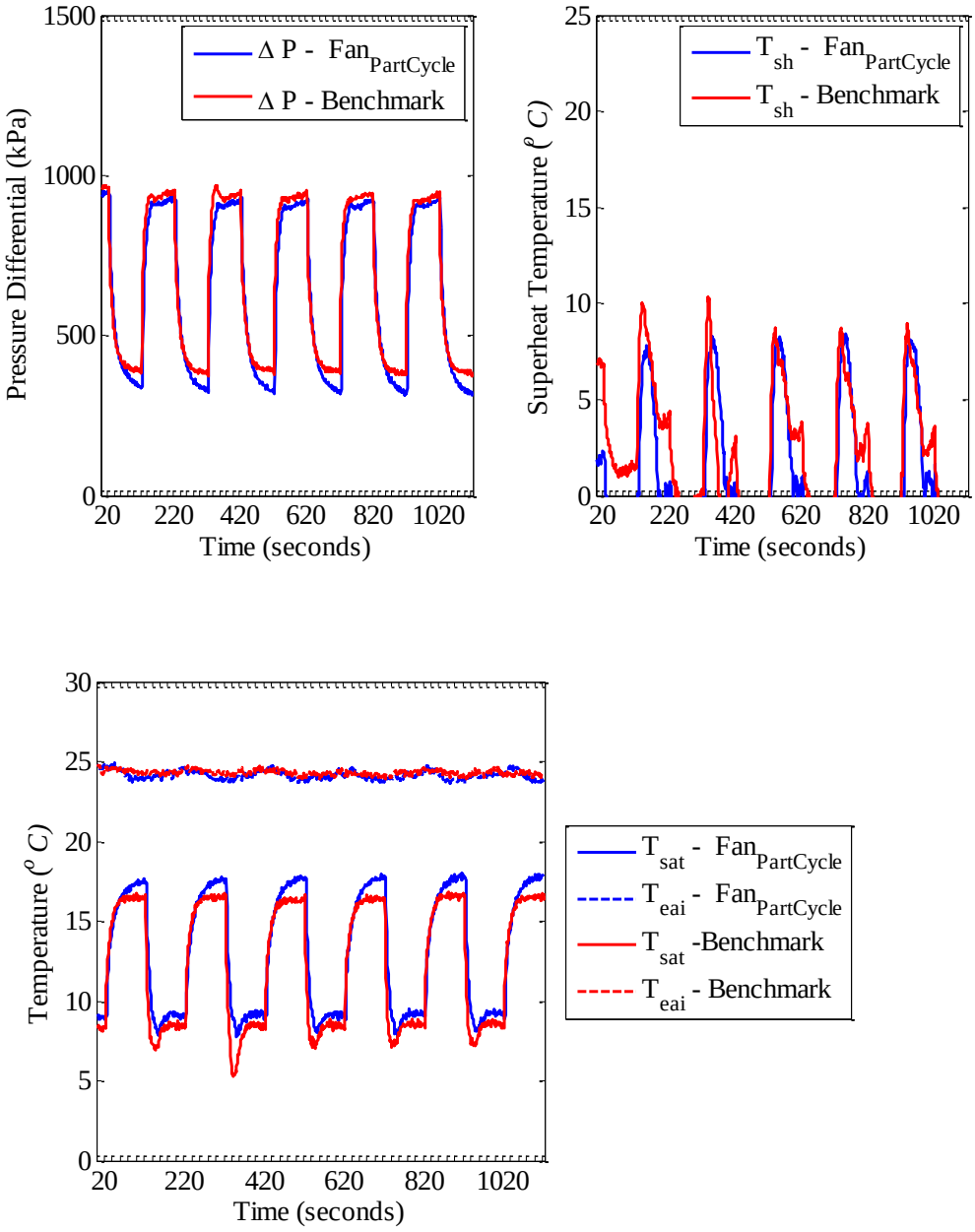

Figure 6.19 Pressure Differential and Superheat – Fan Part Cycle Vs Benchmark – Short Cycle – Experiment

The 'Fan Part Cycle' condition has almost similar pressure and temperature responses as benchmark, shown in Figure 6.18. This is because the valve is cycling similar to benchmark condition and the valve is the main factor for maintaining the pressure differential and super heat as shown in Figure 6.19. Figure 6.20 shows that there is an increase in efficiency for 'Fan Part Cycle'. This is mainly because of the cooling obtained during the initial part of the off cycle shown in the instantaneous cooling in Figure 6.20.

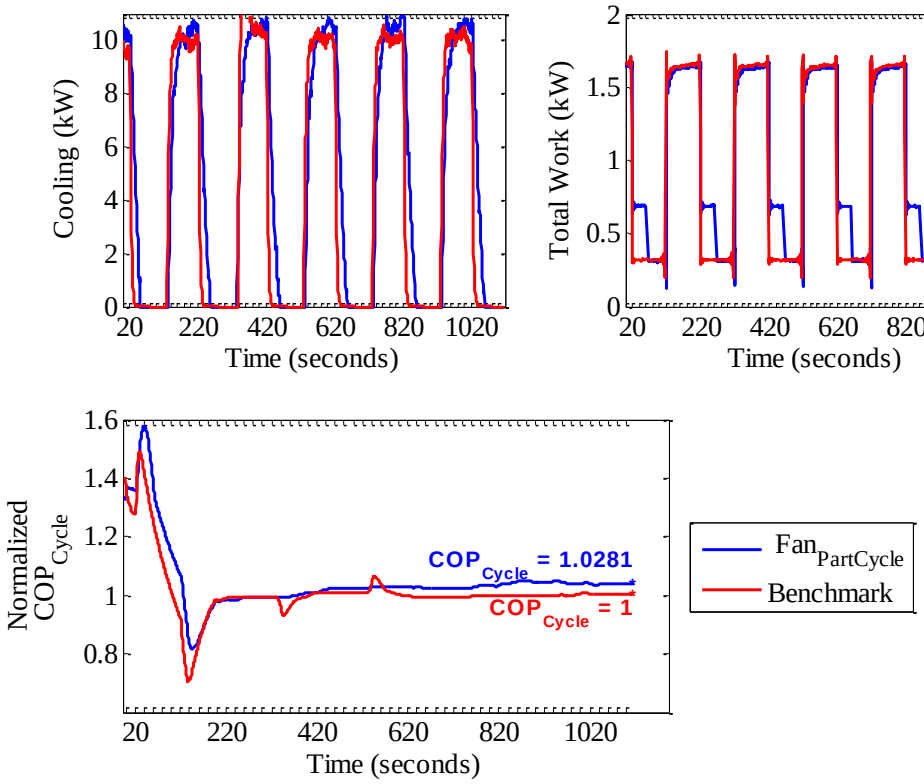

Figure 6.20 Cooling, Work and COP_{Cycle} – Fan Part Cycle Vs Benchmark – Short Cycle - Experiment

Despite having to spend some power being on during the off cycle, the scheme results in a net increase in efficiency because of extraction of the potential cooling. Fan being part-on can be verified by looking at the instantaneous work in Figure 6.20. Figure 6.21 shows the work and cooling per cycle for the two conditions in discussion. There is an increase in both cooling and the work but this time since the fan switches off after 20 seconds, the cooling does more than to trade off the extra work put in.

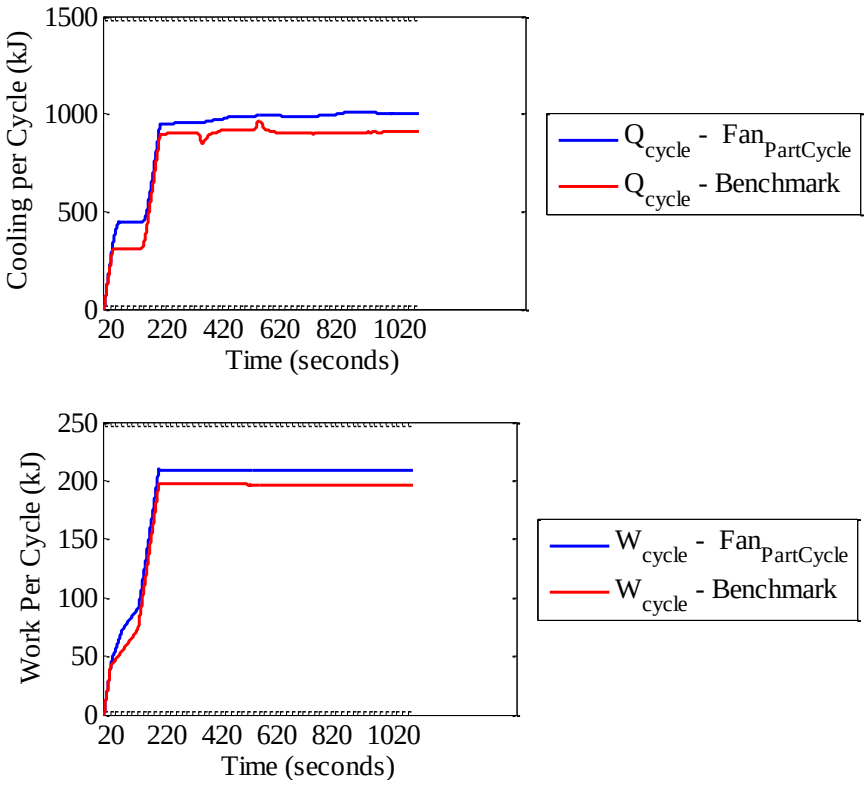

Figure 6.21 Work, Cooling Per Cycle – Fan Part Cycle Vs Benchmark – Short Cycle - Experiment

Thus the various cycling schemes show the important dynamics that affects the cyclic efficiency of the system. There is still a need to investigate the expansion valve and the evaporator fan cycling S-curve parameters individually.

6.1.1.2 Expansion Valve

The expansion valve was first considered as the cycling component, while the evaporator fan was assumed to be running for the entire length of the cycle. The values of the S-curve parameters used for this simulation are specified in Table 5.2. To refresh, higher values of slope correspond to steeper transients in the S-curve. Negative time values mean a lead operation (act before the compressor) whereas positive value means a delayed operation (act after the compressor).

Similar to the simulation, the detailed trend analysis was one dimensional. Thus one parameter was varied according to the range in Table 5.2, the other parameters were held constant at their benchmark values. Figure 6.22 present the results of the detailed trend analysis for the individual S-curve parameters for the expansion valve profile.

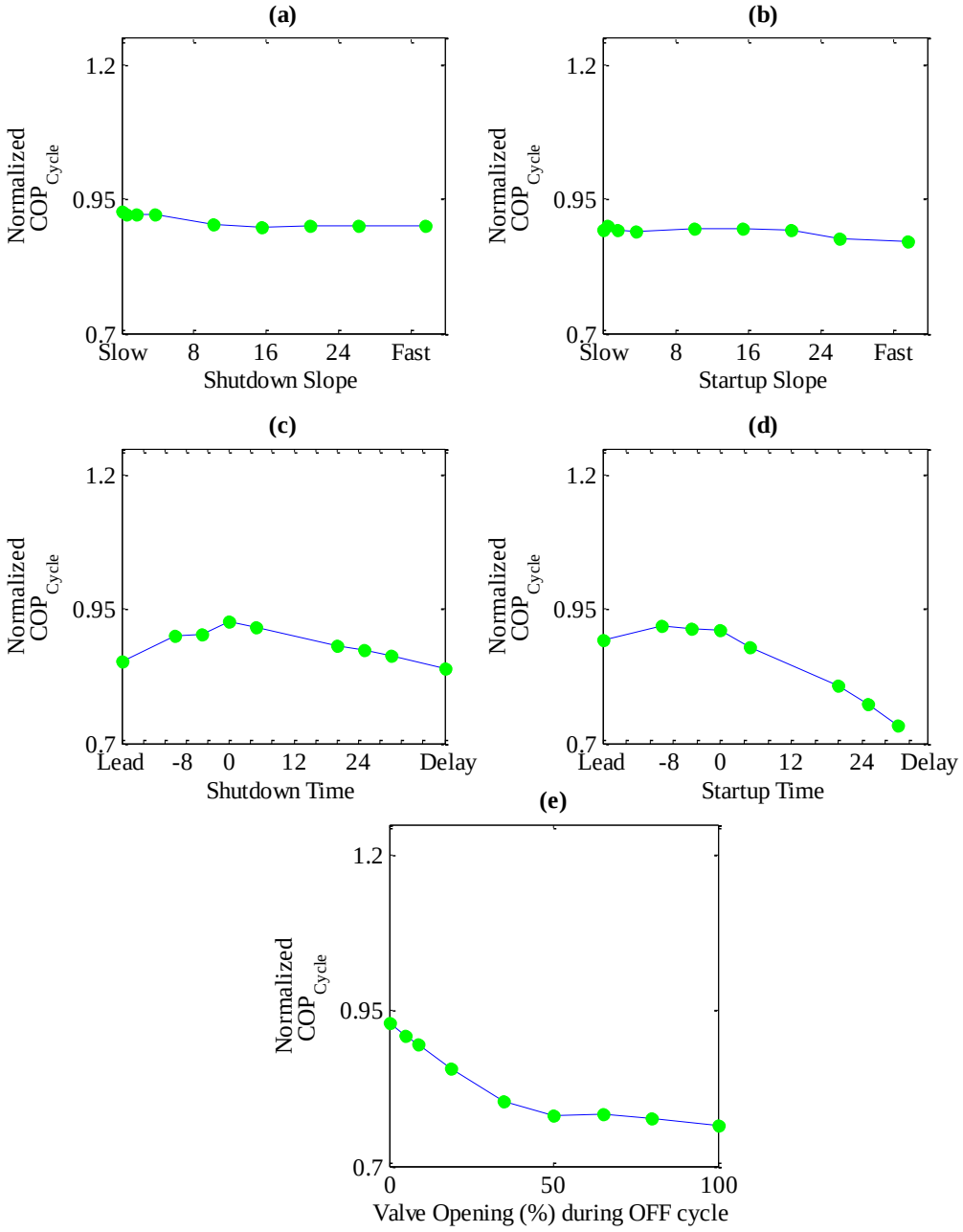

Figure 6.22 Detailed Trends in COP_{Cycle} – Expansion Valve – Short Cycle - Experiment

Figure 6.22(a) and 6.22(b) show the effect of shutdown slope and startup slope respectively on COP_{Cycle}. They show the relatively negligible effect that the slope has in the system efficiency. Figure 6.22(e) shows the trend of COP_{Cycle} when the valve opening during the off cycle was changed as the parameter. This characteristic notes that the valve has to be strictly closed during the off cycle for the best cyclic efficiency of the system. Thus any small leakage in the valve means loss of system efficiency. Figure 6.22(c) presents the effect of shutdown time on COP_{Cycle}. Leading/Delaying the valve closing with respect to compressor shutdown is observed to have negative effect on the system efficiency. Figure 6.22(d) shows the effect of startup time on COP_{Cycle} where trends show that a lead/delay of the valve opening at startup is not at all preferred for better cyclic efficiency. Thus benchmark valve cycling seems to give the best efficiency whereas in the simulation trends showed that leading the valve at shutdown and delaying it during startup is better. The following analyses discuss why leading the valve during shutdown and delaying it while startup is not a good idea for the experiment.

Figure 6.23 shows the system pressures and temperatures in the case of 'Valve Shutdown Lead' compared with the benchmark. In this case because the valve closes before the compressor shuts down, the evaporator is at a much lower pressure compared to benchmark. Figure 6.24 shows the pressure differential and superheat responses for the condition. The early closing of the valve results in a larger pressure differential but undesirably high superheat.

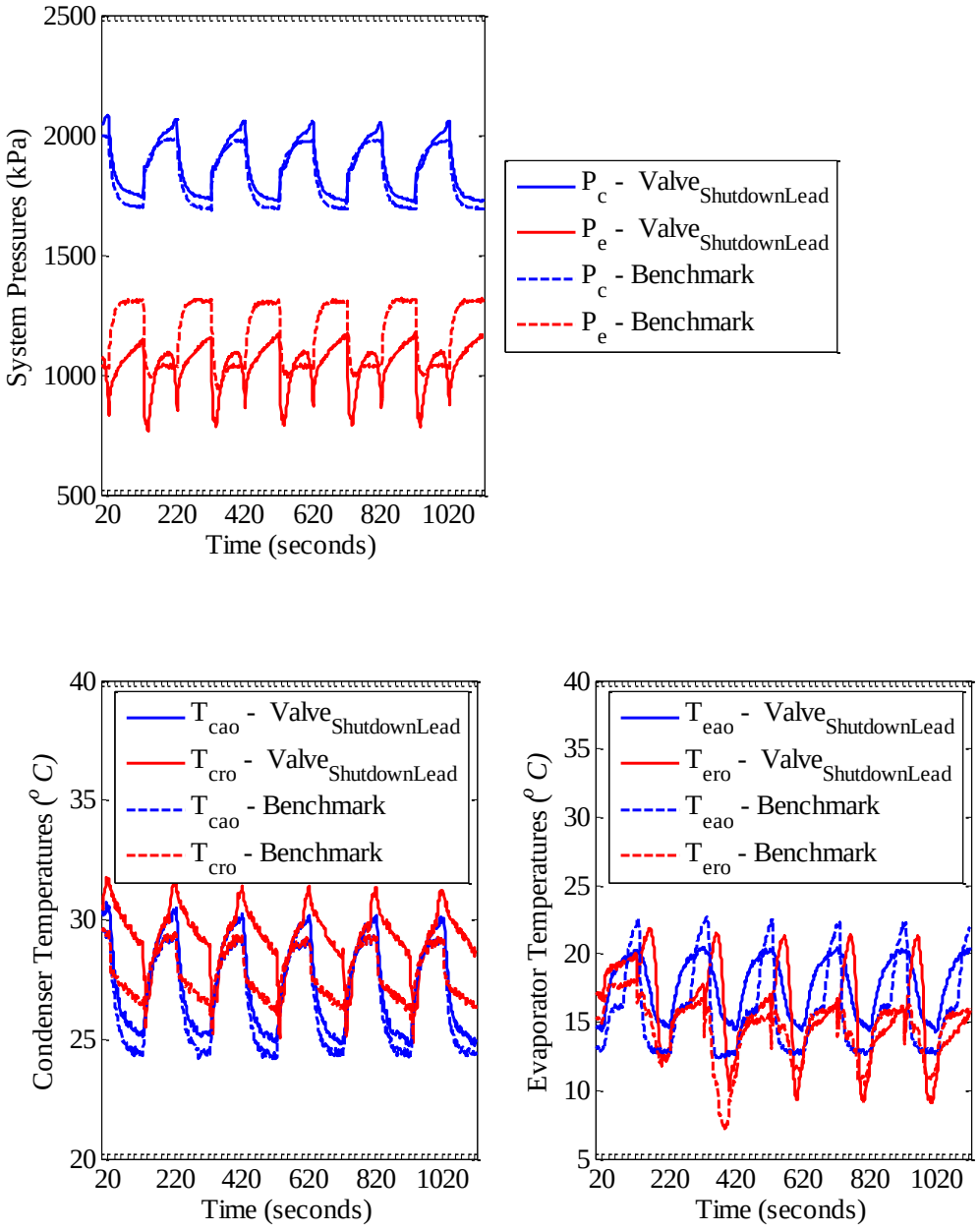

Figure 6.23 System Pressures and Temperatures – Valve Shutdown Lead Vs Benchmark – Short Cycle - Experiment

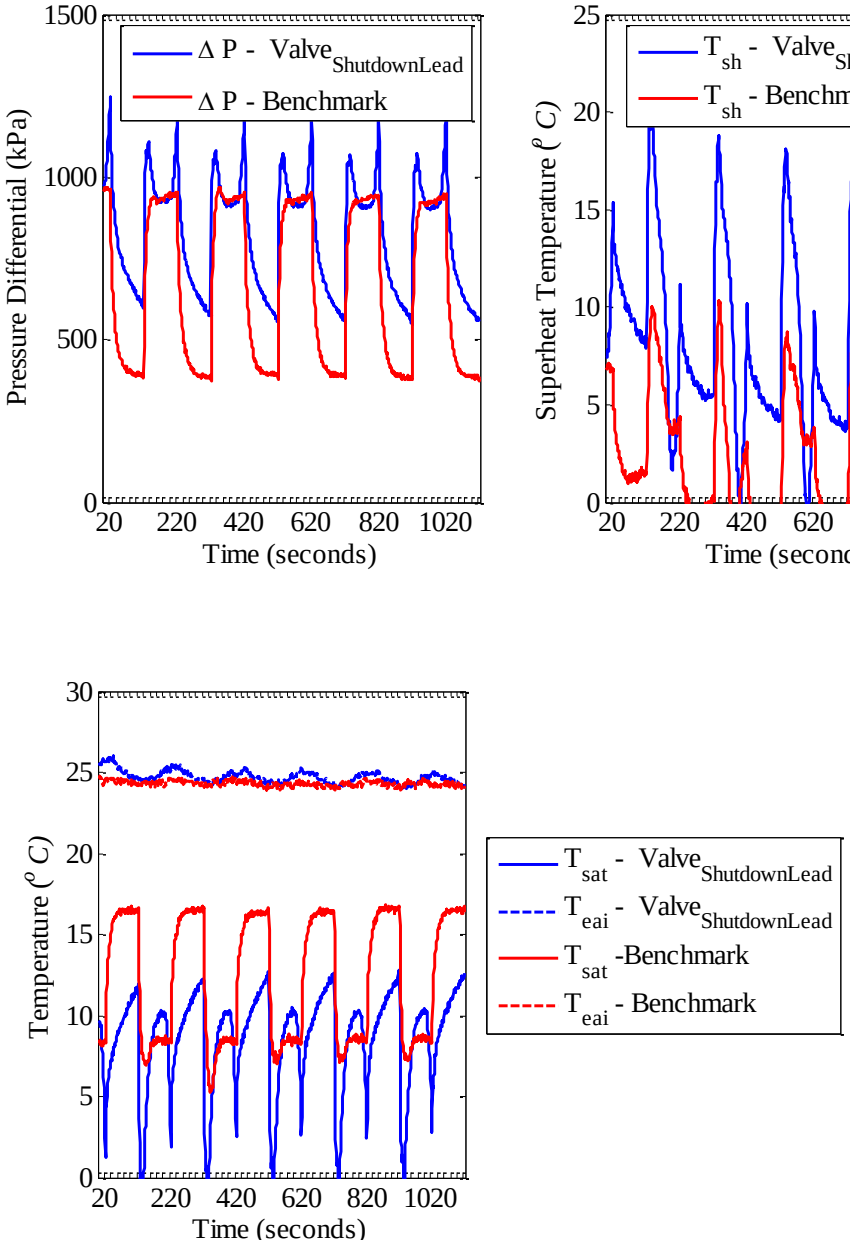

Figure 6.24 Pressure Differential and Superheat – Valve Shutdown Lead Vs Benchmark – Short Cycle – Experiment

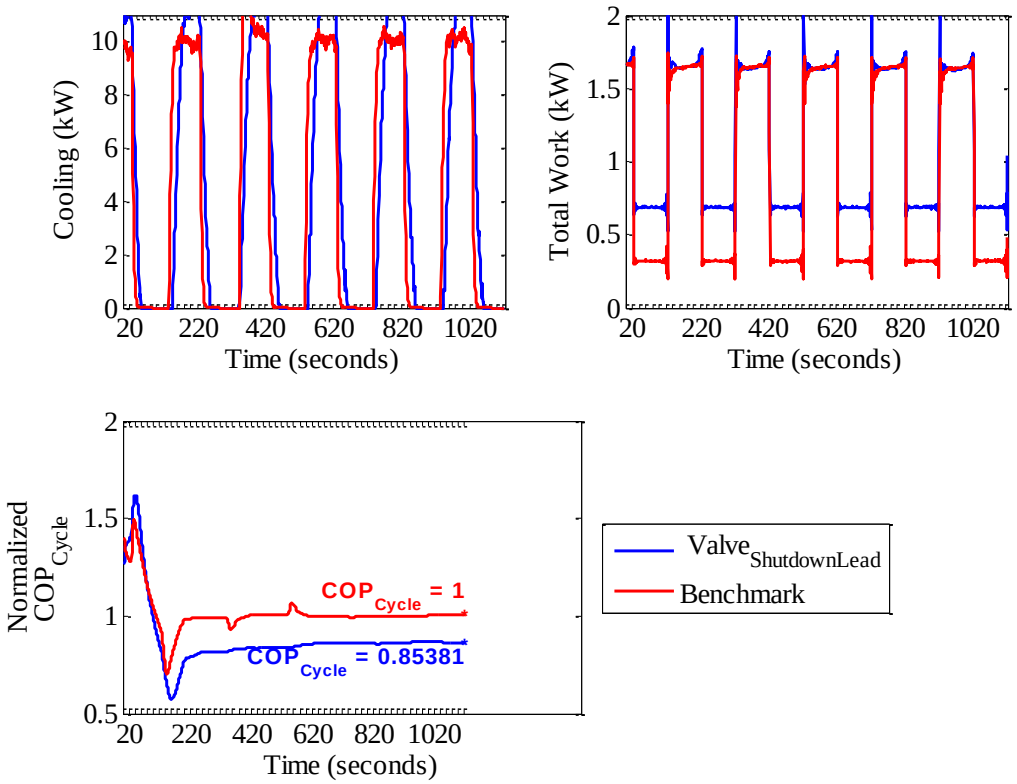

Figure 6.25 Cooling, Work and COP_{Cycle} – Valve Shutdown Lead Vs Benchmark – Short Cycle - Experiment

One of the reasons for this approach having less efficiency is that the cooling at startup is sluggish as shown in Figure 6.25. There is a time lag at startup because by the time the evaporator pressure reaches its operating value, the valve closes and thus the evaporator becomes low pressurized. Figure 6.26 shows that the fan power consumption throughout the off cycle influences the work per cycle to be higher thus having a negative effect on the efficiency.

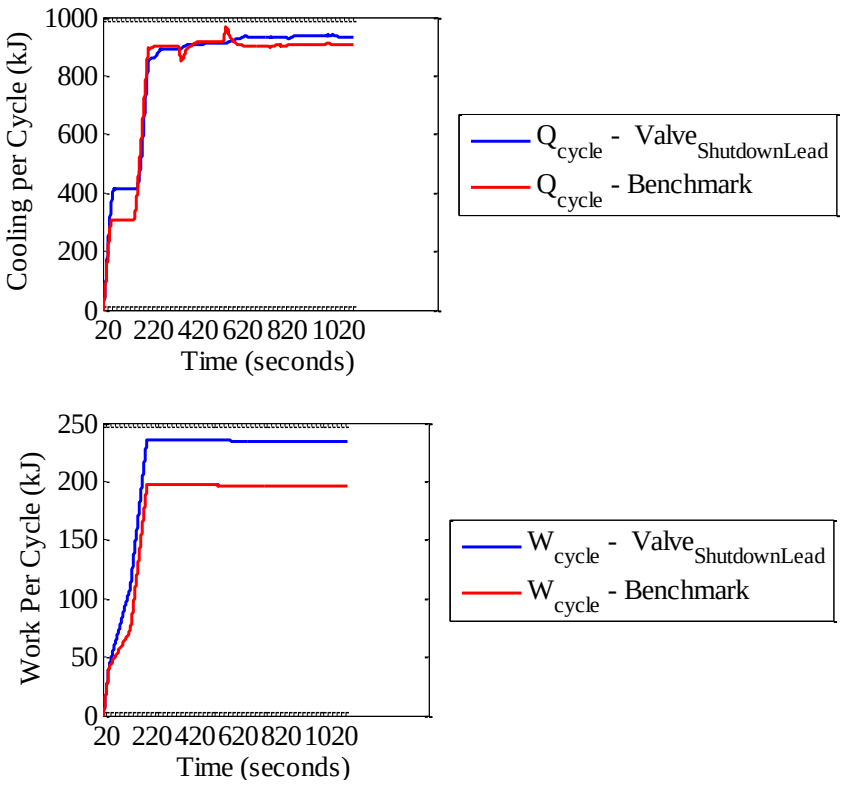

Figure 6.26 Work, Cooling Per Cycle – Valve Shutdown Lead Vs Benchmark – Short Cycle - Experiment

The final condition is the 'Valve Startup Delay' which by far has the worst efficiency. Figure 6.27 shows the pressure and temperature plots. Since the valve is held closed at startup, the evaporator becomes really low pressurized. Once the valve is opened after the delay the pressure starts to build up. The pressure response can be viewed in Figure 6.28 looking at the pressure differential. It spikes at the startup and starts reducing. Figure 6.28 also shows the undesirably high superheat for the 'Valve Startup Delay' condition.

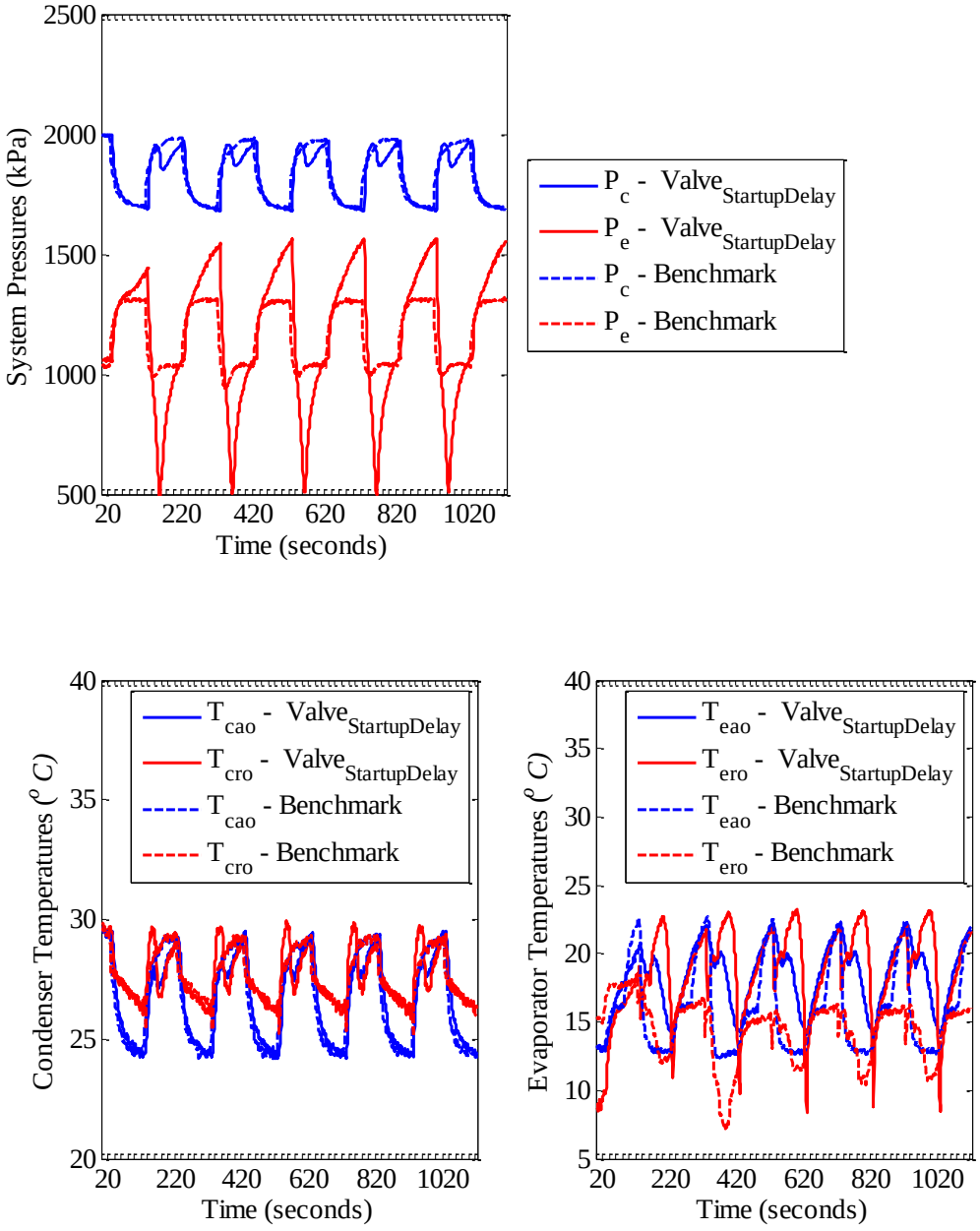

Figure 6.27 System Pressures and Temperatures – Valve Startup Delay Vs Benchmark – Short Cycle - Experiment

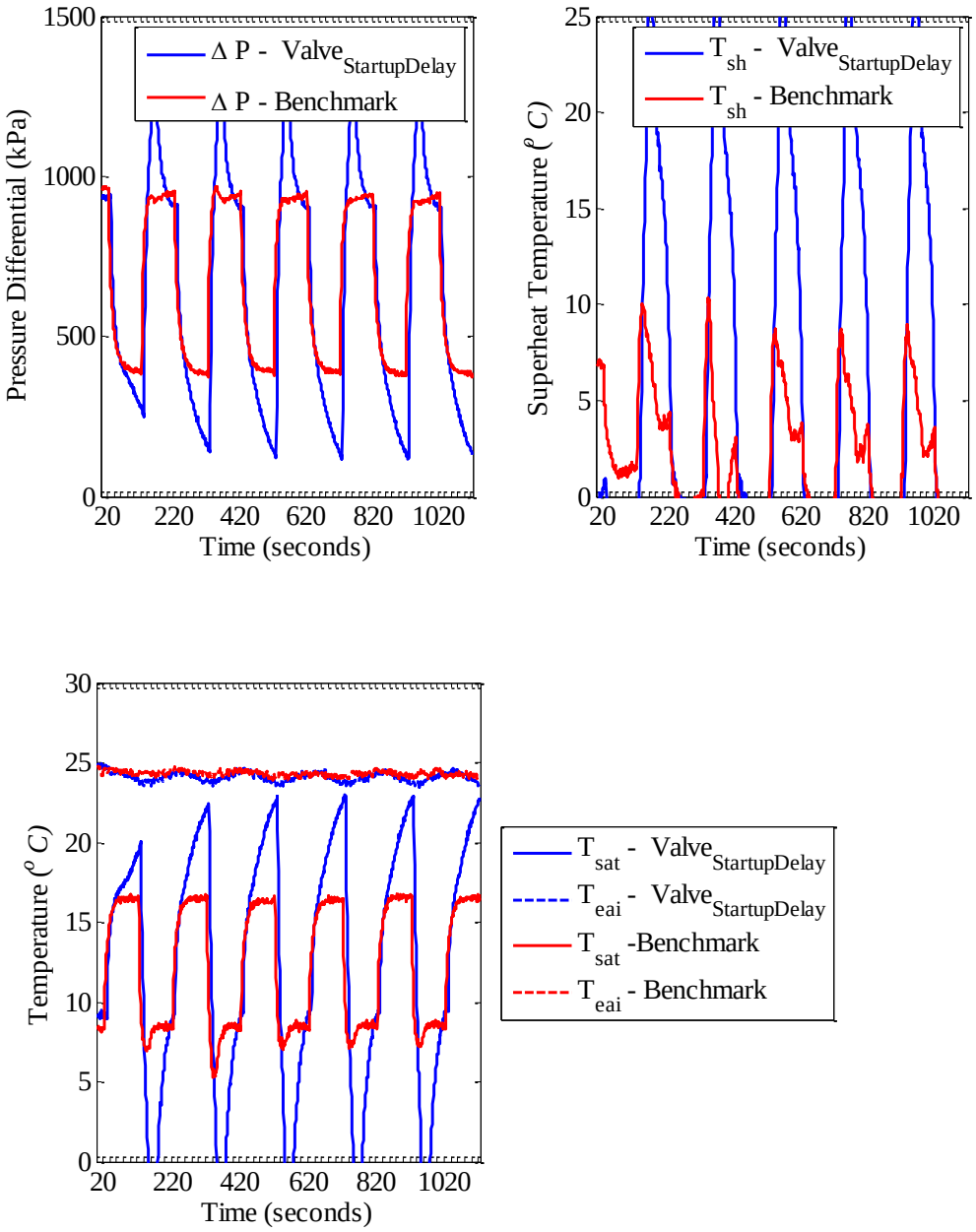

Figure 6.28 Pressure Differential and Superheat – Valve Startup Delay Vs Benchmark – Short Cycle – Experiment

Figure 6.29 shows the effect of 'Valve Startup Delay' on both cooling and work. There is a big loss on startup cooling because the valve is not open to supply refrigerant

for the heat transfer to occur. The power consumed by the compressor is higher than benchmark during startup because the evaporator pressure is higher than nominal during startup.

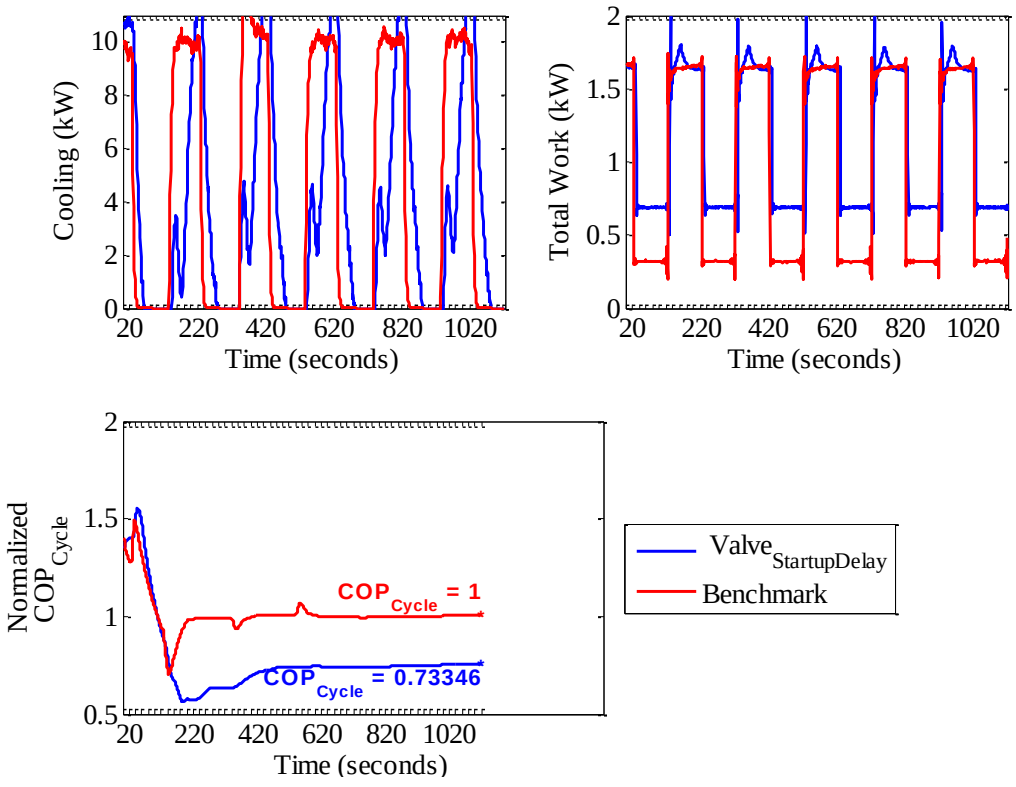

Figure 6.29 Cooling, Work and COP_{Cycle} – Valve Startup Delay Vs Benchmark – Short Cycle - Experiment

Figure 6.30 shows the less cooling per cycle and more work per cycle for the 'Valve Startup Delay' condition when compared to benchmark. A little bit of cooling is got during the initial part of the off cycle but this is not enough to trade of the work that the fan is going to do for the rest of the off cycle.

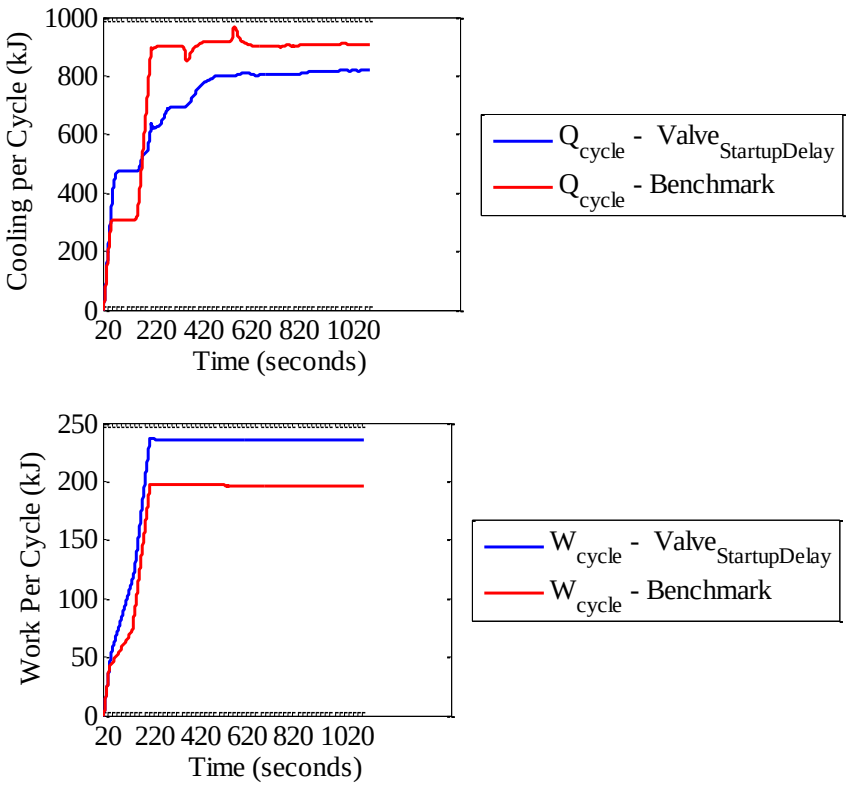

Figure 6.30 Work, Cooling Per Cycle – Valve Startup Delay Vs Benchmark – Short Cycle - Experiment

Table 6.1 Trend Analysis Summary for Expansion Valve – Experiment

Expansion valve cycle S-curve parameter	Recommendations for better cycle efficiency	Representative figures
Shutdown Slope	No significant change	Figure 6.22(a)
Startup Slope	No significant change	Figure 6.22(b)
Shutdown Time	With Compressor	Figure 6.22(c)
Startup Time	With Compressor	Figure 6.22(d)
Valve opening (%) during OFF cycle	Zero	Figure 6.22(e)

To summarize the benchmark valve cycling seems good enough scheme to follow for the short cycle. The consequence of delaying or leading it has a negative effect on cyclic efficiency as tabulated in Table 6.1. Valve cycling mainly affects the startup efficiency of the system by pulling down the pressure faster and thus achieving full cooling capacity faster.

6.1.1.3 Evaporator Fan

The effects of evaporator fan S-curve parameters on COP_{Cycle} is analyzed here. Similar to the simulation conditions, the valve was cycling in sync with the compressor. The valve was not left on throughout the cycle since the effect of fan cycling could not be captured by cycling the fan alone. This approach was also justified since the previous subsection has already established that valve cycling is mandatory for good startup efficiency.

Similar to the expansion valve analysis, the detailed trend analysis was one dimensional where, one parameter was varied according to the range in Table 5.2, the other parameters were held constant at their benchmark values. Figure 6.31 present the results of the detailed trend analysis for the individual S-curve parameters for the evaporator fan profile.

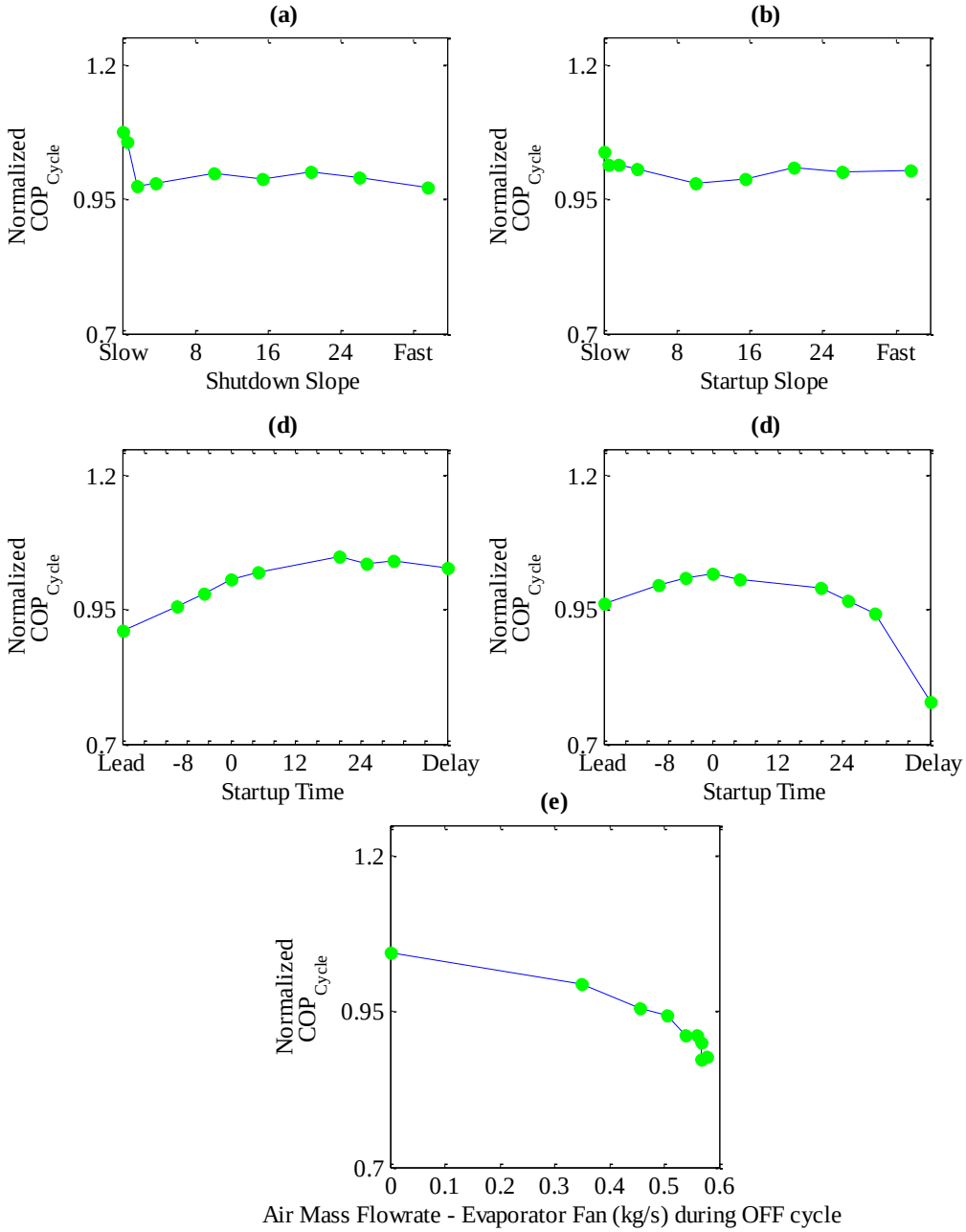

Figure 6.31 Detailed Trends in COP_{Cycle} – Evaporator Fan – Short Cycle - Experiment

Figure 6.31(a) and 6.31(b) show the effect of shutdown slope and startup slope respectively on COP_{Cycle}. They show the relatively negligible effect that the slope has in the system efficiency. Figure 6.31(e) shows the trend of COP_{Cycle} when the air mass flow rate (kg/s) during the off cycle was changed as the parameter. Physically this means leaving the fan on at the specified speed throughout the off cycle. This characteristic notes that the fan has to be strictly OFF during the off cycle for the best cyclic efficiency of the system. Figure 6.31(c) presents the effect of shutdown time on COP_{Cycle}. Delaying the fan switching off with respect to compressor shutdown is observed to have higher efficiency compared to benchmark when the valve is also cycling. Figure 6.31(d) shows the effect of startup time on COP_{Cycle} where trends show that the fan is better off with starting along with the compressor rather than lead/delay it during startup. The effect of delaying the fan during shutdown has already been discussed in Subsection 6.1.1.1 when analyzing the 'Fan Part Cycle' condition. The reasons were also analyzed in the same discussion. The evaporator fan trends were in accordance with the simulation.

The conclusions that were drawn from the trend analysis are summarized in Table 6.2. On an overall note, with the OFF position fixed at zero and the slope effects ignored (since they have relatively less impact on cyclic efficiency), the fan startup time synchronous with the compressor startup, the shutdown time played a big role in the overall optimization of the system as seen in Figure 6.31(c). Fan cycling results in power regulation on the cycle while providing better cooling during shutdown thus, improving the cyclic efficiency of the system.

Table 6.2 Trend Analysis Summary for Evaporator Fan – Experiment

Evaporator fan cycle S-curve parameter	Recommendations for better cycle efficiency	Representative figures
Shutdown Slope	No significant change	Figure 6.31(a)
Startup Slope	No significant change	Figure 6.31(b)
Shutdown Time	Delay (Fan OFF after compressor startup)	Figure 6.31(c)
Startup Time	With the compressor	Figure 6.31(d)
Air mass flow rate during OFF cycle	Zero	Figure 6.31(e)

6.1.2 Long Cycle

Results obtained for a long cycle length of 1000 seconds are presented here. This was to understand how COP_{Cycle} varies with respect to the S-curve parameters during conventional cycling times. Also, since the longer cycle gives enough time for the pressures and temperatures to assume equilibrium, the effect of not having a pressure/temperature differential on the optimum expansion valve, evaporator fan profile was an interesting study. Due to the nature of the length of the cycle only selected test were done to arrive at a conclusion. Detailed expansion valve and evaporator fan were not done for the same reason.

6.1.2.1 Gross Trends

To see whether the normalized COP_{Cycle} changes are significant enough to merit a further detailed investigation, a quick comparison of some possible cycling schemes was done like in simulation. Figure 6.32 shows the gross trends for the various cycling schemes. With the benchmark for comparison at 1 the other cycling schemes are presented. The cycling schemes are explained in Table 5.1.

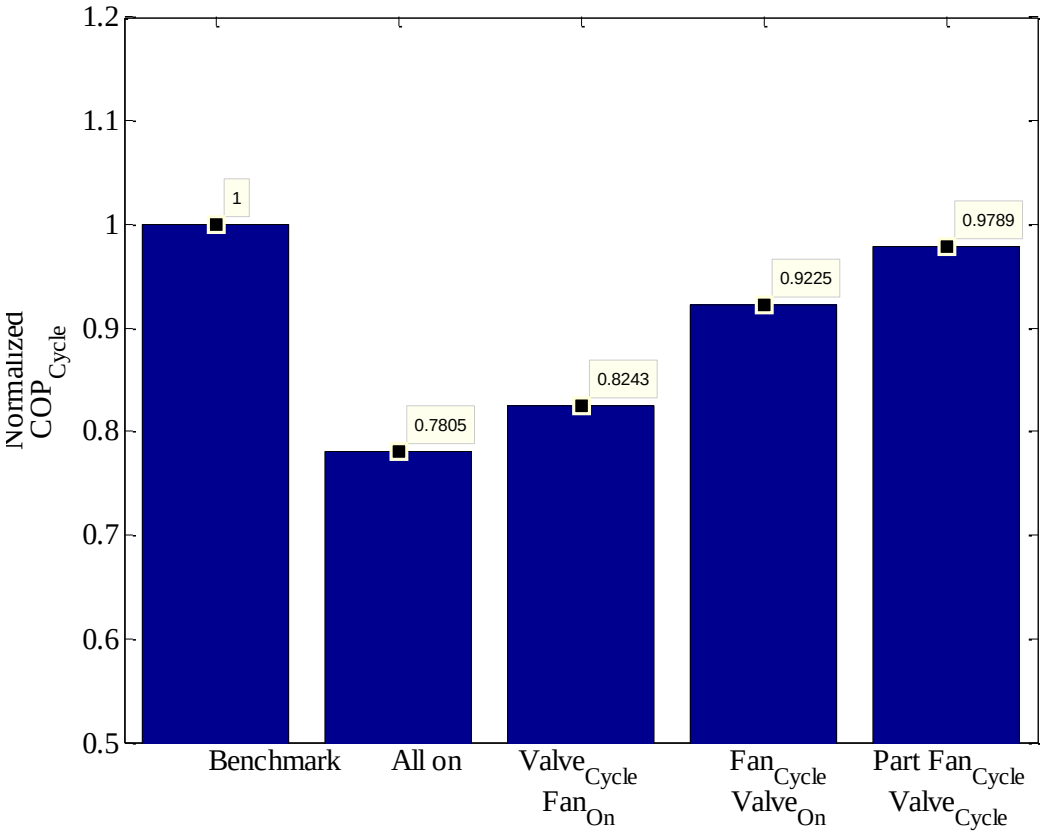

Figure 6.32 COP_{Cycle} Gross Trends of Various Cycling Schemes – Long Cycle - Experiment

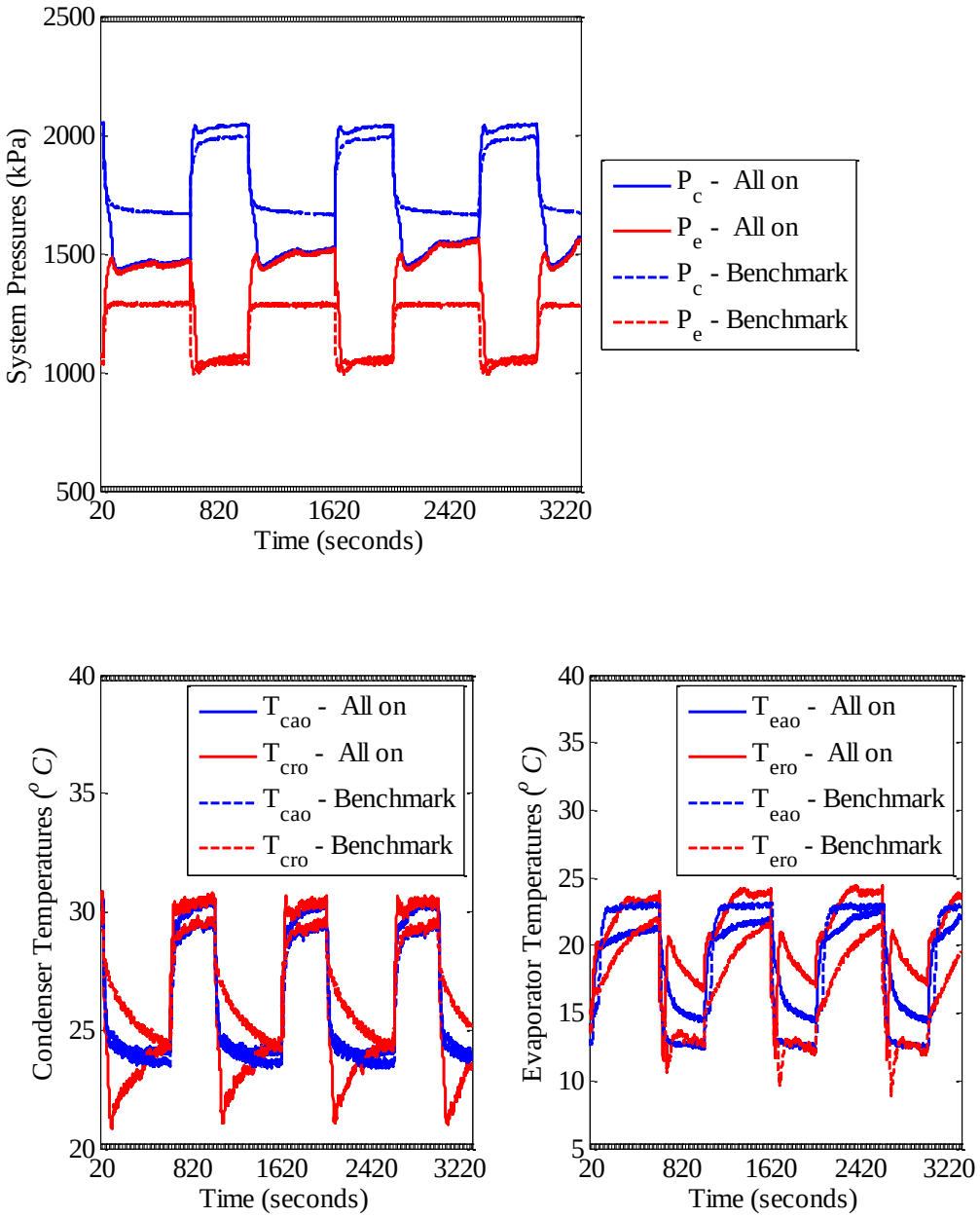

Figure 6.33 System Pressures and Temperatures – All On Vs Benchmark – Long Cycle - Experiment

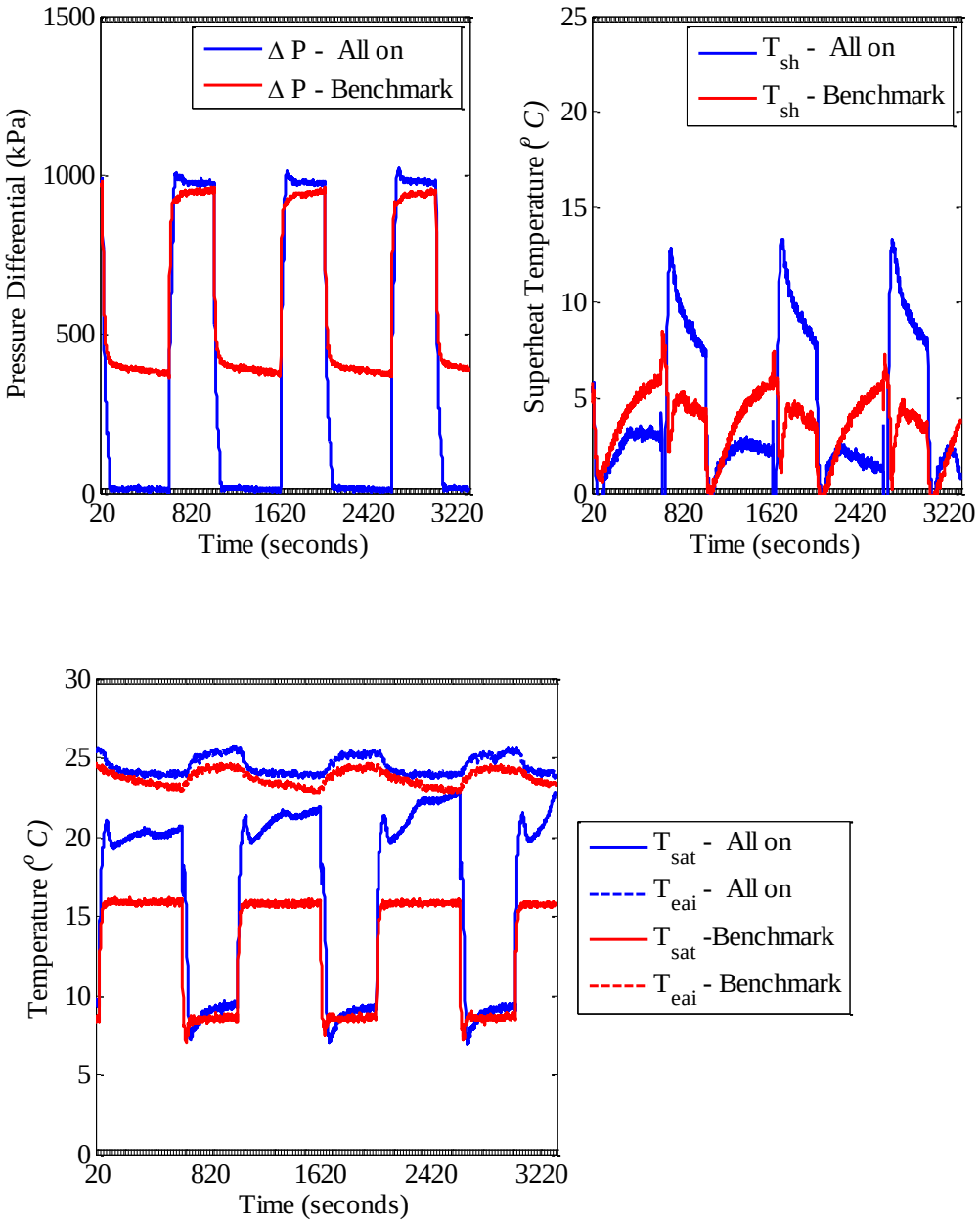

Figure 6.34 Pressure Differential and Superheat – All On Vs Benchmark – Long Cycle – Experiment

Figure 6.33 presents the system pressures and temperatures for the all on condition against the benchmark. As expected, the pressures equalized because the valve was on throughout the cycle. Figure 6.34 shows the pressure differential going to zero. This leads to some cooling loss at startup as shown in Figure 6.35. However this is not the main culprit for the loss in efficiency. Since the fan is on during the relatively long off cycle, it consumes more power while not providing any cooling in return.

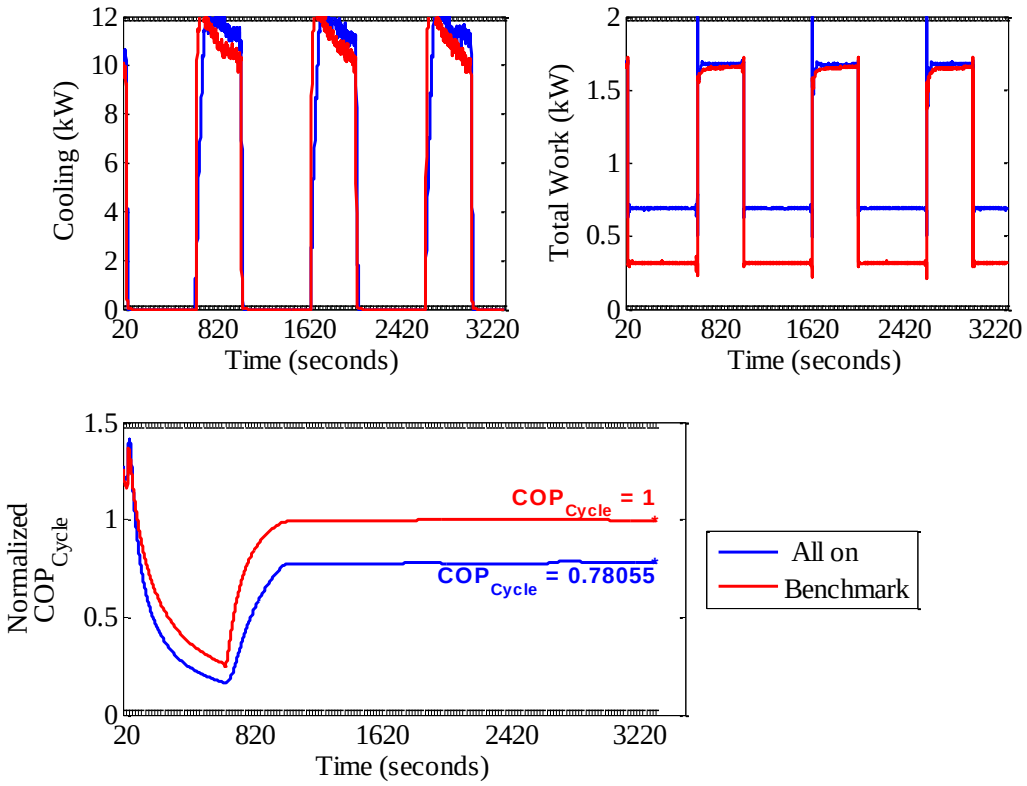

Figure 6.35 Cooling, Work and COP_{Cycle} – All On Vs Benchmark – Long Cycle - Experiment

Figure 6.36 shows the cooling and work per cycle. Because the fan is being on throughout the length of the cycle, the work per cycle is really high. The loss in startup cooling does not affect cyclic efficiency too much in the long run.

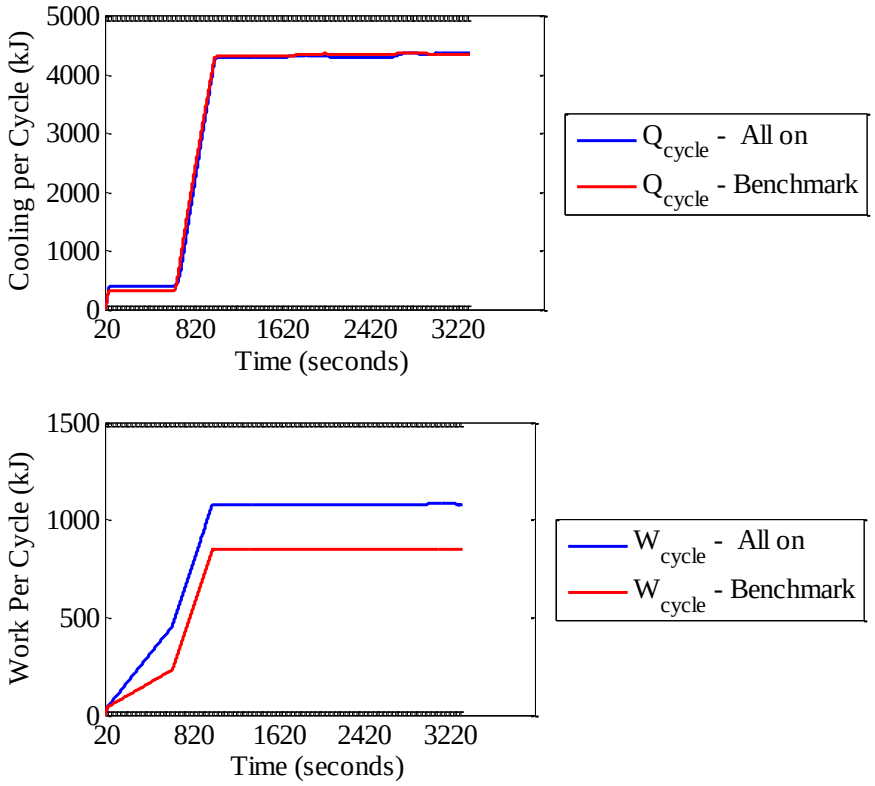

Figure 6.36 Work, Cooling Per Cycle – All On Vs Benchmark – Long Cycle – Experiment

The next case is the 'Valve Cycle Fan On' condition. Compared to the short cycle where this scheme performed moderately well, here it is one of the worst performers. This is again because the fan is on for the length of the cycle. As discussed in simulation, fan cycling plays a much important role during the long cycle. Figure 6.37

shows the system pressures and temperatures. As the cycle kicks in there is some pressure differential as shown in Figure 6.38 but during subsequent cycles the system loses the pressure differential during the off cycle.

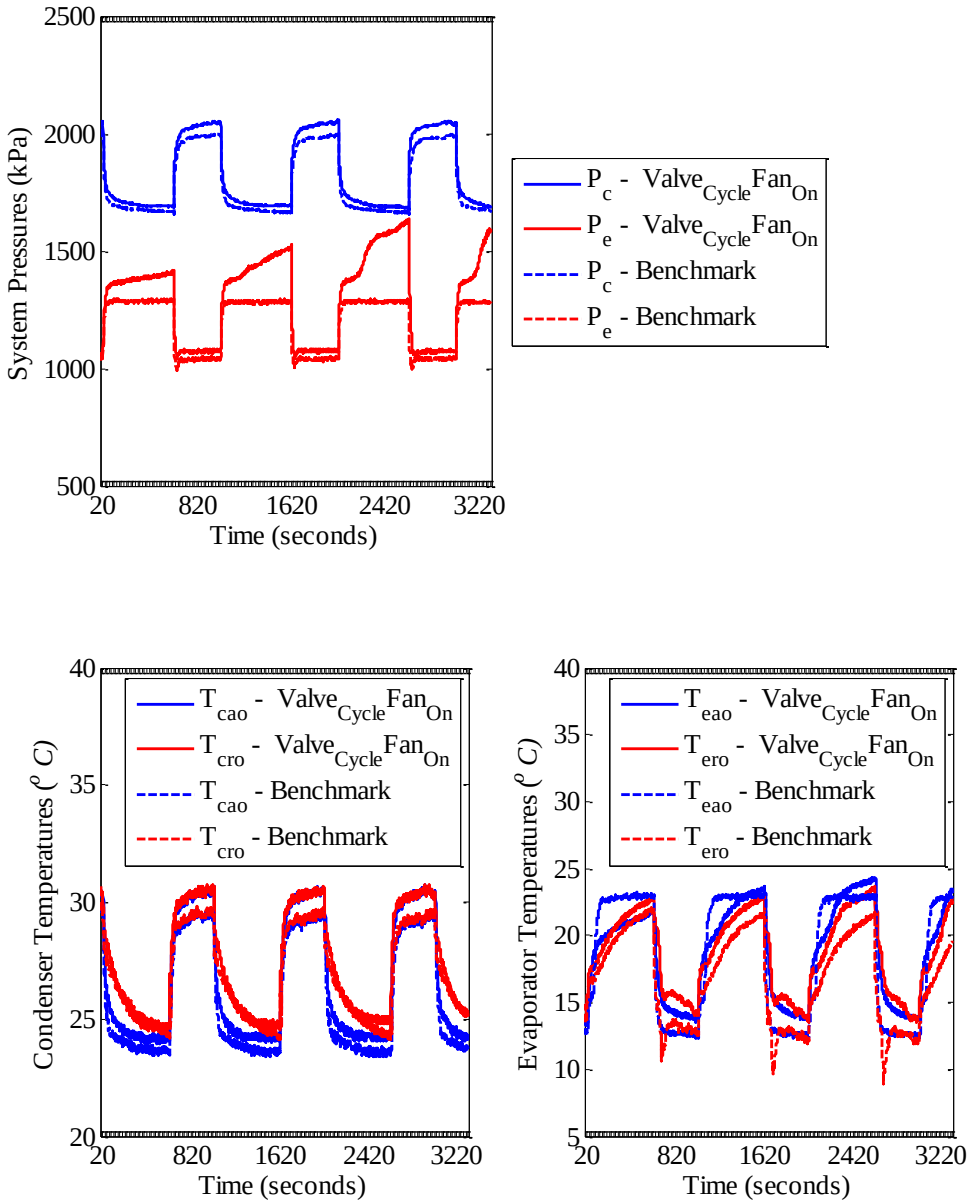

Figure 6.37 System Pressures and Temperatures – Valve Cycle Fan On Vs Benchmark – Long Cycle - Experiment

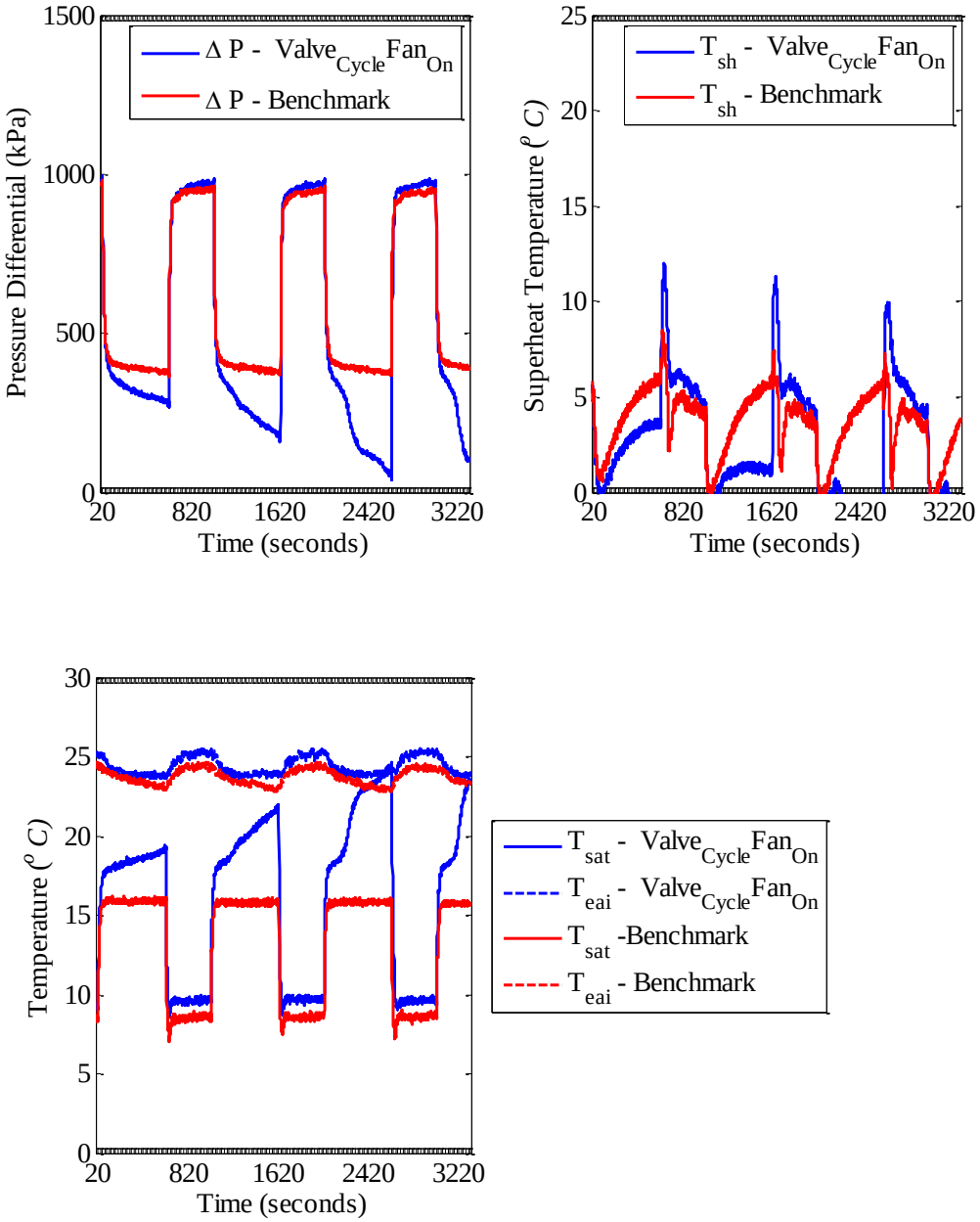

Figure 6.38 Pressure Differential and Superheat – Valve Cycle Fan On Vs Benchmark – Long Cycle – Experiment

Figure 6.39 shows that the 'Valve Cycle Fan On' condition gives a little bit more cooling because the fan is on through the off cycle also. This can be seen from the cooling per cycle in Figure 6.40. However the power consumed by the fan during the off cycle is much more so that the cooling is more than traded off by the fan power as shown in Figure 6.40. Hence this scheme results in a low efficiency.

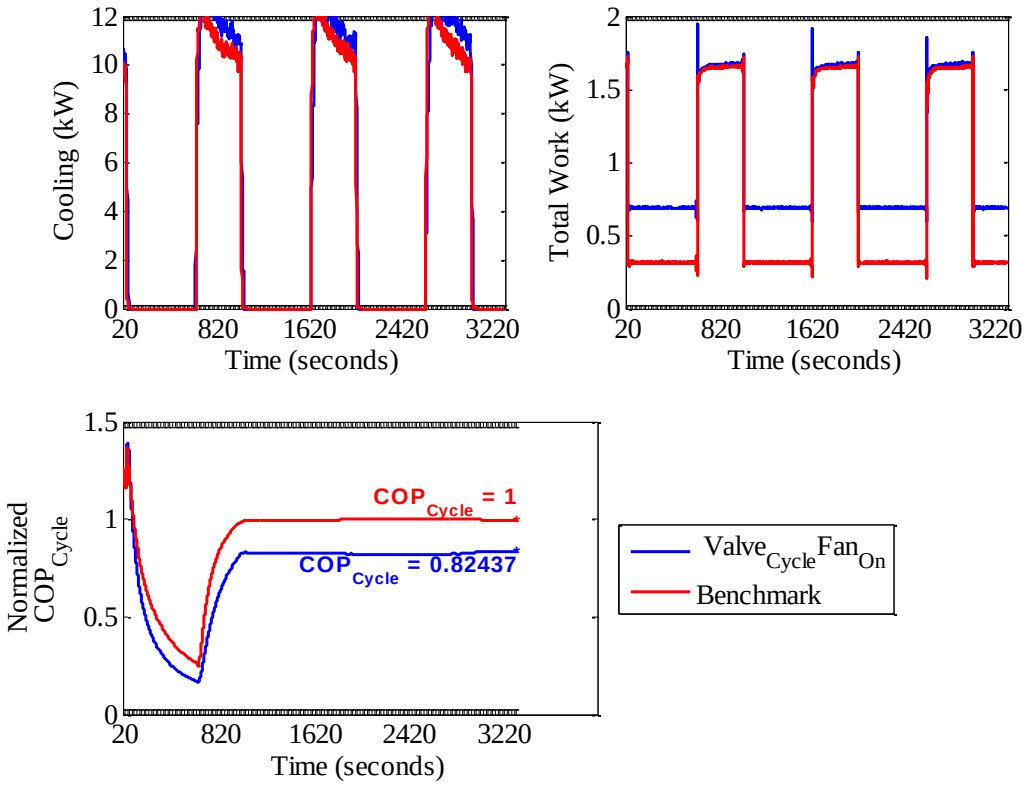

Figure 6.39 Cooling, Work and COP_{Cycle} – Valve Cycle Fan On Vs Benchmark – Long Cycle – Experiment

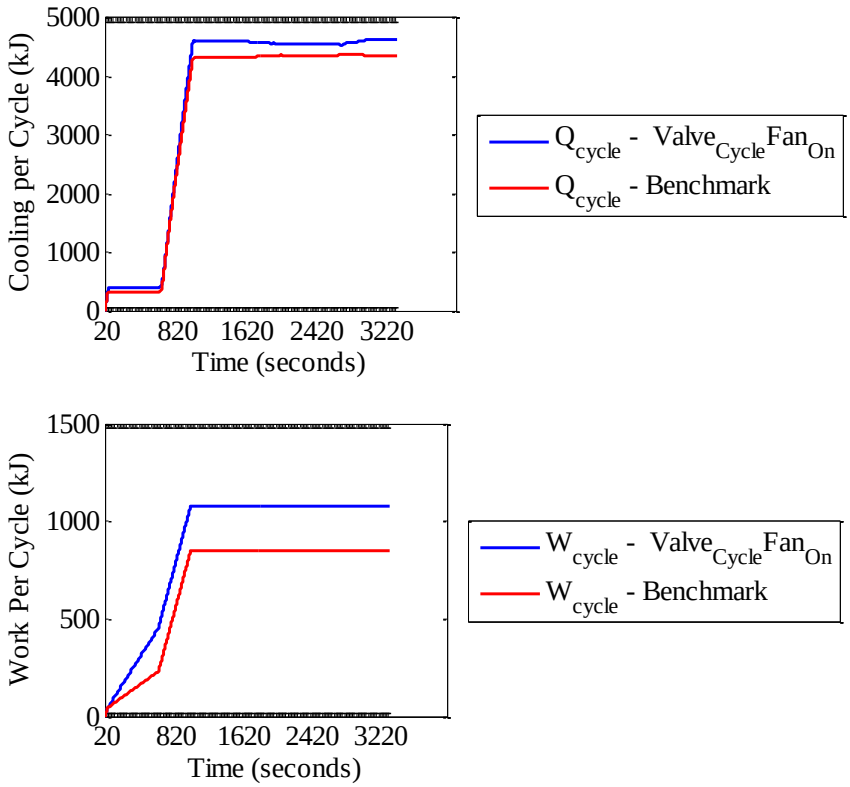

Figure 6.40 Work, Cooling Per Cycle – Valve Cycle Fan On Vs Benchmark – Long Cycle – Experiment

'Fan Cycle Valve On' was one of the worst schemes in terms of effect to cyclic efficiency in the short cycle. But here it is one of the better schemes. This proves that effect of fan cycling is much more in long cycle. Figure 6.41 presents the system temperatures and pressures. Since the valve is on, the pressures equalize almost instantaneously at shutdown. This can also be visualized as pressure differential going to zero in Figure 6.42.

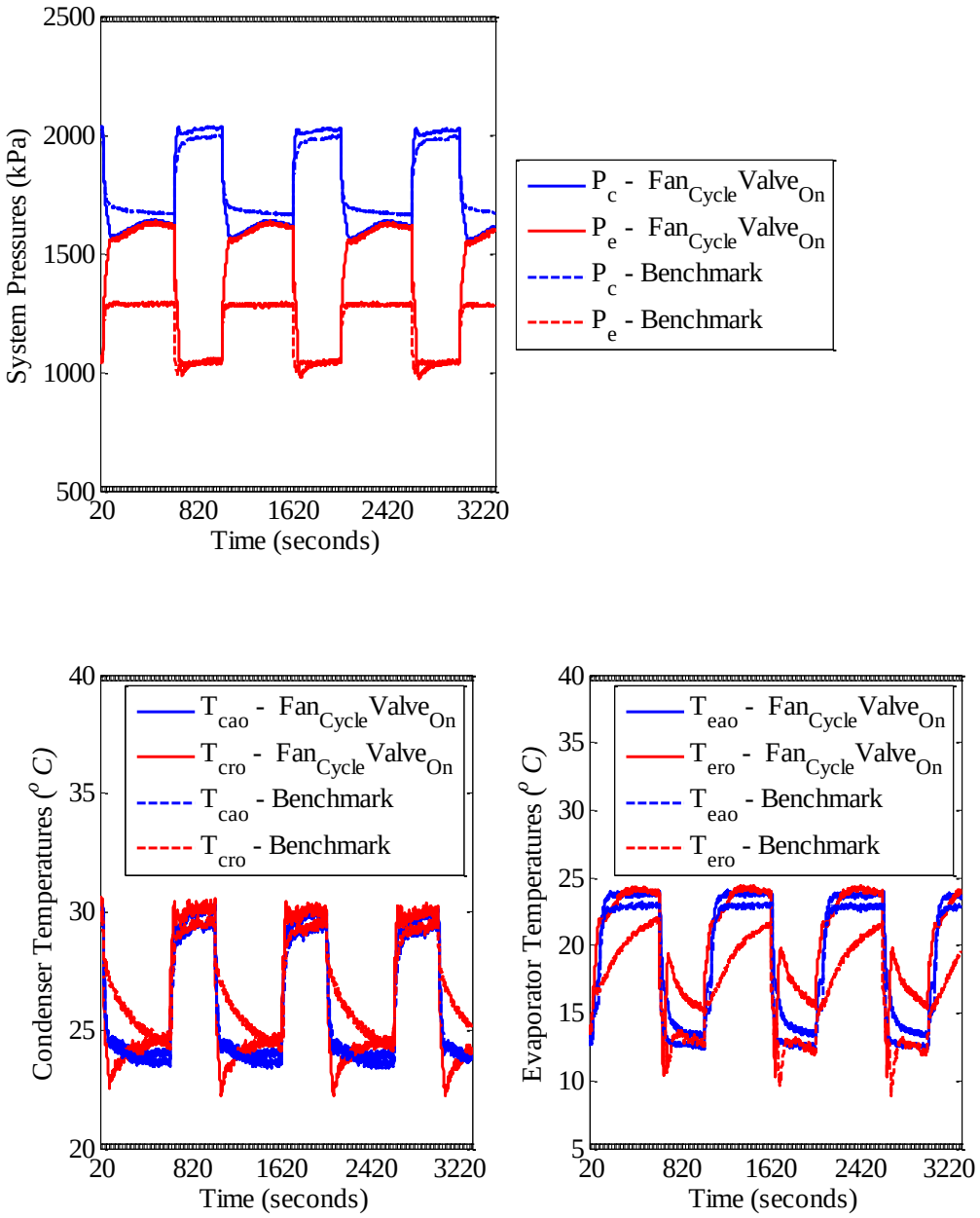

Figure 6.41 System Pressures and Temperatures – Fan Cycle Valve On Vs Benchmark – Long Cycle - Experiment

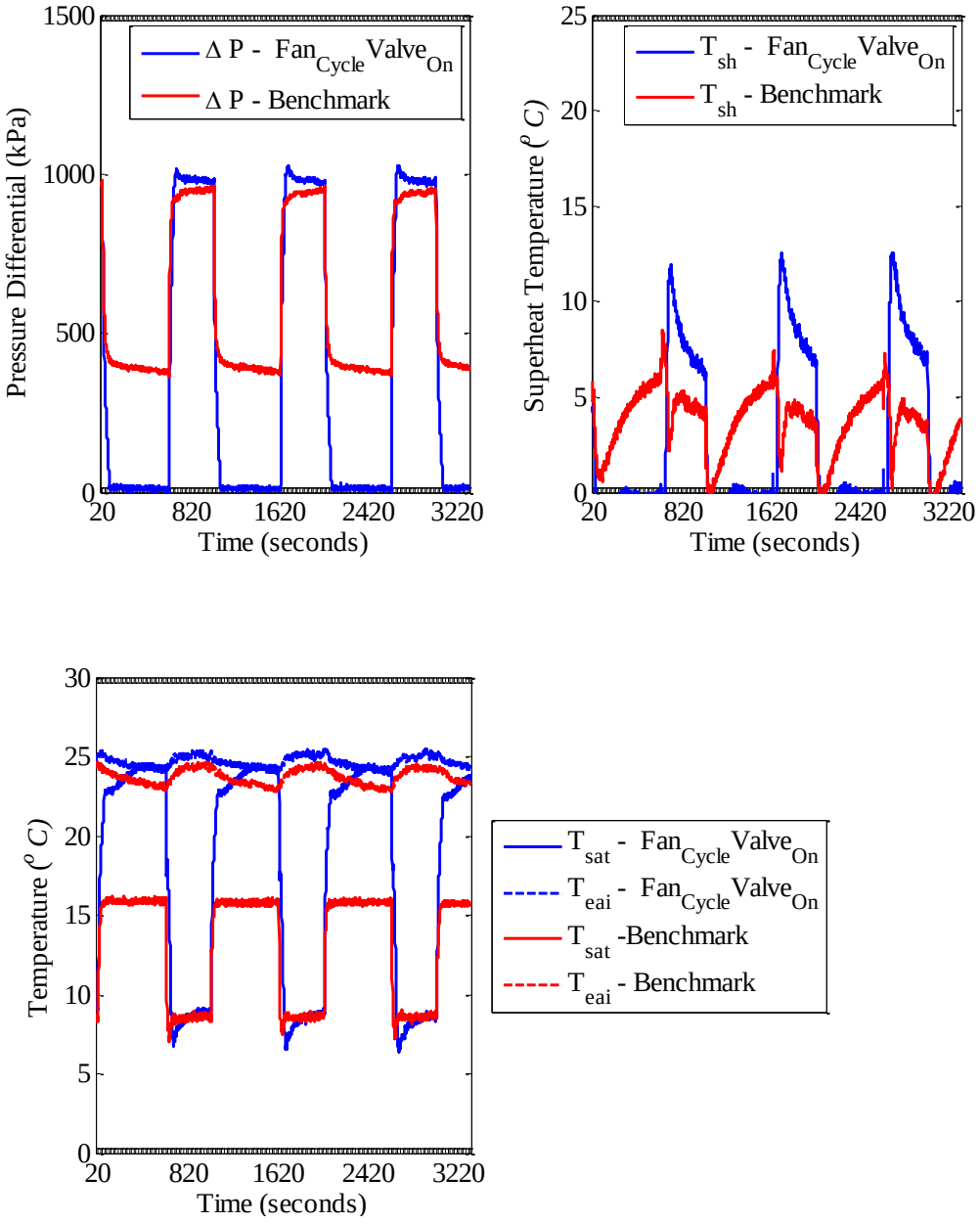

Figure 6.42 Pressure Differential and Superheat – Fan Cycle Valve On Vs Benchmark – Long Cycle – Experiment

Figure 6.43 shows that 'Fan Cycle Valve On' is just 8% away from benchmark efficiency. This is because the fan cycling is similar to that of benchmark thus saving all

the power not being on during the off cycle. The downside in this approach is that since the valve is on, the evaporator has much more refrigerant than benchmark condition and the compressor has to do all the work to build up the flow. This is the cause for losing some cooling during startup as shown in Figure 6.43.

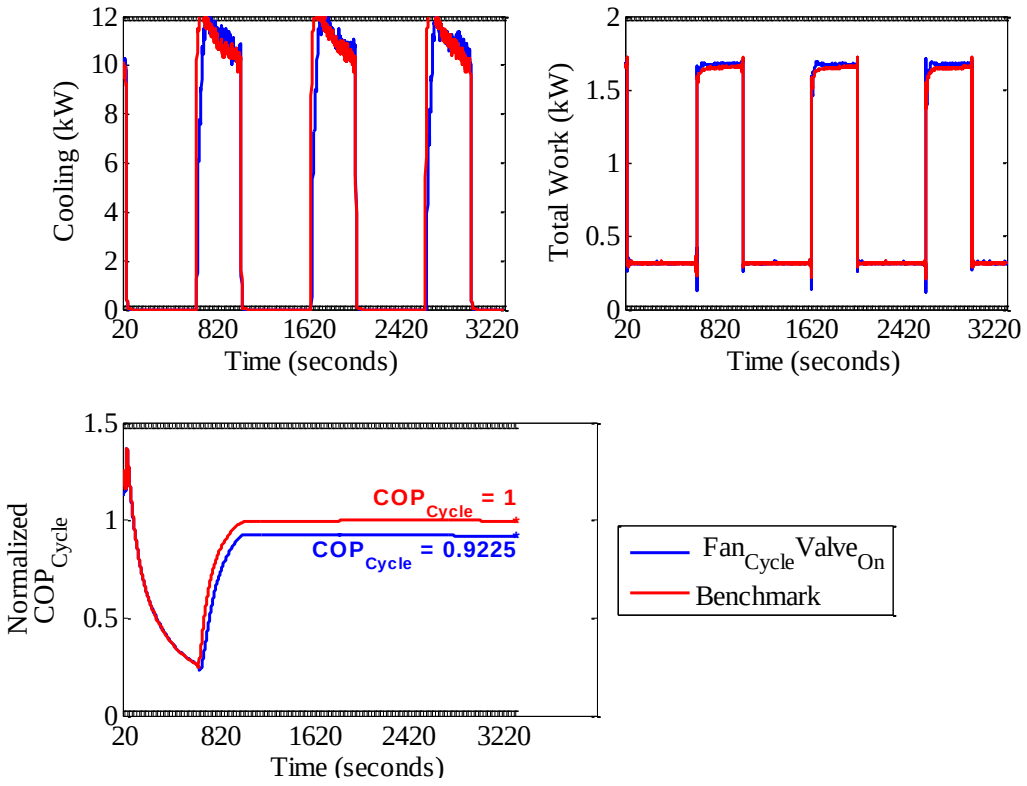

Figure 6.43 Cooling, Work and COP_{Cycle} – Fan Cycle Valve On Vs Benchmark – Long Cycle – Experiment

The cooling loss during startup is visualized in the cooling per cycle in Figure 6.44. Since the power consuming components are cycling in the same way in the

benchmark and the ‘Fan Cycle Valve On’ condition, the work per cycle remains the same.

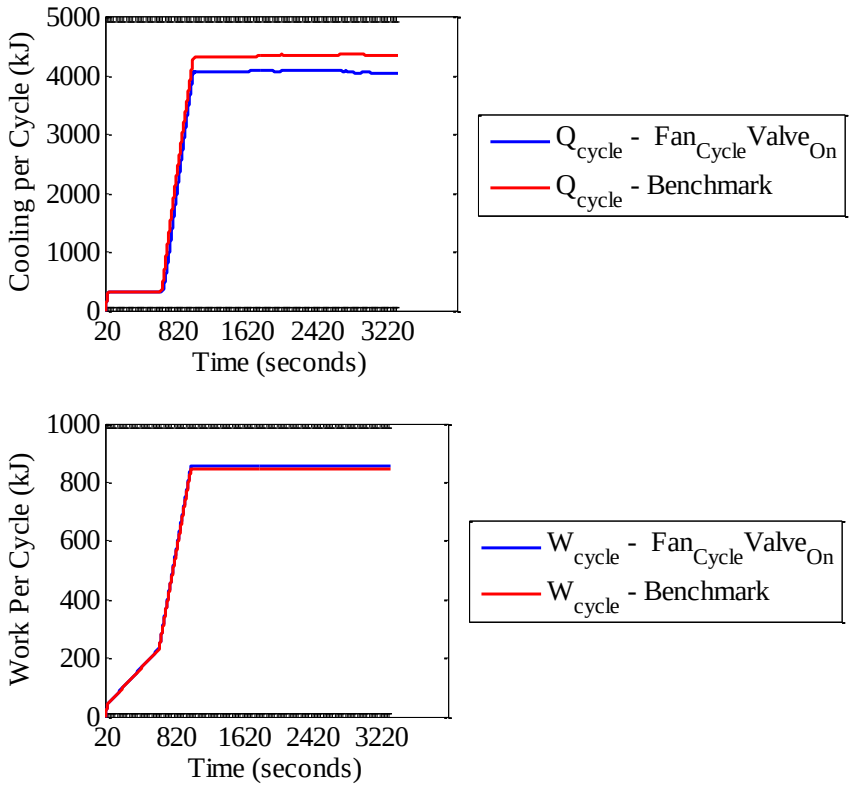

Figure 6.44 Work, Cooling Per Cycle – Fan Cycle Valve On Vs Benchmark – Long Cycle – Experiment

The final case is ‘Fan Part Cycle’, where the fan is on for 20 seconds after the compressor shuts down. The valve cycles according to benchmark. Figure 6.45 presents the system pressures and temperatures. They look essentially the same for the ‘Fan Part

Cycle' and the benchmark conditions. This means the fan being on for just 20 seconds more does not have the kind of effect it had for short cycle.

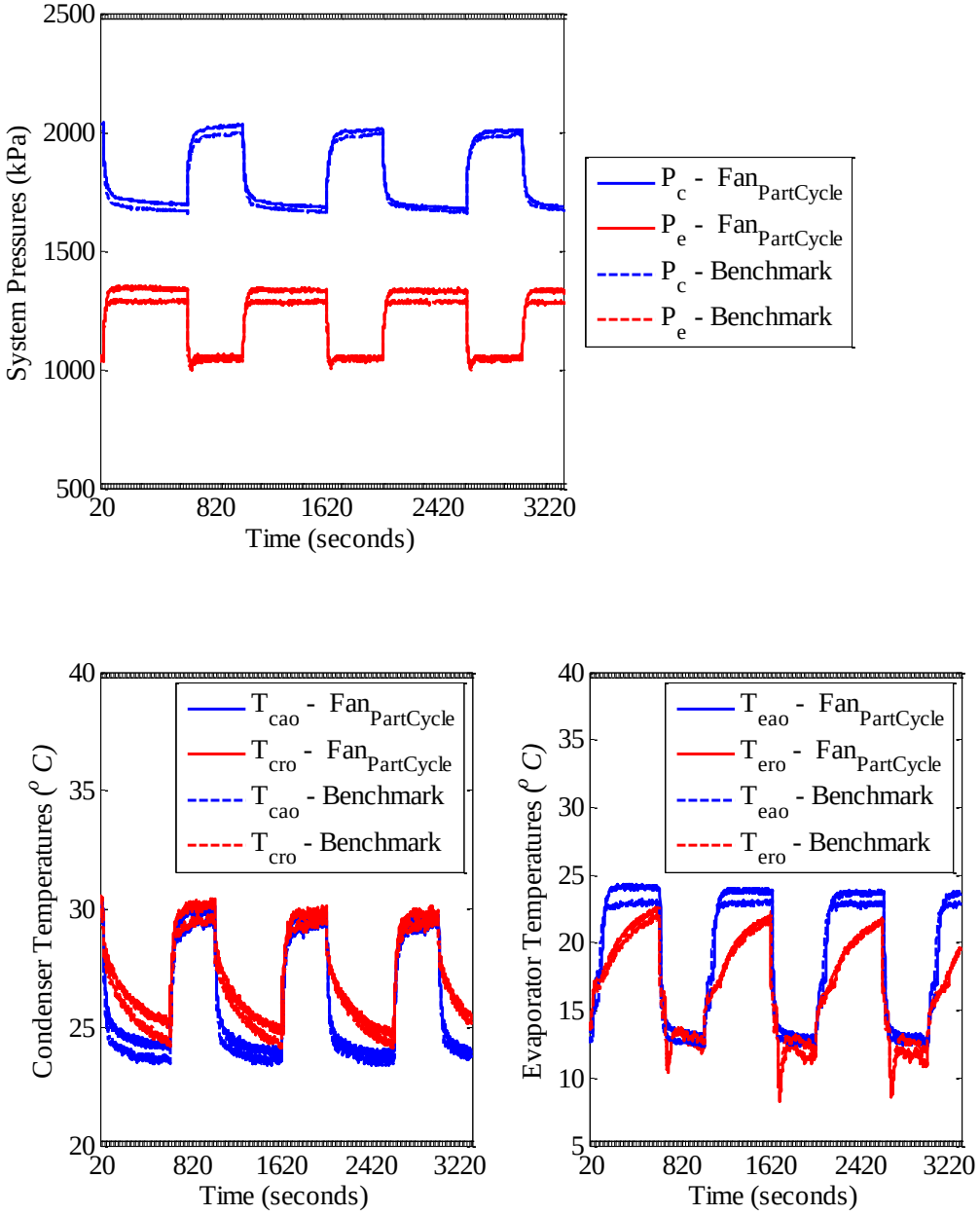

Figure 6.45 System Pressures and Temperatures – Fan Part Cycle Vs Benchmark – Long Cycle - Experiment

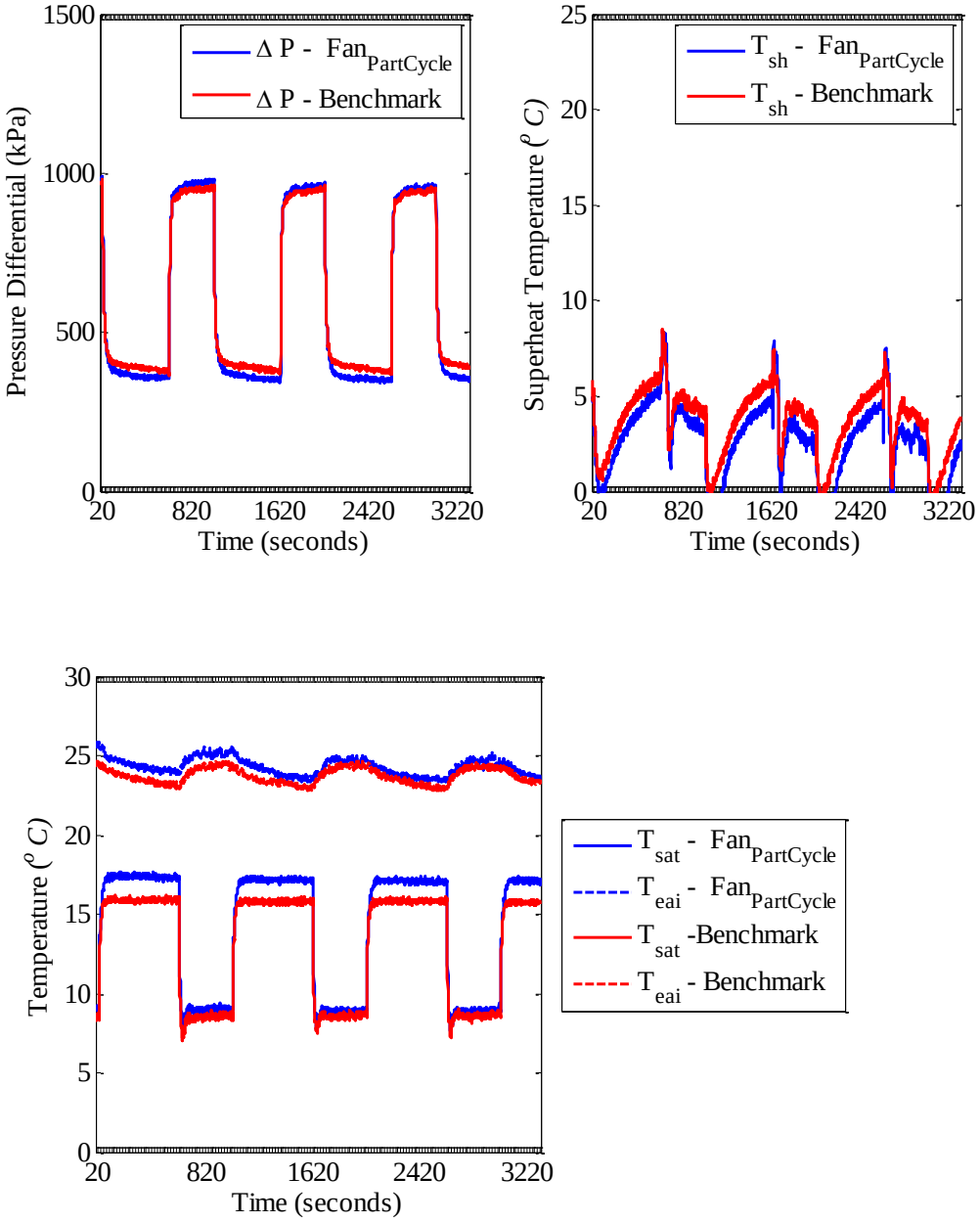

Figure 6.46 Pressure Differential and Superheat – Fan Part Cycle Vs Benchmark – Long Cycle – Experiment

The pressure differential and the superheat also look similar for the two conditions as shown in Figure 6.46. Figure 6.47 shows the instantaneous work and cooling curves which looks essentially the same except for the extra 20 seconds of fan power in the beginning of the off cycle.

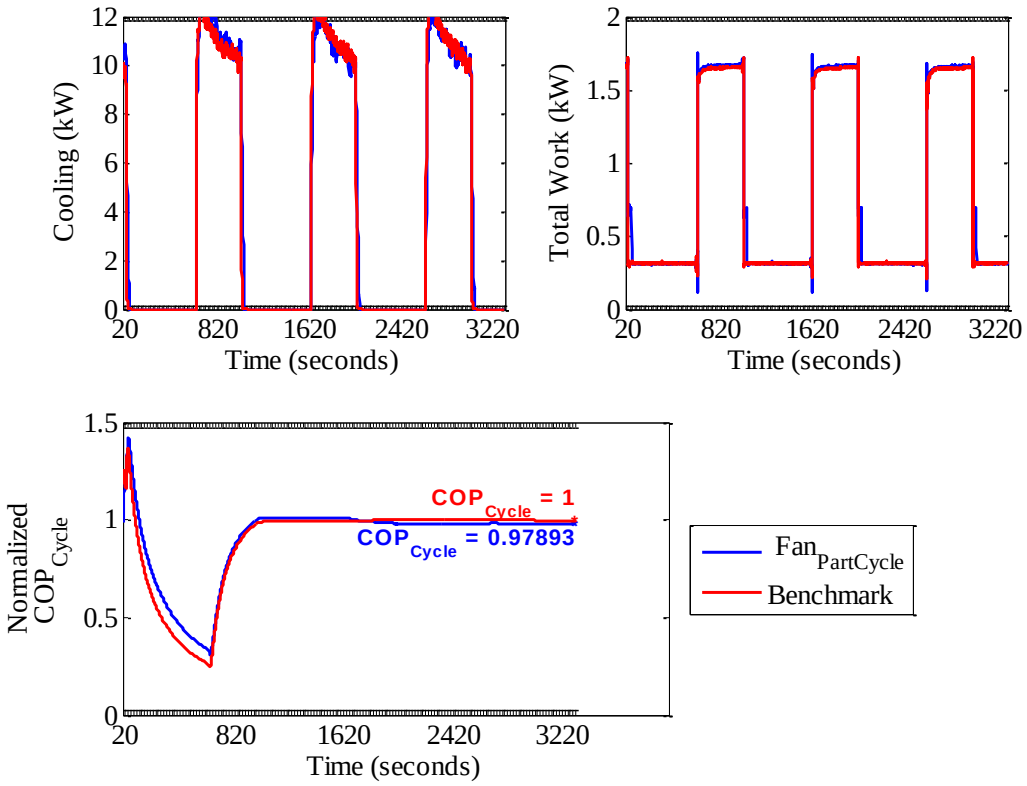

Figure 6.47 Cooling, Work and COP_{Cycle} – Fan Part Cycle Vs Benchmark – Long Cycle - Experiment

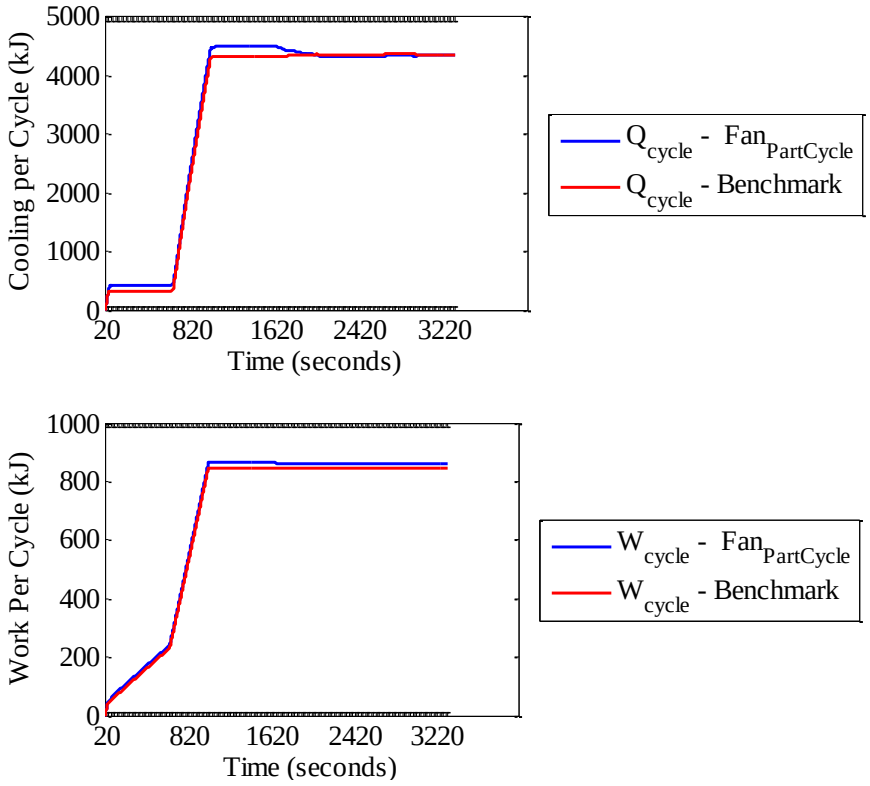

Figure 6.48 Work, Cooling Per Cycle – Fan Part Cycle Vs Benchmark – Long Cycle – Experiment

Unlike the short cycle where this scheme seemed to show a gain in efficiency, here it was just about the same if not lesser as can be seen from cooling and work per cycle in Figure 6.48. The extra fan power does not achieve any significant cooling during the initial part of the cycle.

Overall, the various cycling schemes show that there is not much room to improve in terms of efficiency change. One of the discerning characteristic in the long cycle is the major effect of fan cycling on cyclic efficiency. Whereas valve cycling was

of primary importance in short cycle, it is intuitive to think that fan cycling plays a major part in the long cycle. This is because, switching of the fan during the long off cycle allows for less power consumption thus giving efficiencies close to benchmark. The relatively less effect of valve cycling here compared to short cycle is attributed to the fact that the longer period of the cycle allows for the pressures and temperatures to settle to equilibrium and any losses in startup efficiencies as such will be insignificant given the length of the cycle. At this point it is concluded that changing the S-curve parameters would not yield much change in the COP_{Cycle}. To prove this fact, selected tests were done to see the effect of evaporator fan cycling on COP_{Cycle}. These tests are described in Table 6.3.

Table 6.3 Selected Fan Part Cycling Schemes – Long Cycle - Experiment

TEST	DESCRIPTION
1	Benchmark: Valve, Fan cycled synchronous with compressor
2	Fan runs at full speed for T1 seconds AFTER compressor shutdown and then switch off
3	Fan runs at 30% speed for T1 seconds AFTER compressor shutdown and then switch off
4	Fan runs at 30% speed for T2 seconds AFTER compressor shutdown and then switch off (T2 = Time for fan to consume same power as it runs full speed for T1)
5	Fan runs at 30% speed for the entire OFF cycle

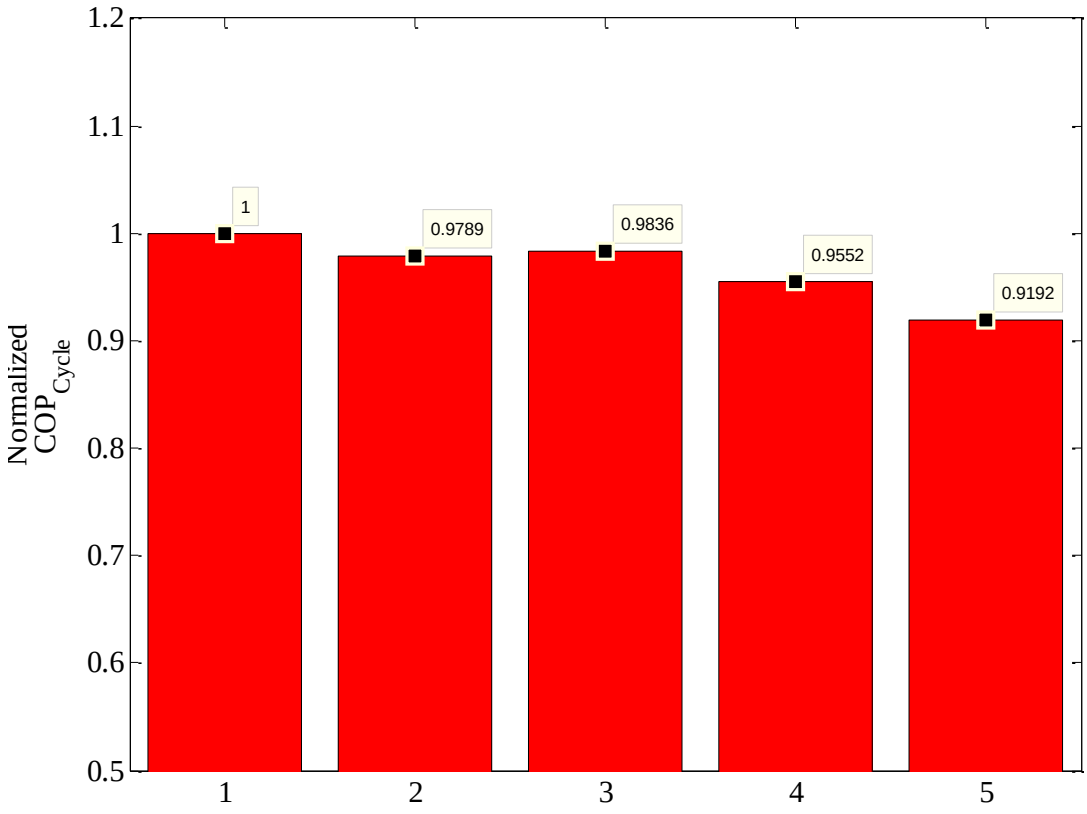

Figure 6.49 COP_{Cycle} Trends Selected Part Fan Cycling Schemes – Long Cycle - Experiment

Figure 6.49 shows the results of the selected part fan cycling schemes. Test 3 which is the 'Fan Part Cycle' discussed before is the scheme that comes closest to benchmark. The other tests come slightly close to it which shows how little things change when it comes to the long cycle. With the available information on the long cycle, the recommendations for the expansion valve and evaporator fan is the same as benchmark.

6.2 Optimization

Subsection 5.4 presented the results of the optimization done through simulation. In this subsection the effect of similar optimization on the experimental TRANE system is discussed.

The prospect of real time optimization was first explored by having the optimization algorithm solve for iterates after each cycle experiment was completed. The objective function was the same $ICOP_{Cycle}$ as was used in the simulations. Experimental data after each cycle experiment was processed and the value of objective function was determined based on the cooling output and the work input as discussed in Subsection 5.1. Cooling on the air side (equation 6.1) was used to calculate the objective function. Appropriate humid air properties were considered for the necessary calculation of the objective function.

$$Q_{air} = \dot{m}_{air}\, C_P\, (T_{in} - T_{out}) \qquad 6.1$$

The next step was to run the optimization routine on the experiment. This was carried out with ease since the data acquisition system used (WinCon 5.0) was MATLAB/Simulink based and thus the minimization algorithm used in the simulation was available directly for use here. The only downside to this approach was the time taken to complete one function evaluation. Considering that the cycle length was 200 seconds and the system had to reach steady state before the cycling began, the test took approximately around half an hour to complete six cycles and give a value of the objective function. So even if an assumption was made that a maximum of 25 function evaluations would be required to converge on the optimal parameters, in real time it

would take around 12 hours. The experiment was carried out with the Nelder Mead simplex search algorithm used in the simulation optimizations because it was the only way to prove the approach. This algorithm did not seem to work that well for real time optimization because the algorithm kept getting trapped at the initial guess value no matter where it was placed. This was understandable because, for small steps local to the initial guess, the $ICOP_{Cycle}$ trend did not follow the global pattern. This was attributed to any sensor noise/disturbance that could affect the system. Thus any point had the probability to act as local minima because of the noise. There is no way to alter the way in which the Nelder Mead simplex method works because it's a systematic non gradient numerical approach.

The only way the real time optimization was expected to work was when the step size of the optimization algorithm could be changed. By making the minimum step size of the algorithm bigger, the routine was expected to escape local troughs on the surface, thus effectively seeing what the bigger picture with respect to the global trends was. MATLAB allows changing the minimum step size only for its constrained minimization algorithms. Thus, the next step was to run the real time optimization with one of the constrained minimization algorithms namely, the active set algorithm. However even this algorithm had hard time keeping to the feasible descent approach. In other words, the algorithm hard time finding iterates that always resulted in a descent from the previous iteration. A part of the problem was the sensors installed in the system. The uncertainty in the instantaneous COP was around 4% of the steady state value. From these experiences the feasibility of the optimization procedure in a practical setting could

be seen. Laboratory conditions were not controlled enough to perform the online optimization. This meant that the optimization procedure on the site of the installation (say a home or supermarket) is not warranted due to the lack of controlled conditions. Thus strictly controlled environment such as a psychrometric chamber is recommended to do the optimization procedure.

6.3 Discussion

The benchmark set in this thesis is valve and fan cycling synchronously with the compressor. However in practice the valve is controlled for superheat by a controller. There is a need to look at how the optimized cycle does in practice. Since the optimization was not possible for the experimental system, a comparison of the assumed benchmark cycle to a superheat controlled cycle is done here to see the effect of a practical controller. Similar to the simulations, there are two types of control that is compared with the benchmark cycle:

- Control Scheme 1: Valve position is determined by the superheat controller through the on and off cycle.
- Control Scheme 2: Valve position is determined by the superheat controller through the on cycle. During the off cycle the controller is over ridden and is completely shut off to avoid migration.

The controller used in the two schemes was a simple PI controller. With control scheme 1 as the new benchmark set at 1, a comparison with the previously set benchmark cycle is done. There is a vast change in efficiency of the previously set

benchmark cycle with respect to control scheme 1. The main reason for this inefficiency is that the controller is still in action during the off cycle. This lets some refrigerant into the evaporator which presents the migration problem. However in the previously set benchmark cycle, the valve shuts off before the compressor shuts down thus preventing the refrigerant from occupying the evaporator. The valve command for control scheme 1 is shown in Figure 6.50. During the off cycle the valve is still open at some percentage.

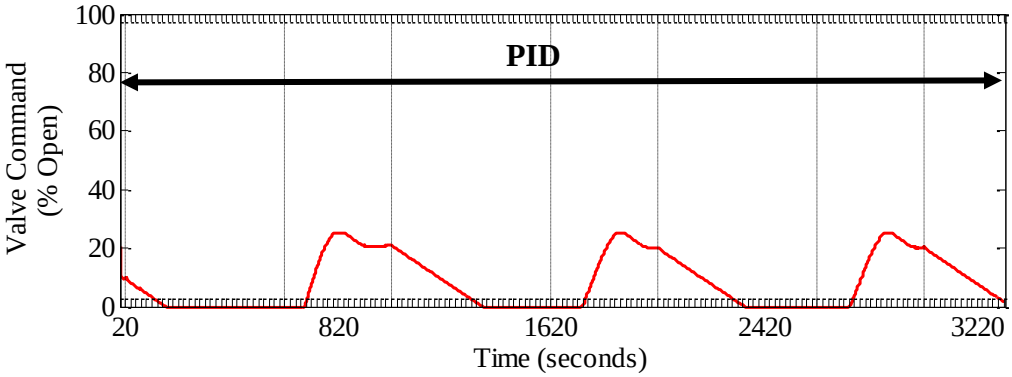

Figure 6.50 Valve Command for Control Scheme 1 - Experiment

The valve command for control scheme 2 is shown in Figure 6.51. Basically the control signal gets multiplied by the compressor signal so that the controller works only during the on cycle whereas in the off cycle it is switched off and the valve goes to zero position. This method aims to couple the controller's ability to attain superheat faster while also turning off the valve during shutdown for better startup performance.

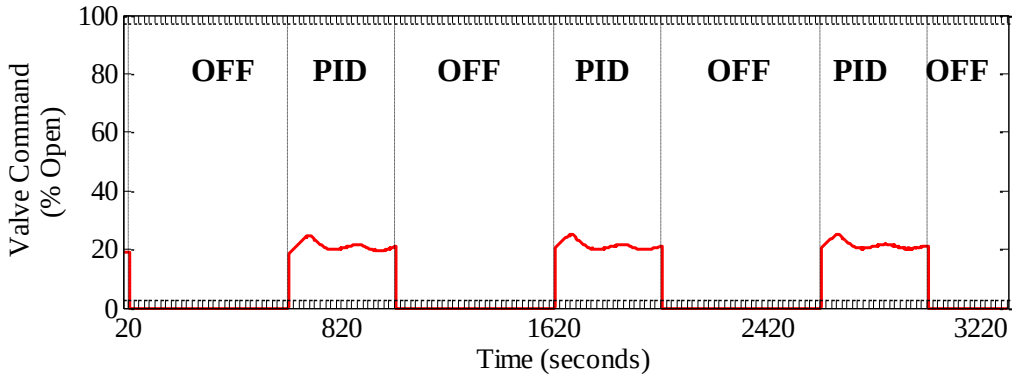

Figure 6.51 Valve Command for Control Scheme 2 - Experiment

Figures 6.52 – 6.55 compare control schemes 1 and 2 with the previously set benchmark cycle. Figure 6.52 presents the system pressures and temperatures. Since the valve is not completely shut off during the off cycle for control scheme 1, the pressures get closer to each other when compared to the control scheme 2 or the benchmark condition. The benchmark cycle has a faster superheat build up as shown in Figure 6.53. Control scheme 2 has similar superheat build up when compared to benchmark. The poor controller performance of control scheme 1 is attributed to the integrator windup that happens during the off cycle. This is because the controller is still in action during the off cycle. This is the reason for the cooling to reach its rated capacity so fast for the benchmark and control scheme 2 compared to control scheme 1. Figure 6.54 shows the instantaneous cooling got at the startup. The power consumed by the compressor and the fan are almost similar for the three conditions. Figure 6.55 shows the cooling and work per cycle. Because of the better startup performance the benchmark and control scheme 2 cycles have significantly more cooling compared to control scheme 1.

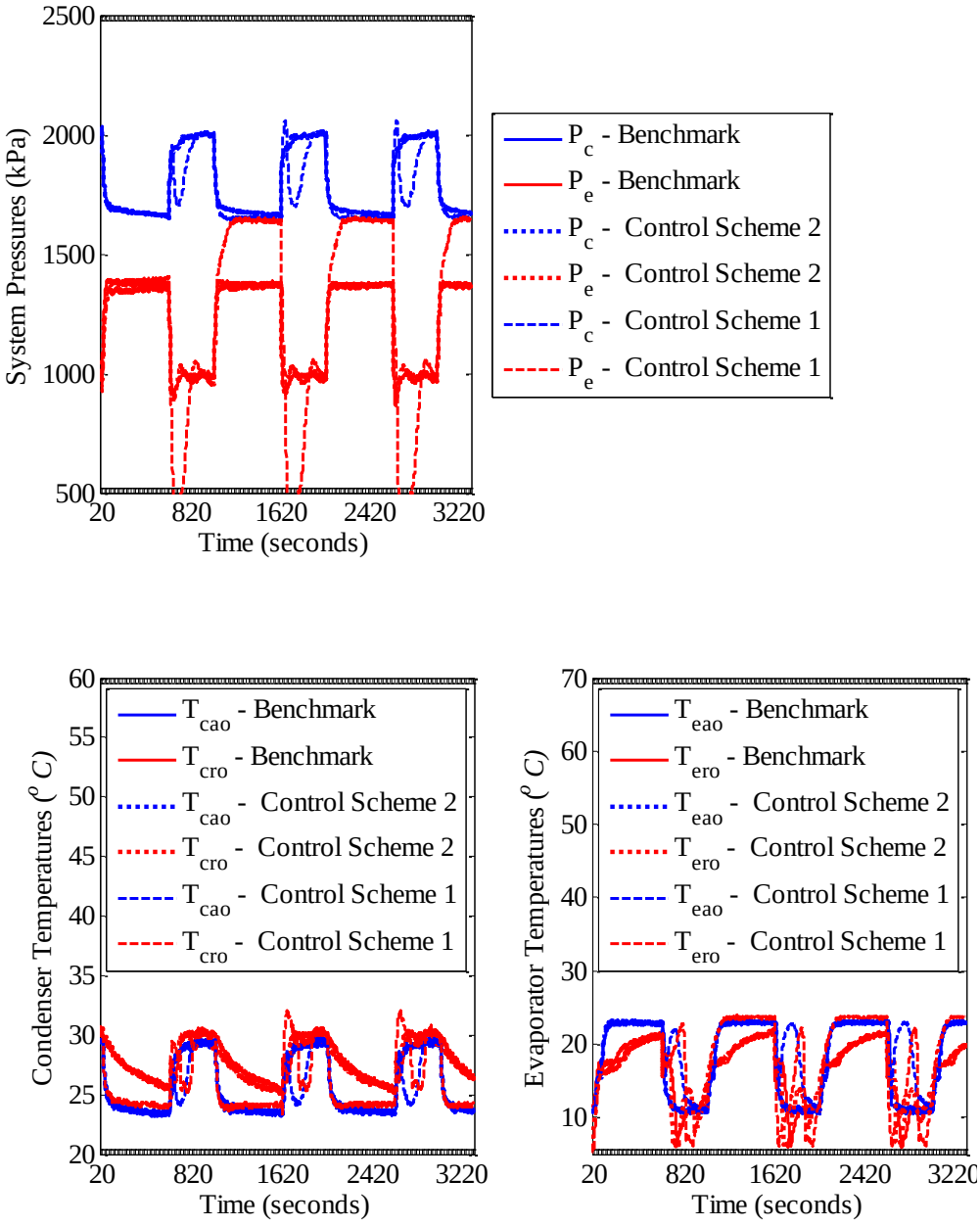

Figure 6.52 System Pressures and Temperatures – Benchmark Vs Control Scheme 2 Vs Control Scheme 1 - Experiment

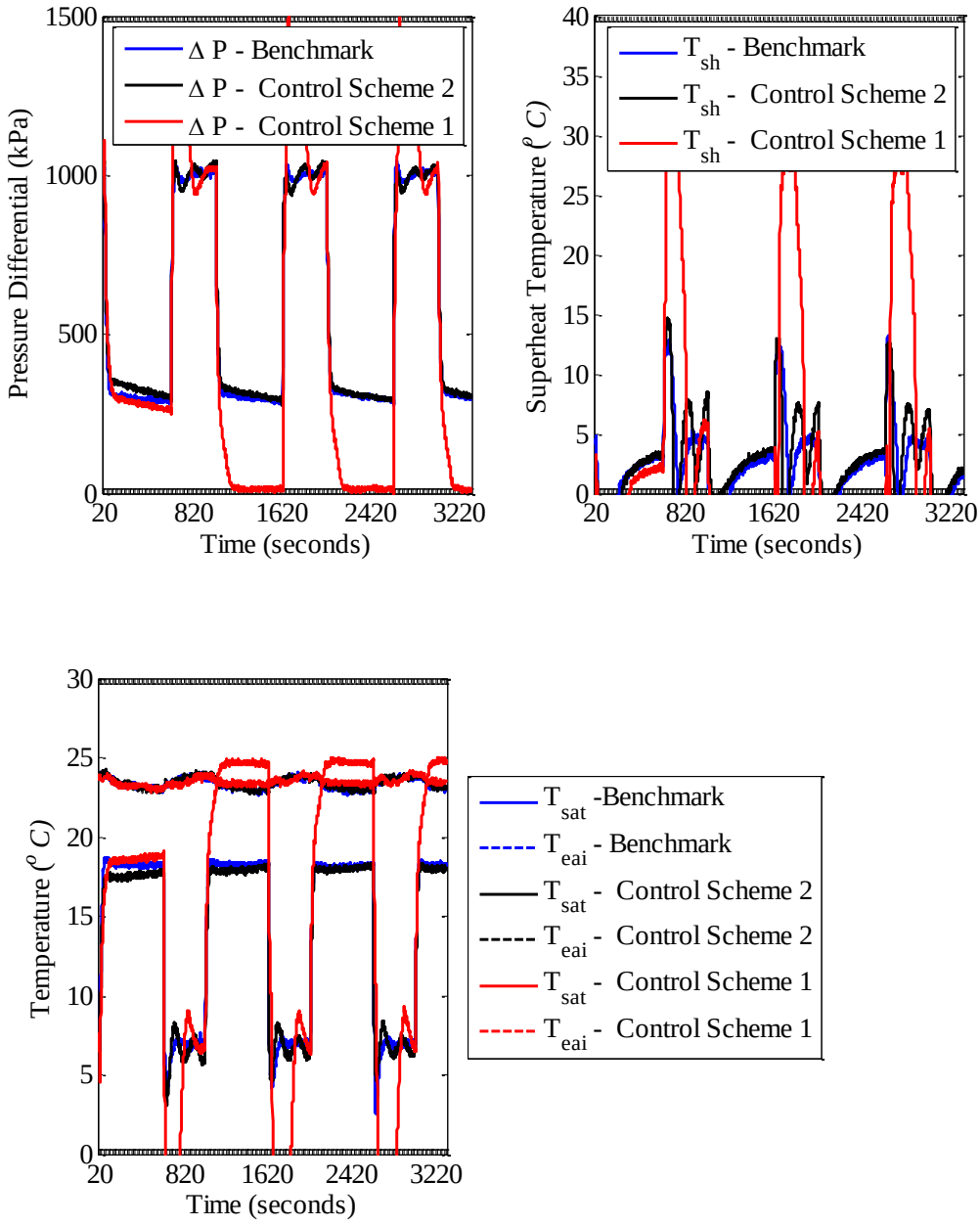

Figure 6.53 Pressure Differential and Superheat – Benchmark Vs Control Scheme 2 Vs Control Scheme 1 - Experiment

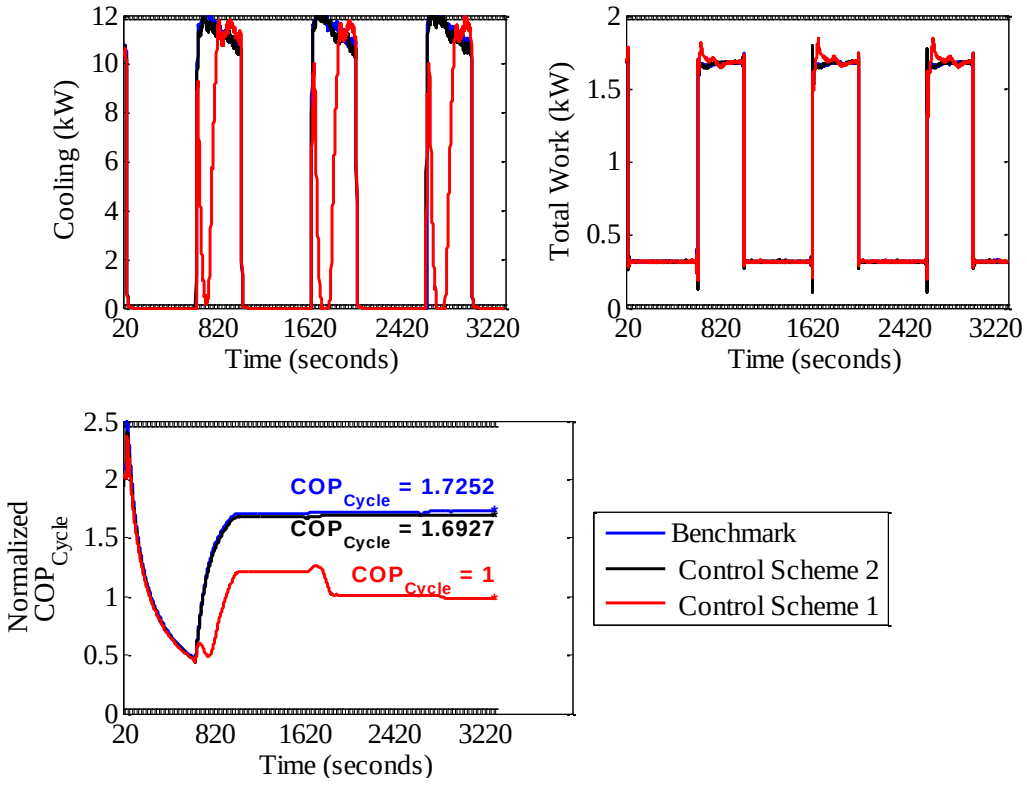

Figure 6.54 Cooling, Work and COP_{Cycle} – Benchmark Vs Control Scheme 2 Vs Control Scheme 1 – Experiment

The comparisons of control scheme 1 and control scheme 2 with the benchmark cycle shows that the benchmark cycle does better. The main reason is how the cycle regulates superheat. By forcing control scheme 1 to cut off the valve during off cycle, there is an increase in the startup performance. Also it proves that just using the superheat controller is not that efficient a strategy so in practice the controller should at least be turned off during the off cycle to prevent integrator windup and refrigerant migration.

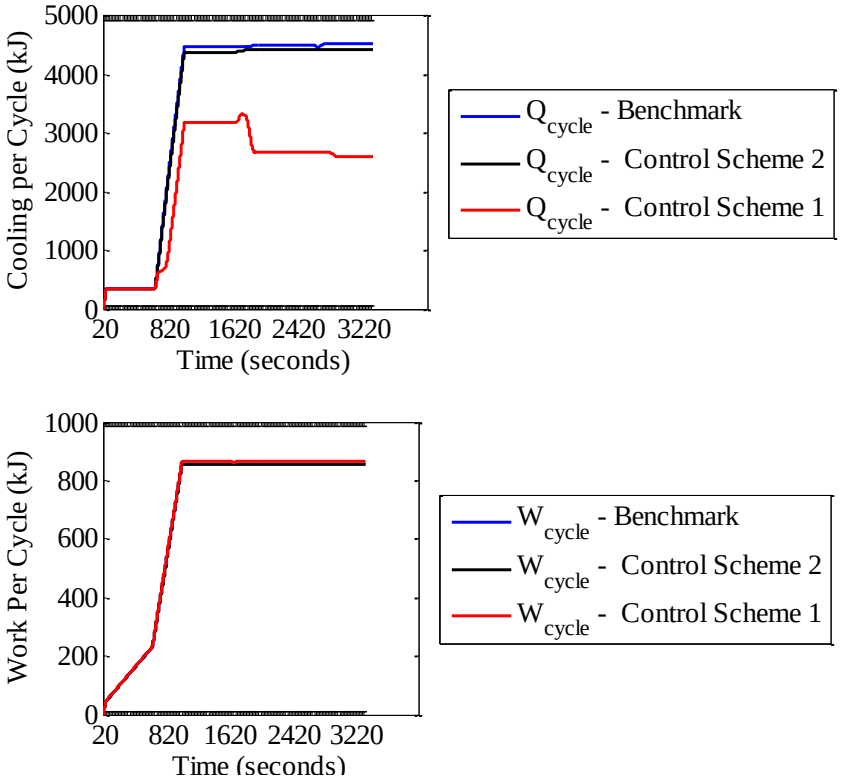

Figure 6.55 Work, Cooling Per Cycle – Benchmark Vs Control Scheme 2 Vs Control Scheme 1 - Experiment

7. CONCLUSION AND FUTURE WORK

This thesis makes specific contributions to the field of air conditioning cycling. To the author's knowledge, no research was done previous to this work to look at the effect, specific expansion valve and evaporator fan cycling schemes had on an air conditioning system's cyclic efficiency. As a first step, dynamic modeling of vapor compression systems was done with the FCV approach. Through extensive simulation analysis, several key vapor compression system dynamics were identified as causes for increasing/decreasing system's cyclic efficiency. Later, recommendations for expansion valve and evaporator fan cycle parameters were given for the simulation model using a robust optimization algorithm to optimize the expansion valve and evaporator fan cycle parameters. Finally, extensive experimental tests on a residential air conditioning system proved the effect of valve/fan cycle on a real system's efficiency. Based on the trends seen from these tests, recommendations were given for the experimental system. A real time optimization method was also explored to optimize for the experimental expansion valve and evaporator fan cycle parameters online. Following are the key outcomes of the research:

- In short cycle simulation the largest gains (~18%) were achieved by
    - Leading the valve during shutdown and delaying it during startup
        - This gain is caused by superior superheat control which results in good startup efficiency
    - Delaying the fan during shutdown

        - This gain is caused by extracting potential cooling off the refrigerant during shutdown
- In short cycle experiment the largest gains (~3%) were achieved by
    - Delaying the fan during shutdown
        - This gain is caused by extracting potential cooling off the refrigerant during shutdown
- The cycling schemes for which the losses were high in both the short cycle simulation and experiment are
    - Valve on during OFF cycle
        - This loss (~17-25%) is attributed to the worst startup efficiency that occurs because of refrigerant migration
- Valve/Fan cycles generally did not result in cyclic efficiency gain for the long cycle whether in simulation or experiment however, the worst performance (~15 – 22% loss) was shown by
    - Any scheme where fan was not cycled because
        - This resulted in unnecessary power consumption during the lengthy off cycle thus bringing down the efficiency
- By comparing cycle strategies to practical control schemes, the problems of refrigerant migration and integrator windup were showcased
    - Operating a PI superheat controller throughout the length of cycle is not that efficient a strategy so in practice the controller should at least be turned off during the off cycle

- This prevents integrator windup and refrigerant migration

This research has some aspects yet to be explored and also opens doors for new research possibilities. Firstly, the effect of condenser fan has been overlooked. Similar to the valve/evaporator fan analysis, the effect of varying the cycling of the condenser fan needs to be seen. There is also the practical aspect of comfort in the air conditioned space determined by the humidity and the temperature swings. Comparing the obtained valve/fan strategies for thermal comfort with the existing strategies will be an interesting study. Future work might explore similar approach towards multi-evaporator systems. Such systems will have a combination of expansion valves for the multiple evaporators and might show some interesting expansion valve behavior against each other. Finally the effect of valve/fan cycling on any other refrigeration cycle such as the transcritical cycle could be evaluated to compare against the vapor compression cycle.

REFERENCES

[1] U. S. DOE. (12/18/2010) Energy savers: Space heating and cooling. Available: http://www.energysavers.gov/your_home/space_heating_cooling/index.cfm/mytopic=12300

[2] EIA. (12/18/2010) Annual Energy Outlook 2010 with Projections to 2035. Available: http://www.eia.doe.gov/oiaf/archive/aeo10/demand.html

[3] Y.-C. Chang, F.-A. Lin, and C. H. Lin, "Optimal chiller sequencing by branch and bound method for saving energy," *Energy Conversion and Management,* vol. 46, pp. 2158-2172, 2005.

[4] D. Honglian, L. Larsen, J. Stoustrup, and H. Rasmussen, "Control of systems with costs related to switching: Applications to air-condition systems," in *IEEE Control Applications, (CCA) & Intelligent Control, (ISIC)*, 2009, pp. 554-559.

[5] W.-L. Jian and M. Zaheeruddin, "Sub-optimal on-off switching control strategies for chilled water cooling systems with storage," *Applied Thermal Engineering,* vol. 18, pp. 369-386, 1998.

[6] B. Li and A. G. Alleyne, "Optimal on-off control of an air conditioning and refrigeration system," in *American Control Conference (ACC)*, 2010, pp. 5892-5897.

[7] M. Rampazzo, Efficient management of HVAC systems, Ph.D. dissertation, Dipartimento di Ingegneria dell'Informazione, Università Degli Studi Di Padova, Padova, Italy, 2010.

[8] S. Bendapudi, J. E. Braun, and E. A. Groll, "A comparison of moving-boundary and finite-volume formulations for transients in centrifugal chillers," *International Journal of Refrigeration,* vol. 31, pp. 1437-1452, 2008.

[9] G. L. Wedekind and W. F. Stoecker, "Theoretical model for predicting transient response of mixture-vapor transition point in horizontal evaporating flow," *Journal of Heat Transfer,* vol. 90, p. 165, 1968.

[10] G. L. Wedekind, B. L. Bhatt, and B. T. Beck, "A system mean void fraction model for predicting various transient phenomena associated with two-phase evaporating and condensing flows," *International Journal of Multiphase Flow,* vol. 4, pp. 97-114, 1978.

[11] M. Dhar, Transient analysis of refrigeration system, Ph.D. dissertation, Department of Mechanical Engineering, Purdue University, West Lafayette, IN, 1978.

[12] W.-D. Gruhle and R. Isermann, "Modeling and control of a refrigerant evaporator," *Journal of Dynamic Systems, Measurement, and Control,* vol. 107, pp. 235-240, 1985.

[13] J. W. MacArthur and E. W. Grald, "Prediction of cyclic heat pump performance with a fully distributed model and a comparison with experimental data," *ASHRAE Transactions,* vol. 93 Part 2, pp. 1159-1178, 1987.

[14] E. W. Grald and J. W. MacArthur, "A moving-boundary formulation for modeling time-dependent two-phase flows," *International Journal of Heat and Fluid Flow,* vol. 13, pp. 266-272, 1992.

[15] P. Mithraratne, N. E. Wijeysundera, and T. Y. Bong, "Dynamic simulation of a thermostatically controlled counter-flow evaporator," *International Journal of Refrigeration,* vol. 23, pp. 174-189, 2000.

[16] J. Chi and D. Didion, "A simulation model of the transient performance of a heat pump," *International Journal of Refrigeration,* vol. 5, pp. 176-184, 1982.

[17] S. Bendapudi and J. E. Braun, *A review of literature on dynamic models of vapor compression equipment*. Atlanta, GA: American Society of Heating, Refrigerating, Air-Conditioning Engineers, 2002.

[18] V. W. Goldschmidt and W. E. Murphy, "Transient performance of air conditioners," in *Proc. of Technical Groups, New Zealand Institute of Engineers*, 1979, vol. 5, pp. 715-738.

[19] J. Wang and Y. Wu, "Start-up and shut-down operation in a reciprocating compressor refrigeration system with capillary tubes," *International Journal of Refrigeration,* vol. 13, pp. 187-190, 1990.

[20] W. J. Mulroy and D. A. Didion, *A laboratory investigation of refrigerant migration in a split unit air conditioner*. Washington, DC : Springfield, VA. : U.S. Dept. of Commerce, National Bureau of Standards ; National Technical Information Service, distributor, 1983.

[21] A. Gado, Development of a dynamic test facility for envirnomental control systems, Ph.D. dissertation, Department of Mechanical Engineering, University of Maryland, College Park, MD, 2006.

[22] R. G. Kapadia, S. Jain, and R. S. Agarwal, "Transient characteristics of split air-conditioning systems using R-22 and R-410A as refrigerants," *HVAC & R Research,* vol. 15, pp. 617-649, 2009.

[23] C. J. Marquand, S. A. Tassou, Y. T. Wang, and D. R. Wilson, "An economic comparison of a fixed speed, a two speed, and a variable speed vapour compression heat pump," *Applied Energy,* vol. 16, pp. 59-66, 1984.

[24] M. J. P. Janssen, J. A. de Wit, and L. J. M. Kuijpers, "Cycling losses in domestic appliances: An experimental and theoretical analysis," *International Journal of Refrigeration,* vol. 15, pp. 152-158, 1992.

[25] F. Wicks, "2nd law analysis of on/off vs. frequency modulation control of a refrigerator," in *Energy Conversion Engineering Conference and Exhibit, 2000. (IECEC) 35th Intersociety*, 2000, vol. 1, pp. 340-344.

[26] A. Leva, L. Piroddi, M. Di Felice, A. Boer, and R. Paganini, "Adaptive relay-based control of household freezers with on-off actuators," *Control Engineering Practice,* vol. 18, pp. 94-102, 2010.

[27] S. M. Ilic, C. W. Bullard, and P. S. Hrnjak, "Effect of shorter compressor on/off cycle times on A/C system performance," *Air Conditioning and Refrigeration Center Contract Report 43,* 2001.

[28] M. J. Poort and C. W. Bullard, "Applications and control of air conditioning systems using rapid cycling to modulate capacity," *International Journal of Refrigeration,* vol. 29, pp. 683-691, 2006.

[29] W. J. Mulroy, "Effect of short cycling and fan delay on the efficiency of a modified residential heat pump," *ASHRAE Transactions,* vol. 92, pp. 813-826, 1986.

[30] B. Rasmussen, Dynamic modeling and advanced control of air-conditioning and refrigeration Systems, Ph.D. dissertation, Department of Mechanical Engineering, University of Illinois, Urbana, IL, 2005.

[31] A. Gupta, Reduced order modeling of heat exchangers using high order finite control volume models, Master of Science Record of Study, Department of Mechanical Engineering, Texas A&M University, College Station, TX, 2007.

[32] J. P. Wattelet, "Heat transfer flow regimes of refrigerants in a horizontal-tube evaporator," Air Conditioning and Refrigeration Center, Urbana-Champaign, IL TR-55, 1994.

[33] V. Gnielinski, "New equations for heat and mass transfer in turbulent pipe and channel flow," *International Chemical Engineering,* vol. 16, pp. 359-368, 1976.

[34] M. K. Dobson, "Heat transfer and flow regimes during condensation in horizontal tubes," Air Conditioning and Refrigeration Center, Urbana-Champaign, IL, TR-57, 1994.

[35] J. Holman, *Heat transfer*. New York, NY: McGraw-Hill, 2002.

[36] S. G. Nash and A. Sofer, *Linear and Nonlinear Programming* New York, NY: McGraw-Hill Science/Engineering/Math, 1995.

[37] W. C. Davidon, "Variable metric method for minimization," *SIAM Journal on Optimization,* vol. 1, pp. 1-17, 1991.

[38] C. G. Broyden, "The convergence of a class of double-rank minimization algorithms 1. General considerations," *IMA Journal of Applied Mathematics,* vol. 6, pp. 76-90, March 1, 1970 1970.

[39] D. Goldfarb, "A family of variable-metric methods derived by variational means," *Mathematics of Computation,* vol. 24, pp. 23-26, 1970.

[40] C. G. Broyden, "A class of methods for solving nonlinear simultaneous equations," *Mathematics of Computation,* vol. 19, pp. 577-593, 1965.

[41] J. A. Nelder and R. Mead, "A simplex-method for function minimization," *Computer Journal,* vol. 7, pp. 308-313, 1965.

[42] B. Bras. (12/18/2010) Penalty and Barrier Methods. Available: http://www.srl.gatech.edu/education/ME6103/Penalty-Barrier.ppt

[43] U. Ascher. (12/18/2010) CPSC 542g : Introduction to Numerical Methods Lecture Notes. Available: http://www.cs.ubc.ca/~ascher/542/chap11.pdf

APPENDIX

FCV Model Derivation

The detailed derivation of the FCV evaporator model found in Gupta is presented here.

Conservation of Refrigerant Energy

The rate of change of refrigerant energy in the system is given by equation 1. Here, $\dot{H}_{in}$ is the rate of energy into the region due to refrigerant flow, $\dot{H}_{out}$ is the rate of energy leaving the region due to refrigerant flow and $\dot{Q}_w$ is the rate of energy due to heat transfer between the refrigerant and the tube wall. At a point the rate of energy due to refrigerant flow is given by equation 2 where $\dot{m}$ is the refrigerant mass flow rate and h is the refrigerant enthalpy at that point. The rate of energy due to heat transfer to the tube wall $\dot{Q}_w$ is given by equation 3 where α_i is the lumped parameter heat transfer coefficient between the fluid and the tube wall, T_w and T_r are the lumped parameter tube wall and refrigerant temperatures. Expanding all the necessary terms, the conservation of refrigerant energy for all the control regions are derived in equation 4.

$$\dot{U} = \dot{H}_{in} - \dot{H}_{out} + \dot{Q}_w \tag{1}$$

$$\dot{H} = \dot{m}\, h \tag{2}$$

$$\dot{Q}_w = \alpha_i A_i (T_w - T_r) \tag{3}$$

$$\begin{bmatrix} \dot{U}_1 \\ \vdots \\ \dot{U}_k \\ \vdots \\ \dot{U}_n \end{bmatrix} = \begin{bmatrix} \dot{m}_{in} h_{in} - \dot{m}_1 h_1 + \alpha_{i,1} A_{i,1} (T_{w,1} - T_{r,1}) \\ \vdots \\ \dot{m}_{k-1} h_{k-1} - \dot{m}_k h_k + \alpha_{i,k} A_{i,k} (T_{w,k} - T_{r,k}) \\ \vdots \\ \dot{m}_{n-1} h_{n-1} - \dot{m}_{out} h_{out} + \alpha_{i,n} A_{i,n} (T_{w,n} - T_{r,n}) \end{bmatrix} \tag{4}$$

Conservation of Mass

The conservation of refrigerant mass is given by difference of the amount of refrigerant entering the region and the amount leaving it. Equation 5 gives the conservation of refrigerant mass for all regions. These can be composed into a single equation by adding them to give equation 6 where, $\dot{m}_{in}$ and $\dot{m}_{out}$ are the mass flow rates of the refrigerant entering and exiting the heat exchanger.

$$\begin{bmatrix} \dot{m}_{e,1} \\ \vdots \\ \dot{m}_{e,k} \\ \vdots \\ \dot{m}_{e,n} \end{bmatrix} = \begin{bmatrix} \dot{m}_{in} - \dot{m}_1 \\ \vdots \\ \dot{m}_{k-1} - \dot{m}_k \\ \vdots \\ \dot{m}_{n-1} - \dot{m}_{out} \end{bmatrix} \quad (5)$$

$$\dot{m}_e = \dot{m}_{in} - \dot{m}_{out} \quad (6)$$

Conservation of Tube Wall Energy

The rate of change of tube wall energy is given by the equation 7 where, $\dot{Q}_a$ is the rate of heat transfer between the tube wall and the external fluid. $\dot{Q}_a$ is given by equation 8 where, α_o is the lumped parameter heat transfer coefficient between the tube wall and the external fluid. A_o is the outside surface area and T_a is the lumped parameter external fluid temperature for each region. Finally, substituting for the necessary terms equation 9 presents the law of conservation of tube wall energy for all regions.

$$\dot{E}_w = \dot{Q}_a - \dot{Q}_w \quad (7)$$

$$\dot{Q}_a = \alpha_o A_o (T_a - T_w) \quad (8)$$

$$\begin{bmatrix} \dot{E}_{w,1} \\ \vdots \\ \dot{E}_{w,k} \\ \vdots \\ \dot{E}_{w,n} \end{bmatrix} = \begin{bmatrix} \alpha_{o,1}A_{o,1}(T_{a,1} - T_{w,1}) - \alpha_{i,1}A_{i,1}(T_{w,1} - T_{r,1}) \\ \vdots \\ \alpha_{o,k}A_{o,k}(T_{a,k} - T_{w,k}) - \alpha_{i,k}A_{i,k}(T_{w,k} - T_{r,k}) \\ \vdots \\ \alpha_{o,n}A_{o,n}(T_{a,n} - T_{w,n}) - \alpha_{i,n}A_{i,n}(T_{w,n} - T_{r,n}) \end{bmatrix} \quad 9$$

Governing Equations

The equations described in 4, 5 and 9 can be compressed into a single expression as in equation 10. The internal energy of the refrigerant could be defined by equation 11 where, $m_{e,k}$ and $u_{e,k}$ are the mass of the refrigerant and the average of refrigerant internal energy. The time derivative of the same could be found out as in equation 12. This is followed by the substitution for the mass of the refrigerant using the average refrigerant density $\rho_{e,k}$ as in equation 13 where $V_{e,k}$ is the volume of the control region. The density and the internal energy could be in terms of pressure, P_e and enthalpy, $h_{e,k}$ so, the time derivatives could be presented with respect to them, which is shown in equation 15. In the next step, the enthalpy $h_{e,k}$ is substituted for in equation 17. The partial derivatives in equations 18 and 19 are then used to obtain equation 21. Equations 22-25 further expand the conservation of mass equations to add to the description. The tube wall energy is then expressed as a product of thermal capacitance and the lumped parameter wall temperature in equation 26. This helps in getting the time derivative of the same as in equation 27. Equation 28-30 remove the intermediate mass flow terms to get the final equation 31.

$$\begin{bmatrix} \dot{U}_1 \\ \vdots \\ \dot{U}_k \\ \vdots \\ \dot{U}_n \\ \dot{m}_e \\ \dot{E}_{w,1} \\ \vdots \\ \dot{E}_{w,k} \\ \vdots \\ \dot{E}_{w,n} \end{bmatrix} = \begin{bmatrix} \dot{m}_{in}h_{in} - \dot{m}_1 h_1 + \alpha_{i,1}A_{i,1}(T_{w,1} - T_{r,1}) \\ \vdots \\ \dot{m}_{k-1}h_{k-1} - \dot{m}_k h_k + \alpha_{i,k}A_{i,k}(T_{w,k} - T_{r,k}) \\ \vdots \\ \dot{m}_{n-1}h_{n-1} - \dot{m}_{out}h_{out} + \alpha_{i,n}A_{i,n}(T_{w,n} - T_{r,n}) \\ \dot{m}_{in} - \dot{m}_{out} \\ \alpha_{o,1}A_{o,1}(T_{a,1} - T_{w,1}) - \alpha_{i,1}A_{i,1}(T_{w,1} - T_{r,1}) \\ \vdots \\ \alpha_{o,k}A_{o,k}(T_{a,k} - T_{w,k}) - \alpha_{i,k}A_{i,k}(T_{w,k} - T_{r,k}) \\ \vdots \\ \alpha_{o,n}A_{o,n}(T_{a,n} - T_{w,n}) - \alpha_{i,n}A_{i,n}(T_{w,n} - T_{r,n}) \end{bmatrix} \quad (10)$$

$$U_{e,k} = m_{e,k}\, u_{e,k} \quad (11)$$

$$\dot{U}_{e,k} = \dot{m}_{e,k}\, u_{e,k} + m_{e,k}\, \dot{u}_{e,k} \quad (12)$$

$$m_{e,k} = V_{e,k} \cdot \rho_{e,k} \quad (13)$$

$$\dot{U}_{e,k} = V_{e,k}(\dot{\rho}_{e,k}\ u_{e,k} + \rho_{e,k}\ \dot{u}_{e,k}) \quad (14)$$

$$\dot{U}_{e,k} = V_{e,k}\left[\left(\left(\frac{\partial \rho_{e,k}}{\partial P_e}\bigg|_{h_{e,k}}\right)\dot{P}_e + \left(\frac{\partial \rho_{e,k}}{\partial h_{e,k}}\bigg|_{P_e}\right)\dot{h}_{e,k}\right)u_{e,k} + \left(\left(\frac{\partial u_{e,k}}{\partial P_e}\bigg|_{h_{e,k}}\right)\dot{P}_e + \left(\frac{\partial u_{e,k}}{\partial h_{e,k}}\bigg|_{P_e}\right)\dot{h}_{e,k}\right)\rho_{e,k}\right] \quad (15)$$

$$h_{e,k} = u_{e,k} + \frac{P_e}{\rho_{e,k}} \quad (16)$$

$$\dot{U}_{e,k} = V_{e,k}\left[\left(\left(\frac{\partial \rho_{e,k}}{\partial P_e}\bigg|_{h_{e,k}}\right)u_{e,k} + \left(\frac{\partial u_{e,k}}{\partial P_e}\bigg|_{h_{e,k}}\right)\rho_{e,k}\right)\dot{P}_e + \left(\left(\frac{\partial \rho_{e,k}}{\partial h_{e,k}}\bigg|_{P_e}\right)u_{e,k} + \left(\frac{\partial u_{e,k}}{\partial h_{e,k}}\bigg|_{P_e}\right)\rho_{e,k}\right)\dot{h}_{e,k}\right] \quad (17)$$

$$\left.\frac{\partial u_{e,k}}{\partial P_e}\right|_{h_{e,k}} = \frac{-1}{\rho_{e,k}} + \frac{P_e}{\rho_{e,k}^2}\left.\frac{\partial \rho_{e,k}}{\partial P_e}\right|_{h_{e,k}} \quad (18)$$

$$\left.\frac{\partial u_{e,k}}{\partial h_{e,k}}\right|_{P_e} = 1 + \frac{P_e}{\rho_{e,k}^2}\left.\frac{\partial \rho_{e,k}}{\partial h_{e,k}}\right|_{P_e} \quad (19)$$

$$U_{e,k} = V_{e,k}\left[\left(\left(\left.\frac{\partial \rho_{e,k}}{\partial P_e}\right|_{h_{e,k}}\right)\left(u_{e,k} + \frac{P_e}{\rho_{e,k}}\right) - 1\right)\dot{P}_e + \left(\left(\left.\frac{\partial \rho_{e,k}}{\partial h_{e,k}}\right|_{P_e}\right)\left(u_{e,k} + \frac{P_e}{\rho_{e,k}}\right)\rho_{e,k}\right)\dot{h}_{e,k}\right] \quad (20)$$

$$\dot{U}_{e,k} = V_{e,k}\left[\left(\left(\left.\frac{\partial \rho_{e,k}}{\partial P_e}\right|_{h_{e,k}}\right)h_{e,k} - 1\right)\dot{P}_e + \left(\left(\left.\frac{\partial \rho_{e,k}}{\partial h_{e,k}}\right|_{P_e}\right)h_{e,k} + \rho_{e,k}\right)\dot{h}_{e,k}\right] \quad (21)$$

$$\dot{m}_e = \sum_{i=1}^{n} \dot{m}_{e,i} \quad (22)$$

$$\dot{m}_{e,k} = V_{e,k} \cdot \dot{\rho}_{e,k} \quad (23)$$

$$\dot{m}_{e,k} = V_{e,k}\left[\left(\left.\frac{\partial \rho_{e,k}}{\partial P_e}\right|_{h_{e,k}}\right)\dot{P}_e + \left(\left.\frac{\partial \rho_{e,k}}{\partial h_{e,k}}\right|_{P_e}\right)\dot{h}_{e,k}\right] \quad (24)$$

$$\dot{m}_e = V_{e,k}\sum_{i=1}^{n}\left[\left(\left.\frac{\partial \rho_{e,i}}{\partial P_e}\right|_{h_{e,i}}\right)\dot{P}_e + \left(\left.\frac{\partial \rho_{e,i}}{\partial h_{e,i}}\right|_{P_e}\right)\dot{h}_{e,i}\right] \quad (25)$$

$$E_{w,k} = (C_P \rho V)_w T_{w,k} \quad (26)$$

$$\dot{E}_{w,k} = (C_P \rho V)_w \dot{T}_{w,k} \quad (27)$$

$$\dot{m}_k = \dot{m}_{in} - V_{e,k}\sum_{i=1}^{k}\left[\left(\frac{\partial \rho_{e,i}}{\partial P_e}\bigg|_{h_{e,i}}\right)\dot{P}_e + \left(\frac{\partial \rho_{e,i}}{\partial h_{e,i}}\bigg|_{P_e}\right)\dot{h}_{e,i}\right] \quad (28)$$

$$\dot{U}_{e,k} = V_{e,k}\left[\left(\left(\frac{\partial \rho_{e,k}}{\partial P_e}\bigg|_{h_{e,k}}\right)h_{e,k} - 1\right)\dot{P}_e + \left(\left(\frac{\partial \rho_{e,k}}{\partial h_{e,k}}\bigg|_{P_e}\right)h_{e,k} + \rho_{e,k}\right)\dot{h}_{e,k}\right] = \quad (29)$$

$$\dot{m}_{in}(h_{k-1} - h_k) + V_{e,k-1}h_{k-1}\sum_{i=1}^{k-1}\left[\left(\frac{\partial \rho_{e,i}}{\partial P_e}\bigg|_{h_{e,i}}\right)\dot{P}_e + \left(\frac{\partial \rho_{e,i}}{\partial h_{e,i}}\bigg|_{P_e}\right)\dot{h}_{e,i}\right] - V_{e,k}h_k\sum_{i=1}^{k}\left[\left(\frac{\partial \rho_{e,i}}{\partial P_e}\bigg|_{h_{e,i}}\right)\dot{P}_e + \left(\frac{\partial \rho_{e,i}}{\partial h_{e,i}}\bigg|_{P_e}\right)\dot{h}_{e,i}\right] = \quad (30)$$

$$\dot{m}_{in}(h_{k-1} - h_k) + \alpha_{i,k}A_{i,k}(T_{w,k} - T_{r,k}) \quad (31)$$

A nonlinear state space of form in equation 32 was used to describe the entire model. This contains *2n+1* states (Enthalpy of *n* regions + Wall Temperature of *n* regions + Pressure across the heat exchanger). These are contained in the state vector *x*, as expressed in equation 33. *u* and *y* are the input and output vectors described in equations 34 and 35 respectively. The matrix $Z(x,u)$consisting of the nonlinear differential equations (equation 36) has all its elements listed in equations 37 through 51. The matrix $f(x,u)$ is presented in equation 52.

$$Z(x,u)\,.\,\dot{x} = f(x,u) \tag{32}$$

$$x = [\;\; P_e \quad h_{e,1} \quad \cdots \quad h_{e,k} \quad \cdots \quad h_{e,n} \quad T_{w,1} \quad \cdots \quad T_{w,k} \quad \cdots \quad T_{w,n} \;\;]^T \tag{33}$$

$$u = [\;\; \dot{m}_{in} \quad \dot{m}_{out} \quad h_{in} \quad T_{a,in} \quad \dot{m}_{air} \;\;]^T \tag{34}$$

$$y = \left[P_e \;\; h_{out} \;\; T_{w,1} \;\; \cdots \;\; T_{w,k} \;\; \cdots \;\; T_{w,n} \;\; T_{a,out} \;\; T_{r,out} \;\; \dot{m}_{e,1} \;\; \cdots \;\; \dot{m}_{e,k} \;\; \cdots \;\; \dot{m}_{e,n}\right]^T \tag{35}$$

$$Z(x,u) = \begin{bmatrix} Z_{11} & Z_{12} & 0 \\ Z_{21} & Z_{22} & 0 \\ 0 & 0 & Z_{33} \end{bmatrix}_{(2n+1)X\,(2n+1)} \tag{36}$$

$$Z_{11} = \begin{bmatrix} Z_{11}^1 \\ \vdots \\ Z_{11}^k \\ \vdots \\ Z_{11}^n \end{bmatrix}_{nX1} \tag{37}$$

$$Z_{11}^1 = V_{e,1}\left(\frac{\partial \rho_{e,1}}{\partial P_e}\bigg|_{h_{e,1}}\right)\left(h_{e,1} - h_1\right) - V_{e,1} \tag{38}$$

$$Z_{11}^k = V_{e,k}\left(\frac{\partial \rho_{e,k}}{\partial P_e}\bigg|_{h_{e,k}}\right)\left(h_{e,k} - h_k\right) - V_{e,k}$$

$$+\left(h_{e,k} - h_k\right)\left(\left(V_{e,1}\left(\frac{\partial \rho_{e,1}}{\partial P_e}\bigg|_{h_{e,1}}\right) + \cdots + V_{e,k-1}\left(\frac{\partial \rho_{e,k-1}}{\partial P_e}\bigg|_{h_{e,k-1}}\right)\right)\right. \tag{39}$$

$$Z_{11}^n = V_{e,n}\left(\frac{\partial \rho_{e,n}}{\partial P_e}\bigg|_{h_{e,n}}\right)\left(h_{e,n} - h_n\right) - V_{e,n}$$

$$+\left(h_{e,n} - h_{out}\right)\left(\left(V_{e,1}\left(\frac{\partial \rho_{e,1}}{\partial P_e}\bigg|_{h_{e,1}}\right) + \cdots + V_{e,n-1}\left(\frac{\partial \rho_{e,n-1}}{\partial P_e}\bigg|_{h_{e,n-1}}\right)\right)\right. \tag{40}$$

$$Z_{12} = \begin{bmatrix} Z_{12}^{11} & 0 & \cdots & 0 & 0 \\ \vdots & & & & \vdots \\ Z_{12}^{k1} & \cdots & Z_{12}^{k(k-1)} & Z_{12}^{kk} & 0 \\ \vdots & & \ddots & \vdots & \vdots \\ Z_{12}^{n1} & \cdots & & Z_{12}^{n(n-1)} & Z_{12}^{nn} \end{bmatrix}_{nXn} \quad (41)$$

$$Z_{12}^{11} = V_{e,1}\left(\frac{\partial \rho_{e,1}}{\partial P_e}\Big|_{h_{e,1}}\right)(h_{e,1} - h_1) + V_{e,1}\rho_{e,1} \quad (42)$$

$$Z_{12}^{k1} = (h_{k-1} - h_k)V_{e,1}\left(\frac{\partial \rho_{e,1}}{\partial h_{e,1}}\Big|_{P_e}\right) \quad (43)$$

$$Z_{12}^{k(k-1)} = (h_{k-1} - h_k)V_{e,k-1}\left(\frac{\partial \rho_{e,k-1}}{\partial h_{e,k-1}}\Big|_{P_e}\right) \quad (44)$$

$$Z_{12}^{kk} = (h_{e,k} - h_k)V_{e,k}\left(\frac{\partial \rho_{e,k}}{\partial h_{e,k}}\Big|_{P_e}\right) + V_{e,k}\rho_{e,k} \quad (45)$$

$$Z_{12}^{n1} = (h_{n-1} - h_n)V_{e,1}\left(\frac{\partial \rho_{e,1}}{\partial h_{e,1}}\Big|_{P_e}\right) \quad (46)$$

$$Z_{12}^{n(n-1)} = (h_{n-1} - h_n)V_{e,n-1}\left(\frac{\partial \rho_{e,n-1}}{\partial h_{e,n-1}}\Big|_{P_e}\right) \quad (47)$$

$$Z_{12}^{nn} = (h_{e,n} - h_n)V_{e,n}\left(\frac{\partial \rho_{e,n}}{\partial h_{e,n}}\Big|_{P_e}\right) + V_{e,n}\rho_{e,n} \quad (48)$$

$$Z_{21} = \left[V_{e,1}\left(\frac{\partial \rho_{e,1}}{\partial P_e}\Big|_{h_{e,1}}\right) + \cdots + V_{e,n}\left(\frac{\partial \rho_{e,n}}{\partial P_e}\Big|_{h_{e,n}}\right)\right]_{1X1} \quad (49)$$

$$Z_{22} = \left[V_{e,1}\left(\frac{\partial \rho_{e,1}}{\partial h_{e,1}}\Big|_{P_e}\right) \cdots V_{e,n}\left(\frac{\partial \rho_{e,n}}{\partial h_{e,n}}\Big|_{P_e}\right)\right]_{1Xn} \quad (50)$$

$$Z_{33} = diag\{|(C_P\rho V)_{w,1} \quad \cdots \quad (C_P\rho V)_{w,n}|\} \quad (51)$$

$$f(x,u)=\begin{bmatrix} \dot{m}_{in}(h_{in}-h_1)+\alpha_{i,1}A_{i,1}(T_{w,1}-T_{r,1}) \\ \vdots \\ \dot{m}_{in}(h_{k-1}-h_k)+\alpha_{i,k}A_{i,k}(T_{w,k}-T_{r,k}) \\ \vdots \\ \dot{m}_{in}(h_{n-1}-h_{out})+\alpha_{i,n}A_{i,n}(T_{w,n}-T_{r,n}) \\ \dot{m}_{in}-\dot{m}_{out} \\ \alpha_{o,1}A_{o,1}(T_{a,1}-T_{w,1})-\alpha_{i,1}A_{i,1}(T_{w,1}-T_{r,1}) \\ \vdots \\ \alpha_{o,k}A_{o,k}(T_{a,k}-T_{w,k})-\alpha_{i,k}A_{i,k}(T_{w,k}-T_{r,k}) \\ \vdots \\ \alpha_{o,n}A_{o,n}(T_{a,n}-T_{w,n})-\alpha_{i,n}A_{i,n}(T_{w,n}-T_{r,n}) \end{bmatrix}_{(2n+1)X1} \quad 52$$

Running Experiments Using Wincon

The nature of the short cycle experiments is explained as follows. Each test starts with 15 minutes of steady state test. This will help bring the experimental system to its appropriate steady state condition before starting the cycle tests. At the end of 15 minutes, cycling starts. The experiment goes through 6 cycles (100 seconds ON and 100 seconds OFF repeat 6 times). At the end of cycling a 5 minute steady state test ends the data set for that experiment. Data is taken for calculations by cutting the cycle data in between the two steady states.

The procedure to run the cycle experiments through Wincon software is presented here. There were basically three MATLAB-script files and a Wincon/Simulink model to run the experiment. The first was a MATLAB-script file that was used to generate the input sequences for the experiments. The input sequences comprised of the valve, the evaporator fan and the compressor sequences. The second was file that setup the MATLAB workspace and compiled the Wincon/Simulink model for running the test.

Once the compilation is complete, the program launches the required plots to record automatically and starts the test. The program also saves the data automatically once every cycle test ends in the '.mat' format and stops the system. To automatically compile the Wincon/Simulink model, open and save the plots, start and stop the test, Wincon scripting commands are used. Once the tests are run the third MATLAB-script file is used to process the data for computation. This file down samples the data and stores it in a structure form for easier access.

VITA

Name:	Swarooph Nirmal Seshadri
Address:	Department of Mechanical Engineering, 3123, TAMU, College Station, TX 77843-3123.
Email Address:	swarooph.nirmal@gmail.com
Education:	B.E., Electronics and Instrumentation, Madras Institute of Technology, 2008 M.S., Mechanical Engineering, Texas A&M University, 2011
Experience:	Graduate Assistant Teaching, Department of Industrial Distribution. Texas A&M University, 06/2009-12/2010, College Station, Texas.
Interests:	Control Systems, Vehicle Dynamics, and Mechatronics.